

X-730-67-10

NASA TM X-55833

**ATS-4**  
**GSFC CONCEPT DESIGN STUDY**

**COMPILED BY**  
**HARRY L. GERWIN**

**JANUARY 1967**



**GODDARD SPACE FLIGHT CENTER**  
**GREENBELT, MARYLAND**

**N67-31355**

FACILITY FORM 80

(ACCESSION NUMBER)

(THRU)

326

(PAGES)

1

(CODE)

TMX-55833

(NASA CR OR TMX OR AD NUMBER)

31

(CATEGORY)

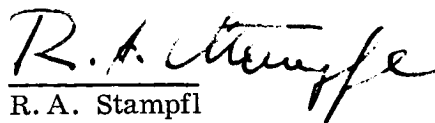
ATS-4

GSFC CONCEPT DESIGN STUDY

Compiled by

Harry L. Gerwin

Approved by:

  
R. A. Stampfl

## CONTENTS

<u>Section</u>	<u>Page</u>
1 INTRODUCTION	1-1
2 PROJECT OBJECTIVES	2-1
3 PROJECT FEASIBILITY	3-1
4 PROJECT JUSTIFICATION	4-1
5 LAUNCH PHASE SEQUENCE	5-1
6 EXPERIMENT DESCRIPTION AND JUSTIFICATION	6-1
7 SYSTEM DESCRIPTION	7-1
8 LAUNCH VEHICLE	8-1
9 LAUNCH AND ORBIT ANALYSIS	
A. ATS-4 NOMINAL ASCENT AND INJECTION SEQUENCE	9-1
B. PAYLOAD TRADE-OFFS AND SPINNING BODY STUDIES	9-13
C. ORBIT ANALYSIS AFTER KICK STAGE FIRING	9-38
10 SPACECRAFT STRUCTURE	10-1
11 A DEPLOYABLE, HIGH GAIN PARABOLIC ANTENNA SYSTEM WITH A SCANNING RF FEED	11-1
12 COMMUNICATIONS SUBSYSTEMS	12-1
13 CONTROLS	13-1
14 PROPULSION SYSTEMS	
A. PROPULSION SYSTEMS ANALYSIS	14-1
B. PROPULSION HARDWARE DESCRIPTION	14-13
15 ATS-4 THERMAL DESIGN	15-1
16 POWER SYSTEM DESIGN CONSIDERATIONS	16-1

## CONTENTS (continued)

<u>Section</u>	<u>Page</u>
17 COMMAND AND TELEMETRY SYSTEM	17-1
18 TM, COMMAND AND GROUND SUPPORT	18-1
19 ORBIT DETERMINATION	19-1
20 ATS-4 EXPERIMENTS	
A. COMMUNICATIONS EXPERIMENTS AND DEMONSTRATIONS CONSIDERATIONS	20-1
B. WHEEL-GRAVITY-GRADIENT BOOM HYBRID	20-40
C. SCANNING CELESTIAL ATTITUDE DETERMINATION SYSTEM (SCADS)	20-40
D. ELECTRIC PROPULSION EXPERIMENT	20-44
E. DEVELOPMENT OF INTERFEROMETER ATTITUDE SENSOR FOR ATS-4 EXPERIMENT	20-45
21 SUMMARY	21-1

## FOREWORD

The conceptual design of the ATS-4 spacecraft required the group efforts of many GSFC personnel. This report is a result of the interchange of ideas, discussions, and critiques among a number of individual authors and groups. Consequently, assigning specific credit is very difficult.

The complete document was reviewed and coordinated by the ATS-4 Study Project Office consisting of Harry L. Gerwin, the Study Manager; Joseph V. Fedor, the Project Technologist; Marius Weinreb, the Spacecraft Manager; and Aldo Merollini, the Project Coordinator.

Sections 1, 2, 3, and 4, consisting of the Introduction, Project Objectives, Project Feasibility, and Project Justification, were written by Harry L. Gerwin.

Sections 5 and 7, covering the Launch Phase Sequence and System Description, respectively, were written by Marius Weinreb.

The Experiment Description and Justification, Section 6, was written by Joseph V. Fedor of the Experiment Engineering Branch.

The Launch Vehicle, Launch and Orbit Analysis, and Propulsion Systems, Sections 8, 9, and 14, respectively, were the efforts of the members of the Auxiliary Propulsion Branch: William Isley, Kenneth Duck, Thomas Cygnarowicz, Curtiss Barrett, Harold Horiuchi, and Albert Yetman. In addition to these individuals, a number of others have provided information and assistance in compiling Sections 8, 9, and 14. Particular acknowledgment should be given to Robert Hunter, Arthur White, Daniel Grant, Robert Gibson, and William Lund. Acknowledgment is also due the Data Systems Division for information and advice pertaining to spacecraft tracking, and to the Stabilization and Control Branch for their cooperation in obtaining the system requirements.

Section 10, describing the Spacecraft Structure, was written by Marius Weinreb and Edwin Stengard of the Systems Division.

Section 11, the descriptions of the 30-foot antenna and its associated RF feeds and beam steering were written by William Korvin with contributions from John Gates, Hossein Bahiman, and Milton Mills; these authors are all

members of the Communications Research Branch.

The Transponders, Section 12, and the Communications Experiment and Demonstration Considerations, Section 20A, were both written by Paul Heffernan of the Communications Research Branch.

The Controls System, Section 13, was written mainly by James Gatlin with contributions from John Hrastar and Walter Raskin of the Stabilization and Control Branch.

The Thermal Approach, Section 15, was written by Joseph Skladany of the Thermal Systems Branch.

The Electrical Power System, Section 16, was authored by Edwin Moses of the Space Power Technology Branch.

Section 17, Telemetry and Command Logic, was written by Joseph Silverman and Marvin Maxwell of the Systems Engineering Branch.

Sections 18, Telemetry, Command and Ground Support, and 19, Orbit Determination, were both written under the direction of Anthony Durham of the Tracking and Data Systems Directorate (T&DS) in cooperation with Howard W. Shaffer and David Stewart of T&DS and Charles N. Smith of the Communications Research Branch.

Section 20B, on the experiment consisting of the Wheel-Gravity Gradient Boom Hybrid, was written by James Gatlin.

The SCADS Experiment, Section 20C, was written by Irving Lowen of the Systems Engineering Branch.

The Electric Propulsion Experiment, Section 21D, was written by Robert Hunter, Head of the Auxiliary Propulsion Branch.

The Interferometer Experiment, Section 21E, was written by David Nace of the Communications Research Branch.

The Summary and Foreword were written by the ATS-4 Study Project Office.

In addition, appreciation, is expressed to Alton Jones and R. A. Stampfl for their suggestions and ideas in overall systems engineering.

## SECTION 1

### INTRODUCTION

One of the major factors which pace the advancement of on-board radio communication and radar in orbiting spacecraft is the progress made in antenna technology. The 30-foot precision antenna to be developed in the A T S - 4 program will be a significant step forward in the technology of large spacecraft antennas. It is fitting that NASA should select Goddard Space Flight Center, having engineers and scientists who are particularly versed in the antenna and control technology required to advance this field, to undertake this project. Control technology is especially relevant because precise aiming is necessary to properly direct the narrow beams of large antennas.

Obviously, such advancements in technology cannot be monitored from behind a desk. Thus, certain critical portions of the program will be done as in-house activities and others, including all manufacturing, will be contracted. Following this reasoning, Goddard established an in-house study team, headed by a project manager, to carry out two functions. The first was to direct the the three mission study contractors and to provide them with the technical information necessary to effectively carry out their studies. The second was to conduct studies to complement and/or supplement the effort of the mission study contractors.

For the in-house study, constraints in certain areas and freedom in other areas were applied. A constraint imposed during the early phases was the use of the SLV-3C Atlas-Centaur as the launch vehicle. No in-house launch vehicle evaluation was undertaken because it was believed that the analyses being conducted by three separate contractors would be sufficiently complete and accurate to permit the correct final vehicle selection with minimum in-house effort. Free thinking was encouraged in terms of allowable experiments and evaluation of proposed experiments. As a result, a spacecraft configuration evolved utilizing experiments other than those proposed in the mission study. This configuration and experiments, when considered with contractor proposals, should provide a comprehensive view of the technology being developed.

During the six months duration of this study, the in-house team examined closely the A T S - 4 antenna system, control system, orbital mechanics, experiments, and launch problems. Both a team spirit and team play have evolved as evidence of the nucleus of an effective in-house team. This Goddard team is technically updated and knowledgeable in the specific problems related to the A T S - 4 project. They are, thus, well qualified to make sound decisions on the design concept and technical approaches selected for the final system.

## SECTION 2

### PROJECT OBJECTIVES

Stated briefly, the A T S - 4 project objectives are:

- Demonstrate a 30-foot diameter deployable spacecraft antenna
- Provide spacecraft fine pointing (0.1 degree) and slewing (17.5 degrees in 30 minutes)
- Provide an oriented platform at synchronous altitude for advanced technology experiments

The spacecraft design is dictated largely by the first two objectives. Provisions are being made for additional experiments which require an oriented platform in synchronous orbit. Experiments which are being considered (subject to Headquarters approval) are discussed in Section 6, Experiments Description and Justification.

For the demonstration of a 30-foot diameter deployable spacecraft antenna, the antenna reflector will be folded to fit inside a launch shroud. When deployed, it will form a reflecting parabolic surface of sufficient accuracy to provide proper performance for frequencies up to 8 GHz. The feed will be capable of performing at several frequencies. Electronic scanning of the beam to  $\pm 12$  beamwidths in the east-west or pitch axis and mechanical scanning of  $\pm 6$  beamwidths in the north-south or roll axis will be provided at the GHz frequency. To provide error control signals in roll and pitch monopulse feeds at 8 GHz and 400 MHz will be provided. At 8 GHz, the error signal accuracy will be 0.01 degree.

Since antenna pattern beamwidths in the order of 0.3 degree are feasible, a necessary and complementary technology is that of precise spacecraft attitude control. Attitude control is necessary for quick pointing toward pre-determined rf energy sources or receivers located on the earth's surface or in space. This control technology involves the use of angle error detection devices such as earth sensors, rf angle-measuring sensors, and star trackers. It involves the technology of forcing systems such as micro-thrust impulse thrusters, high performance inertia wheels, and gimbal gravity gradient booms. It also involves the design of spacecraft which have structural dynamics response characteristics compatible with 3-axis closed loop precise attitude control. The magnitude and effect of the perturbing forces, which the control system must correct, can be predicted. The noise and error sources in the

attitude sensors can be estimated. These factors cannot be completely measured on earth since all the environments cannot be duplicated. Therefore, a significant part of the control system operational program is to determine, by operational measurements, what aspect of the control problem limits precision pointing.

## SECTION 3

### PROJECT FEASIBILITY

Goddard Space Flight Center considers that, based on the absence of any known scientific limitations which require research, it is feasible to achieve the objectives set forth in Section 2 of this report. There are, however, many elements of the problem which pose engineering challenges requiring the highest quality engineering talent.

The feasibility of the project can be best illustrated by examining three specific elements of the problem:

- Launch vehicle capability
- Antenna and feed feasibility
- Control system feasibility

To determine the total spacecraft weight that could be put into synchronous orbit, it was necessary to establish the total weight that the selected launch vehicle SLV-3C Atlas-Centaur could put into the transfer orbit. This was established at 4,000 pounds when the existing Surveyor shroud is used. Since lengthening of the Surveyor shroud would be necessary to provide adequate volume for the A T S - 4 spacecraft, it was also established that each foot extension of the shroud would reduce the 4,000-pound reference weight by 5.0 pounds. Assuming an existing apogee motor (TE-364-3) and the above constraints, it was determined that 1797 pounds could be injected into synchronous orbit. After jettisoning the apogee motor case, adapter structure, transfer orbit control, and thruster system, an orbited on-station weight of 1415 pounds results. The total weight of the spacecraft as now configured is 1287 pounds. This leaves 128 pounds of reserve. It is anticipated that studies by Lewis Research Center will show that the 4,000-pound figure can be increased by 200 to 400 pounds, yielding a 35- to 65-pound increase in spacecraft weight. In addition, an optimized kick stage could provide an additional spacecraft weight growth of 100 to 150 pounds. Based on these data, it is considered completely feasible to design a spacecraft to the weight capability of the SLV-3C Atlas-Centaur.

The feasibility of manufacturing and deploying a 30-foot parabolic reflector can best be examined by considering manufacturing accuracy, deployment reliability, and reflector accuracy when subjected to the environments of space.

Parabolic reflectors can and are being manufactured to a surface accuracy of 0.050 inch. Thus, there should be no reason why these same accuracies cannot be maintained in the manufacturing of a deployable antenna. The hinged petal configuration, deployed in a one-operation driving sequence, is considered very reliable. The flight model antenna deployment system will be cycled through its deployment sequence several times to prove its operability before it is flown.

The surface accuracy achieved with such structures when subjected to the environment of space can only be measured in space. Particular emphasis was placed on this problem by a review in depth of the work carried out by Goodyear and General Electric in their A T S - 4 Phase A mission study. Both companies conducted relatively complete computer analyses, starting with heat flow as the input condition and rf gain and pattern plots as the outputs. Several computer programs were required to conduct the analyses. A program was used to compute the thermal gradient and temperature contour on the reflector due to heat flow. This included shadowing effects as the spacecraft traveled through its 24-hour orbit. From these gradients and temperature contour a second program computed the surface distortions of the reflector. A third program computed antenna gain and pattern using the reflector shape previously calculated. These computer programs made it possible to construct and test various design concepts to arrive at an optimized paper redesign. Computer evaluation of the redesign indicated that, under the worst conditions, the loss in gain resulting from thermally induced deformation was 0.2 dB at 8 GHz.

While the antenna and feed system are considered feasible, they will pose the most challenging engineering problem in the A T S - 4 project. The principal obstacle is the inability to simulate zero g, solar radiation, and vacuum simultaneously. Since tests are limited to those which can be conducted with available facilities, it will be necessary to extrapolate from the test results to the expected performance in space. This approach applies to the correlation of results from structural vibration tests conducted in a vacuum to the dynamic performance of the spacecraft as it will affect spacecraft control performance in space. It also applies to correlation between structural distortion of the antenna as measured in a thermal test chamber under a one g field and antenna performance under flight conditions.

An orbital control system capable of meeting the 0.1 degree pointing requirement is considered within the state-of-the-art. Goddard has considerable experience programing such control systems on analog and digital computers. This technique, along with analytical analysis, was used to examine a variety of proposed control systems. A limiting element in such a control system is the attitude measuring transducer. It appears that an earth sensor will

satisfy the 0.1 degree pointing requirement. However, either an interferometer sensor or a monopulse sensor utilizing the large dish will permit control system performance better than a 0.1 degree pointing requirement. In no case has the slewing requirement been considered a serious problem. Based on these factors, it is considered that the orientation control system required for A TS - 4 is completely feasible.

## SECTION 4

### PROJECT JUSTIFICATION

As stated in Section 1, on-board spacecraft antennas have been a major pacing item in the advancement of radio communications and radar. Since 2-way space communication is a relatively new field, spacecraft antennas will probably be a pacing item in this field. The development of a 30-foot diameter reflector, which has good rf performance up to 8 GHz, is obviously a difficult technical problem. From a scientific viewpoint, achieving this objective is, in itself, a justification. Even so, the successful achievement of this objective will be only the beginning. It will only provide temporary relief to the demands of future communications systems. Demands for higher data rates and for additional channel assignments will increase greatly with time. These demands can be met most efficiently by utilizing the microwave region of the spectrum. Thus, the 8-GHz reflector technology is only a forerunner of the requirements which must be met for future programs.

Concurrent with and of equal importance is the ATS-4 control technology. The narrow antenna beam (0.3 degree half-power beamwidth) can neither be tested nor used in an operational system until control technology is available to point it with an accuracy substantially better than one antenna beamwidth. The control system must be able to slew the spacecraft axis quickly from one angular position to another. It must be able to track a fixed position on earth or a moving position, such as a near-earth satellite. It must be able to perform these functions with a minimum expenditure of consumable fuel to achieve a long lifetime in operational spacecraft. The ATS-4 control technology is also the first step in achieving the pointing accuracy needed for shorter-wave-length microwave and optical communication links. These communication systems, which appear both feasible and practical, can open up a whole new spectrum of communication channels.

While the foregoing might be considered adequate justification for the program, the control technology to be developed for the ATS - 4 program will be useful because of its adaptability to a number of specific applications. These are:

Considerable interest has been expressed in utilizing satellites at synchronous orbit as TV and voice broadcast stations. Figures 4-1 and 4-2 show the antenna pattern coverage that can be achieved with the 30-foot diameter reflector for four selected cases of satellite location, orientation, and carrier frequency. The rf link calculations shown in Section 9 indicate that operating tests could be

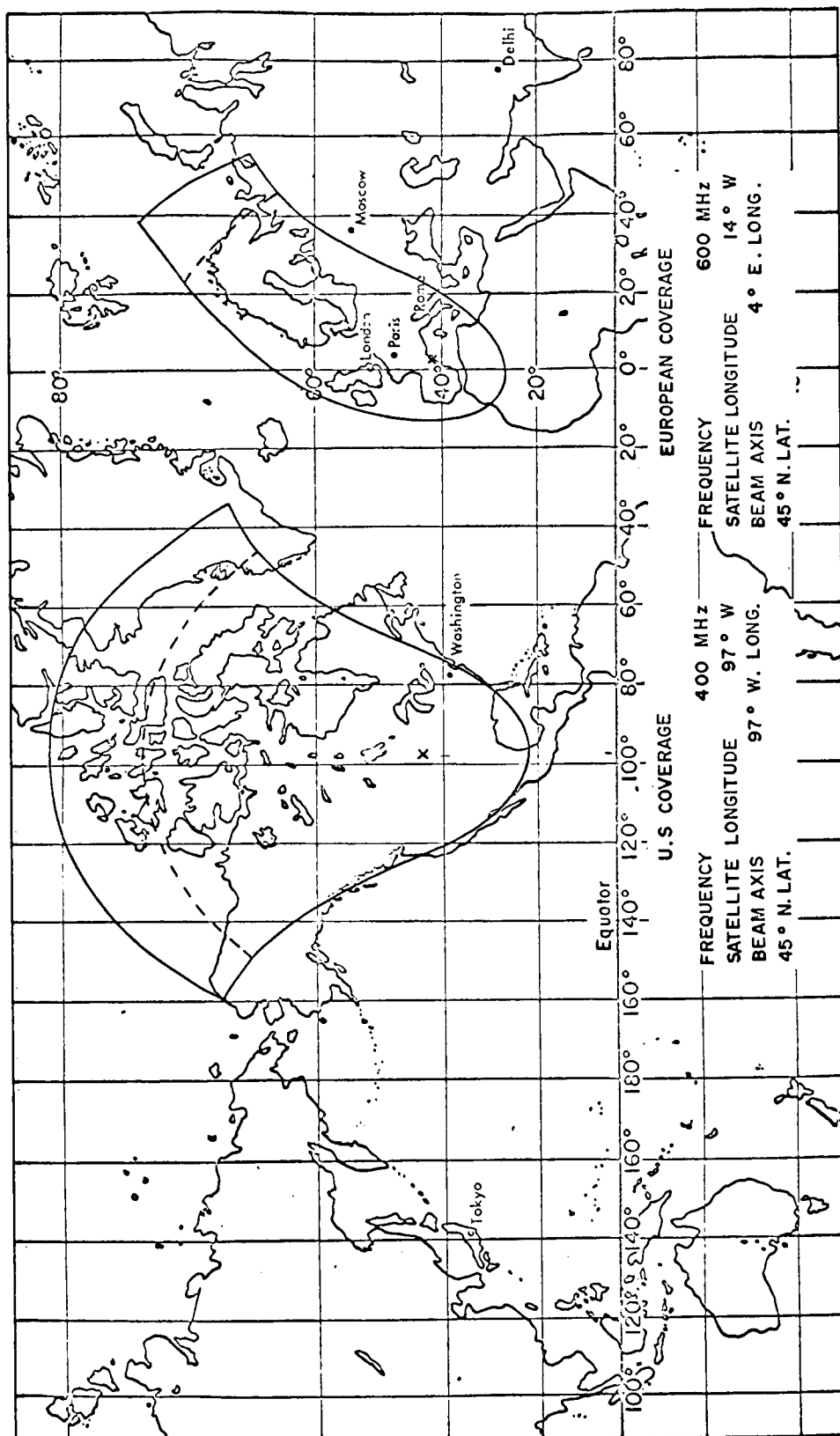


Figure 4-1. Antenna pattern earth coverage with 30-foot parabolic reflector at 400 MHz and 600 MHz.

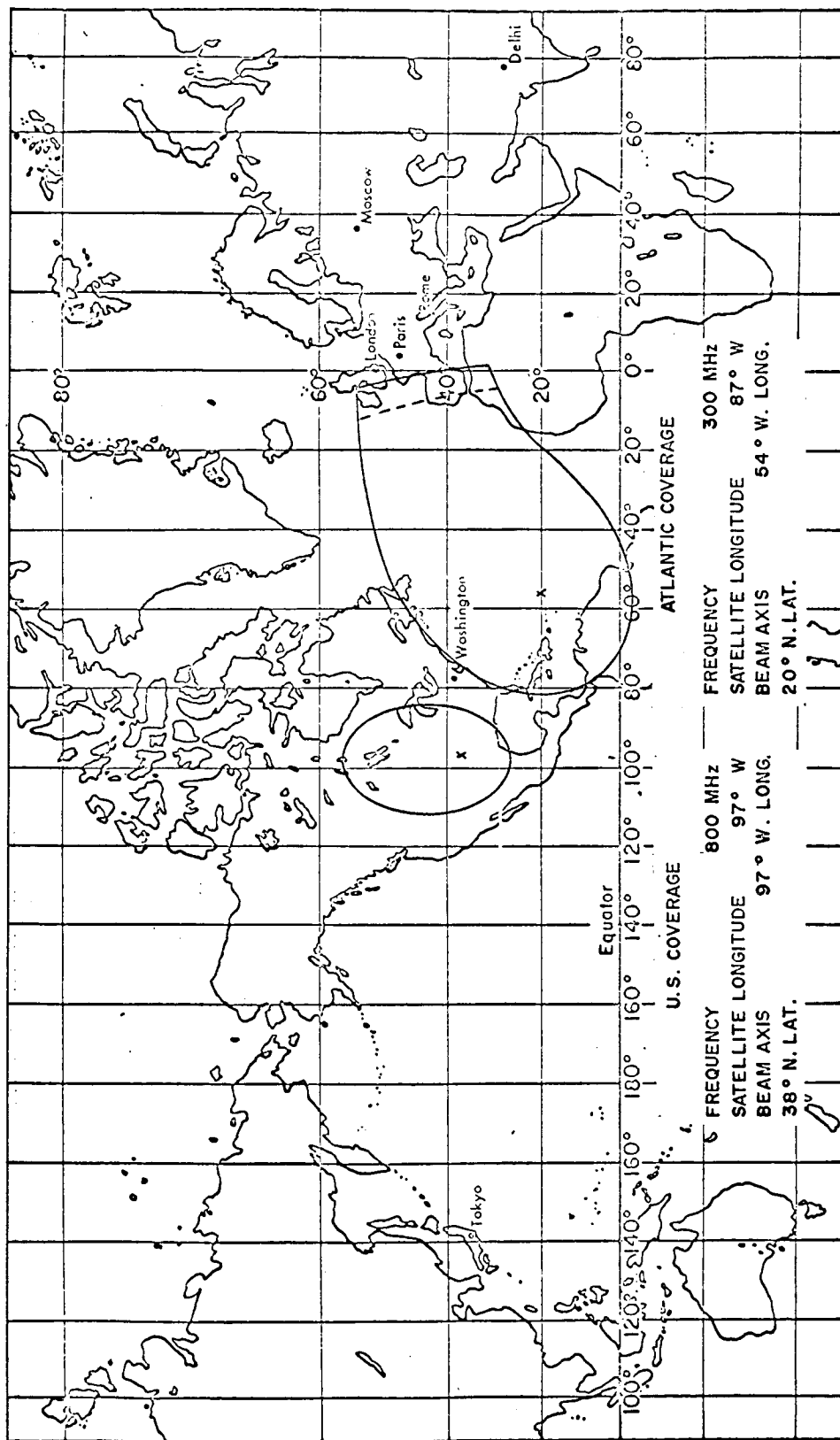


Figure 4-2. Antenna pattern earth coverage with 30-foot parabolic reflector at 800 MHz and 300 MHz.

conducted, even with the A T S - 4 transmitter power levels, of TV relay, military standard voice or facsimile, multiple-access man-pack communications, and air traffic communications. Characteristics of the multipath propagation due to specular water reflection and of radio interference could be studied.

The A T S - 4 antenna technology is directly applicable to the high gain antennas needed to achieve acceptable data rates for deep space probes. For instance, real time TV communications from Mars (480 kilobits per second) could be achieved with less than 1 watt of transmitter power on the satellite and an 85-foot receiving dish on the ground.

An A T S - 4 type spacecraft located at synchronous orbit will be able to track and communicate with an Apollo spacecraft. While the Apollo is in its parking orbit, a data rate of 400 kilobits per second could be provided. While it is on course to the moon, coverage could be provided during those periods when ground station coverage is limited due to rotation of the earth.

Two satellites located at the libration points could provide communications from the earth to the hidden side of the moon. With 10 watts of transmitter power and a 10-foot diameter antenna aperture on the moon, a link channel capacity of 100 megabits per second is achievable.

The A T S - 4 spacecraft will embody the basic control and antenna configuration required in an orbital radio astronomy station. Measurements of radio sources could be conducted in the frequency region where the earth's absorption is high. These measurements are difficult to make on earth.

The A T S - 4 system can be used as a signal source to make pattern measurements and calibrate large earth based antennas.

The control technology to properly orient the spacecraft and the time of firing of the apogee motor for changing from transfer orbit to synchronous orbit will be established and available for future programs involving other large spacecraft with an unfavorable moment of inertia.

A control system to provide an accurately oriented, very stable platform in space will be available on this flight for other advanced technology experiments. This control technique will be available for future programs.

## SECTION 5

### LAUNCH PHASE SEQUENCE

The sequence of events from launch through corrected synchronous orbit is established for the in-house study. A more detailed description is given in Section 9. Launch will occur from ETR with a launch azimuth of 90 degrees utilizing the Atlas-Centaur combination to achieve a 100-nautical mile nominally circular orbit inclined at 28.5 degrees. At the first equatorial crossing, which occurs south of Nigeria, Africa, the transfer orbit is established with a second Centaur burn. A 8.6-degree inclination reduction is included in the burn maneuver. The latter maneuver, in combination with the existing apogee kick motor (TE-364-3), provides the optimum combination for inserting the payload into synchronous orbit. Following the Centaur second burn, the launch vehicle orients the spacecraft to the correct attitude for the kick-stage burn at the second apogee. The spacecraft is spun-up for stabilization. Active damping is used for nutation control. While in the transfer orbit, spin-axis attitude is measured, and small corrections are made to achieve the precise attitude required for apogee kick motor firing. This occurs approximately 17 1/4-hours after launch, and the motor burns for approximately 40 seconds. This operation circularizes the orbit and removes approximately 19.9 degrees of inclination. The spacecraft is then at synchronous altitude located at 53 degrees W longitude or approximately above French Guiana, South America. This location is within the communications range of the Mojave and Rosman ground stations.

Firing the apogee motor could increase the spin-axis cone angle considerably. The thruster system, which provided the active nutation damping while the spacecraft was in the transfer orbit, is used to reduce the coning angle to a small value. Following this operation, the spin-axis orientation is accurately measured using sun sensors and RF polarization sensors. Concurrently, the preliminary orbit is established, using data from the Goddard range and range-rate system. With the spacecraft orientation and orbit established, the required computations to remove injection errors (eccentricity and inclination) are made. To remove eccentricity, the spacecraft axis is first precessed to the computed eccentricity correction attitude. Both thrusters in the thruster system are then fired at the computed time and for the computed firing interval, thereby completely circularizing the orbit. Following another period of orbit determination and spacecraft axis measurement, the inclination error is removed. Again, the spacecraft is precessed to the computed inclination correction attitude, and both thrusters are fired at the computed time and for the computed firing interval.

After inclination correction, the thruster system has completed its function and is jettisoned along with the kick stage. This triple-function hydrazine thruster system provided nutation damping by firing thrusters out of phase and in synchronism with the nutation frequency. It provided precession control by firing thrusters in synchronism with the spin rate and phased to precess the axis in the required direction. It provided inclination and eccentricity correction by firing both thrusters simultaneously and continuously for the desired interval.

Next, the spacecraft spin rate is reduced to a residual of 1 degree/sec by the use of a yo-yo system. After despin of the spacecraft, the 3-axis control system begins operating by acquiring the sun in the roll axis. The spacecraft antenna is then deployed, and a slow roll is initiated. When the earth appears in the field of view of the earth sensor, pitch and roll control is transferred to an earth reference. Yaw control is then transferred to a digital sun sensor. A yaw bias is set in the control system, and when Polaris appears in the field of view of the Polaris tracker, yaw control is transferred to Polaris. The spacecraft is now under 3-axis control and ready to begin operation at a longitude of 53 degrees W. The elapsed time to this point is about 58 hours. The triaxiality of the earth will cause a slow drift toward the stable point at about 108 degrees W. When the satellite reaches about 100 degrees W it will be stopped using the on-board stationkeeping system.

Tracking and data acquisition coverage during the launch sequence is provided by use of the following stations:

1. Launch to injection into circular parking orbit--Cape Kennedy and Bermuda.
2. Coast phase - no coverage is available with present stations.
3. Second burn, 8.6 degrees inclination removal, Centaur separation - ship off the coast of Africa if available from the Apollo program.
4. Remainder of trajectory (except at perigee) - covered by a number of Goddard range and range-rate stations.

The performance reliability of the spacecraft was given careful consideration. This consideration is reflected in the following tabulation.

<u>Failure modes</u>	<u>Reliability approach</u>
Spacecraft separation from Centaur	Redundant squibbs
Spin-up	Redundancy but at reduced spin rate
Active nutation damping	Redundant nozzles
Spin-axis measurement	Redundant system
Spin-axis precession	Redundant nozzles
Kick-stage firing	
Inclination or eccentricity removal	Redundant nozzles
Jettison adapter	Redundant squibbs
Yo-yo despin	Control nozzle back-up
Deploy solar paddles and antenna	Redundant squibbs and deployment motors
Control system acquisition	Back-up sensors and back-up nozzles

## SECTION 6

### EXPERIMENT DESCRIPTION AND JUSTIFICATION

The intent of the Application Technology Satellite Program of which ATS-4 is a part is to develop progressively the technology required for various spacecraft applications of the future. The technology for spinning satellites is being developed by ATS-B and ATS-C; the technology for passive gravity gradient systems is being developed by ATS-A, ATS-D, and ATS-E. It is the intent of the ATS-4 project to develop the technology for the deployment, 3-axis control, and utilization of large, high gain antenna system(s).

In addition to the primary antenna and the 3-axis fine control technology experiments, which were covered earlier, specific experiments being considered in the in-house study are listed below, with a brief description of each. No implication is intended as to their approval or exclusive desirability.

The Interferometer is a radio frequency sensor which measures spacecraft attitude (3-axis) during the mission phase. The basic sensor consists of two antennas whose phase centers are separated by a fixed distance and by electrical phase - comparing elements. A transmitted radio wave intersecting the two antennas results in a measurable phase shift between the signals received by each antenna. The amount of phase shift depends upon the angle made by arrival of the wave and the baseline axis between the antennas. When orthogonal pairs of antennas are appropriately combined with the main axis of the spacecraft, the resulting measured phase gradients are indicative of spacecraft attitude. Also, the interferometer can be used to generate error signals for attitude control of the spacecraft.

The Self-Steering Phased Array Communication Repeater is a microwave repeater consisting of a self-phasing antenna system which automatically forms high-gain beams to both receive and transmit microwave communications signals between two or more earth bound stations. The stations acquire the beams by sending a CW pilot signal to the satellite (repeater) which has an RF pattern encompassing the earth. The antenna electronics then direct the beam toward that station and the beam remains fixed to the station as long as the CW pilot is in operation. A wideband signal can be received, amplified, and frequency converted to a new frequency band for retransmission. Another ground station that wishes to receive the signal transmit a CW pilot signal to the repeater. This pilot directs a high-gain transmit beam toward the second station, which contains the wideband signal sent by the first station. The mission study contractors have investigated phased arrays. These systems are described in their reports; and therefore have not been included in this study.

The Scanning Celestial Attitude Determination System (SCADS) is a star mapping system which provides a simple means to determine spacecraft attitude information for ATS-4 during the transfer ellipse mode (spin stabilized) and during the mission mode (3-axis stabilized). The SCADS concepts consists of a single on-board sensor device and a ground based data reduction system. The sensor device, by observing the generally known star field, provides signals from which the viewed star field can be positively identified and three axis vehicle attitude information derived.

The Inertia Wheel-Gravity Gradient Boom Hybrid is an active control system with a gimbaled two degree of freedom gravity gradient boom. It serves as a source of reaction torque for attitude maneuvers and a source of external torque to prevent wheel saturation and to minimize momentum storage requirements. The inertia wheels and control electronics provide its own control system damping, so that an additional passive damper is not required.

The Colloid Micro-Thruster is an electrostatic thruster in the same general category as ion thrusters: that is, exhaust beam kinetic energy is obtained by accelerating charged particles within an electrostatic field. The colloid thruster differs from the ion thruster in that charged particles are multi-molecular rather than atomic. The characteristic feature of this concept is the use of a charged particle source which utilizes a voltage potential and capillary tubes for particle formation and acceleration. The propellant, a low vapor pressure, moderately conductive liquid, is sprayed from tips of metallic capillary tubes. This is achieved by maintaining the tubes at a high electrical potential. The need for exhaust beam

neutralization is eliminated by having the capillary tubes produce both positive and negative charged particles simultaneously from adjacent tubes. The contemplated thruster would have a nominal thrust level of 200 micro-pounds, specific impulse of 800 to 1000 seconds, and would require less than 20 watts of power. The thruster could serve an operational function such as north-south stationkeeping.

The interferometer and SCADS experiments deal with orientation determination, which is fundamental to 3-axis control and to space flight in general. The phased array repeater experiment takes advantage of the synchronous nature of the ATS-4 orbit and can point and steer in particular directions without spacecraft or ground station ephemeris data and without accurate platform stabilization. The wheel-boom experiment is another use of the gravity gradient force field for other than a reference to the local vertical. It promises to appreciably extend the operational life of 3-axis reaction wheel control systems. The colloid thruster is a significant advance in the electrostatic thruster field, requiring approximately one tenth the power of the ion thruster. All the experiments are untried technology; that is they have not been used in space flight. It is felt that the inclusion of these experiments on ATS-4 would advance the state of technology in these areas. Within the constraints of weight, power, and available volume, other experiments can also be considered.

## SECTION 7

### SYSTEM DESCRIPTION

#### LAUNCH VEHICLE

The Atlas-Centaur has been selected as the launch vehicle. This launch vehicle, with a TE-364-3 (Delta) kick motor, will inject 1797 pounds, including kick-stage inert weight, into equatorial synchronous orbit. Allowing for kick-stage inert weight and adapter, this yields a useful spacecraft weight of 1415 pounds. The shroud will be the one developed for the Surveyor mission, modified in length. An additional cylindrical length of 15 feet is required. The spacecraft is attached to the Centaur at an interface located at station 156.45. The diameter of this interface ring is 5 feet. Optimization of the kick stage would add approximately 200 pounds of useful spacecraft weight, but this is not proposed now for cost reasons. The use of the Titan as a launch vehicle would raise the useful spacecraft weight to about 1865 pounds.

#### SPACECRAFT DESCRIPTION

The A T S - 4 spacecraft is depicted in Figure 10-1. The spacecraft consists of two equipment modules separated 15 feet by a six-member truss. All spacecraft subsystems and components are housed in these modules. One equipment module is earth viewing; the other views space and is referred to as the "aft equipment module." The thirty-foot-diameter parabolic antenna reflector is mounted to the aft equipment module. The solar cell paddles for the solar conversion power supply extend beyond the rim of the reflector. The spacecraft is mounted to Centaur on an adapter. The launch weight of the spacecraft is 3250 pounds. After separation of the adapter the in-orbit useful payload is 1415 pounds. The major contributors to this weight are (1) attitude control and stationkeeping---176 pounds, (2) parabolic reflector, instrumentation, feed, and RF systems---345 pounds, (3) structure---235 pounds, (4) solar power supply---241 pounds, (5) telemetry and command---60 pounds, (6) interferometer---35 pounds, and (7) miscellaneous (harness, thermal control, additional experiments, etc.)---323 pounds. A complete weight breakdown is given in Section 10. The major spacecraft components and subsystems will now be described in somewhat more detail. For complete descriptions of these items, including trade-off analysis, refer to Sections 9 through 18.

The parabolic antenna reflector has an  $f/d$  of 0.5. The reflecting surface is a mesh with high RF reflectivity and high optical transparency. This mesh

is mounted on a system of petals which form the desired parabolic contour. The parabolic contour of the antenna must be maintained over the two-year lifetime in orbit. The sun's energy is the primary cause of deviations, as a function of orbital position. Varying incidence of the sun's rays on the reflector will cause varying thermal gradients over the structure, hence mechanical deformations. Minimization of these deformations can be effected by a clever thermal design. The thermal design of the antenna is therefore of primary importance to the success of the mission. A combination of thermal coatings that will give acceptable deformation limits is as follows: a buffed-metal front surface, black painted edges, and a metallized back surface (low emittance). If required, better performance can be obtained by wrapping the structure with a super-insulation. However, this technique will be held as reserve. For stowage in the launch condition (Figure 10-1), it is folded to fit into the shroud. The folding technique features triangular- and rectangular-shaped petals, which are hinged at the attachment points to the aft equipment module. In addition, each petal is hinged to its adjacent petals so that only unfolding action is required to deploy the antenna. The antenna petals are manufactured to form the correct parabolic contour, then hinged to each other, and the entire assembly is mounted on the aft module. In this condition, the antenna is in an unstressed state. To accomplish stowage, each hinge line is first straightened, thereby putting the petals into a stressed condition. Then the petals are folded, accordion style, to fit into a cylindrical envelope 8-1/2 feet in diameter and 10 feet in length. Reinforcement for launch is obtained by snubbing the upper ends of the petals to a ring on the interconnecting truss. Fastening is accomplished with a circumferential band clamp. Once in orbit, the clamp is released pyrotechnically and the stored energy in the petals causes deployment to begin. Deployment is then continued by use of an active mechanism. This deployment mechanism acts to control the deployment rate while the stored energy in the petals is being dissipated, and then takes over and pulls the hinge lines into place. A detailed design of the deployment mechanism is still in process. The RF-feed system for the antenna is housed on the aft end of the earth-viewing module. The many frequencies suggested by the Headquarters RFP are dictated by various applications and are all of interest for ATS-4. The in-house study has attempted to bracket these frequencies: on the low end 400 MHz was selected; on the high end 7-8 GHz was selected. The 400-MHz feed is comprised of four radiating elements arranged symmetrically to perform a monopulse function. The gain of the sum channel is 27 db. The beamwidth of the sum channel is about 6 degrees and when used in connection with the difference channel, it provides full earth coverage in a monopulse mode. When used for data collection, the beam can be swept by slewing the spacecraft. In this way the entire earth's disk can be swept in an hour's time. The 7- 8-GHz feed provides for scanning with the RF beam. It has a scan capability of  $\pm 12$  beamwidths in the East-West direction and  $\pm 6$  beamwidths in the North-South direc-

tion. The scanning in the East-West direction is done by electronically switching 32 horns. The North-South scanning is accomplished by mechanically moving the row of horns. A monopulse system capability is incorporated into the center horns. The on-axis gain at this frequency is approximately 50 db. Beside the parabolic reflector, the spacecraft structure consists of the two equipment modules separated by a distance of 15 feet and interconnected by a 6-member beryllium tube truss. The separation distance is dictated by the required distance between the reflector and feed. The earth-viewing module contains, besides the feed, all equipment that has an earth-viewing requirement. The bulk of the spacecraft equipment is located in the aft equipment module.

Spacecraft thermal control is accomplished by a system of active thermal louvers located on both the forward and aft equipment modules. The active system is augmented by application of passive insulation. If the necessary techniques become available in the time frame of ATS-4, in-orbit repairs by astronauts may be a desirable feature. To this end, the spacecraft is being designed so that all equipment is easily accessible. For example, all equipment in the aft module becomes exposed when a layer of thermal insulation is peeled off. Similarly, the equipment in the earth-viewing module becomes exposed by rotating the thermal shutter assemblies out of the way. The entire spacecraft is mounted on the Centaur stage on an adapter. This adapter performs three functions: (1) structural mount for the spacecraft, (2) housing for the apogee kick motor, (3) and housing for the vernier auxiliary propulsion system. The apogee kick motor is the TE-364-3 developed to be a third stage on the Delta vehicle. Its 1440 pounds of solid propellant burn for approximately 40 seconds. A more detailed description of this motor is given in Section 14.

To provide for spacecraft maneuvers, coning control, and velocity error corrections during the launch phase, a vernier auxiliary propulsion system is provided. This system uses hydrazine as fuel. The hydrazine system consists of the two nozzles, two hydrazine tanks, two nitrogen pressurization tanks, a catalyst bed, and related valving. The nozzle axes are parallel to and offset from the spacecraft spin axis. The entire system, including 85 pounds of hydrazine, weighs approximately 110 pounds.

The specific impulse of the hydrazine system will vary from 115 to 235 seconds, depending on the length and number of the pulses. The major pulse requirement will occur at an average specific impulse approaching 235 seconds.

Following is a description of the major orbital spacecraft subsystems.

## ORBITAL THRUSTER SYSTEM

Orbital stationkeeping and attitude control thrusting is accomplished by a system of ammonia Resistojet thrusters. Four multijet thermal storage Resistojet thrusters are provided on the spacecraft. They are mounted on the aft equipment module. Each thruster contains four nozzles aligned such that they provide tangential thrust for stationkeeping and moments about the pitch, roll, and yaw axes for attitude control.

Because the spacecraft design constrains the location of thrusters off the center of gravity, it is necessary to utilize the attitude nozzles simultaneously with the tangential nozzles to correct attitude errors imparted by the stationkeeping operation. The tangential thruster provides the desired motion while the attitude control thruster counteracts any disturbance torques. The net effect of this mode of operation is a resultant thrust vector through the center-of-mass of the spacecraft. This technique of thrusting through the center-of-mass was chosen over the technique of canting and thrusting with a single nozzle. The reason is that a degree of redundancy is obtained in attitude control.

The resistance jet system consists of the nozzles, a zero gravity propellant feed tank, and a power conditioner subsystem. The weight of the entire system, excluding the propellant, is approximately 38 pounds. The calculated auxiliary propulsion fuel requirements to accomplish East-West stationkeeping for a period of 2 years, to achieve initial precise orbital adjustment, to provide attitude control, and to demonstrate the capability of North-South stationkeeping is 40 pounds of ammonia.

The resistance jet is designed to operate at temperatures up to 2000° F. Ammonia gas passes through a resistive heater in the thruster module and is heated before exiting through the nozzle. The heat increases the specific impulse of the gas. The design of the resistance jet is such that it can be operated at any temperature from ambient up to approximately 2000° F, depending on power input. This feature presents the option of increasing specific impulse by increasing power input. The daily attitude control functions will be performed at a power input of 5 watts to each thruster module. This provides a specific impulse of about 150 seconds. The East-West stationkeeping will be done every 10 or 11 days at a power input of 35 watts with a corresponding specific impulse of about 250 seconds. (Cold ammonia gas has a specific impulse of about 100 seconds.)

## ATTITUDE CONTROL SYSTEM

The basic operational attitude control system is a wheel-jet hybrid. The operational (on-station) requirements are:

1. Steady-state pointing:  $\pm 0.1$  degree
2. Offset range:  $\pm 8.5$  degrees
3. Horizon-to-horizon slew (17 degrees): 30 minutes

The basic operational control system uses an infrared earth sensor for pitch and roll error signals and a Polaris tracker (electronically gimballed) for yaw error signals. The Polaris tracker also makes available a roll error signal.

The horizon scanner principal requirements are:

1. Offset capability:  $\pm 8.5$  degrees in each axis
2. Accuracy:  $\pm 0.05$  degree

The device utilizes mechanical scanning of the earth's disk. Offset pointing is achieved by gimbaling the optical axis by use of mirrors.

The Polaris star tracker requirements are:

1. Field of view: 4 x 25 degrees
2. Accuracy: 1 arc minute

The tracker is electronically gimballed to give the offset pointing capability.

While the infrared earth scanner and the Polaris tracker are the primary sensors for the 3-axis earth-pointing mode, additional experimental sensors are being considered. The RF interferometer can be used for an open-loop measurement of attitude or to provide control error signals. The star-field mapper (SCADS) will be used only for an open-loop attitude measurement and should be accurate to better than 0.01 degree. The main dish can be used in the monopulse mode to provide attitude measurements of roll and pitch errors to an accuracy of better than 0.01 degree.

An in-house analog simulation study (which includes effects of structural vibrations) has shown that a pulse-modulated reaction-jet control system can fulfill the acquisition control requirements and could possibly fulfill the operations control requirements. However, it is proposed to utilize this capability only as a backup mode and provide the wheel-jet hybrid control system for the operational mode for the following reasons:

1. Less sensitive to sensor noise.
2. Less sensitive to structural vibrations and disturbances.
3. Smaller orbital stationkeeping disturbance.
4. Gas consumption less dependent on the operational program.
5. Adaptable to a gimbaled gravity gradient boom experiment.

The wheels required are similar to the OAO fine wheels.

Spinning-body control is used during the transfer ellipse and initial synchronous-orbit corrections. Control is obtained with one axial thruster (two are carried for redundancy) using the techniques pioneered on Syncom and used on ATS D&E. The requirements placed upon the control system are active nutation damping, spin-axis precession, and spin-axis orientation measurements. Coarse spin-axis measurements are made, utilizing a Syncom-type sun sensor and ground station measurement of the RF polarization of the spacecraft beacon. A potential method for making fine axis-orientation measurements is the star-field mapper presently being developed.

The sensors utilized during the acquisition are:

1. Acquisition sun sensor - Four linear null detectors plus an array of logic cells to provide 2-axis inertial orientation towards the sun will be used. The sensor will have a spherical field of view of  $\pm 0.5$ -degree accuracy at null.
2. Digital sun sensor - A slit-type sensor will be used to provide yaw control for Polaris acquisition. The sensor will have a linear range of  $\pm 40$  degrees with an accuracy of  $\pm 0.75$  degree, and sensitivity sufficient to operate at a sun incident angle as low as 30 degrees. A digital command word will provide the appropriate bias, determined by time of day and time of year, to place the spacecraft roll-axis within  $\pm 1.5$  degrees of the equatorial plane.
3. Body rate sensors - A 3-gyro package is required for rate control and damping during the acquisition sequence. The required minimum commandable rate is 0.2 degree/sec with a threshold of 0.02 degree/sec.

## POWER SYSTEM

The electric power supply is a solar conversion type, utilizing nickel-cadmium batteries for umbra and peak loads. The design loads are 200 watts average, regulated during the illuminated portion of the orbit; and 100 watts average, regulated during umbra conditions.

The system consists of two fixed solar paddles, oriented like a cruciform and aligned parallel with the pitch axis. The paddles are mounted on two extended antenna deployment trusses. Each paddle surface provides 40 square feet of area for mounting solar cells. Cells are mounted on both sides of the structure. N-on-P solar cells having a 10-percent, air mass zero efficiency have been selected. After 2 years, the solar array provides 275 watts of average power under worst-case orientation of the solar array. (Two-hundred sixty-five watts are required.) Fixed solar paddles were selected on the basis of higher reliability. The following trade-off factors are applicable:

	<u>Fixed array</u>	<u>Oriented array</u>
Solar cell area	160 sq ft	50 sq ft
Solar panel weight	128 lb	54 lb
Solar array drive weight (2)	0	18 lb
Slip ring weight (2)	0	8.0 lb
Cost-tested panels/spacecraft	700k	300k
Development cost of array drive	0	750k
Reliability	high	requires array drive and slip rings

Two packs of 12 ampere-hour, third-electrode, nickel-cadmium batteries have been chosen to provide the necessary power during nighttime and peak loading. Each pack consists of 22 series-connected cells. Maximum depth of discharge during the longest eclipse is 25 percent. Charge current is controlled by two temperature-varied, constant-potential regulators. The third-electrode feature provides overcharge protection by signaling the regulator to reduce the charge rate to C/60 (200 ma) constant current. Ground command can also provide this same reduction.

The solar array and batteries are diode-gated to redundant 400-watt buck-boost voltage regulators that provide a +28 volt  $\pm 2$  percent regulated bus. The 400-watt size is derived from the total peak load of the spacecraft. A fault, sensed on the regulated bus, initiates automatic switchover to the standby regulator. This switchover can also be commanded from the ground.

## COMMAND AND TELEMETRY SYSTEM

The command and telemetry system for ATS-4 has been designed to provide a high degree of flexibility. During the spacecraft lifetime, the system

requirements vary widely, depending on the state of the spacecraft. The telemetry requirements are such that only certain parameters require continuous readout. The intermittent requirements vary from a time period of a few minutes to several hours. To best satisfy these requirements, a Telemetry Data Processing System is proposed which can vary the sampling rates and sampling points through the use of various stored programs.

This system is generally called the "adaptable" or "programmable" concept, and it allows wide variations in sampling rates, points, and formats. This removes many of the restrictions imposed by hardwired systems. It provides two basic data transmission rates:

40 samples/second (prior to deployment)  
400 samples/second (after deployment)

It provides also an optional ground programming mode. The proposed spacecraft command system design is straightforward and conforms to all requirements of the GSFC Aerospace Data Systems standards. The current command requirements are:

1. Approximately 160 latching-type relay commands.
2. Approximately 170 10-bit digital command-type words.
3. Approximately 8 timed tone-execute commands for real-time control of spacecraft functions.
4. Real-time operation only.

Internal spacecraft verification of the command will be performed prior to spacecraft execution. The communication system for telemetry and command will be at S-band. In this way, utilization of this same equipment is made for the range and range-rate tracking system.

## SECTION 8

### LAUNCH VEHICLE

The launch vehicle evaluation conducted for the in-house study was limited to the SLV-3C Atlas-Centaur. For the A T S - 4 launch, the Atlas burn and two Centaur burns are used to place the spacecraft into a Hohmann transfer ellipse having a perigee altitude of 100 nautical miles, apogee altitude of 19,323 nautical miles and line of apsides lying on the equator.

The Atlas booster which is mated with Centaur is essentially the same vehicle which has been used in such programs as Project Mercury, the Ranger series of lunar spacecraft, and the Mariner II Venus fly-by. It was initially developed by General Dynamics, Convair for the U. S. Air Force. For use with the Centaur high energy upper stage, the tapered nose section of the Atlas vehicle is modified to a constant 10-foot diameter, and eight 500 pound-thrust retro-rockets have been added to the aft section to increase the rate of separation from Centaur. The modified vehicle is designated the SLV-3C. The Atlas vehicle has no internal bracing. It maintains its cylindrical shape by use of internal pressurization. The fully loaded Atlas stage weighs 266,000 pounds at lift-off. This lift-off weight is composed of a jettisonable booster section, sustainer and propellant tankage system, and the interstage adapter section. It is propelled by the Rocketdyne NA-5 propulsion system which includes two booster engines, a sustainer engine, and two small vernier engines. These five engines produce a lift-off thrust of 389,000 pounds. All the engines are gimbal-mounted for directional control.

The standard Centaur vehicle is the first successful space vehicle to use a combination of liquid hydrogen and liquid oxygen as propellants. It is manufactured by General Dynamics, Convair and has a diameter of 10 feet and length of 30 feet. It is powered by two Pratt and Whitney engines developing a total thrust of 30,000 pounds. These engines can be ignited, shut down, and re-ignited in a space environment as long as the period between the first shut down and second ignition is less than 25 minutes. The Centaur like the Atlas contains no internal bracing; i. e., any environmental structural loads are supported by use of the pressurized tanks. Prior to the first ignition, the Centaur vehicle weighs approximately 35,000 pounds. Of this weight 30,000 pounds constitutes propellant weight.

Figure 8-1 shows the Atlas-Centaur vehicle in the Surveyor configuration. For the A T S - 4 mission, the vehicle would be exactly the same except for a

cylindrical extension added to the current Surveyor nose fairing. The payload penalty resulting from this extension is 1 pound per 13 pounds of additional shroud weight.

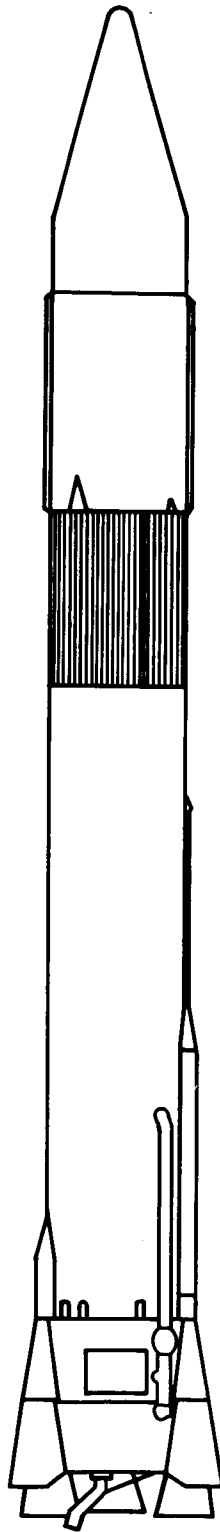


Figure 8-1. Atlas-Centaur Vehicle.

## SECTION 9

### LAUNCH AND ORBIT ANALYSIS

#### A. ATS-4 NOMINAL ASCENT AND INJECTION SEQUENCE

The ATS-4 nominal ascent and injection sequence has been established on the basis of using the SLV-3C Atlas-Centaur vehicle from ETR (Cape Kennedy) with launch conditions being 28.5 degrees latitude and 90 degrees due east launch azimuth. The trajectory profile, illustrated in Figure 9-1, consists of ascent to a low-altitude inclined parking orbit, followed by injection into a transfer orbit having its apogee at a near-synchronous, near-equatorial altitude. The kick stage (solid-propellant TE-364 motor) is employed to inject the spacecraft at second apogee into a near-synchronous equatorial orbit at approximately 53 degrees West longitude above the earth. A ground trace of sub-satellite, longitude and latitude during ascent and injection is shown in Figure 9-2. This trajectory sequence is the result of a large number of performance trade-off studies designed to maximize the payload deliverable into the final synchronous orbit within operational constraints imposed by the launch vehicle, kick stage, and spacecraft. Further consideration of optimization studies is included in the following individual sections.

Table 9-1 lists the time-altitude profile and major tracking events during various stages of the nominal ascent trajectory up to the firing of the solid kick stage rocket. Table 9-2 provides the chronological sequence of major operational events which occur from liftoff through spacecraft station-seeking to the point where a fully operational status is achieved.

Table 9-1

Time Altitude Profile and Major Tracking Events

	Time (seconds)	Altitude (n. m.)	Event
0		0	Lift-off
1	250	79	Atlas burnout, shroud separation Centaur first ignition

Table 9-1 (cont.)

	Time (seconds)	Altitude (n. m.)	Event
2	567	100	Termination of first Centaur burn injection into circular parking orbit initiation of coast phase
3	668	100	Coast phase continued
4	1477	100	Pick up local tracking station (station type & location not defined, possibly ship station) C/S stage attitude reorientation for plane change
5	1620	100	Initiate Centaur second burn (8.6° plane change)
6	1713	116	Centaur burnout transfer orbit established  $e = 0.7306$ $i = 19.9^\circ$ $h_p = 100 \text{ n. m.}$ $h_a = 19323 \text{ n. m.}$ $\lambda_p = 4.5^\circ \text{E}$
7	1891	245	Pick up Madagascar tracking station
8	2891	2150	
9	3491	3560	Pick up Carnarvon tracking station
10	8690	12,150	First subsatellite longitude reversal
11	20,530	19,323	First apogee
12	39,430	100	Second perigee
13	58,330	19,323	Second apogee (53° W) Fire kick motor

Table 9-2

## Ascent Sequence Into an Operational Orbit

Sequence no.	Time after launch (hr)	Remarks
0	0	Launch site-ETR; $28.5^{\circ}$ latitude, $90^{\circ}$ azimuth
1	0.070	Atlas burnout, shroud separation, first Centaur ignition
2	0.158	Termination of first Centaur burn
3	0.185	Parking orbit established; 100 n. miles circular
4	0.410	Execute C/S attitude maneuvers for plane change
5	0.450	Initiate second Centaur burn and $8.6^{\circ}$ plane change
6	0.476	Transfer orbit established; reorient Centaur/Spacecraft stage
7	0.526	Separation of spacecraft from Centaur and spinup
8	0.804	Active nutation damping through 1-1/2 orbits and initiation of spin axis measurement
9	0.970	Obtain updated orbit for transfer ellipse
10	2.410	Complete spin axis measurement
11	5.710	Execute spin axis precession (in vicinity of first apogee)
12	10.950	Obtain updated orbit and initiate repeated spin axis measurement
13	16.210	Execute vernier spin axis precession followed by firing of kick stage at second apogee
14	----	Active nutation damping of spacecraft attitude motions introduced by apogee kick
15	20.000	Spin axis measurement and ground tracking to establish injection orbit
16	32.21	Preliminary orbit obtained (16 hours following injection into synchronous altitude)
17	----	Spin axis precession for eccentricity and/or inclination removal resulting from injection errors based upon preliminary orbit information

Table 9-2 (cont.)

Sequence no.	Time after launch (hr)	
18	44.21	Final orbit obtained (28 hours following injection)
19	Note (a)	Execution of inclination and/or eccentricity removal in conjunction with vernier precession of spin axis. Precess spin axis normal to orbit plane
20	53.000	Jettison adaptor section
21	53.050	Yo-Yo despin
22	53.060	Damping of rotational rates to less than $1^{\circ}/\text{sec}$
23	53.200	Acquire roll axis to sun line
24		Deploy solar panels and antenna (controls off)
25		Reacquire roll axis to sun line
26		Acquire local vertical reference using horizon sensor
27		Transfer yaw control to digital sun sensor
28		Transfer yaw control to Polaris tracker
29		Fire east-west station keeping thrusters to remove mean drift and make vernier eccentricity adjustment
30	67.0	Spacecraft fully operational at $53^{\circ}$ West longitude (minimum time of 67 hours after launch)

Note (a): The time required for sequence 19 is based upon a low-altitude injection into near-synchronous orbit.

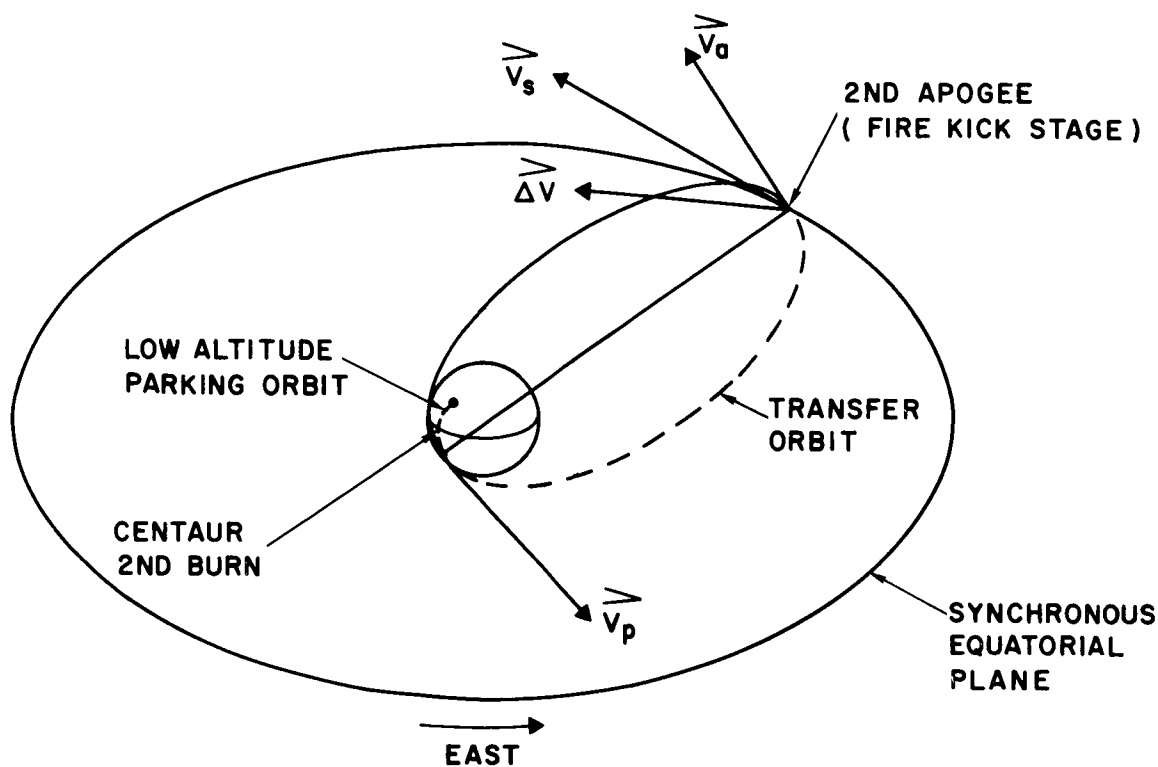


Figure 9-1. ATS-4 ascent and injection geometry.

Consider first the ascent and initial injection sequence into a near-synchronous orbit. The Atlas burn and first Centaur burn are employed to inject the Centaur/Spacecraft (C/S) stage into a nominal 100-nautical-mile parking orbit, inclined at an angle of 28.5 degrees with respect to the equator. After an approximately 20-minute coast period in this parking orbit, Centaur attitude control jets are utilized to execute attitude reorientation for a 8.6-degree plane change as shown in Figure 9-3. The plane change maneuver is established to maximize synchronous orbit payload injection capability in terms of Centaur performance and a fixed capability for the TE-364 kick stage. At approximately 27 minutes after liftoff, the C/S stage is at the point of first equator crossing (descending node). At this instant, the Centaur is reignited for a second burn which places the stage into the inclined transfer orbit shown in Figure 9-1. Orientation of the C/S stage during second Centaur burn is shown in Figure 9-4. Shortly following injection into the transfer orbit, the C/S stage is reoriented as shown in Figure 9-5. The maneuvers consist of a

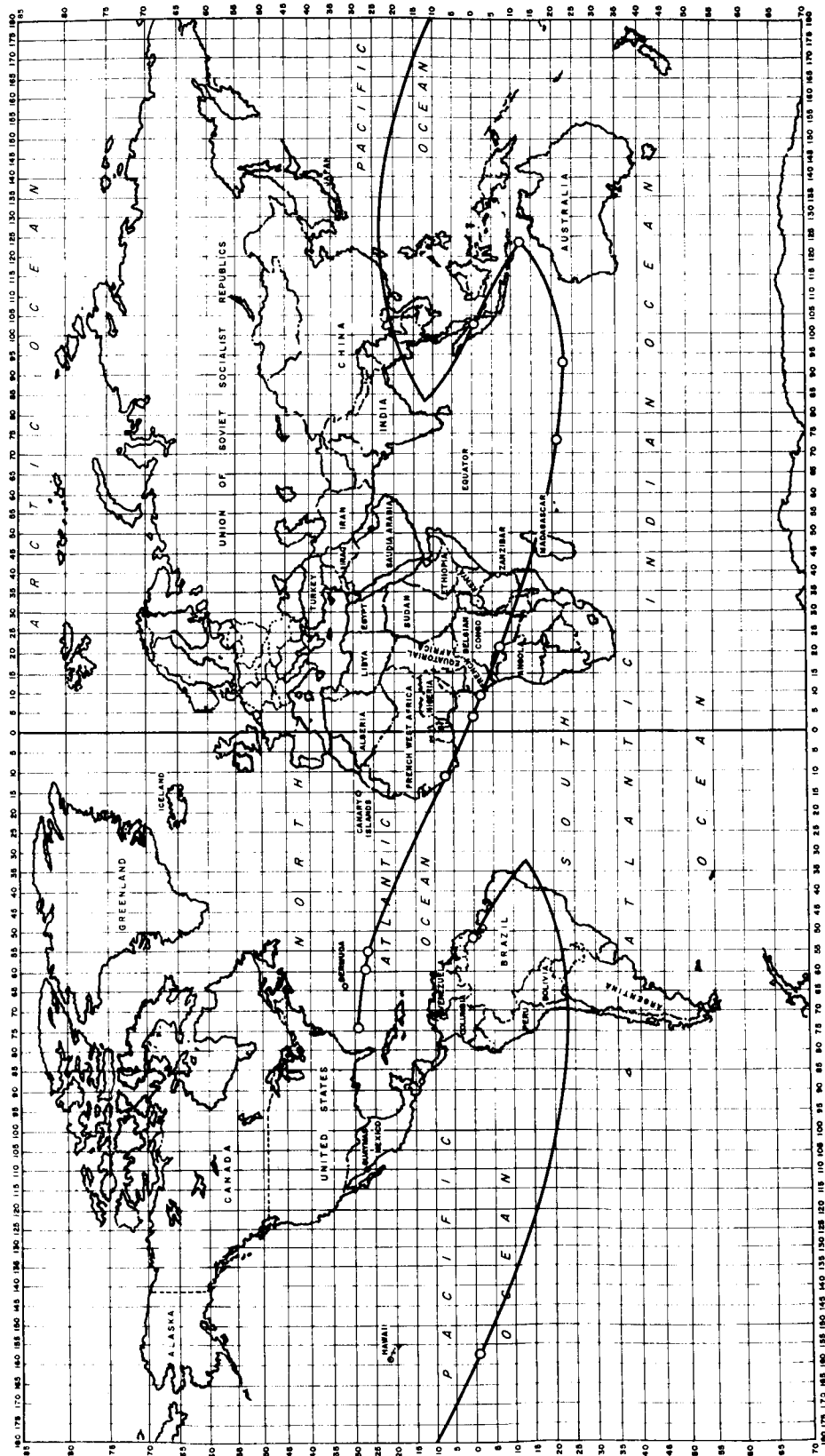
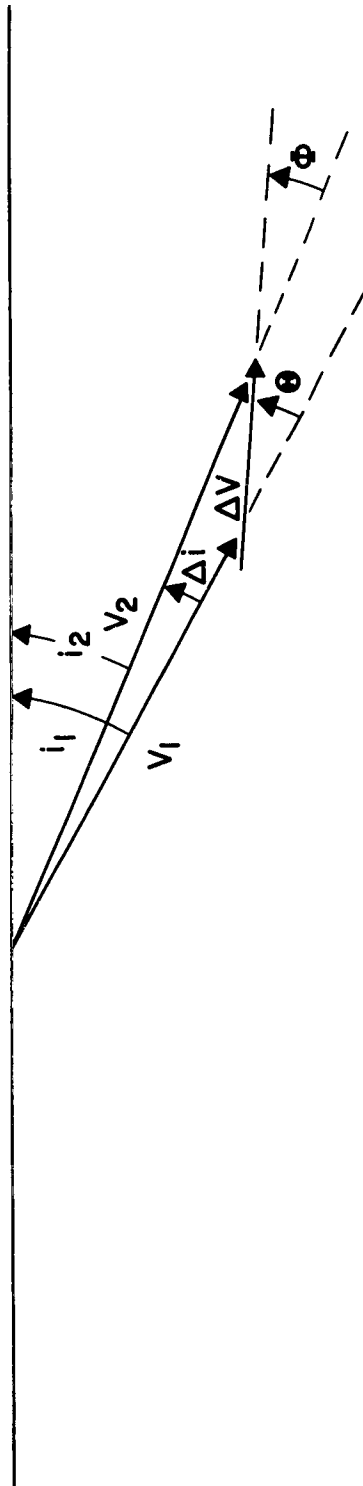


Figure 9-2. Proposed ATS-4 launch trajectory.

# EQUATORIAL PLANE



$$i_1 = 28.5^\circ$$

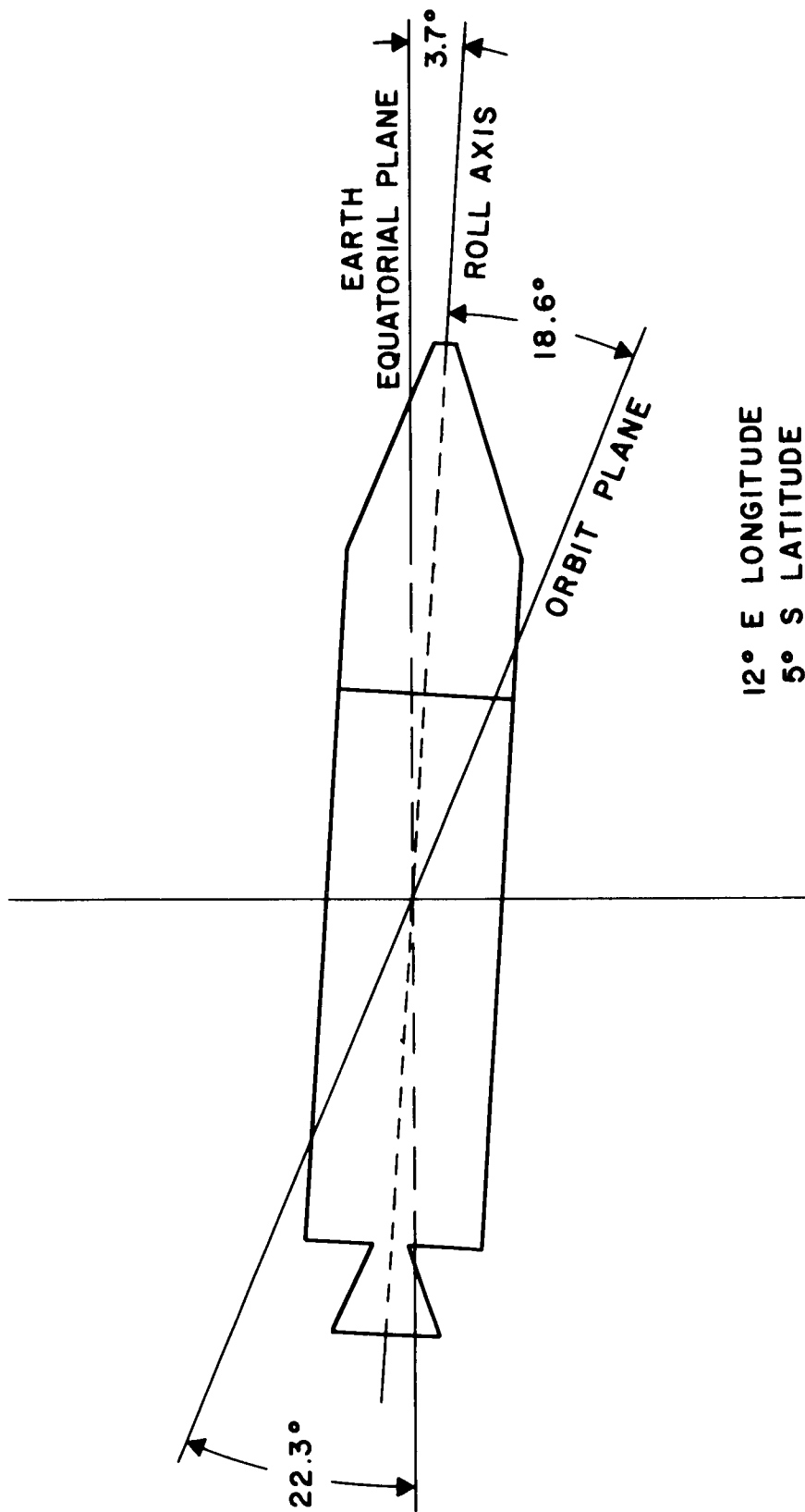
$$i_2 = 19.9^\circ$$

$$\Delta i = 8.6^\circ$$

$$\theta = 33.2^\circ$$

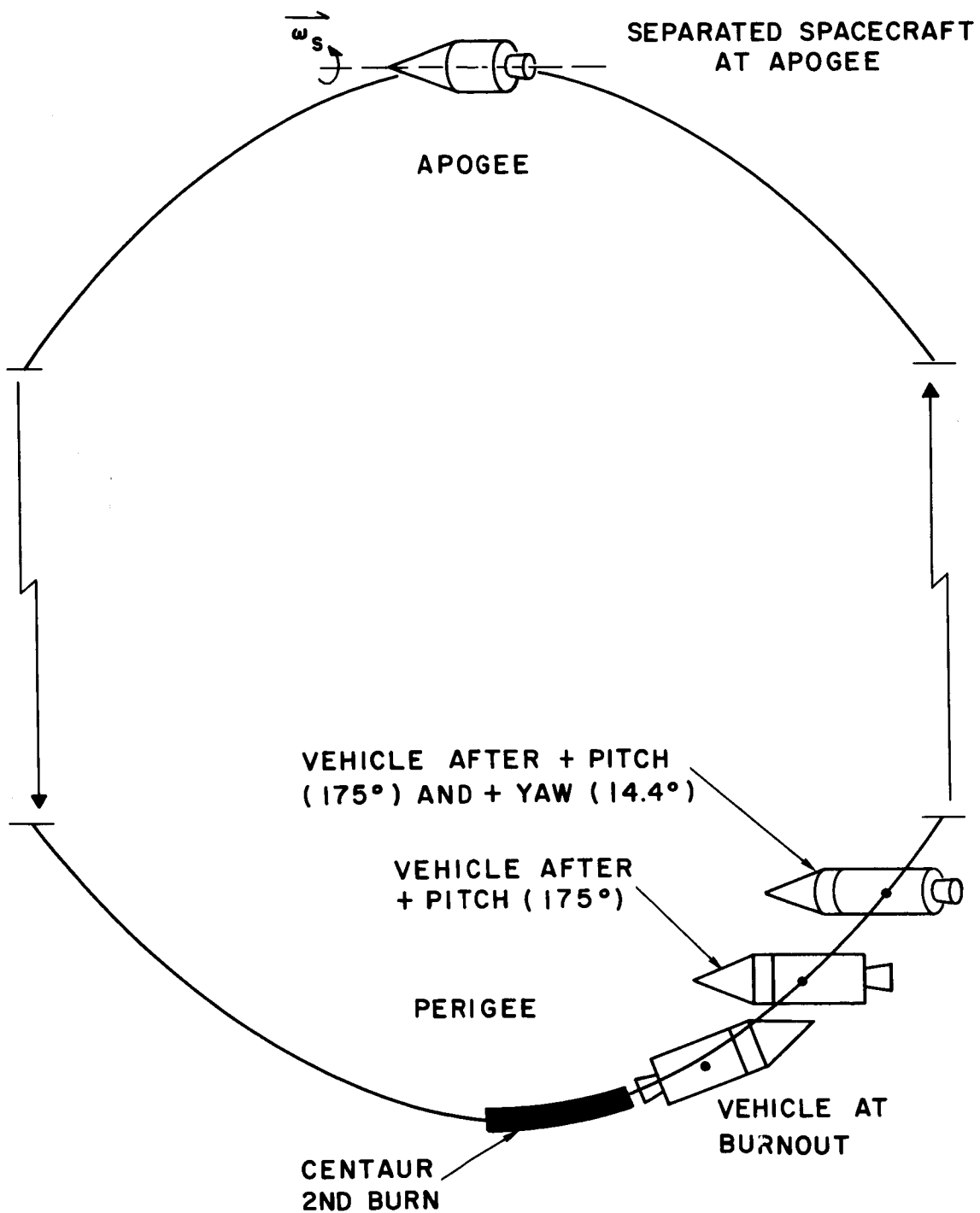
$$\Phi = 24.6^\circ$$

Figure 9-3. Centaur second burn (ATS-4 mission).



12° E LONGITUDE  
5° S LATITUDE

Figure 9-4. Centaur second burn termination.



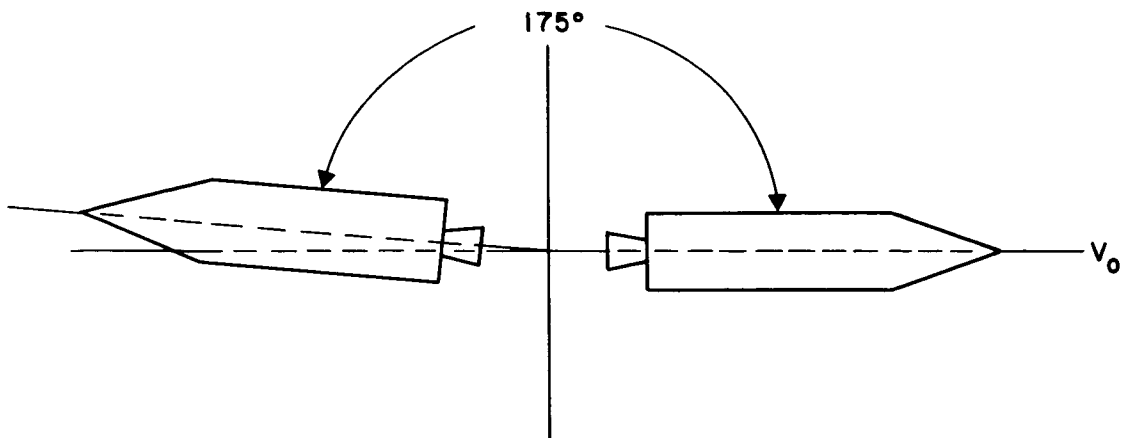
NOTE: PLANE OF PAPER DENOTES TRANSFER ORBIT PLANE

Figure 9-5. Centaur attitude maneuvers after second burn.

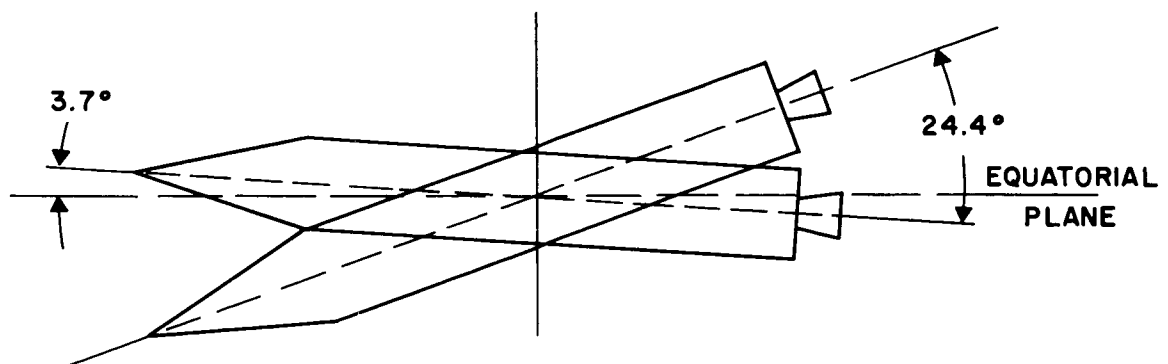
175-degree pitch-axis rotation in the orbit plane and a 14.4-degree yaw-axis rotation normal to the orbit plane as shown in Figure 9-6. This action places the spacecraft in the approximate attitude desired for firing the kick stage at second apogee. At the completion of the reorientation maneuver, the C/S stage separation sequence is initiated. This is followed by spacecraft spinup using solid rocket motors attached to the adapter section. Attitude errors introduced by tipoff and any thruster misalignment during spinup will cause the spacecraft stage to undergo nutation and to be misaligned with respect to the attitude reference. An onboard hydrazine rocket system will provide active nutation damping and any necessary precession-control torque. After the required period of nutation damping and a coast phase suitable for sensor acquisition, a measurement will be performed to ascertain precession requirements for the spin axis. At first apogee (5.71 hours after launch) a command will be given to precess the spin axis to the reference attitude. Spin-axis measurements will be repeated during the second transfer orbit with a vernier correction applied shortly before the second apogee. At the second apogee (16.21 hours after launch) the spacecraft stage will be oriented as shown in Figure 9-7. At this point, the kick stage motor will be fired to remove inclination and circularize the orbit at near-synchronous altitude.

The second phase of the injection sequence involves tracking of the near-synchronous orbit to determine injection errors, to execute removal of nutation from the spinning spacecraft introduced by firing of the kick stage, and to execute removal of injection errors using an onboard hydrazine propulsion system. There are three possible error-correction cases as described in later material, namely low injection orbit, high injection orbit with descending node, and high injection orbit with ascending node. The correction sequence is based upon availability of a preliminary orbit from ground tracking stations within 16 hours after injection, and a final orbit within 28 hours after injection. The minimum adjustment period for eccentricity and inclination is 52.21 hours following launch. The maximum period could be an additional 48 hours based upon possible additional corrections for inclination or eccentricity. Prior to removal of injection errors, the following operations are considered. For 16 hours, tracking information is obtained to establish the satellite orbit. During this period, the hydrazine rockets will be used for active nutation damping and vernier precession of the spin axis. Upon determination of the orbit, the spinning spacecraft will be sequentially precessed to adjust inclination, eccentricity, or both. At the termination of the orbit correction period, the spacecraft will be precessed in a manner that will orient its spin axis normal to the orbit plane.

The third phase of the injection sequence includes jettison of the adapter section, spacecraft despin, rate damping, sensor acquisition, deployment of solar panels and antenna, and a final reacquisition to obtain a fully operational status. The despin mode is performed by a yo-yo device. The residual rates



I. PITCH AXIS REORIENTATION ( IN ORBIT PLANE )



II. YAW AXIS REORIENTATION ( NORMAL TO ORBIT PLANE )

Figure 9-6. Centaur reorientation following second burn termination.

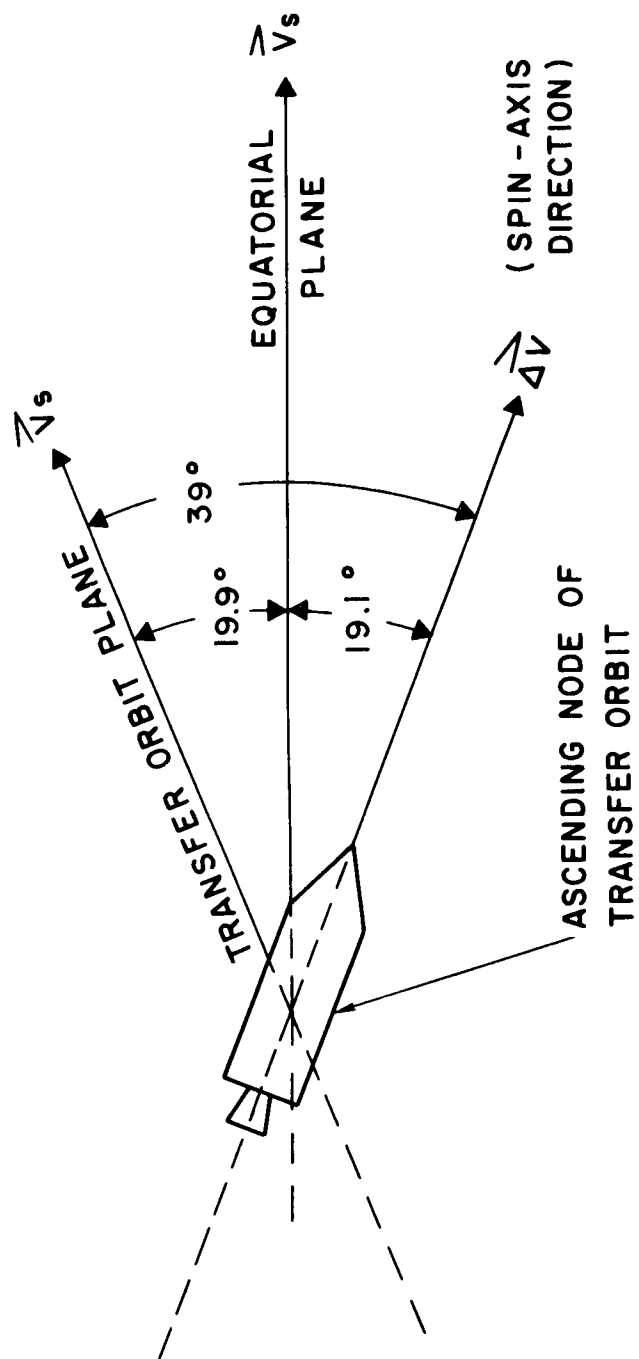


Figure 9-7. Orientation for apogee kick.

are reduced to within allowable limits using an ammonia thermal storage Resistojet system. The first acquisition mode consists of stabilizing the roll axis along the sun line. Once this is achieved, attitude control is temporarily turned off and the deployment is carried out for solar panels and the antenna. Upon completion of the deployment phase, controls are reactivated and the spacecraft is once again stabilized along the sun line. The next acquisition mode consists of earth-line (local vertical) capture using a horizon sensor. The final acquisition phase is to transfer yaw control to a digital sun sensor and ultimately to a star tracker. Up to 18 hours can be required for completing the despin and acquisition phase. The minimum mission time (from launch) required to obtain an operational status is 67 hours. The spacecraft is now positioned at 53 degrees West longitude in a very nearly synchronous equatorial orbit and is fully deployed and receiving power for experiments. Small eccentricity errors and possibly small altitude error, which will give rise to a mean daily drift motion, are expected at this time. The onboard ammonia Resistojet system will be employed to correct any such errors and to provide necessary east-west station keeping during the mission life. No further north-south adjustment during the operational life of the spacecraft is considered in this study.

#### **B. PAYLOAD TRADE-OFFS AND SPINNING BODY STUDIES**

##### **ATS-4 ATLAS-CENTAUR/TE-M-364 PAYLOAD CAPABILITIES**

The nominal ascent trajectory for synchronous missions using the Atlas Centaur vehicle is achieved by using the Atlas burn and a Centaur burn to place the Centaur/Spacecraft combination into a 100-nautical-mile, nominally circular, inclined parking orbit, by coasting to the first equator crossing (15 to 20 minutes) and reigniting the Centaur to place the spacecraft into a Hohmann transfer orbit having an apogee altitude equal to the synchronous altitude (19,323 nautical miles). The Centaur vehicle is limited to a 25-minute coast period between the first main engine cutoff (MECO) and the second ignition because of the boil-off of cryogenically stored propellant and oxidizer (liquid hydrogen and liquid oxygen). The Hohmann transfer orbit is inclined, and the spacecraft is injected into a final, near-synchronous orbit by an onboard or attached propulsion system. One of the constraints placed on this study is that some version of the Thiokol Chemical Corporation TE-M-364 motor is used as the propulsion system to inject the ATS - 4 spacecraft into the final, near-synchronous orbit. Using a 90-degree launch azimuth, the Atlas-Centaur vehicle is capable of placing a 4000-pound payload into the previously described transfer ellipse. A payload trade-off study has been made with the following cases examined.

1. A 90-degree launch azimuth, unmodified TE-M-364 motor,
2. A 90-degree launch azimuth, modified TE-M-364 motor,
3. Deviation of launch azimuth from 90 degrees,
4. Effect of an apogee bias (overshooting or undershooting the apogee),  
and
5. Effect of a nose shroud extension.

The parameters used in the trade-off studies are summarized as follows:

A. Centaur

Propellant weight (second burn): 6342.17 lb

Dry weight: 4310 lb

Specific impulse: 442 sec

Reference weight into transfer: 4000 lb

B. Spacecraft

Propellant weight: 1440 lb (unmodified motor)

Reference velocity increment: 6028 fps

Motor structure fixed weight: 140 lb

Specific impulse: classified

Figure 9-8 is a summary of the payload optimization for the 90-degree launch azimuth-unmodified TE-M-364 motor case. This Figure shows that the maximum payload placed into the final synchronous orbit using a 90-degree launch azimuth existing Centaur shroud and unmodified kick motor weighs 1678 pounds excluding motor and motor case.

Results of a 90-degree launch azimuth and a modified TE-M-364 motor are shown in Figure 9-9. The modified TE-M-364 motor consists of a small cylindrical section (10.3 inches) placed between the hemispheres of the unmodified motor. Since the throat and nozzle area are not changed in the modification, the only decrease in propellant specific impulse (1 to 2 percent) results from the modification of the combustion chamber. The increase in propellant weight ( $W_p = 660$  lb), however, gives a significant increase in total impulse capability. Figure 9-9 shows that the modified motor will inject a maximum payload (excluding motor and motor case) of 1946 pounds

into the final synchronous orbit. It was decided, however, not to use this motor version because of the extremely large development cost (\$1.5 to \$3 million).

The effect of changing the launch azimuth is shown in Figure 9-10. The payload is plotted against Centaur second-burn plane change for launch azimuths of 90, 95, 100, 105, and 110 degrees. Changing the launch azimuth moves the apogee of the transfer orbit in a westward direction. This movement increases the elevation angle with respect to the Mojave-Rosman ground stations (Figure 9-11). The longitude of the second apogee is shown with respect to launch azimuth as follows:

Launch azimuth	2nd apogee longitude
90	53°W
95	52.5°W
100	72.0°W
105	80.5°W
110	88.0°W

Figure 9-10 indicates that there is a significant decrease in useful payload weight as the launch azimuth deviates from 90 degrees. The reasons for this payload decrease are that there is approximately a 2-pound-per-degree transfer orbit payload penalty resulting from the change in azimuth and that the orbit inclination with respect to the equator increases as the azimuth deviates from 90 degrees. This increase in inclination creates a  $\Delta V$  penalty for the apogee motor burn, and if the  $\Delta V$  penalty were plotted against the deviation of azimuth from 90 degrees. One would observe that the graph of the  $\Delta V$  penalty is approximately a parabola. This accounts for the nonlinear payload penalty as the azimuth deviates from 90 degrees.

The effect of a  $\pm 800$ -nautical-mile bias (undershooting and overshooting the apogee of the transfer orbit) was studied to determine whether it was applicable to the ATS - 4 mission. The apogee bias allows the spacecraft to be purposely injected with either an eastward or a westward drift in order to position the spacecraft at some longitude other than the normal apogee longitude. The following constraint was later placed on the study: that the spacecraft be launched without a bias and be injected into a synchronous orbit rather than in an orbit with slightly more or less energy. This analysis showed results similar to those in Figures 9-8 and 9-9 since the  $\pm 800$ -nautical-mile bias is not a very large amount compared with the synchronous altitude. There would be an additional payload penalty resulting from the vernier propulsion requirements to add or subtract the necessary energy to make a synchronous orbit when the proper longitude is reached after drifting.

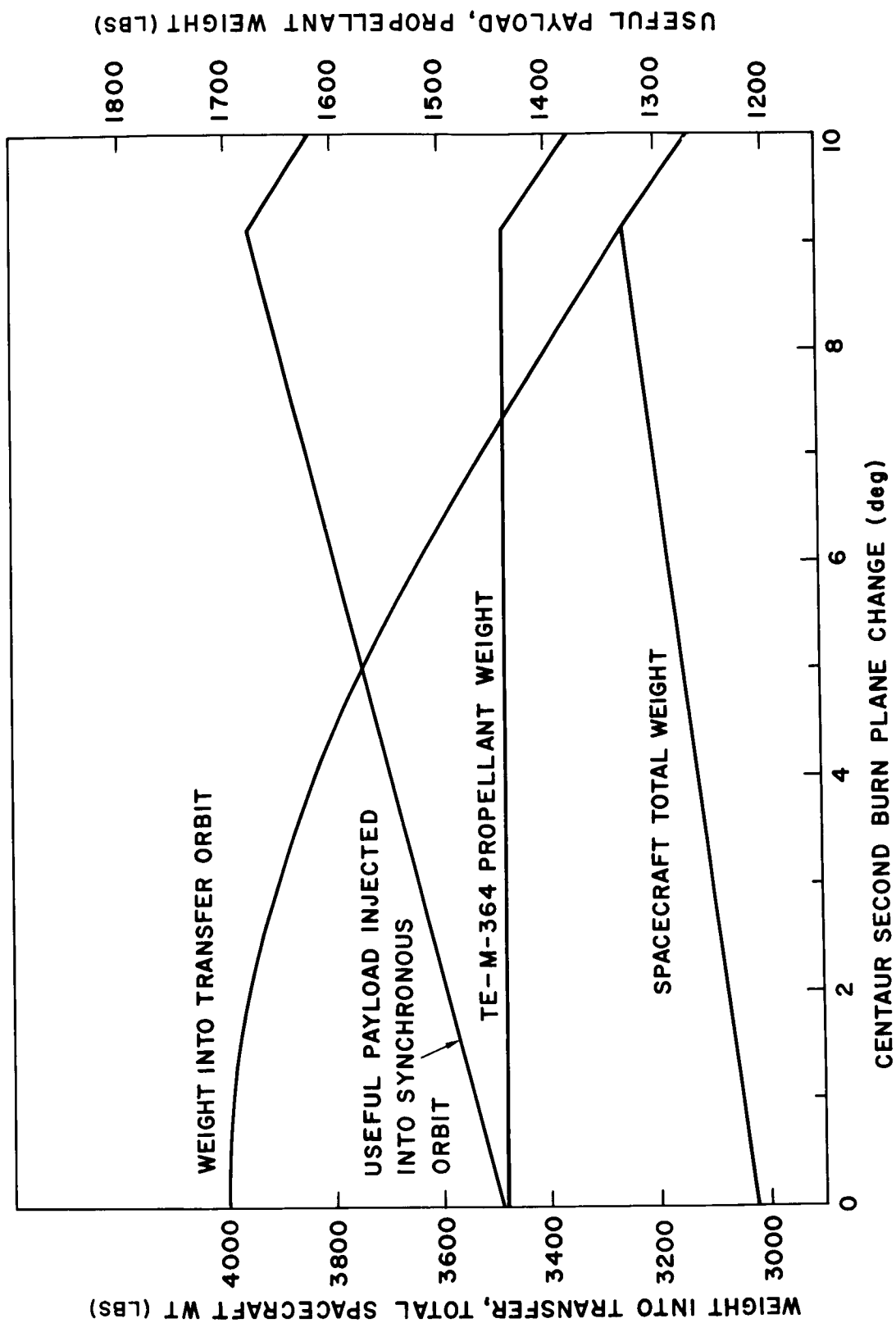


Figure 9-8. Atlas/Centaur/TE-M-364 payload optimization study.

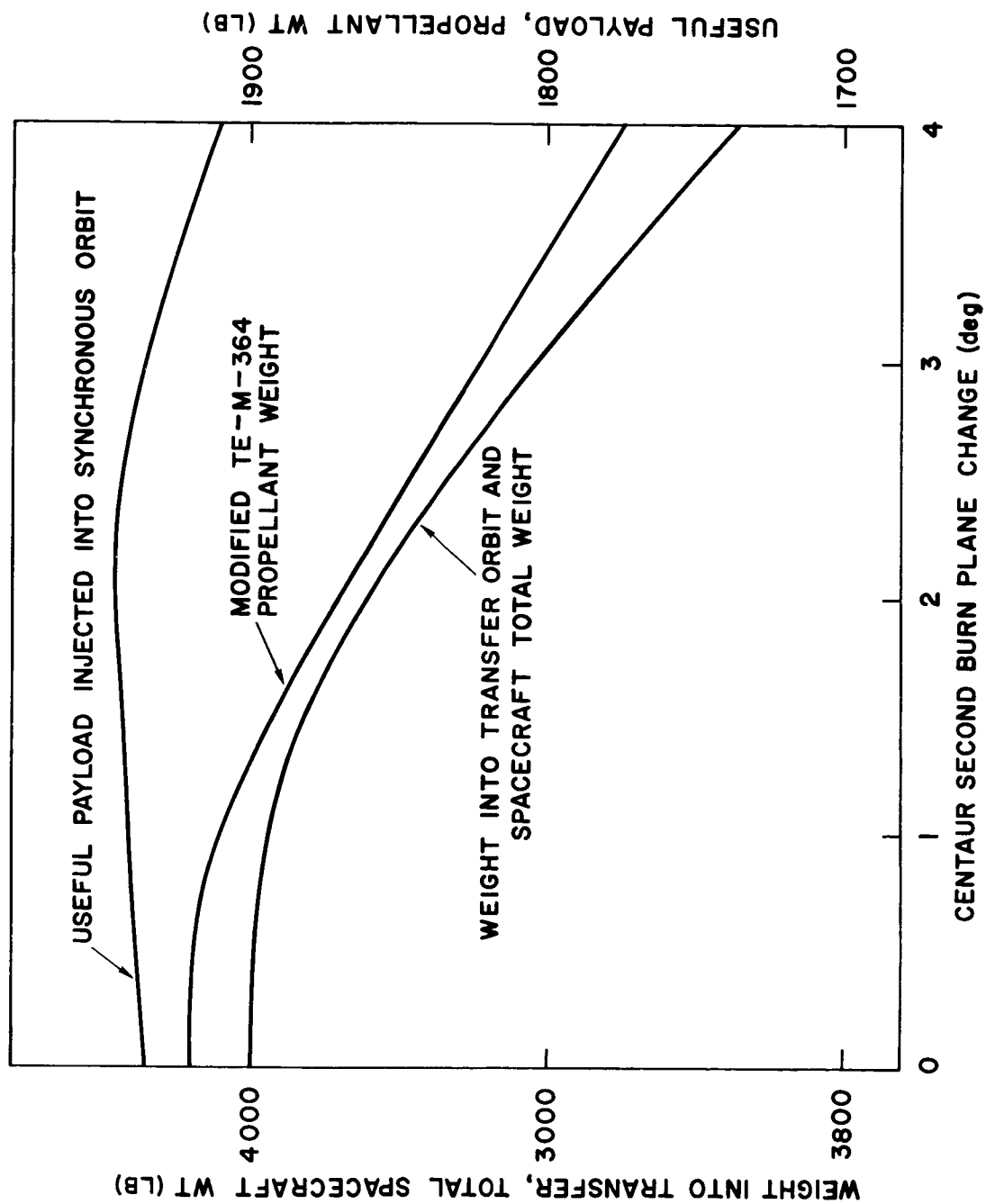


Figure 9-9. Atlas/Centaur/modified TE-M-364 payload optimization study.

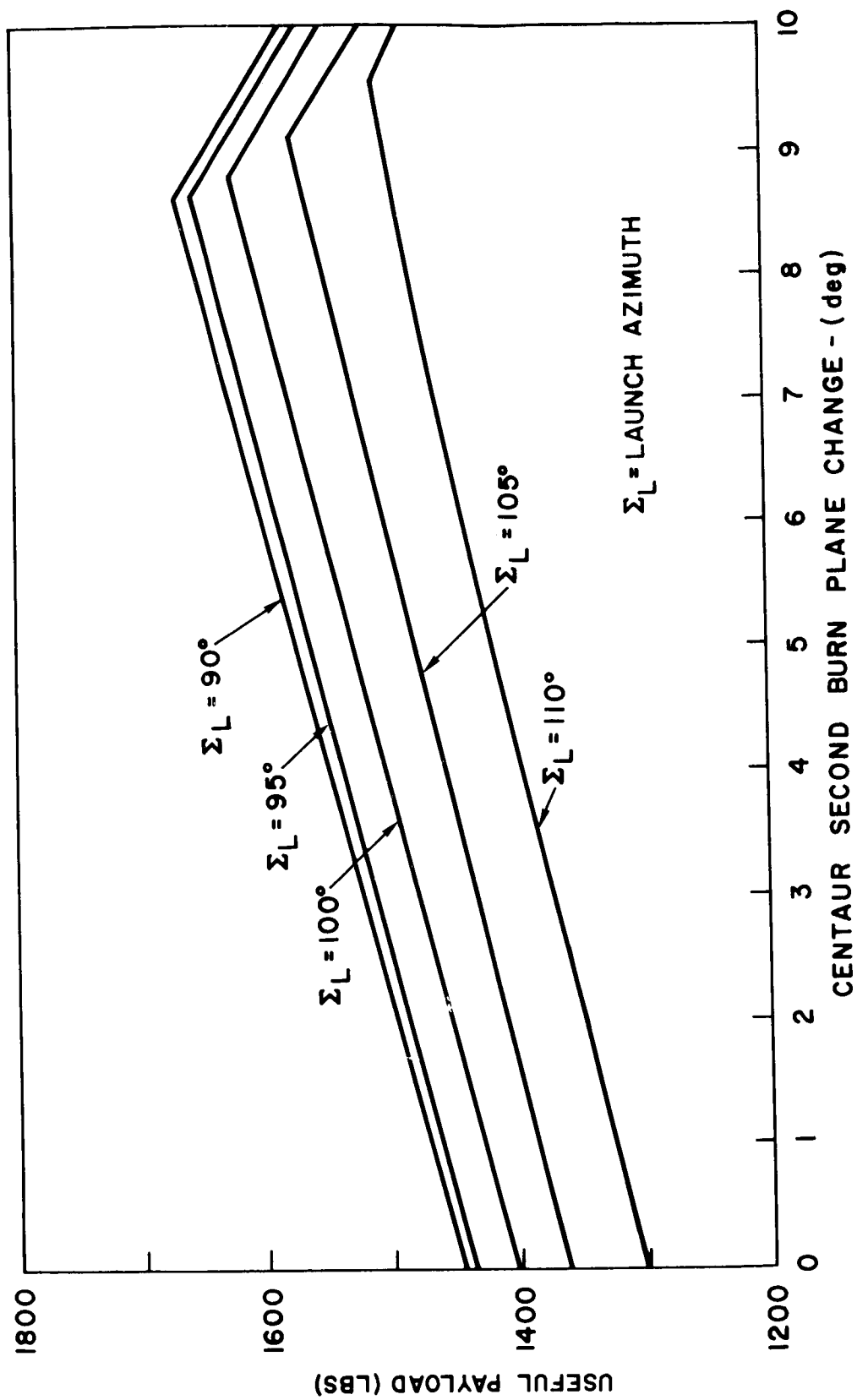


Figure 9-10. Useful payload injected into synchronous orbit using the Atlas/Centaur/TE-M-364.

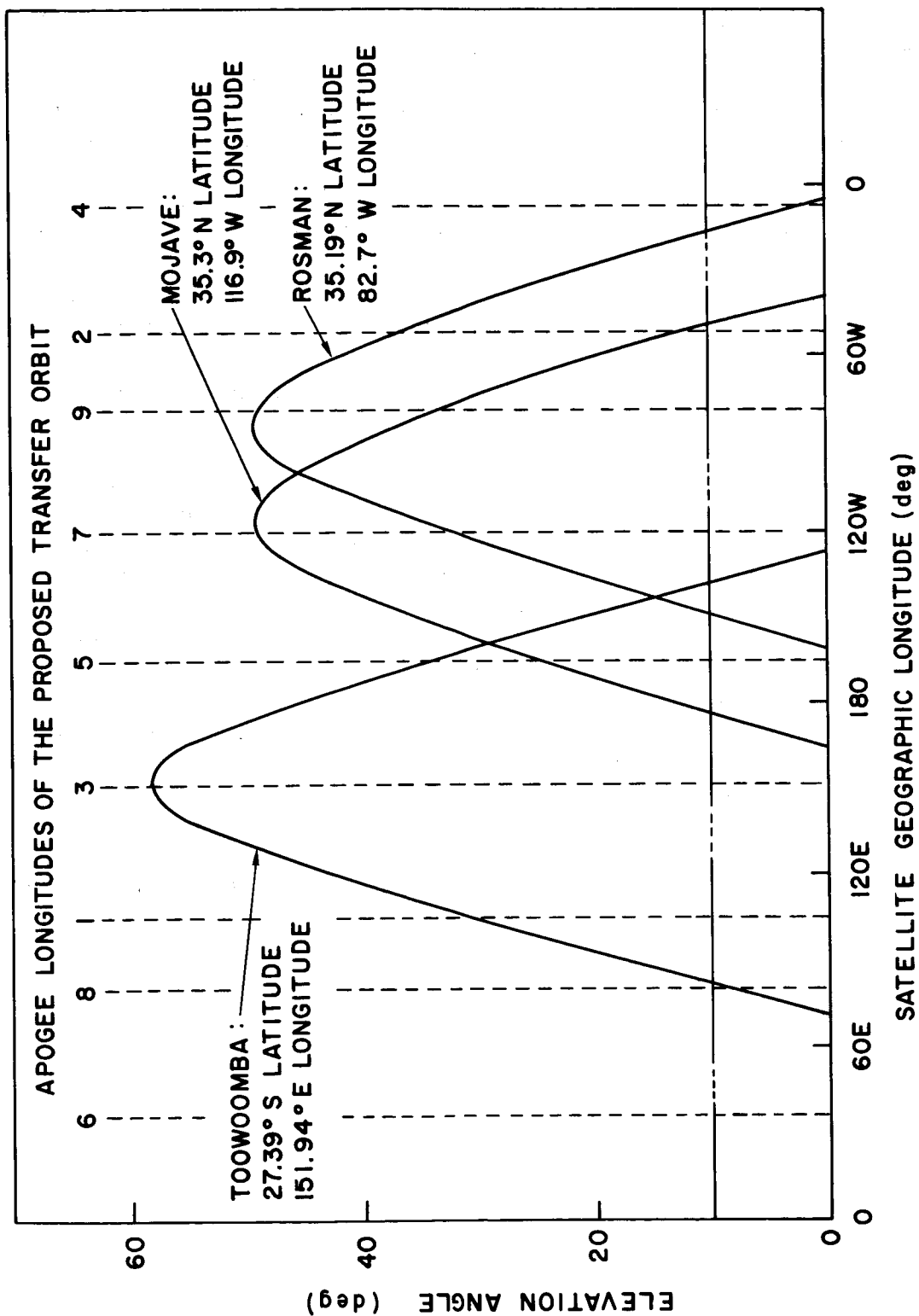


Figure 9-11. ATS-4 elevation angle with respect to three ATS ground stations

It is apparent from the results of the in-house A T S - 4 structure study that the current Atlas-Centaur shroud is inadequate for the A T S - 4 mission. The current Atlas-Centaur shroud is a 5-foot cylinder topped by a 15-foot, 30-degree cone. It has been deemed feasible to add up to a 15-foot cylindrical extension to the existing 5-foot cylindrical section. This extension weighs 5.4 pounds per inch and, there exists a 13-to-1 payload trade-off in conjunction with the shroud extension; i.e., for every 13-pound increase in shroud weight there is a 1-pound transfer orbit payload penalty. Figures 9-12 and 9-13 are similar to Figures 9-8 and 9-9 in illustrating the payload trade-off except that Figures 9-12 and 9-13 reflect an 8-foot shroud extension. These figures indicate that a 1657 pound useful payload (excluding motor and motor case) can be injected with an unmodified motor, while an 1916-pound useful payload (excluding motor and motor case) can be injected using the modified motor.

Based on these studies, it is recommended that the A T S - 4 mission be achieved by launching at a 90-degree launch azimuth with the Atlas-Centaur vehicle, and executing a 8.6-degree plane change with the Centaur second burn to optimize the payload injected into the final synchronous orbit, using the unmodified Thiokol Chemical Corporation TE-M-364 solid-propellant motor. As previously mentioned, the modified motor has been eliminated because of high development and testing costs. Of all the launch schemes studied, the recommended launch scheme allows the maximum useful spacecraft payload to be injected. A detailed weight breakdown is shown in Table 9-3. It is further recommended that the Delta version of the TE-M-364 be used, since it is being manufactured for a GSFC project; also because this version has extra insulation mounted inside the motor casing to hold the external-case temperature to a minimum both during and after firing. Actual motor-firing data show that the maximum case temperature for the Delta version of the motor is less than 500<sup>0</sup> F compared with 700<sup>0</sup> F for the Surveyor and Burner II versions of the motor. The Delta motor is designated as the TE-M-364-3 motor.

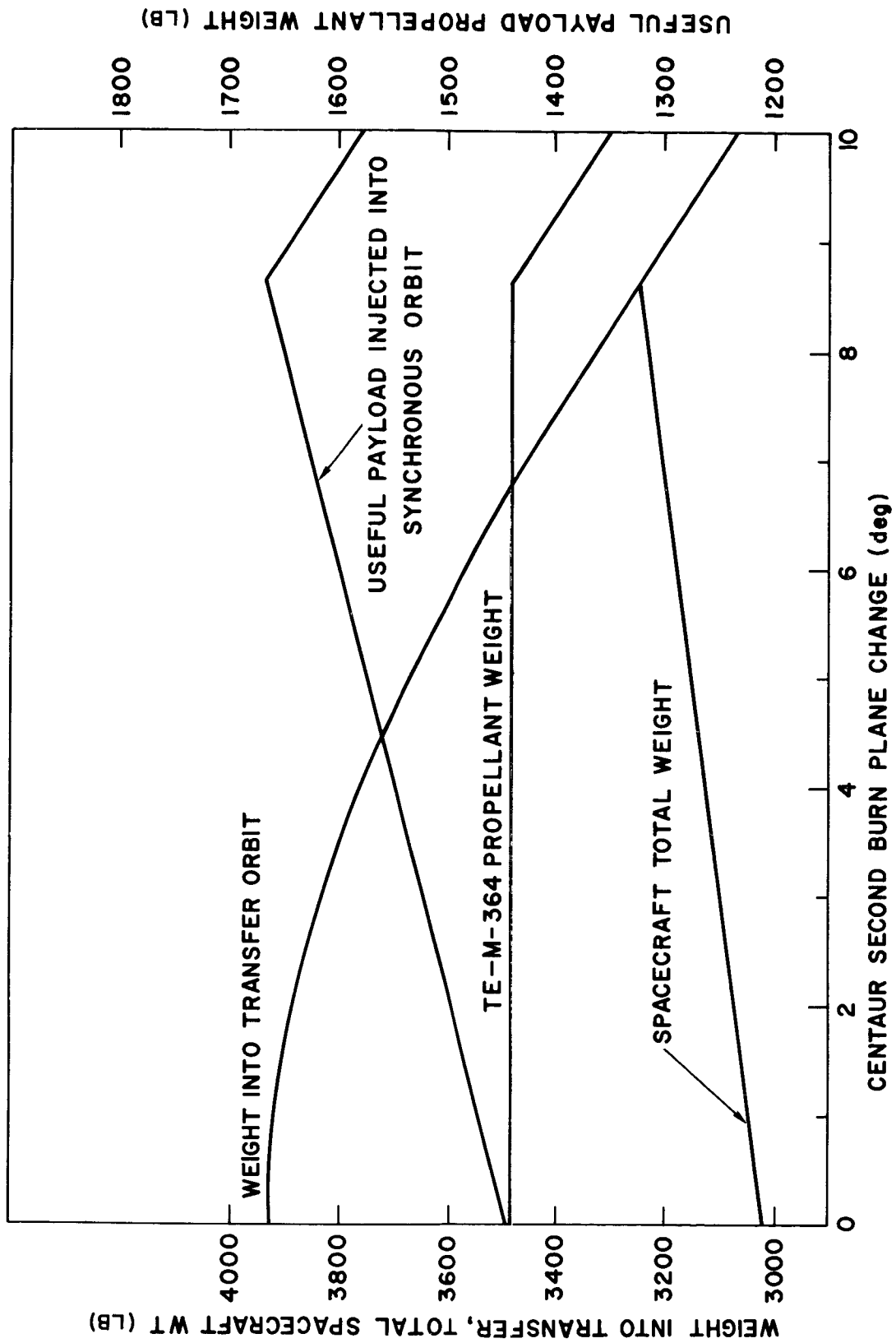


Figure 9-12. Atlas/Centaur/TE-M-364 payload optimization study including an 8-foot shroud extension.

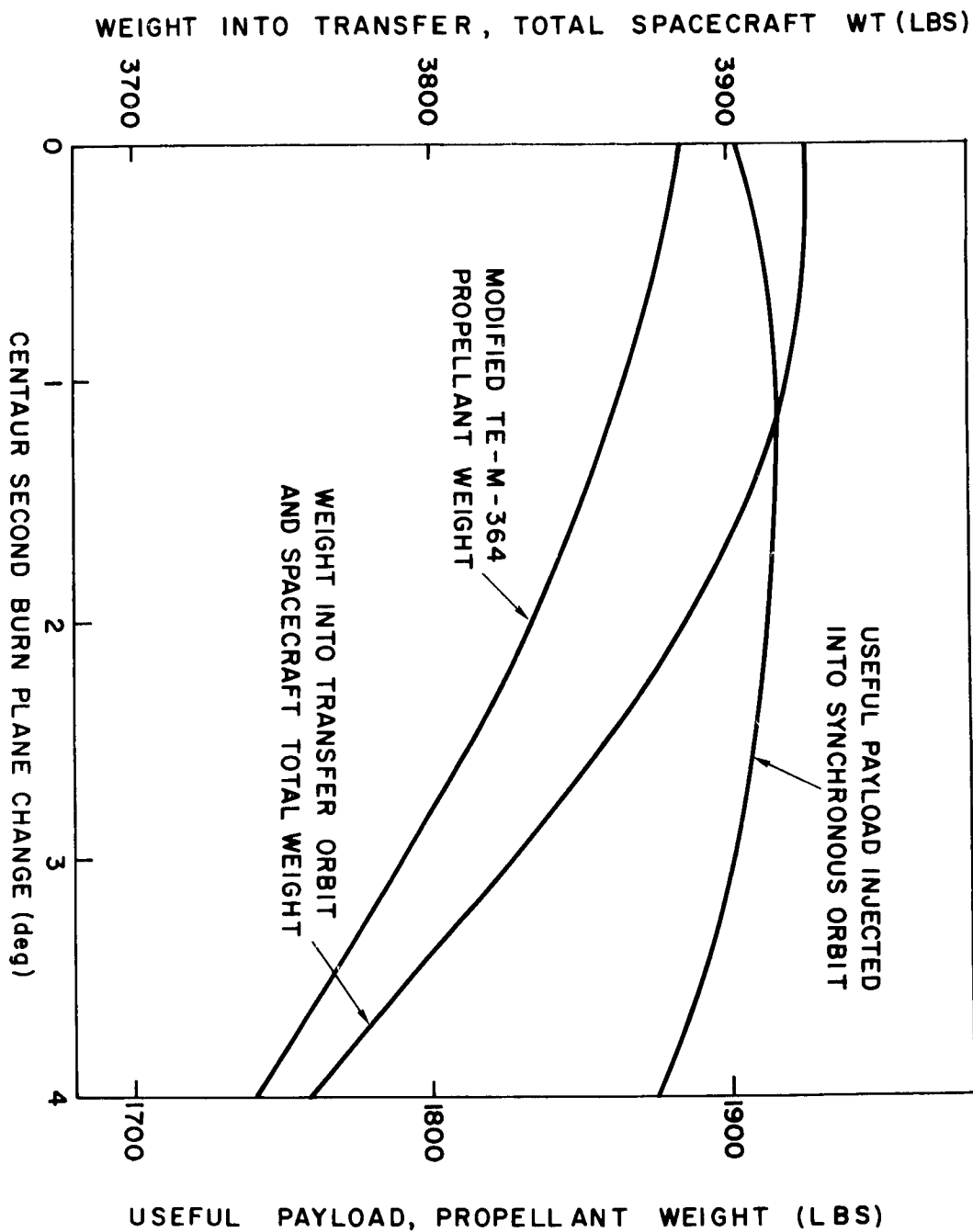


Figure 9-13. Atlas/Centaur/modified TE-M-364 payload optimization including an 8-foot shroud extension.

Table 9-3

## Weight Breakdown Based on Payload Optimization

Atlas-Centaur baseline capability	+4000 lb
15-foot shroud extension penalty	-75 lb
8.6-degree perigee plane change penalty	<u>-675 lb</u>
Launch weight	3250 lb
Mass expulsion for spinup and coning control	<u>-13 lb</u>
Weight delivered to 2nd apogee	3237 lb
Apogee motor fuel weight	<u>-1440 lb</u>
Weight into synchronous orbit	1797 lb

## INJECTION ERROR ASSESSMENT

Because there is no such thing as a perfect launch, a set of injection errors is associated with any spacecraft mission. Normally a statistical analysis is performed using the error tolerances of every component in the system to determine a distribution for the entire set of injection conditions. This process is long and involved and requires that every phase of the mission be defined; i. e., the entire mission profile must be completely stipulated. It usually requires approximately six months and a great deal of computer time to determine such a statistical distribution. Also, each analysis is mission-peculiar. For a study such as the current one, where all the mission parameters are not defined, the analysis is based on estimated  $3\sigma$  dispersions for launch vehicle and spacecraft-induced errors. For the launch vehicle-induced errors, the  $3\sigma$  estimates are based on previous missions and mission studies similar to the one at hand. For the spacecraft-induced errors, an estimate of system accuracy is obtained from individuals responsible for their respective systems (e. g., attitude pointing accuracy, any spacecraft propulsion system total impulse tolerances, total impulse reduction resulting from vehicle coning if a spin-stabilized mode is employed, and any timing errors in firing a propulsive device). The injection error assessment for the GSFC in-house ATS - 4 study is based on the following items: (1) General Dynamics Corporation estimate for Atlas-Centaur vehicle induced  $3\sigma$  errors for transfer to the synchronous

altitude, (2)  $\pm 0.6$  percent TE-M-364 motor total impulse dispersion (based on actual motor firing test data), (3)  $\pm 0.5$ -degree,  $\pm 1.5$ -degree respective pitch and yaw tolerances for attitude pointing (based on estimates of A T S - 4 attitude accuracy by the GSFC Stabilization and Control Branch), (4) net thrust reduction resulting from vehicle coning during the firing of the apogee motor (4 degrees), and (5) a  $\pm 2$ -minute timing error in igniting the apogee motor. The values given were obtained by taking the individual total derivatives for each of the error sources previously described and then obtaining their root-sum-square to provide a basis for sizing vernier propulsion requirements for removing the injection errors to obtain the final orbit. In addition to the error sources just described, the injection errors resulting from use of the GSFC-developed star-field-mapper system (SCADS) of an attitude-sensing system are computed and compared with the nominal sensing system (the one described above with the  $\pm 0.5$ -degree,  $\pm 1.5$ -degree pitch and yaw tolerances) and a perfect sensing system, i. e., one with no pointing errors. It is believed by the system developer, however, that much smaller tolerances can be achieved. At present, the Stabilization and Control Branch proposes that the star-field mapper system be flown on the first A T S - 4 as an experiment rather than as the primary attitude-sensing system, since the SCADS system has not as yet been flown as a flight system. Preliminary ground tests have been performed on the system, and the results have been excellent. Based on the error sources previously described, the injection dispersions have been calculated and are tabulated in Table 9-4.

Table 9-4

ATS-4 Injection Errors (Nominal)

Source	$\Delta h$ (n. m.)	$\Delta V_s$ (fps)	i (degrees)	e
Launch vehicle	$\pm 101$	$\pm 56.4$	$\pm 0.1313$	0.01620
Apogee motor total impulse	0	$\pm 31.4$	$\pm 0.0676$	0.00623
Coning ( $4^\circ$ )	0	$\pm 15.9$	$\pm 0.0342$	0.00315
Attitude pointing ( $\pm 0.5^\circ$ , $1.5^\circ$ )	0	$\pm 52$	$\pm 0.471$	0.0110
$\pm 2$ min. timer error	0	$\pm 22.5$	$\pm 0.1286$	0.00446
RSS Total	101	87.3	0.497	0.02126

Table 9-5

## ATS-4 Injection Errors (SCADS)

Source	$\Delta h$ (n. m.)	$\Delta V_s$ (fps)	i (degrees)	e
Launch vehicle	$\pm 101$	$\pm 56.4$	$\pm 0.1313$	0.0162
Apogee motor total impulse	0	$\pm 31.4$	$\pm 0.0676$	0.00623
Coning	0	$\pm 15.9$	$\pm 0.0342$	0.00315
Attitude pointing ( $\pm 0.2^\circ$ )	0	$\pm 6.9$	$\pm 0.0616$	0.00205
$\pm 2$ min timer error	0	$\pm 22.5$	$\pm 0.1286$	0.00446
RSS Total	101	70.5	0.209	0.0183

Table 9-6

## ATS-4 Injection Errors (Perfect Sensors)

Source	$\Delta h$ (n. m.)	$\Delta V_s$ (fps)	i (degrees)	e
Launch vehicle	$\pm 101$	$\pm 56.4$	$\pm 0.1313$	0.0162
Apogee motor total impulse	0	$\pm 31.4$	$\pm 0.0676$	0.00623
Coning	0	$\pm 15.9$	$\pm 0.0342$	0.00315
Attitude pointing (0)	0	0	0	0
$\pm 2$ -minute timer error	0	$\pm 22.5$	$\pm 0.1286$	0.00446
RSS Total	101	70.1	0.175	0.00182

Tables 9-4, 9-5, and 9-6 indicate that the injection errors obtained in using the SCADS system are significantly less than those obtained when using the proposed ATS - 4 primary sensor system, which uses an earth sensor, sun sensor, and Polaris sensor. There is no significant difference between the errors obtained in using the SCADS sensing system and the system with perfect sensors. These facts will be borne out when the in-plane and out-of-plane vernier velocity increment requirements are compared.

To correct the final spacecraft orbit, the injection errors previously discussed must be removed. There are basically two types of errors: in-plane or eccentricity errors and out-of-plane or orbit inclination errors. The eccentricity or in-plane errors are removed by thrusting which occurs in the orbit plane at some point and changes the position and in-plane velocity component to proper values for the desired orbit. The most efficient method to adjust the orbit inclination is to thrust normal to the current orbit at some node of the current orbit with respect to the desired orbit. Both of these maneuvers will be described in much greater detail in a subsequent section.

From the "Orbital Flight Handbook" (NASA Publication SP 33) it can be shown that

$$\Delta V_{in} \approx (V_s/2) (e - \Delta r/r) \quad (1)$$

and

$$\Delta V_{out} = V_s \sin \Delta i, \quad (2)$$

where:  $V_{in}$  - velocity-in-orbit plane  
 $V_{out}$  - velocity-out-orbit plane  
 $V_s$  - velocity-synchronous orbit  
 $e$  - eccentricity  
 $r$  - radius of orbit  
 $i$  - inclination

Based on Equations 1 and 2, the vernier propulsion system velocity increments were calculated for the various conditions described above and are outlined in Table 9-7.

Table 9-7

ATS-4 Vernier  $\Delta V$  Requirements

Sensor system	$\nabla V_{in}$ (fps)	$\nabla V_{out}$ (fps)	$\nabla V_{out} + \nabla V_{in}$ (fps)
ATS-4 Primary system	85.0	87.5	172.5
SCADS system	70.3	36.8	107.1
Perfect system	69.7	30.8	100.5

Table 9-7 shows that there is a 38-percent saving in vernier propulsion system  $\Delta V$  requirements if the SCADS system is used instead of the proposed system. If a perfect sensing system existed, the  $\Delta V$  requirement would be reduced by 42 percent, as compared with the 38-percent reduction resulting from use of the SCADS system. If the SCADS system were to work out for the ATS - 4 launch, extra mission flexibility would result from the savings in propulsion-system  $\Delta V$  requirements. It is on this basis that the vernier propulsion system is being sized on the earth, sun, and Polaris sensors because they are flight-proven components. The vernier propulsion system will be elaborated upon in the hardware section.

#### SPIN STABILIZATION VERSUS THREE-AXIS STABILIZATION FOR ATS-4 DURING THE TRANSFER-ORBIT PHASE

The purpose of the comparison below is to justify the choice of spin stabilization for the ATS - 4 spacecraft during the transfer-orbit phase. The comparisons given below are based on 1-1/2 revolutions in the transfer orbit (proposed ATS-4 trajectory) before firing the apogee kick motor to inject the spacecraft into an equatorial synchronous circular orbit. All data relating to the three-axis stabilized system is based on the Boeing Burner II stage. It is believed that the Burner II control system is a representative system for three-axis stabilization of the ATS-4 spacecraft during the transfer-orbit phase.

A spin-stabilized-vehicle attitude-control system requires spinup motors, despin devices (motors or yo-yo's) and spin-axis precession-control devices in order to exercise control over the spacecraft attitude. In addition, for ATS-4 nutation control is required because of the nature of the spacecraft body configuration in the undeployed condition; i.e., unstable moment of inertia ratio and semi-flexible structure. It has been determined in the in-house study that both precession and nutation control can be achieved using the same propulsion system.

A three-axis attitude-stabilized vehicle of the ATS-4 type requires two sets of thrusters in the transfer-orbit phase; i. e., a set of low-impulse control jets to be used during the coast phase for pitch and yaw control and a set of high-impulse devices to be used during the burn of the apogee kick motor to offset any attitude disturbance resulting from thrust-vector misalignment, jet damping, etc.

The relative advantages and disadvantages of both spin-stabilized and three-axis stabilized control systems for the ATS-4 mission transfer-orbit phase are outlined in Tables 9-8 and 9-9, respectively. Based on a comparison of these tables, it is recommended that spin stabilization be used during the transfer-orbit phase of the ATS-4 mission.

Table 9-8

#### Spin Stabilization

A. Advantages

1. Simple on-board system
2. Low cost
3. Flight proven
4. Larger useful payload injected into final orbit (~200 pounds)
5. High chance of mission success if a thruster hardware component failure occurs

B. Disadvantages

1. 100 percent larger injection errors
2. Required spinup and despin devices for final spacecraft configuration

Table 9-9

Three-Axis Stabilization

A. Advantages

1. Flight proven (Surveyor 1, Burner II)
2. Small injection errors (50 percent less than for spin stabilization)
3. Does not require spinup and despin devices

B. Disadvantages

1. Complex on-board system
2. High cost
3. Smaller payload injected into final orbit due to increased expendables and batteries for the long coast phase
4. Smaller chance of mission success if pitch or yaw thruster failure occurs, unless a redundant system is carried; this further decreases the useful payload ratio.

4. DETERMINATION OF SPIN-RATE REQUIREMENTS FOR ATTITUDE STABILIZATION OF THE ATS-4 SPACECRAFT DURING TRANSFER-ORBIT PHASE

The purpose of this analysis is to determine the minimum angular velocity at which the ATS-4 spacecraft must be kept in order to be attitude-stabilized during the transfer-orbit phase of the mission. In this phase, the ATS-4 spacecraft is in its undeployed configuration; i. e., the parabolic antenna and solar arrays are folded about the vehicle axis of symmetry. In the undeployed configuration, the ATS-4 spacecraft is a symmetric body (two equal moments of inertia) having an unfavorable inertia ratio (i. e.,  $I_{\text{roll}} < I_{\text{pitch}} = I_{\text{yaw}}$ ). Some disturbances that can act on a spinning spacecraft are (1) thrust misalignment of one or all spinup motors, (2) failure of a spinup motor, (3) structural energy dissipation, (4) thrust-level variation of spin rockets, (5) misalignment

between spin axis and principal axis, and (6) orbit-change propulsion system net thrust misalignment. According to Reference 1, these disturbances are subordinate in comparison to the primary propulsion system net thrust misalignment. Based on this fact, a computation of the spin rate was made by studying the effect of the thrust misalignment on the spacecraft during the burn of the TE-M-364 solid-propellant motor.

The motion of the ATS-4 spacecraft was simulated on a digital computer by numerically integrating the Eulerian rigid-body equations of motion using the fourth-order Runge-Kutta method. The equations programmed included the effects of mass expulsion, changing moments of inertia resulting from mass expulsion, changing c.m. location due to mass expulsion, jet damping, initial transverse rates (coning) and primary-propulsion-system thrust misalignment. The moments of inertia and c.m. changes were assumed to move along the spacecraft axis of symmetry. According to Reference 2 these are valid assumptions. The equations programmed for the simulation are

$$\dot{\omega}_x = \frac{\dot{I}_x}{I_x} \omega_x + \omega_y \omega_z \frac{(I_y - I_z)}{I_x} \quad (\text{spin-axis motion})$$

$$\dot{\omega}_y = \frac{\dot{I}_y}{I_y} \omega_y + \omega_x \omega_z \frac{(I_z - I_x)}{I_y} + \frac{M_y}{I_y} + \frac{\dot{m} r^2 \omega_y}{I_y}$$

$$\dot{\omega}_z = \frac{\dot{I}_z}{I_z} \omega_z + \omega_y \omega_x \frac{(I_x - I_y)}{I_z} + \frac{M_z}{I_z} + \frac{\dot{m} r^2 \omega_z}{I_z}$$

$$\dot{\psi} = \frac{1}{\cos \theta} (\omega_y \sin \phi + \omega_z \cos \phi)$$

$$\dot{\theta} = \omega_y \cos \phi - \omega_z \sin \phi$$

$$\phi = \omega_x + \psi \sin \theta$$

$$\beta = \tan^{-1} \frac{I_y \sqrt{\omega_y^2 + \omega_x^2}}{I_x \omega_x}$$

$$I_x = I_{x0} + \dot{I}_x t$$

$$I_y = I_{y0} + \dot{I}_y t$$

$$I_z = I_{z0} + \dot{I}_z t$$

$$M_y = F l$$

$$M_z = F l$$

$$l = \rho \sin \delta$$

$$\rho = \rho_0 + \dot{\rho} t$$

$$m = m_0 + \dot{m} t$$

$$r = r_0 + \dot{r} t,$$

where

$t$  = time

$I_x, I_y, I_z$  are spacecraft instantaneous moments of inertia

$\dot{I}_x, \dot{I}_y, \dot{I}_z$  = time rate of change of moments of inertia

$\omega_x, \omega_y, \omega_z$  = instantaneous Euler body rates

$\psi, \theta, \phi$  = instantaneous yaw, pitch, and roll Euler angle

$m$  = instantaneous spacecraft mass

$\dot{m}$  = mass expulsion due to primary propulsion system

$F$  = primary propulsion system thrust

$\delta$  = net thrust misalignment

- $\rho$  = distance along axis of symmetry between total vehicle c.m. and primary propulsion system c.m.
- $\dot{\rho}$  = time rate of change of c.m. along axis of symmetry
- $l$  = net thrust moment arm
- $r$  = instantaneous distance between vehicle c.m. and primary propulsion system nozzle exit plane
- $\beta$  = coning half angle.

The simulation described above was run for apogee motor thrust misalignments of 1, 0.5, 0.25 and 0.1 degrees and for initial spin rates varying between 10 and 100 rpm. It was assumed that spin rates greater than 100 rpm might impose a hardship on the ATS-4 vehicle structure; for this reason, spin rates greater than 100 rpm were not studied. The results from this simulation are shown in Figure 9-14. On Figure 9-14 the maximum coning half angle obtained from the simulation is plotted versus spin rate and net thrust misalignment. The apogee motor for the proposed ATS-4 spacecraft is some derivative of the Surveyor retro motor, the Thiokol Chemical Corporation TE-M-364. From actual ground static firing tests the thrust excursion from the nominal direction was found to be less than 0.3 degree (Reference 3). The mechanical motor misalignment can safely be said to be less than 0.1 degree (Reference 4). The root-sum-square of these two excursions results in a net thrust misalignment of 0.316 degree which lies in the region mapped on Figure 9-14 by thrust misalignments of 0.25 and 0.50 degree. According to Reference 5, a coning angle greater than 2.5 degrees is undesirable, because this is in the region where thrust degradation is very rapid as coning angle increases (see Figure 9-15). Using a 0.5-degree thrust misalignment as a conservative estimate and 5 degrees as the maximum half cone angle, Figure 9-14 shows that the minimum spin rate for the ATS-4 mission is approximately 60 rpm. This results in approximately a 9-percent net thrust reduction.

## SEPARATION AND SPINUP ANALYSIS

Immediately following the Centaur second burn the vehicle is pitched and yawed to align the spacecraft thrust axis for apogee burn. After this attitude reorientation, the spacecraft is separated from the Centaur vehicle and is spun up by use of propulsive devices. The spacecraft attitude dispersions could be reduced if the Centaur could be given a small roll rate (1 or 2 rpm). According to Reference 6, the Centaur could spin at 1 or 2 rpm after burnout, but this has never been done before. Thus it was decided to make the present analysis assuming that the Centaur could supply no spin.

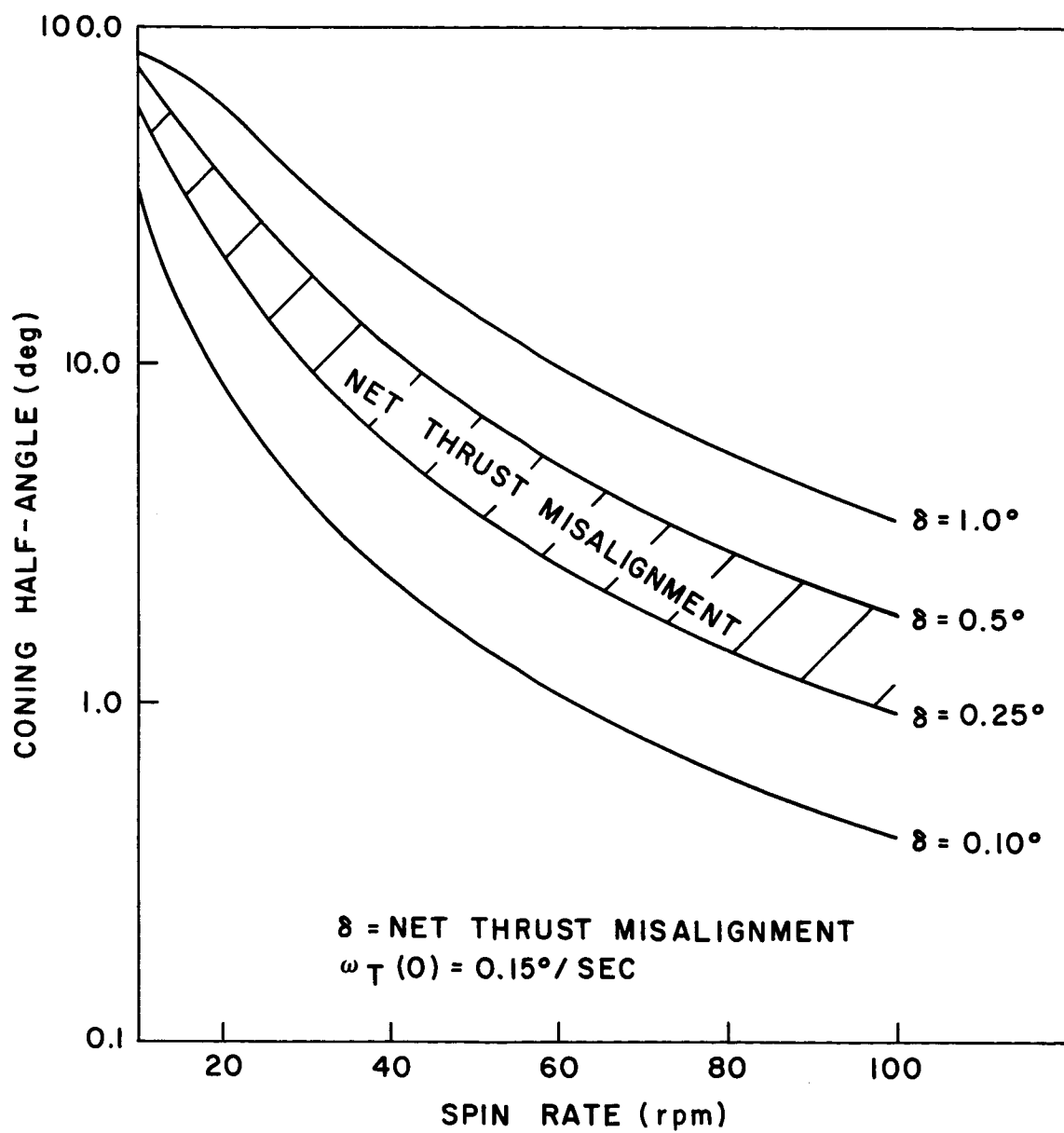


Figure 9-14. Coning half angle versus spin rate.

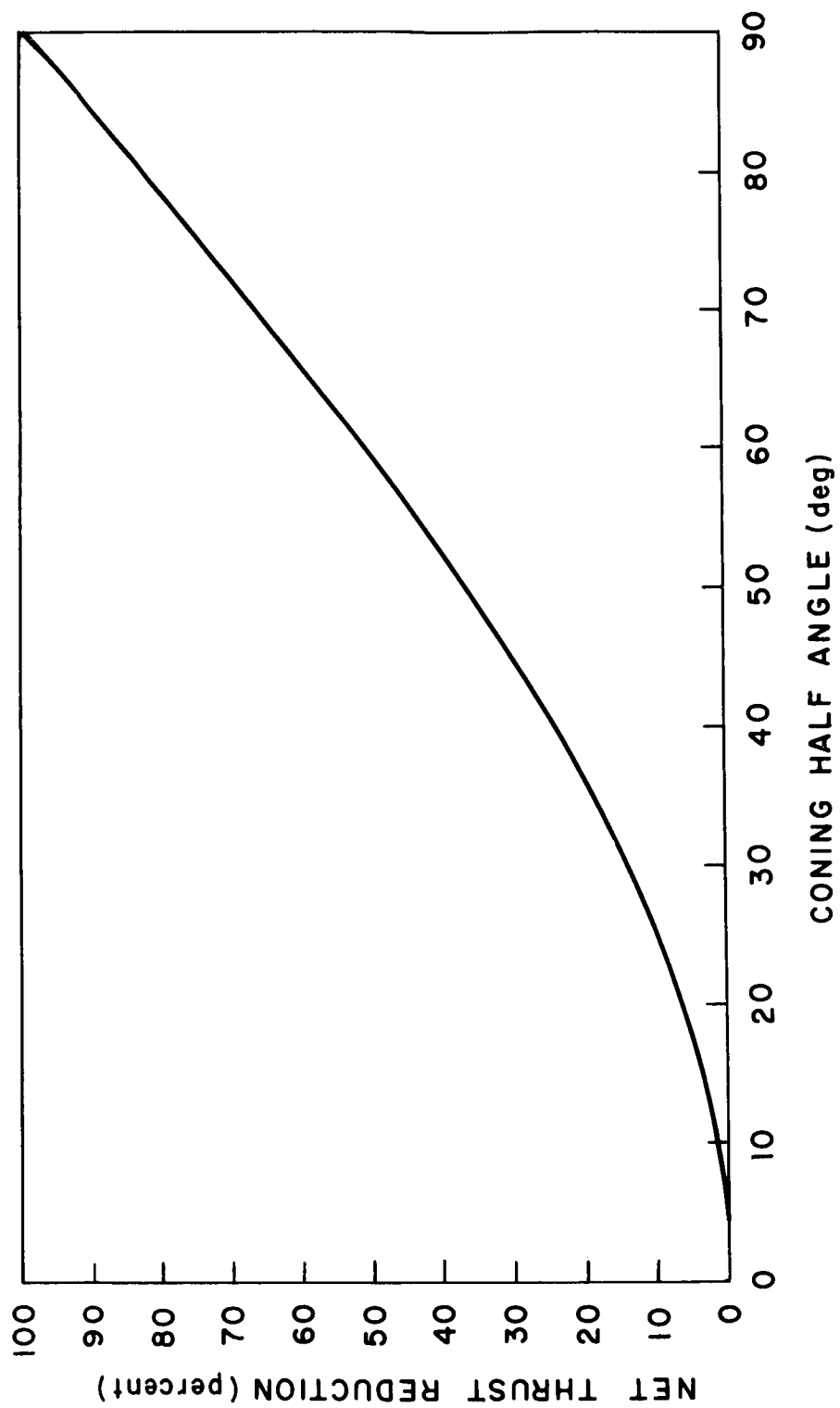


Figure 9-15. Thrust reduction resulting from vehicle coning.

It is assumed that the ATS-4 spacecraft is separated from the Centaur vehicle after the attitude maneuvers with the relative separation velocity being imparted by a specially manufactured set of matched springs. The reason for matching the springs is to hold to a minimum any transverse angular momentum applied to the spacecraft from spring mismatch. Following the separation, a small time delay is made in order to ensure, before ignition, complete separation of the propulsive devices for vehicle spinup; this delay is approximately 2 seconds (Reference 7). The spacecraft motion during separation and spinup was simulated on a digital computer. This simulation consisted of numerically integrating the Eulerian equations of motion for a rigid body. The equations programmed are

$$\dot{\omega}_x = \omega_y \omega_z \frac{(I_y - I_z)}{I_x} + mn \frac{Fl}{I_x}$$

$$\dot{\omega}_y = \omega_x \omega_z \frac{(I_z - I_x)}{I_y}$$

$$\dot{\omega}_z = \omega_y \omega_x \frac{(I_x - I_y)}{I_z}$$

$$\dot{\psi} = \frac{1}{\cos \theta} (\omega_y \sin \phi + \omega_z \cos \phi)$$

$$\dot{\theta} = \omega_y \cos \phi - \omega_z \sin \phi$$

$$\dot{\phi} = \omega_x + \dot{\psi} \sin \theta,$$

where

$\omega_x, \omega_y, \omega_z$  are instantaneous body rates

$I_x, I_y, I_z$  are instantaneous moments of inertia

$l$  is the thrust moment arm

$m$  is the digital signal (1 for thrust on, 0 for thrust off)

$n$  is the number of thrusters

$\psi, \theta, \phi$  are instantaneous yaw, pitch, and roll Euler angles.

According to Reference 8 the separation rates associated with the Centaur vehicle are less than 3 degrees per second. It is pointed out in Reference 7 that these rates can be reduced to less than 1 degree per second if a set of matched springs such as those described above were used. Cases run in the simulation included separation rates of 1, 2, and 3 degrees per second.

It is now necessary to determine the total impulse required to spinup the ATS-4 spacecraft to at least 60 rpm. It is known that

$$\Delta\omega = \frac{l I_t}{I_s},$$

where

$I_t$  = total impulse

$I_s$  = spin moment of inertia

$l$  is as defined above.

Solving for  $I_t$ ,

$$I_t = \frac{\Delta\omega I_s}{l}.$$

For the in-house ATS-4 spacecraft design,

$$I_s = 391 \text{ slug-ft}^2$$

$$\Delta\omega = 60 \text{ rpm} = 6.28 \text{ rad/sec}$$

$$l = 2.9 \text{ feet}$$

$$I_t = \frac{(6.28)(391)}{2.9} = 847 \text{ lb-sec.}$$

Now that the minimum total impulse required for spinup is known, a spinup system can be chosen from the available hardware.

It is the opinion of this writer that solid rockets should be used for spinup of the ATS-4 spacecraft because of their light weight, reliability, and total system simplicity. Other possibilities are use of monopropellant or bipropellant thrust systems or a blow-down system. These are relatively complicated systems requiring a great deal of plumbing; thus they have a large total system weight.

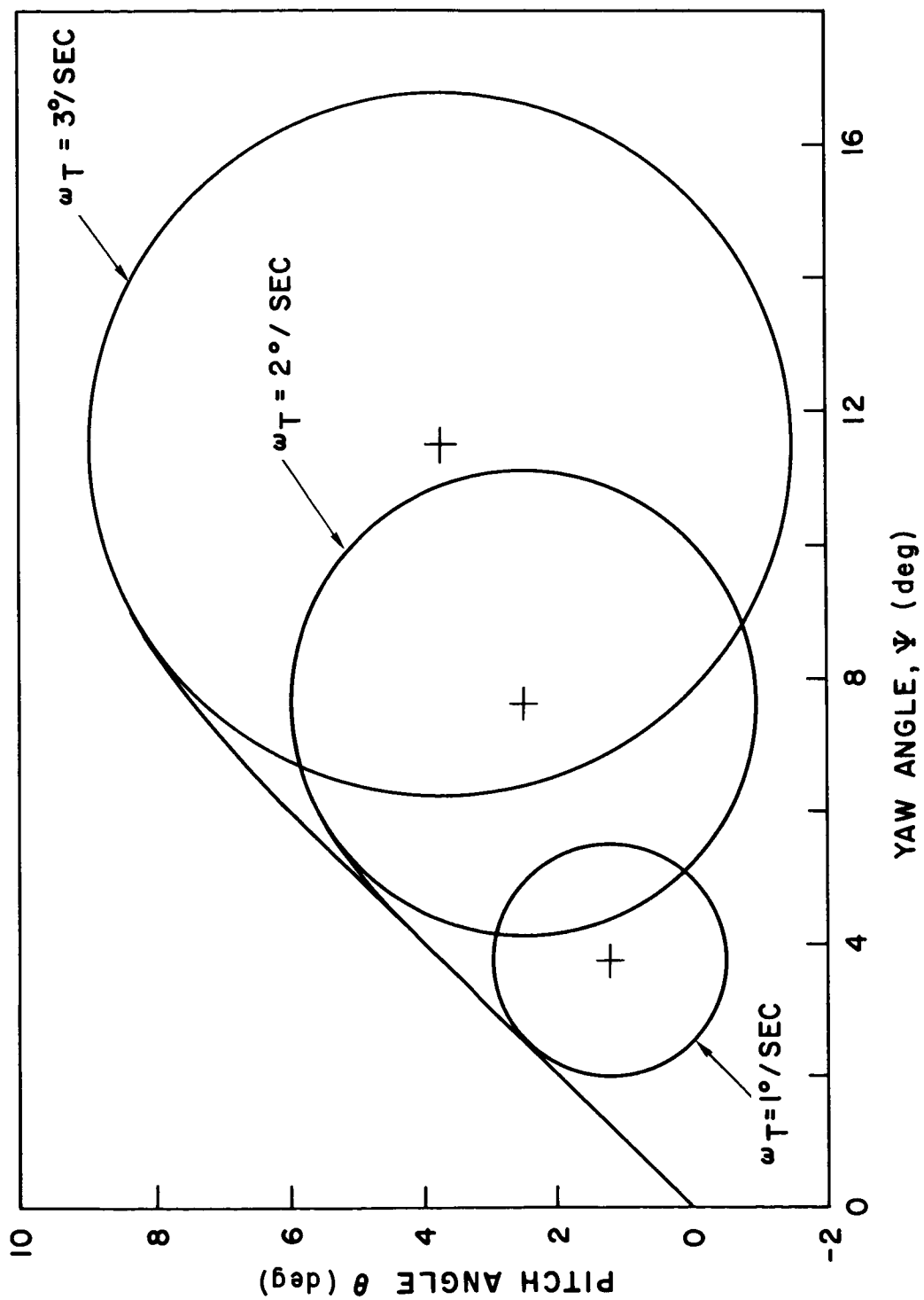


Figure 9-16. Locus of spin-axis motion during and after separation and spinup.

The thrusters mounted on the spacecraft for purposes of spinup are mounted along the periphery of the vehicle so that the thrust vectors of the individual thrusters cancel each other statically. The reason for this is to eliminate any translational force on the spacecraft while imparting maximum rotational energy to the vehicle. Total impulse to the spacecraft can be provided by a set of four Atlantic Research Corporation MARC 6A1-KS-210 solid propellant rockets. The 1-KS-210 rocket is described in detail in another section. There are rockets that will allow the spinup system to consist of fewer motors, but it is believed that net mission reliability is less with such a system. This belief is based on the fact that if a motor failure occurs, the system with fewer rockets would not obtain as high a percentage of the nominal angular rate and would also have a much larger translational force acting on the vehicle. The spin rate achieved by using the 1-KS-210 rockets would yield the spin rate

$$\Delta\omega = \frac{4(222)(2.9) 60}{(391)(2\pi)} = 62.9 \text{ rpm}$$

This situation results in a centrifugal acceleration of 0.617g at the periphery of the spacecraft. The motion of the spacecraft spin axis during separation and spinup is shown in Figure 9-16 for initial separation rates of 1, 2, and 3 degrees per second. Figure 9-16 indicates that both precession and nutation damping are required after separation and spinup. The propulsion system requirements for this precession and nutation damping are based on separation rates of 3 degrees per second. If smaller rates are achieved, the total mission propulsion requirements would not change significantly; thus, after separation and spin-up, a precession of 12 degrees and removal of transverse rates of 4.24 degrees per second must be executed.

### C. ORBIT ANALYSIS AFTER KICK STAGE FIRING

As has been previously indicated, the TE-364 kick stage will be fired at the second apogee of the transfer orbit. This occurs nominally at 53 degrees West longitude. Because it is so easily reached and because it is in view of two potential tracking stations, Rosman and Mojave, this longitude has been chosen as the operational longitude for ATS-4. There is no apparent requirement for placing the satellite more to the east. If during the satellite lifetime a longitude more to the west is desired, it can be reached by simply allowing the satellite to drift in response to earth's gravity field, the stable point of which is at 108 degrees West longitude.

This section of the report gives the analysis for (1) station seeking, which will be accomplished with the hydrazine propulsion system, (2) final orbit adjust and station keeping, which will be accomplished with the resistance jet propulsion system, and (3) the yo-yo despin.

## STATION SEEKING

The hydrazine propulsion system used for precession and nutation control during the transfer orbit will be used in this phase of the mission also. It will now provide the translational velocity increments in addition to precession and nutation control.

The three sigma injection errors were given in the previous section and are repeated here as Table 9-10. From these errors, the in-plane boundaries within which the actual orbit should fall can be calculated. The results are shown as Figure 9-17. It is estimated that 16 hours after the injection into the synchronous orbit, sufficient data will have been obtained to provide a preliminary estimate of where within these boundaries the actual orbit lies, and that a final orbit determination can be made within 28 hours. Based upon this information and the further assumption that the orbit injection point must be one of the nodes, if there is any inclination, the sequence of precession and orbit correction can be predicted. Depending on whether the actual injection orbit is high or low as depicted in Figure 9-17, the sequence is as shown in Table 9-11. It is noted that the satellite has been assumed to remain in the attitude required for synchronous orbit injection until the first maneuvers indicated in Table 9-11 are made. It is further noted that a preliminary determination of orbit has been assumed sufficiently accurate for eccentricity correction of the low-orbit condition. This is more or less dictated by the fact the eastward drift is undesirable from the standpoint of keeping Mojave above the horizon with respect to the satellite. The worst-case conditions (having the satellite orbit coincide with the boundaries of Figure 9-17) would result in an eastward drift of 14.6 degrees per day for the low orbit or a westward drift of 14.2 degrees per day for the high orbit. Using the preliminary data is not expected to create any serious problem, as additional in-plane orbit adjust capability is being provided by the resistance-jet-propulsion system. Such is not the case for inclination removal, however; therefore, the inclination error should be known as accurately as possible before any attempt is made to remove it.

The increment of velocity required for inclination removal is 87.3 feet per second. The increment of velocity required for eccentricity removal is 98.2 feet per second which is slightly higher than the injection velocity error of Table 9-9. This is necessary to guarantee an orbit with a mean motion less than or equal to the synchronous rate. If this condition were not met, an eastward drift of the satellite would result. In summary, the hydrazine propulsion system must provide a local incremental velocity of 185.5 feet per second and a maximum of 200.7 degrees precession for the station-seeking phase of the mission.

Table 9-10

Injection Errors

Altitude	- $\pm 101$ nautical miles
Velocity	- $\pm 87.3$ feet per second
Inclination	- $\pm 0.497$ degrees
Eccentricity	- 0.221

Table 9-11

Sequence of Removing Eccentricity, "e", and Inclination, "i", with the Hydrazine Propulsion System.

Low Orbit	High Orbit	
	Injection point is descending node	Injection point is ascending node
Precess $20.7^{\circ}$	Precess $69.3^{\circ}$	Precess $110.7^{\circ}$
Remove "e" at 24 hrs	Remove "i" at 36 hrs	Remove "i" at 36 hrs
Process $90.0^{\circ}$	Precess $90.0^{\circ}$	Precess $90.0^{\circ}$
Remove "i" at 36 hrs	Remove "e" at 48 hrs	Remove "e" at 48 hrs

(The times are measured from injection into the synchronous orbit.)

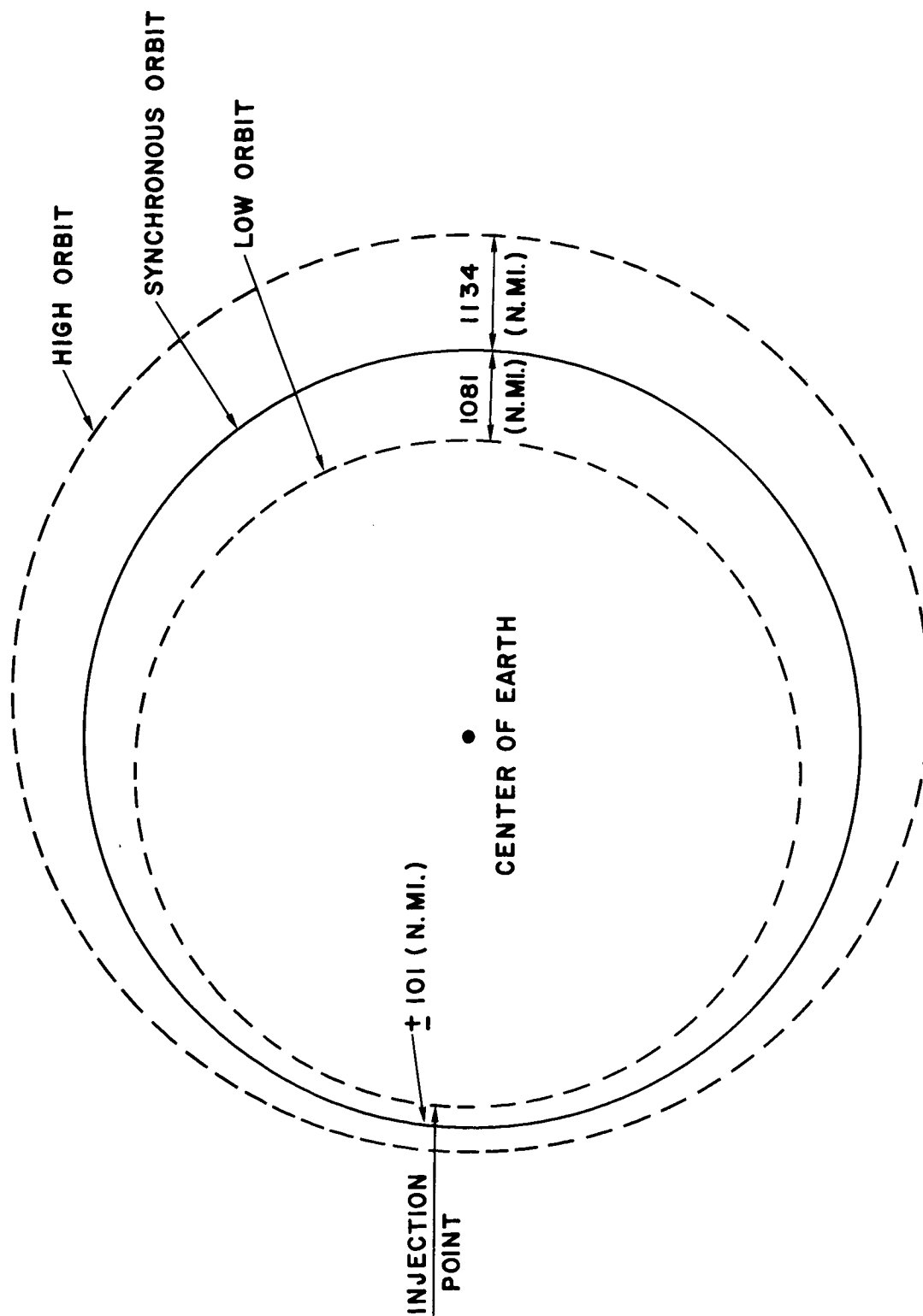


Figure 9-17. In-plane orbital error boundaries due to injection errors

## FINAL ORBIT ADJUST AND STATION-KEEPING

At the completion of the orbit corrections by the hydrazine propulsion system, no inclination error should remain. However, in-plane orbital errors will not have been completely removed. Since all in-plane velocity increments have been applied at or near the injection point (see Table 9-10), the attitude error of  $\pm 101$  nautical miles at injection still remains. In addition, provision was made above to eliminate as quickly as possible any eastward drift. This may well mean that the orbit will be 101 nautical miles high at the point 180 degrees from injection. These error boundaries are shown as Figure 9-18. The velocity increment required (two pulses) to remove these errors is 22.0 feet per second.

As has been previously indicated, the geometry of the resistance-jet-propulsion system is not ideal for providing translational velocity increments. The sketch shown as Figure 9-19 reveals the inefficiency. When the satellite is in its preferred attitude, a radial component of thrust 4.6/3.6 times as great as the tangential component must be applied to maintain the attitude. Therefore, in order to provide a tangential velocity increment of 22.0 feet per second, a total velocity increment of  $(4.6 + 3.6)/3.6$  times 22.0, i. e. 50.1, feet per second must be supplied for the final orbit adjust. It should be noted that this number is based on optimum timing, meaning that thrust should be applied at or near (say  $\pm 1.5$  hours) apogee or perigee. Any detrimental effects of the radial thrust component are minimized and the tangential correction is maximized in this region. In order to estimate the total time for the final orbit adjust, it is assumed that 0.026 pounds of tangential thrust is applied to the 1400-pound satellite for three hours twice a day at a ten-percent duty cycle. The total correction time is then approximately 17 days for the worst case.

A further task to be performed by the resistance-jet-propulsion system is that of station keeping. From this standpoint the longitude,  $53^{\circ}$  West, chosen for the satellite position is the worst-case condition, as the  $J_{22}$  gravitational perturbation is maximum at this point. This station could theoretically be maintained by applying a constant, very small thrust against the perturbation which would produce a total velocity increment of 5.36 feet per second per year. The radial component of thrust must also be provided to maintain attitude. This results in a total requirement of 12.2 feet per second per year. In actuality the thrust will not be applied constantly but in pulses after an error has appeared. Using an analog simulation, it can be shown that the inefficiency of operating in this manner increases the above figure to 15.3 feet per second per year. In the analog simulation two thrust pulses, of 4 minutes duration each, applied 12 hours apart and repeated every 10 to 11 days, were sufficient to maintain the station. Note that a total incremental velocity correction of 30.6 feet per second must be supplied for a two-year mission.

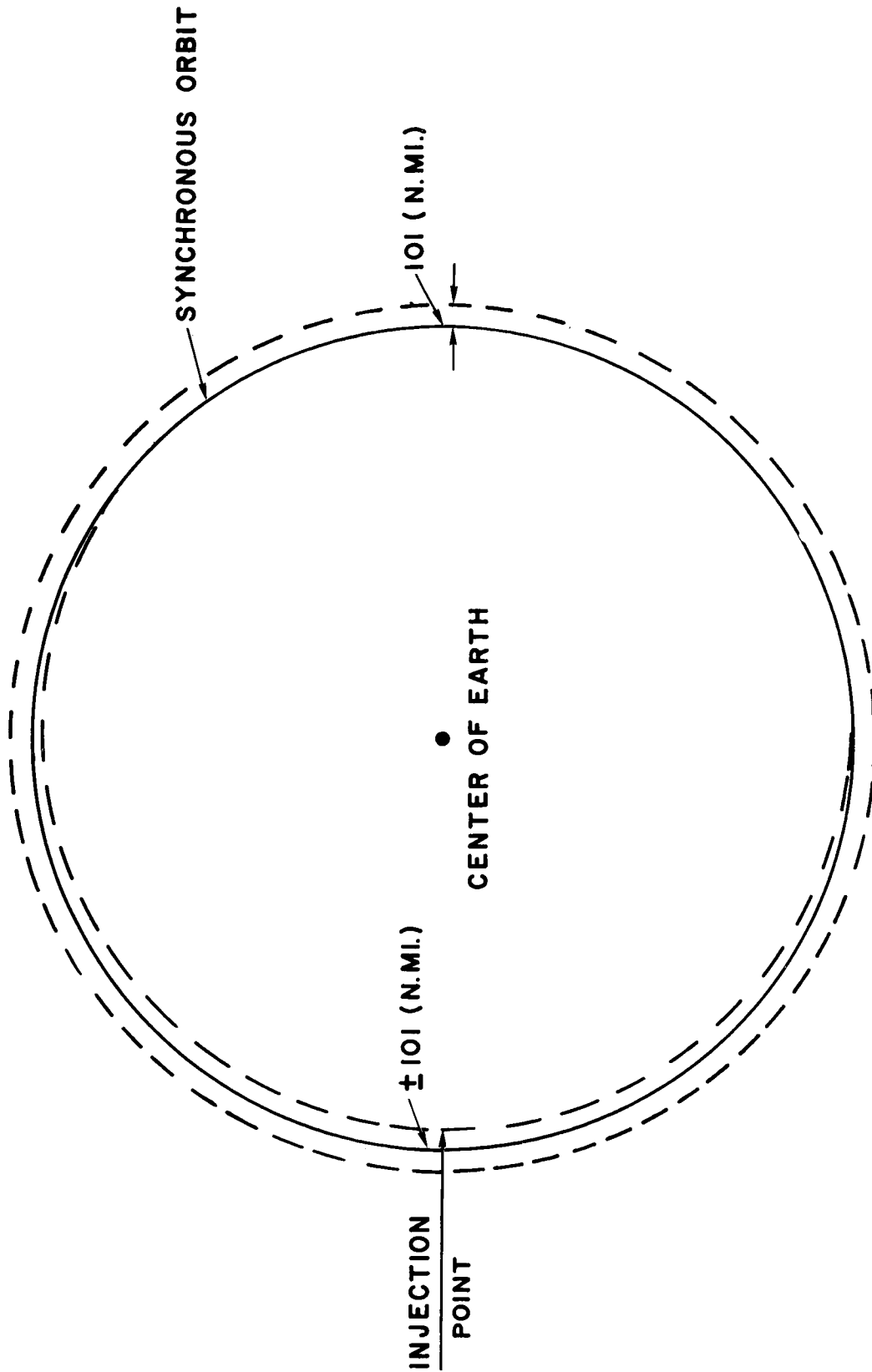


Figure 9-18. In-plane orbital error boundaries after correction by hydrazine propulsion system.

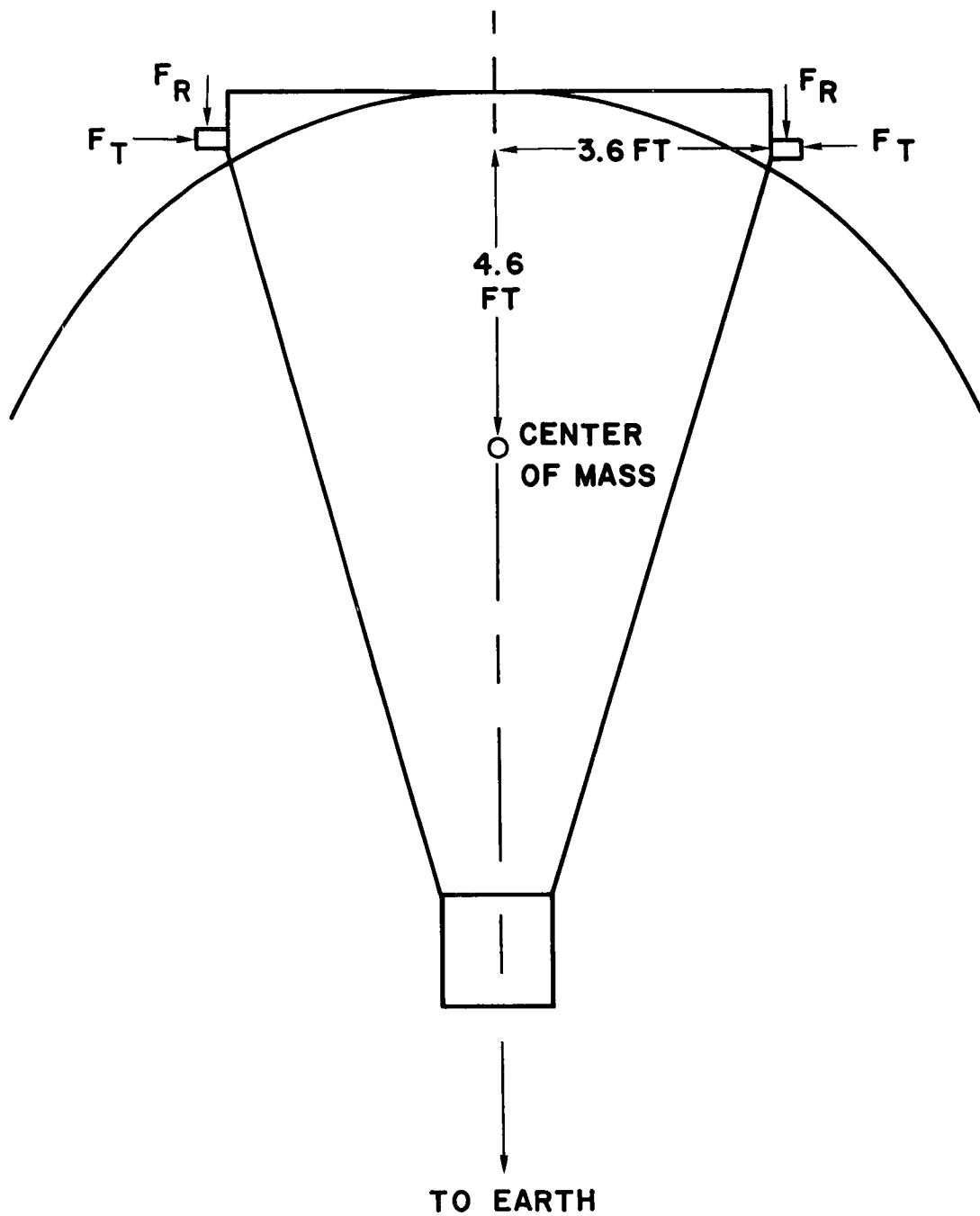


Figure 9-19. Schematic of ATS-4 showing thruster location with respect to center of mass.  $F_T$  is Tangential thrust and  $F_R$  is radial thrust.

The total of the velocity increments required for final orbit adjust and station keeping is then 50.1 plus 30.6, i.e. 80.7, feet per second. It would seem that provision of 100 feet per second is reasonable for design purposes as additional orbit adjust due to secular perturbations may be required during the satellite's lifetime. It is noted that there is no requirement for additional station seeking. This is true if there is no desire to place the satellite east of  $53^{\circ}$  West longitude. As has already been pointed out, a station to the west can be reached by allowing satellite drift, caused by the  $J_{22}$  perturbation. It would require approximately 200 days for a satellite in a perfect synchronous orbit at  $53^{\circ}$  West longitude to drift 45 degrees.

#### YO-YO DESPIN

After the initial station seeking with the hydrazine propulsion system and before deployment into the final flight configuration, the satellite must be despun from its nominal spin rate of 62.9 revolutions per minute. The simplest device for performing this maneuver is the yo-yo, consisting of two wires and two masses. The wire length was chosen to make two wraps around the circumference of the satellite. The satellite has a four-foot radius; therefore the wire length is 25 feet. Based on this number and the spin moment of inertia of 355 slug-feet squared and the desire to completely despin, the two masses and wires weigh approximately 13.7 pounds. Actually the two wires weigh only about 0.15 pounds for some materials. Therefore, most of the weight is in the two masses. The despin is accomplished in approximately 1.5 to 2.0 seconds.

A rather crude error analysis was performed to estimate the possible residual spin rate left after the despin. Assumed errors and resulting spin rates are shown as Table 9-12. It is noted that an error in the initial spin rate is propagated to an error in the final spin rate only through the errors in inertia, mass, and length. In other words, error due to initial spin rate error is produced by second-order effects. The root sum square of final spin rate errors is 0.123 radians per second, i.e. seven degrees per second. This residual spin rate must be removed by the resistance-jet-propulsion system during the satellite's earth-acquisition phase.

Table 9-12

## Yo-yo Despin Error Analysis

Cause of Error	Final Spin-Rate
$\frac{\Delta I}{I} = \pm 3\text{-}1/3\%$	$\pm 0.031 \text{ rpm}$
$\frac{\Delta m}{m} = \pm 2/3\%$	$\pm 0.116 \text{ rpm}$
$\frac{\Delta l}{l} = \pm 1/8\%$	$\pm 0.023 \text{ radians per second}$
$\frac{\Delta \omega_o}{\omega_o} = 10\%$	$\pm 0.008 \text{ rpm}$
	<hr/>
RSS =	$\pm 0.015 \text{ rpm}$

(I = moment of inertia, m = yo-yo mass, l = yo-yo wire length, and  $\omega_o$  = initial spin rate.)

## REFERENCES

1. "Determination of Spin Rate Requirement for Attitude Stabilization of the Aerostar Vehicle," Aerojet-General Corporation Report No. 2084.
2. Private conversation with Dr. Joseph Fedor, Mechanical Systems Branch, GSFC.
3. Private conversation with S. A. Racik, Thiokol Chemical Corp.
4. Private conversation with Arthur Sprott, Delta Project, GSFC.
5. "ATS System Summary," Hughes Aircraft Corp. Report No. SSD 60028R.
6. Private conversation with Norman Weisberg, Centaur Project Office, NASA Lewis Research Center.
7. ATS System Summary, Hughes Aircraft Co. Report No. SSD 60028R.
8. Atlas-Centaur Payload users Manual, Published under Lewis Research Center Contract No. NAS 3-8701.

## SECTION 10

### SPACECRAFT STRUCTURE

The study has evolved the spacecraft configuration shown in Figures 10-1 and 10-2. The main elements of this configuration consist of two structural modules connected by a six-member tubular truss. In orbit, the smaller of these modules views the earth and the larger one views space. A 30-foot-diameter parabolic reflector is fastened to the larger structural module and is snubbed at the earth viewing module for launch support. During launch, the solar paddles are folded around the earth viewing module, but are primarily supported by a truss which is an extension to the antenna deployment truss. The larger module is mounted on an adapter, which is mounted to the Centaur launch vehicle.

The primary purpose of the spacecraft adapter is to transmit the spacecraft loads to the Centaur stage and to provide a mounting for the apogee kick stage. In or on its surface are the spin-up rockets, separation systems, and the vernier propulsion system.

The adapter is an aluminum alloy structural shell reinforced with longitudinal and circumferential stiffeners. It features riveted construction as used on similar adapters in other programs. Its diameter at the Centaur interface is 5.5 feet, and at the spacecraft interface is 6.5 feet. The total adapter height is 34.5 inches.

The bulk of the adapter's inside volume is occupied by the TE-364-3 stage, which is mounted to the adapter by a six-member truss. Alignment of the motor thrust axis can be accomplished by adjustable end fittings on this truss. The separation system features a V-band clamp which is explosively released at the desired separation time. The separation relative velocity is obtained by a system of coil springs which are activated upon release of the clamp. (Spin-up and vernier propulsion systems are discussed in Section 14.) The entire adapter is separated just prior to spacecraft despin.

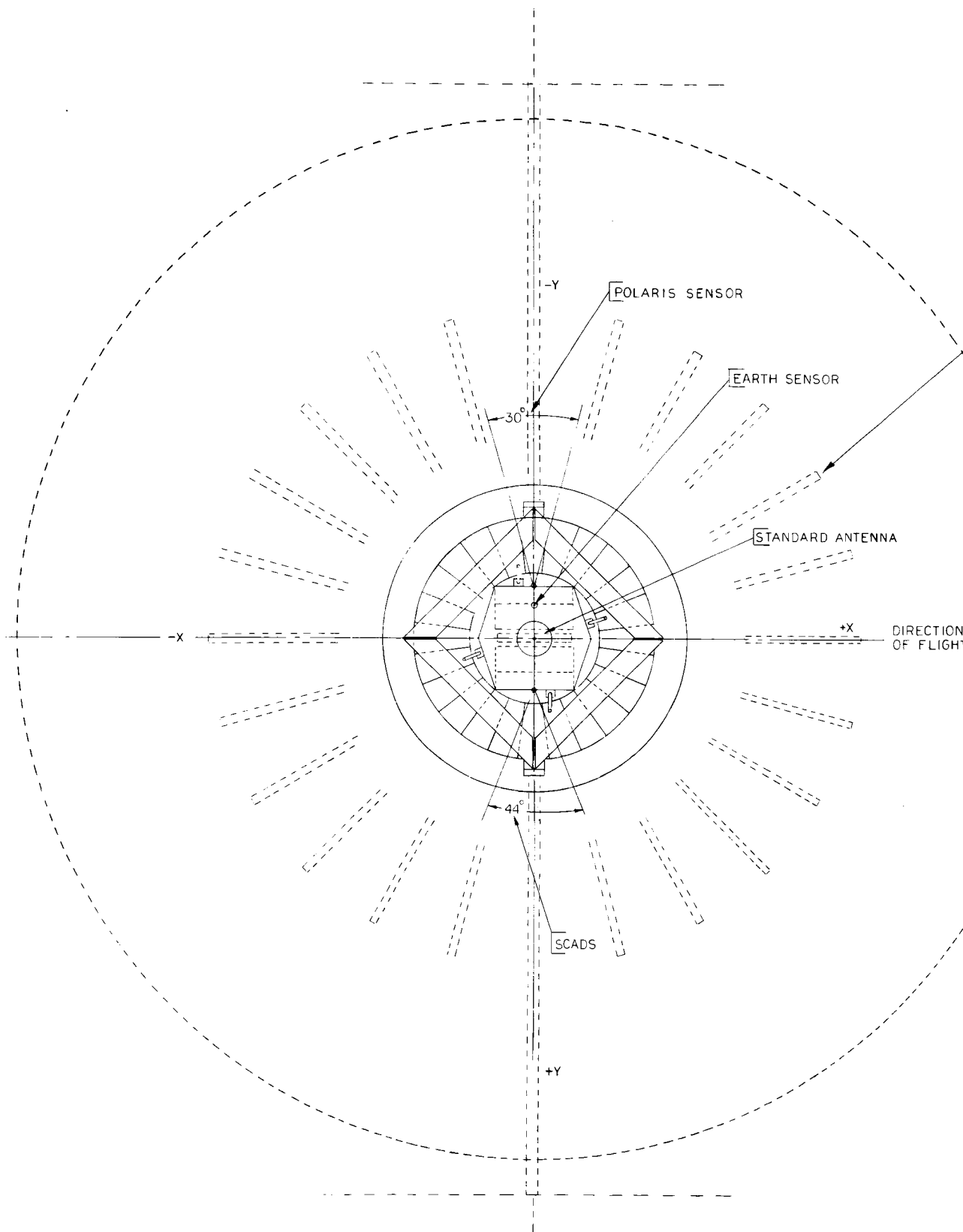
The aft-equipment module (so called because it is located at the rear of the spacecraft) is mounted to the spacecraft adapter. The structural purpose of this item, which is load transmission to the adapter of the major spacecraft weight, is accomplished by a reinforced aluminum alloy shell. The configuration is such that all major loads from the spacecraft are transmitted through this shell. The equipment contained within this module is mounted to a structural honeycomb plate. Eighteen standard size equipment packages can be

accommodated in the module, and additional volume is available for equipment that cannot conform to the standard size. Also mounted to this module is the parabolic antenna reflector, which mounts to an interface ring of the same diameter as the equipment module. (Although the reflector is an integral part of the spacecraft structure, it is discussed in detail in Section 11.) Where necessary to keep spacecraft temperatures within reasonable limits, thermal louvers will be used and mounted to the structural shell.

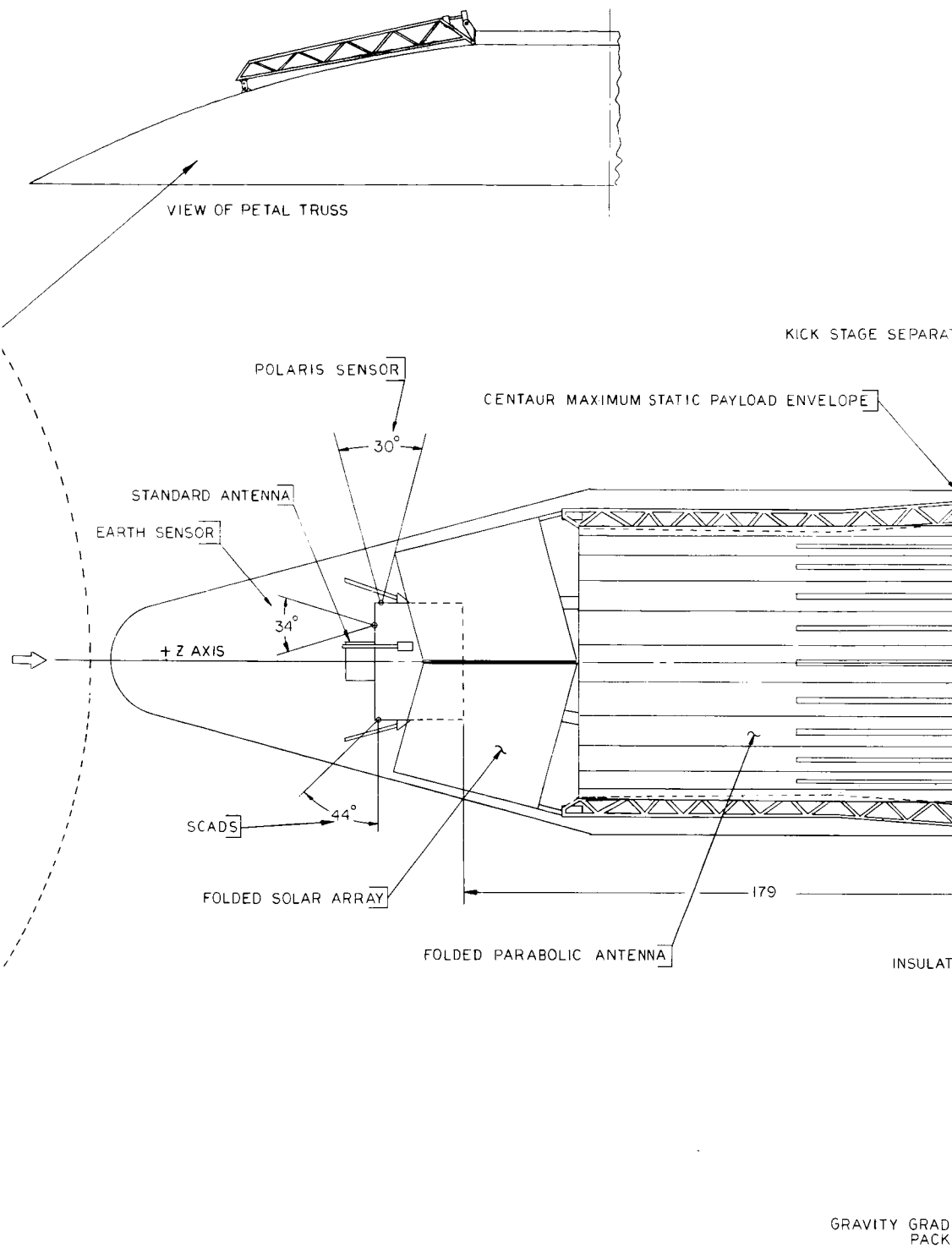
The earth viewing equipment module contains the UHF and X-band feeds, transponders, interferometer, attitude control sensors, and all other equipment that must view the earth. The hexagon-shaped module is constructed of aluminum alloy structural members and aluminum alloy panels. To keep RF blockage a minimum, the frontal area of the module will be kept as small as possible and will be closely controlled. There will be a number of thermal louver assemblies on this module.

The separation distance between the reflector and the RF feed is dictated by the required focal length. For ATS-4 this length is 15 feet; hence the earth viewing module is mounted to the aft module on a structure with separation distance of that amount. This structure is a six-member truss formed of individual beryllium struts. According to preliminary calculations, the struts will be 4 inches in diameter with a wall thickness of .060, and will terminate in a bonded stainless steel end fitting. This technique is used to avoid the necessity of machined beryllium parts. The struts are attached to the equipment modules by means of adjustable monoball mounts. Because the ball joints do not transmit bending moment, the truss members will always be in either tension or compression, a condition necessary for a minimum weight truss. Another function of the adjustable feature of the monoball mounts is that they permit adjustment of the strut length, allowing precise boresight alignment. Very precise alignment has been accomplished on the Nimbus spacecraft using the same type of system. Because this support system is not optimum from an RF standpoint, additional work is being done to devise a support system to improve RF performance. Section 11 describes another candidate system under consideration.

The solar paddles, in their deployed configuration, extend beyond the rim of the antenna. They are mounted on two extended and reinforced antenna deployment trusses. (See Section 11.) No additional deployment mechanism is required to extend the solar paddles to their position. The solar paddles will be made of aluminum honeycomb, reinforced with internal aluminum alloy structural members. Each paddle will have a single fold to permit stowage around the earth viewing module, as indicated by Figure 10-1. As stated earlier, the paddles will deploy along with the antenna. They will then unfold



10-3-1



Figure

10-3-2

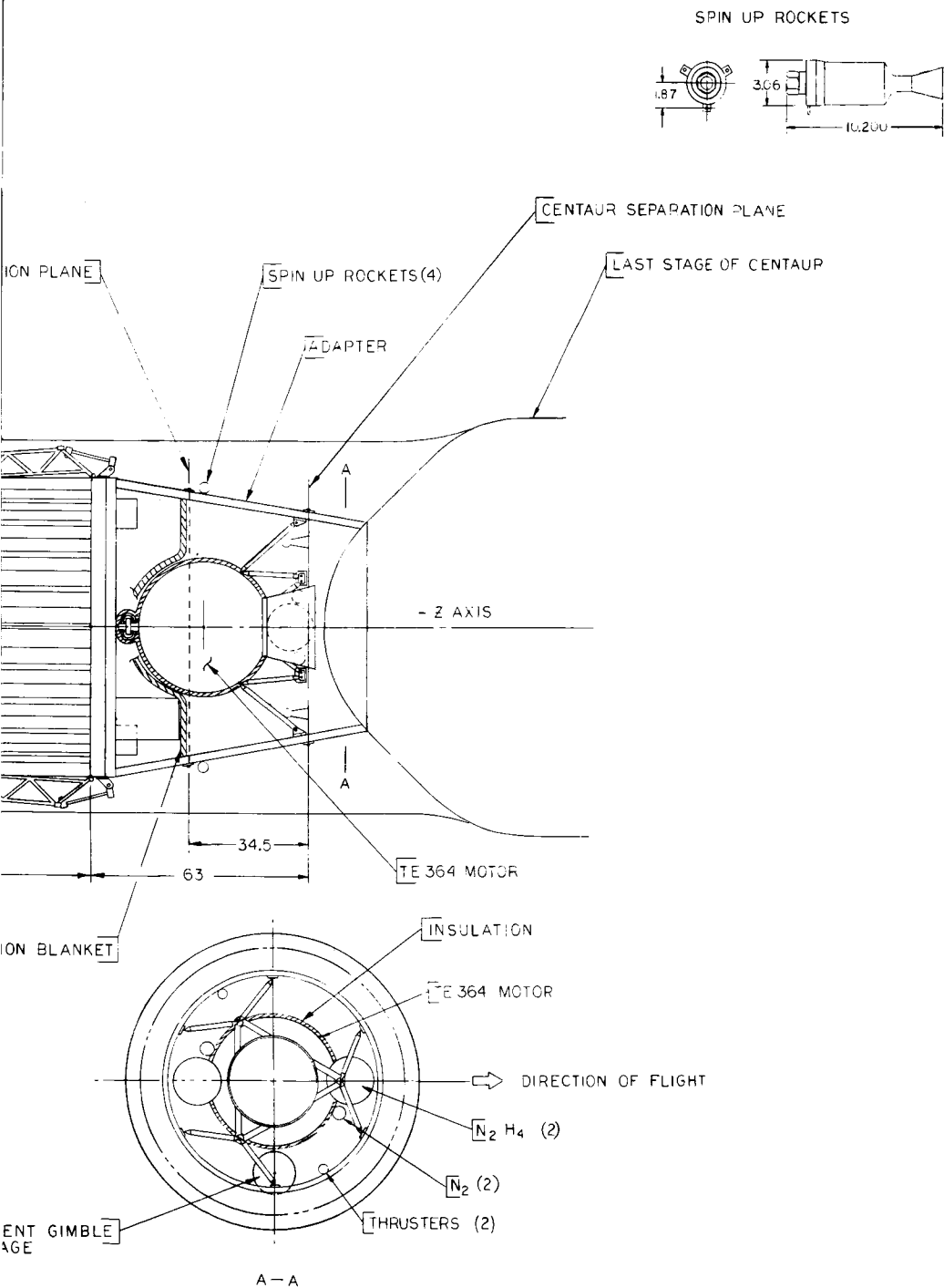
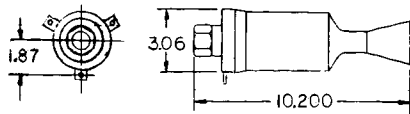


Figure 10-1. Launch Configuration of ATS-4 Spacecraft, GSFC Concept.

# SPIN UP ROCKETS



SPINNING BODY SUN SENSOR

KICK STAGE SEPARATION PLANE  
(O REF. FOR CENTER GRAVITY  
LOCATION)

YO-YO WEIGHTS(2)

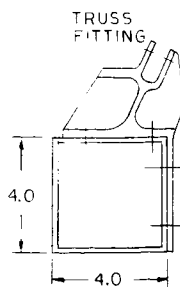
6X6X6  $\frac{1}{2}$  MODULES (18)

DETAIL - A

400 MHz & 8GHz

SOLAR PADDLE 40°  
400 WATTS PER PADDLE  
(WHEN NORMAL TO SUN)

TRUSS SUPPORT

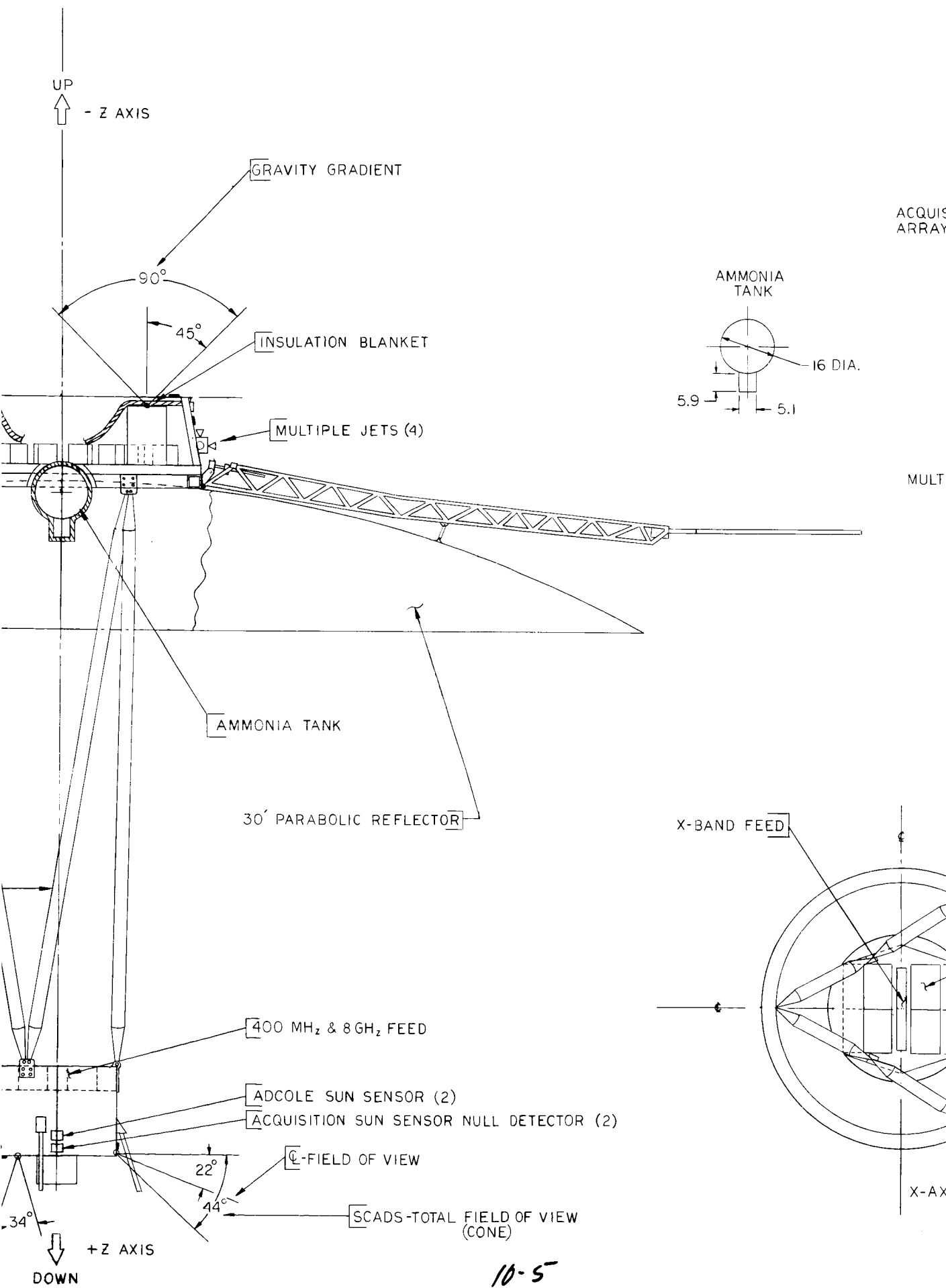


DETAIL - A

T.T. & C ANTENNA  
(4)

POLARIS SENSOR 30°

EARTH SENSOR



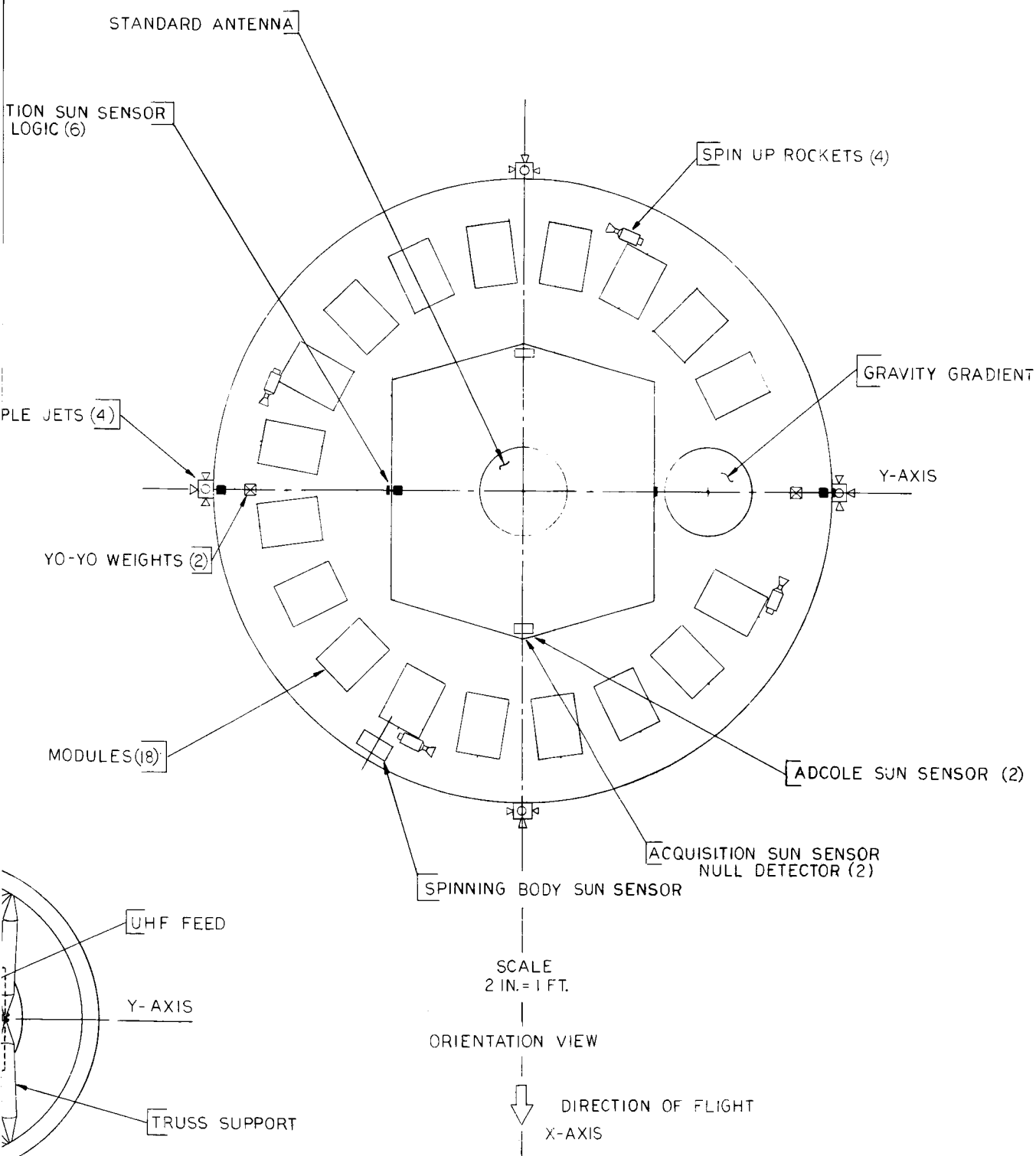


Figure 10-2. Orbital Configuration of ATS-4 Spacecraft, GSFC Concept.

into straight panels, and one panel will be rotated 90 degrees with respect to the other panel to yield the cruciform configuration described in the solar power section of this report.

A preliminary structural and dynamic analysis has been performed on this spacecraft configuration. The spacecraft must withstand the SLV3C/Centaur/TE-364-3 vibration and acceleration requirements. The preliminary analysis indicates that the spacecraft structural concept shown in Figures 10-1 and 10-2 can be designed to withstand these environments and that the spacecraft structure can be designed to meet the weights stated in Table 10-1. This table is a total spacecraft weight breakdown. A computer program was devised to calculate center of gravity and moments of inertia of the spacecraft. This program allows easy recomputation of these numbers when changes in the spacecraft require updated moments of inertia and center of gravity.

Table 10-2 lists the center of gravity and moments of inertia for 2 spacecraft conditions. One of these the spacecraft antenna and solar paddles folded in the launch configuration, and the TE-364 motor full of fuel attached to the spacecraft by its adapter. The second is the launch configuration with the antenna and solar paddles deployed and the TE-364 motor and adapter separated.

The preliminary dynamic analysis indicates that the spacecraft can be designed to stay within the dynamic envelope established by the common interface with the shroud. The analysis also indicates that the transmissibility factor up to the feed module will be high in spacecraft transverse vibration. Values up to 17 have been calculated using a damping factor,  $C/C_c$ , of 0.03. Dynamic excursions resulting from this factor are calculated to be approximately  $\pm 1\frac{1}{2}$  inches.

The shroud selected for this mission is a modified surveyor shroud (See Figure 10-1). The modification involves an extension in length of 15 feet. As shown in the drawing, a preliminary static spacecraft envelope has been determined. The final spacecraft static envelope will be determined as an interface with the shroud, after consideration of the dynamic envelope of the shroud. Use of the modified surveyor shroud appears to be the best solution for this program. The alternates would be a modification and extension of the OAO shroud or development of an entirely new shroud. Both would be more expensive than the selected solution. Extension of the shroud has the effect of lowering the launch availability. This item is now under investigation by the Lewis Research Center.

Table 10-1

## Spacecraft Weight Breakdown

Control System-----	108.0
Sensors -----	43.0
Sun--4.0	
Earth--8.0	
SCADS--7.0	
Polaris--10.0	
Rate int. gyro.--6.0	
3 rate gyro.--8.0	
Electronics-----	35.0
Control computer--30.0	
Power converter--5.0	
Reaction Wheels -----	30.0
Gravity Gradient Experiment -----	30.0
Auxillary Propulsion-----	188.0
NH <sub>3</sub> resistance jets -----	78.0
Propellant--40.0	
Power conditioner--10.0	
Tankage & lines--19.0	
Thrusters--9.0	
Hydrazine -----	110.0
Propellant--85.0	
Prop tanks--14.0	
N <sub>2</sub> tanks--3.0	
Lines, valves, etc.--8.0	
Telemetry and Command -----	60.0
Telemetry logic--35.0	
Command logic--15.0	
Telemetry Transmitter--6.0	
Command receiver--4.0	
Power System-----	241.0
Solar paddles, cells, and booms--144.0	
Batteries--73.0	
Array shunt limiter--6.0	
Volt reg.--18.0	

Table 10-1 (continued)

## Spacecraft Weight Breakdown

Transponders-----	60.0
8 GHz--40.0	
4 GHz--20.0	
Structure-----	235.0
Back--120.0	
Feed--40.0	
Feed support--75.0	
Adapter -----	125.0
Harness-----	75.0
Thermal Control -----	50.0
Large-Aperture Antenna -----	250.0
Reflector trusses & mech.--200.0	
8GHz & 0.4GHz feeds--50.0	
Interferometer-----	35.0
Spin Up and Despin -----	20.0
Balance Weights -----	30.0
Antenna Instrumentation -----	35.0
Apogee Motor-----	1580.0
Fuel--1440.0	
Structure--140.0	
<u>Totals:</u>	
Spacecraft-----	1287.0
Spacecraft, Adapter & Apogee Motor-----	3122.0
Launch Vehicle Capability-----	3250.0
Margin-----	128.0

TABLE 10-2

ATS-4 Spacecraft Moments of Inertia and Centers of Gravity

Condition 1-----Launch Configuration

Center of gravity 32.3 inches in the +Z direction from the kick stage separation plane

$$CGx = 0.0 \text{ inches}$$

$$CGy = 0.3 \text{ inches}$$

Moments of inertia about CG:

$$Ix = 3700 \text{ slug-ft}^2$$

$$Iy = 3707 \text{ slug-ft}^2$$

$$Iz = 237 \text{ slug-ft}^2$$

Condition 2-----Orbit Configuration

$$CGz = +71.8 \text{ inches}$$

$$CGx = 0.0 \text{ inches}$$

$$CGy = -0.9 \text{ inches}$$

Moments of inertia about CG:

$$Ix = 3322 \text{ slug-ft}^2$$

$$Iy = 1910 \text{ slug-ft}^2$$

$$Iz = 1781 \text{ slug-ft}^2$$

## SECTION 11

### A DEPLOYABLE, HIGH-GAIN PARABOLIC ANTENNA SYSTEM WITH A SCANNING RF FEED

#### INTRODUCTION

The purpose of this section is to present briefly the various concepts and techniques for developing a large-aperture, parabolic antenna reflector and scanning RF feed system which can be placed in a synchronous orbit as part of the ATS-4 spacecraft mission. In addition, a preferred concept and proposed system design will be presented.

Because of the large size of the parabolic reflector (minimum of 30 feet in diameter), it is necessary that the concept allow for packaging within the constraints of the Atlas-Centaur shroud or modified Atlas-Centaur shroud. The weight of the antenna system must be in the order of 200 to 300 pounds including the reflector, RF feed structure support, and RF feed system in order that a standard booster such as SLV-3C/Centaur can place the spacecraft in a synchronous orbit. Finally, the antenna system must be capable of reliably deploying to its full 30-foot minimum diameter and possess a surface tolerance for use at X-band ( $\pm 0.050$  from true parabolic contour). This tolerance may be exceeded somewhat at or near the periphery of the dish where relatively low RF energy exists and at several small localized areas.

#### DEPLOYABLE REFLECTOR CONCEPTS

Available techniques for the operational achievement of a space-deployable antenna are described in the following paragraphs. The desirability of a deployable structure stems from the enhanced RF gain to be derived from a large-aperture reflector, e.g., 30 feet or larger, at X-band. The volume restraints imposed by the booster orbital delivery systems under consideration (such as the SLV-3C/Centaur), govern the size of a prior-to-launch erected reflector. These restraints limit the aperture size of a pre-launch assembled reflector to approximately 10 feet. The various factors, advantages, and disadvantages involved are described, and conclusions are stated concerning the probability of obtaining an optimized reflector design using a specific technique, both from the standpoint of state-of-the-art and from possible future development points of view.

Certain design techniques lend themselves to classification because of similar deployment mechanisms and gross structural characteristics. For the purpose of this discussion, the four main subheadings are defined as (1) Inflatable (any technique using gas pressurization as the primary method of deployment and a primary structural material with extreme flexibility in the prior-to-deployment state), (2) Mechanical (any technique using a mechanical method of deployment other than inflation and a primary structural material with a minimal amount of flexibility), (3) Memory (any technique using the structural

material characteristics as the primary means for obtaining deployment and a structural material with great to extreme flexibility at some period in the prior-to-deployment state), and (4) Hybrid (any technique using a combination of the previously mentioned techniques as the method of deployment and/or structural material).

The principal design criteria for evaluation of any of the techniques is the ability of the antenna system to carry out its structural mission, that is, to attain and maintain an optimized RF reflector surface. Other important criteria are (1) the deployed-to-packaged volume ratio, (2) weight of the package, and (3) the ability to attain and maintain the desired structural shape without detriment to mechanisms, experiments, etc. which may be situated in the vicinity of this structure.

Deployment reliability is one of the keystones to attainment of the desired structure. The other keystone is materials application, which includes material physical characteristics and their application in the structural design. The maintenance of this structural shape is wholly dependent upon material application. The evaluation of the reliability of the deployment mechanism is related to the type and number of failures, both critical (system could be rendered inoperable) and non-critical (system performance degraded.)

In lieu of mechanical design and performance data and their analysis, material application evaluation is predicated upon the choice of material with the most promising physical characteristics.

In the following discussion, the specific design techniques are described.

## INFLATABLE TECHNIQUE

### Definition

This antenna system consists essentially of the inflatable antenna dish, the pressurization system, and the vacuum-packed container for carrying the system into orbit. It is obvious that both metallic and nonmetallic materials would be needed so that the mechanical and electronic requirements could be met. It would be impractical to maintain inflation pressure in the structure during the whole life of the antenna system; therefore, the antenna material must be self-rigidizing after the pressurization process has been completed. Inflatable antennas include single-bladder, double-bladder, tubular truss, foam type, and hybrid.

### Advantages

Compactness of the undeployed system, flexibility of packing, simplicity of the deployment mechanism, and light weight are the main features of this system.

### Disadvantages

Five major difficulties exist and must be resolved. These difficulties are (1) developing a reliable way of discarding the container, (2) staying within the permitted geometrical tolerance of the ideal shape during variations of solar radiation on the antenna surface, (3) deviation of the surface beyond the allowable geometrical tolerance caused by the mechanical scanning of the dish, (4) deposition of sublimed material on the optical lenses, etc., and (5) "pumpkinoiding" of the surface (i.e., effect of overpressurization and underpressurization because of reinforcements at the seams). Each of these difficulties may not exist to the same extent. For two geometrically identical dishes, for example, the dynamic stability of the stiffer, foam type structure is much greater than that of a rather flimsy, rigidized mesh. The stress concentration at the junction of the tubes and the dish in the case of a tubular truss, as well as the doubtfulness of X-band frequency surface accuracy in all of them, is not desirable. Except for the single-bladder spherical shape, other geometries (e.g. parabolic) are rather difficult to achieve.

### Conclusions

While this group as a whole seems to be somewhat promising, some of them, such as self-supporting, rigidized mesh, may encounter permanent deformation during the mechanical scanning of the reflector. Since this group and other groups have common thermal problems, no judgement could be made on their thermal merit at this stage. The high rigidity foam type structure may be more accommodating if it is made in such a way (i.e., thermal coatings) that the maximum temperature variation could be limited to a small fraction of the depth of the outer surface.

## MECHANICAL TECHNIQUE

### Definition

This antenna system consists of rigid geometrical shapes which are segments of a desired reflector surface. These segments are stacked or flexed slightly, depending upon the mechanics of the deployment mechanism, into a minimum volume for the packaged configuration. The segments themselves

are usually surfaces that may be visualized by cutting truncated wedges from a projected aperture view of the reflector. The packaged configurations of these wedges or petals may be described roughly as closed flower, compressed iris, and stacked front-to-back types. Movement of these segments from a packaged into a deployed position consists of rotation, translation, and, in some cases, front-to-back surface sliding caused by a system of levers, screws, gears, etc. Because of the package volume allowed, the circular central core or hub of the reflector is packaged in an erected configuration and is the base plate about which the petals are hinged and deployed. The deployment mechanism may be powered by springs, compressed gas, or electrical solenoids or motors. Segments constructed of a single metal have a tendency to alleviate the problems (e.g., bonding and compatibility of physical properties) encountered with the use of a composite material and conductive plastics (i.e., resistivity is approximately one order of magnitude higher than metals.)

### Advantages

Segments are fabricated so that they are interchangeable in the overall reflector structure. Deployment does not invoke a major change in the molecular structure of the reflector surface such as cold working or chemical action as a prerequisite for rigidity of the structure. These conditions facilitate small-scale or segment testing and retesting of the structure; furthermore, the ability to replace damaged or malfunctioning sections of the reflector during ground testing is enhanced greatly. Retest-of-deployment capability is among the best of all techniques considered.

### Disadvantages

The high rigidity inherent in this technique during packaging precludes the possibility of high deployment-to-package volume ratios (approximately an order of magnitude lower than inflation and memory type). The deployment force or leverage must be applied at several points around the packaged structure, if not for all segments individually, as compared to say, one point control for gas pressurization. This situation tends to add to weight and volume requirements. A light, rigid structure may require additional support during the launch phase; this support would be above the strength and rigidity requirements of the orbital maneuver phase.

### Conclusion

The mechanical technique presents few major variables and problems in analyzing deployment and in testing, and although possessing low deployment-to-package ratios, it appears quite feasible to package a 30-foot aperture, space erectable reflector within the volume restrictions. The reflector

surface tolerance requirements imposed by an X-band frequency also appear quite feasible.

## MEMORY TECHNIQUE

### Definitions

This system consists of structural materials which possess some type of memory and which can be activated by a simple mechanism, at least in application. Materials of this type are high modulus materials and molecular distortion materials. The high modulus materials, such as fiber glass, are simply bent into a packaged configuration of almost any shape. Depending upon the use of a grid pattern, the diameter of the fiber glass strands, the type of plastic and metallic coatings, and the minimum bend radius, this material can match or better inflatable deployment-to-package ratios. The deployment mechanism consists of removing the packaged restraint and allowing the memory of the material to deploy the reflector.

Two molecular distortion materials which hold promise are NiTi and crosslinked polymers and copolymers such as polyethylene. The former material must be formed and heat-treated (approximately 500°C) in the desired configuration to implant the memory. Packaging consists of bending the material structure at room temperature into some feasible package configuration. Care must be exercised so that the minimum bend radius is not exceeded. Deployment is accomplished by applying heat so that the temperature of the material rises above room temperature. The speed and force of the deployment reaction are functions of the amount of work applied in packaging and the rate of the temperature rise of the material. The material exhibits almost no spring-back from a packaged position because the material, as soon as it is distorted after being stabilized, begins an intermetallic transformation from one metallic phase to another. This transformation is reversed by heating. The latter material, polyethylene, is formed into the desired shape, irradiated by gamma rays, heated to approximately 140°C, and, depending on the degradation of any metallic coating allowed, can be squeezed into a solid block of any shape and cooled. The package configuration requires no restraining mechanism. Deployment is accomplished by reheating (140°C), which melts the crystalline structure; the crosslinked molecular structure, which was distorted during packing, is permitted to assume its original position, i. e., the desired reflector structure.

### Advantages

The deployment-to-package volume ratios are among the best of all

techniques considered. The more compact the structure, the less tendency there is for the need of additional support during launch. Polymers and copolymers are easily formed at low temperatures ( $140^{\circ}\text{C}$ ) before irradiation. The deployment mechanisms show promise of being very simple and reliable. For instance, the heat could be applied to NiTi and polyethylene by electric current through the NiTi and by implanted wires in the polyethylene (assuming proper use of thermal control coatings). Single, one-piece construction lends itself to improvements in weight and reliability requirements.

### Disadvantages

Tooling for the fabrication of a one-piece, 30-foot structure is cumbersome. Development of the material physical characteristics and fabrication methods is considered to be in a rudimentary stage. The estimated time required to make this technique equal in development with mechanical techniques, for example, is at least two to four years. The ability of these techniques to attain and maintain X-band frequency surface tolerances for a structure of this size is doubtful at this stage of development.

### Conclusions

This technique lacks the development necessary to evaluate its merits properly. However, the potential is promising for packaging efficiencies, possibly higher rigidity for less weight, and simpler, more reliable deployment mechanisms than any of the techniques under consideration.

## HYBRID TECHNIQUE

### Definition

This system consists of combinations of two or more of the previously described techniques of both deployment mechanisms and material applications. The main hybrid types are rigid rib, expandable truss rib, high modulus flexible rib, and inflatable rib. All of these erected antennas are somewhat similar to an umbrella structure possessing ribs upon which a flexible grid of a metallized covering is attached under slight tension in deployment, thus forming the reflector surface.

The rigid rib structure is packaged by folding the ribs (either radially or helically) about their base hinge line. The extreme tips of the ribs move in a vertical or horizontal arc toward the symmetrical axis of the reflector, and the reflective material is stowed in a convenient fashion about the ribs. Deployment is caused by opening the ribs about their base hinge line until a posi-

tion is reached where the inner edge of a rib represents a line on the surface of the desired reflector with the reflective grid material stretched out between lines.

The expandable truss rib is a two-dimensional truss with hinge joints. The truss pattern may be visualized by placing a series of X's side-by-side with their ends jointed together. Three-dimensional stability is gained by joining the radial truss pattern with a similar truss pattern in the tangential direction at various radial distances. This truss can be compressed for packaging in an inward radial direction by expanding one end of the truss system, which is analogous to opening a pair of multi-hinged scissors. The flexible reflective material is attached to the end of each element of the truss on one side of the truss system in such a manner that when the truss is expanded, the reflective material assumes the proper reflective shape.

The high-modulus flexible rib system is similar in general form to the rigid rib type. The flexible rib is simply bent in an inward radial direction along with its reflective material covering and restrained in an appropriate manner for the packaged condition. The general rib shape may be radial or helical, thus lending itself to compact packaging by being bent in the tangential as well as the radial direction.

The inflatable rib structure is formed by gas pressurization of a series of long thin self-rigidizing bladders joined at specific points. This structure can be fabricated such that in a deployed condition almost any geometrical shape can be formed as the backup structure for the attached flexible reflective material. Packaging consists of folding the flexible bladders and reflective material into a suitable shape.

### Advantages

The main advantages of this technique are the extremely low structure weight-to-aperture-size ratios, the simplicity of the deployment mechanism, and the deployed-to-packaged volumes ratios which, on the whole, are comparable to inflatables.

### Disadvantages

Since the reflective surface is attached to the backup structure only at specific points, the reflective surface is made up of a single curved surface which only approximates the double curved surface desired. Also because discrete attachment points are the rule, the gross structural rigidity is rather low. Any creep exhibited by the reflective material, connecting the ribs and under slight tension, could easily cause permanent distortion of the reflective surface.

## Conclusions

Although this technique has distinct advantages, there is a poor possibility of attaining and, especially, maintaining a structure of this size considering the X-band frequency, reflector surface tolerance.

## SELECTED ANTENNA REFLECTOR CONCEPT

Overall study of all the foregoing suggests that the mechanical technique consisting of a segmented (or petaloid), rigid reflector structure which can be deployed in a hinged configuration offers the best probability of achieving the required performance characteristics within the expected time span of the ATS-4 spacecraft launch schedule.

## MECHANICAL AND STRUCTURAL CONSIDERATIONS

### Reflector

The parabolic surface will be an assembly of petal sector subassemblies, each consisting of two triangular and one trapezoidal petals. Twenty-four petal sector subassemblies are contemplated. The shape of each petal is a true, double-curved, radial segment of a paraboloid of revolution. The petals are connected by curved hinges uniformly spaced along the petal edges and by hinges attached to the hub at the base of the trapezoidal petals, so that the composite structure of petals and hinges approaches the equivalent of a one-piece paraboloid (see Figure 11-1). This particular concept was originally proposed by the Goodyear Aerospace Corporation.

The parabolic surface, which can be manufactured from a honeycomb structure, will be formed into a lattice network approximately 80 percent open in order to minimize weight and thermal distortions. The cutouts reduce the reflector to radial legs (some of which contain the side petal hinges), circumferential concentric rings (hoop members), and diagonal members which are added for truss stability. A light-weight RF reflector screen will span the open areas of the reflective structure in order to optimize the weight and solar energy transmission. Titanium is being considered as a material for petal (aluminum core) honeycomb face sheets and the reflective screen because of its high modulus of elasticity and low thermal expansion coefficient.

Packaged (Launch Phase) — The petals will be designed with a flexural stiffness which will permit the petals to be flattened (inducing a state of stored energy) without inducing a high percentage of the allowable yield stress in the

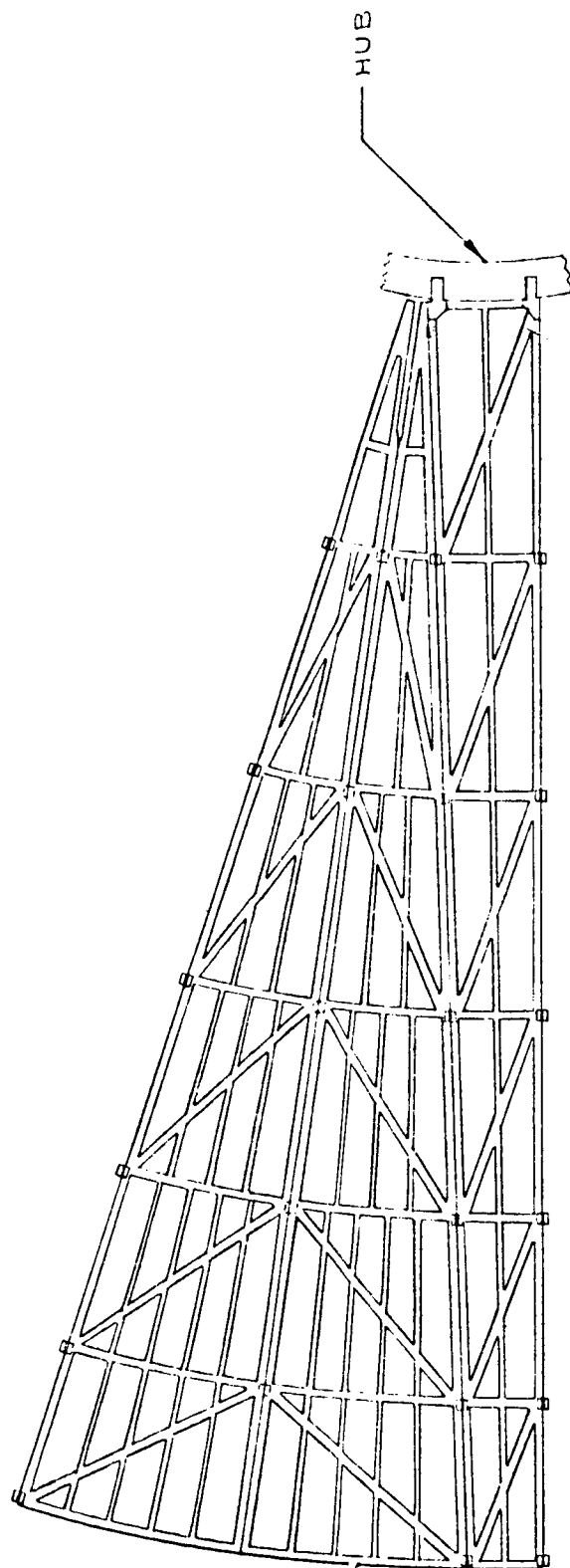


Figure 11-1. Subassembly petal sector.

petal material. This situation will permit the curved hinge lines to become straight-line elements and, in turn, permits an accordion-like folding of the reflector structure. Thus the paraboloid is transformed into a cylinder of a height approximately equal to the length of the petals for the packaged configuration (see Figure 11-2). The folded petals will be banded together and snubbed to the feed support structure to optimize available structural restraints and stiffness during the launch environment.

It appears that the vibrations at launch will, in general, produce the critical design accelerations of the structure. Reflector loads due to longitudinal and lateral vibration and steady state conditions result in concentrated loads at the petal-hub hinge lines. This condition may necessitate the use of reinforced petal material in this area in order to withstand the critical beam-column condition. Petal loads due to centrifugal forces originating from the spin condition appear to be less critical than those present from lateral vibration. Design of the hub ring at the base of the petals is also believed critical since it redistributes the petal loads to the aft equipment module and must have sufficient stiffness to prevent large dynamic coupling between the antenna and the spacecraft during launch. The stowed reflector must be designed with careful consideration to provide adequate resonant frequency separation from the adjacent structure in order to avoid dynamic coupling.

Deployment — A system of deployment trusses will be used to exert an outward radial force to move the petals in radial arcs about the central hub from the packaged to the deployed parabolic state. Each petal subassembly sector is actuated from the rear of the reflector to minimize RF blockage. The outer attachment point of each truss is tied to the hinge-line midpoint of the triangular panels of each sector. The attachment is made by single member links connecting the outboard end of the trusses to accommodate the change in hinge-line length from the folded petal to the deployed contour as well as to provide freedom for radial thermal expansion (see Figure 11-3).

The folding of the reflector petals induces strain energy in the petals and petal hinge-lines. The release of this stored energy must be closely controlled during deployment by providing a slow rate of excursion of the petals. During deployment, the design loads for the petals and deployment trusses and mechanisms occur near the end of the actuator stroke from the force (in the order of three pounds) required to snap through the petals (i. e. forming a double curved surface). These loads are considered to be within design capability.

One proposed actuating device under evaluation uses a single motor to power a continuous chain drive which transmits torque through sprocket pulleys attached directly to a worm gear which, in turn, drives a segment of a wheel gear rigidly attached to each deployment truss. The worm gear in this design,

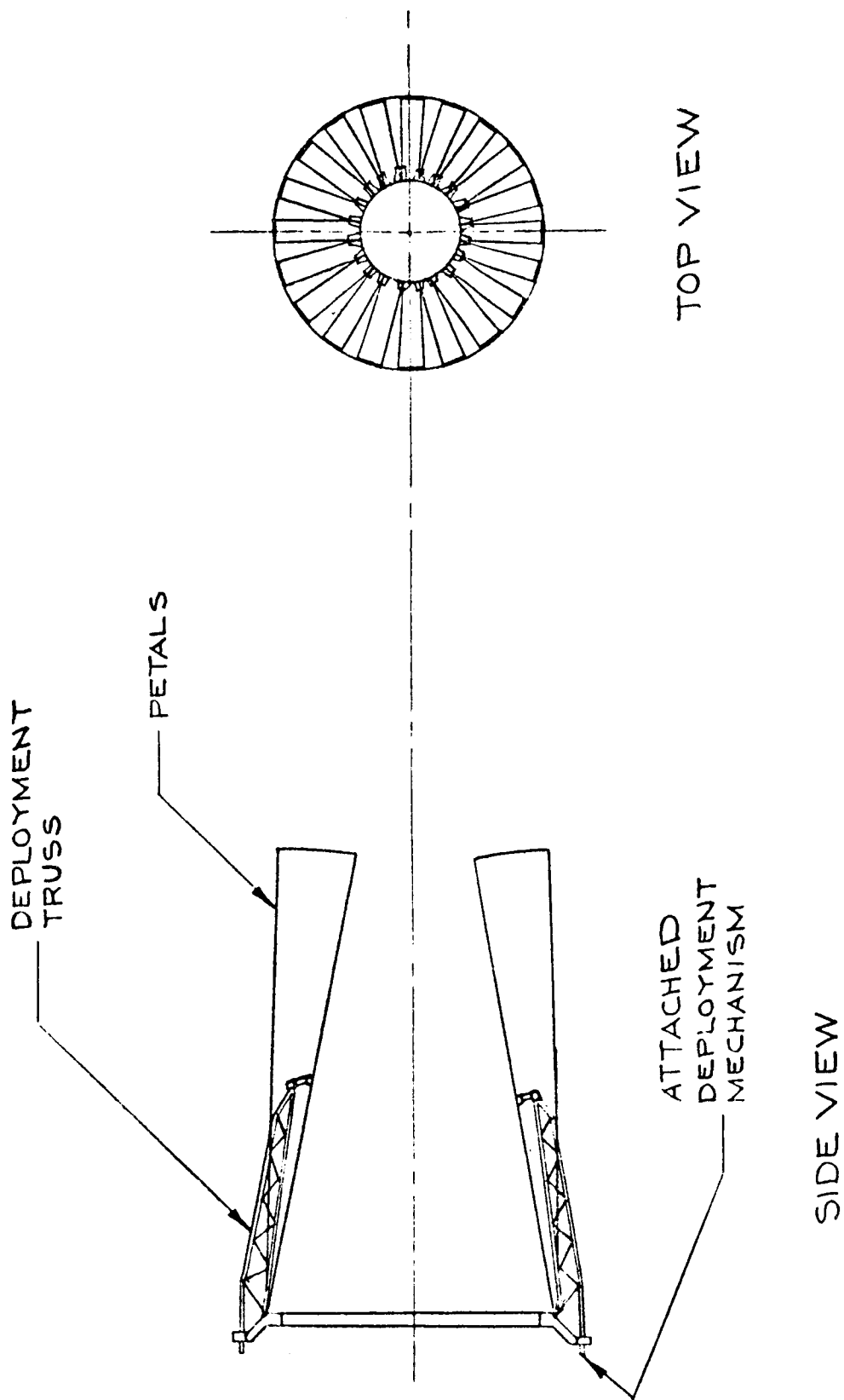


Figure 11-2. Packaged configuration.

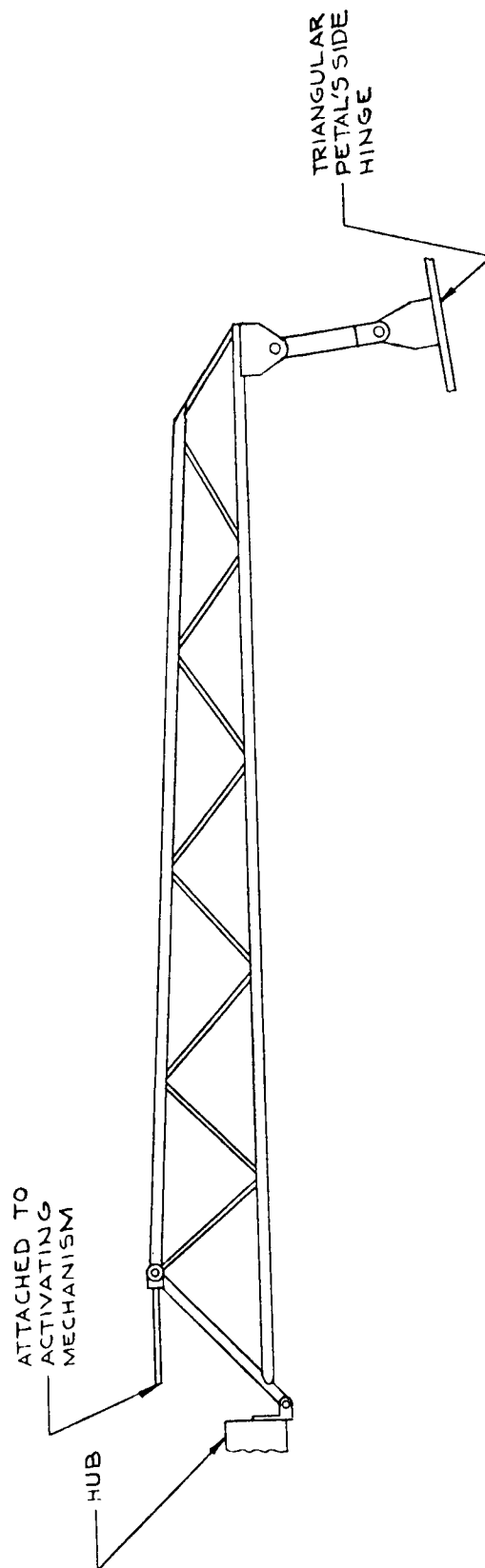


Figure 11-3. Deployment force transmission truss.

as in the first design previously mentioned, acts as a brake during the snap through of the petals and contributes to a controlled rate of deployment. If any petal subassembly sector or its associated individual deployment mechanism should begin to lag behind other sectors, the deployment torque will be reduced automatically for the advanced sectors and torque will be concentrated progressively on the retarded sector. Redundancy may be obtained with minimal addition of weight and complexity by installing a second motor, chain drive, and sprockets mounted on an extension of the original sprocket shaft.

Deployed (Orbital Phase) — Orbital control impulses do not appear to introduce any significant stresses in the reflector design because of its dynamic response, which considers only negligible structure damping. The calculated fundamental frequency of two Hz or greater for the reflector should avoid any strong coupling with the satellite control system. Uneven solar heating of the deployed reflector will produce thermal gradients causing thermal stresses in the hoop members and significant distortions in the structure. However, it is believed possible through proper design to restrict distortions of the reflective surface to highly localized areas, such as the periphery of the reflector, to approximately  $\pm 0.25$  inch. The thermal analysis of the reflector is discussed in Section 15.

Deployed (Ground Test) — Analysis has indicated that with proper design consideration for areas of locally high stresses, this design, in the deployed mode, will permit accelerations as high as 1.5 g's without failure. This capability should permit full-scale testing of the deployed antenna without the necessity of resorting to excessive fixtures.

## FEED SUPPORT

### Strut Type Structures

Two feed support structural approaches are under consideration. The first (shown in Figure 10-1, Section 10) consists of a set of six tubular struts which forms three V's. These are symmetrically located on a truncated right cone in such a way that each two neighboring V's are joined at one end. With the assumption of a 350-pound load supported at one end, the preliminary study has shown that six-tube beryllium struts are sufficiently strong to pass the structural dynamic tests as required by the specification. The length of each tube is about 15 feet. It is estimated that the weight of the support structure, including the end pieces, is 70 pounds.

The length of the tubes might be reduced by use of a composite-type support such that the main tubular truss which is adjacent to the base is

attached to a much slimmer truss which supports the feed and experiment package. The virtue of such a composite system is that substantial reduction in RF blockage could be obtained. If fiber glass is considered instead of high strength metal, attention must be paid to the fact that fiber glass tubes could act in a waveguide mode.

#### Low-Dielectric Foam Cone

The second feed support structural approach under consideration is a low-dielectric foam cone. The principal advantage of this approach is that the material is essentially transparent to RF energy. Successful preliminary axial and lateral flight level vibration tests were completed on December 2, 1966 involving a one-fifth scale structural model of a reinforced, low-dielectric foam cone. The truncated cone was designed to support the feed and experiment packages for a 30-foot-diameter antenna using a scaled 200-pound tip mass. This test was performed in the GSFC Test and Evaluation Division vibration chambers.

Calculations have shown that lateral vibration is by far the most critical structural dynamic test of the three dynamic loadings (axial, lateral, and torsional) for this cone configuration. The lateral resonant frequency was found to be approximately 40 Hz. The cone structure successfully passed the resonant frequency with a 5-g input with a tip amplification factor of 16. The axial test was also performed. The frequency in both tests ranged from 0 to 3000 Hz. The reinforcements included 1-mil fiber glass cloth on each side of the 0.6-inch-thick cone and eight diagonal cables (which correspond to 1/4-inch diameter cable 15 feet long for the full scale spacecraft). The dielectric constant of the foam was slightly higher than unity, and its density approximately 4 pounds per cubic feet.

#### REFLECTOR RF FEEDS

##### FREQUENCY CONSIDERATIONS

The choice of frequencies for the antenna was one of determining those frequencies most advantageous in terms of information, future technology applications, experiments, and versatility. The development of the engineering technology for deploying large-aperture antennas (30-foot diameter) in space to provide high directivity and gain is of first order of importance. Hence, microwave frequencies are most significant in this respect. More specifically, 8 GHz (receive) and 7.3 GHz (transmit) were chosen since this was the highest frequency capability considered achievable, consistent with a practical 30-foot-diameter spacecraft antenna reflector.

Having selected the 8-GHz frequency band, it was considered important and necessary to choose an additional frequency to (a) allow the capability of commanding, upon reception of a coded signal from earth, the entire spacecraft to point in the vicinity of a given or desired ground station in terms of gross directional alignment, and (b) compare the performance of the 30-foot reflector surface at a frequency other than X-band. The frequency range which most readily lends itself to these requirements is 400 MHz. This frequency, when used in conjunction with a 30-foot parabolic reflector and a monopulse-type system, produces an earth disk coverage sum-difference pattern. The sum pattern is approximately 6 degrees wide at the 3-db beamwidth, and the difference pattern extends to either side of the boresight axis. The total angular coverage for accepting earth station commands produced by this sum-difference pattern configuration is nearly 20 degrees. This angular coverage allows the spacecraft to acquire any station on the earth's disk. It should be noted that vernier alignment of the 8-GHz beam for communication with earth should be achieved through a monopulse system incorporated in the 8-GHz feed system design.

The following table summarizes the frequency characteristics of the 30-foot-diameter parabolic reflector.

Freq. /Dia	$\lambda$ (cm)	BW <sup>0</sup> (3 db)	Gain(db)
0.4 GHz/30'	75	6.0 <sup>0</sup>	27
8 GHz/30'	3.75	0.3 <sup>0</sup>	50

## OPTICAL GEOMETRY FOR RF FEED POSITIONS

### Reflector Focal Length to Diameter Ratio (F/D)

In choosing a F/D ratio, a trade-off must be made to best accommodate the overall feed system performance. The effect on system performance as a function of F/D ratio is summarized in the following general comments.

- a. The larger the F/D ratio, the flatter the parabolic surface curvature of the reflector.
- b. Small F/D ratios allow a more compact configuration because the focal point is closer to the reflector.

c. A small  $F/D$  results in a more curved reflector surface and hence greater loss of energy from polarization losses.

d. For beam scanning purposes, the smaller the  $F/D$  ratio, the smaller the required off-axis primary feed displacement for a given angular beam scan. But, the amount of beam scan is much more limited because the secondary beam deteriorates (gain, beamwidth, secondary lobe level) at a greater rate than for large  $F/D$  ratio configurations.

e. With respect to the Cassegrain optics configuration, the greater the  $F/D$  ratio, the greater the subreflector distance becomes from the parabolic reflector vertex. For a given  $F/D$  ratio, the closer that the subreflector is brought to the vertex of the parabolic reflector, (i. e. to make a more compact configuration) the greater the subreflector diameter becomes. The greater the subreflector diameter, the greater the energy blockage becomes. Structurally, the smaller the  $F/D$  ratio (i. e., RF the feed system is closer to the vertex of the reflector), the more rigid and light weight the feed support structure can be made.

With consideration given to all the parameters mentioned, it has been decided to fix the  $F/D$  ratio at 0.5 as a good compromise.

#### Cassegrain Versus Prime Focal Point

The decision to design the antenna system around the prime focus feed rather than the Cassegrain feed is based on the following factors: (a) it is desirable to allow the full structural surface tolerance to be allotted to the parabolic reflector rather than to divide the tolerance between the subreflector and parabolic reflector, (b) the reliability of the system would be degraded in the Cassegrain system because of the three body misalignment problem's feed-subdish misalignment-main reflector misalignment as opposed to only a primary feed-main reflector misalignment in the prime focus feed geometry, (c) a subreflector by the nature of its size for this configuration (6 to 9 feet in diameter) presents more of an RF blockage problem, (d) more data and characteristics on scanning prime focus feed are available than on Cassegrain feed, and (e) an additional alignment problem exists when using a subreflector.

#### Secondary Beam Scanning Considerations

The synchronous satellite presents an earth-satellite geometric arrangement (23,000 miles altitude) which results in a 17-degree, included angle intercepted by the earth's disk. Although this angle is relatively small in terms of an antenna pattern beamwidth, for consideration in monopulse operations it is considered excessively large in terms of off-axis scanning of the secondary

beam of a parabolic reflector. But, if the included angle intercepted by the continental United States is considered (approximately 7 degrees in the East-West direction and 3.5 degrees in the North-South direction), it is seen to be within the state-of-the-art for scanning the secondary beam of the 30-foot-diameter reflector. Therefore, it is proposed that the X-band feed of the large aperture antenna possess the capability to scan the continental United States and/or maintain communication (transmit and receive) between any two stations within this scan limit. To scan the secondary beam of the parabolic reflector when fed at the prime focal point, it is necessary to displace the RF feed center-of-phasing from the reflector axis. This can be accomplished either mechanically or electrically (array).

#### Energy Illumination Taper on Reflector

When the primary feed is directed off-axis, part of the illuminating energy which is normally available for the on-axis condition is spilled over the edge of the dish. It is desirable to minimize this spillover loss when scanning; hence, this situation suggests that larger taper (lower energy level at the reflector periphery) be used to illuminate the reflector on-axis. This results in a small degradation of the on-axis beam gain, a slight increase in beamwidth, and lowering the sidelobe level since the dish is no longer optimally illuminated (i. e. 10 to 12 db points on the periphery of the reflector). But this lower energy level at the periphery and higher energy concentration in the center area of the reflector permits a greater off-axis scan to be realized before the secondary beam is degraded to an unusable degree.

### PROPOSED RF FEED CONFIGURATION

#### X-Band System(Monopulse and Communication)

As was previously mentioned, the scanning of the secondary beam is accomplished by displacing the center of phasing of the primary feed from the axis of the parabolic reflector. This can be accomplished either mechanically or electronically. With an  $F/D = 0.5$ , it is necessary to displace the feed off-axis approximately  $\pm 1$  foot in one plane (roughly equivalent to East-West coverage of the US from synchronous altitude with a 30-foot-diameter reflector at 8 GHz) and approximately  $\pm 1/2$  foot in a direction normal to the above direction (roughly equivalent to North-South coverage of the US under the conditions previously stated.) In summary; this corresponds to  $\pm 12$  beamwidths (3 db) in the East-West scan and  $\pm 6$  beamwidths in the North-South scan. Figure 11-4 shows feed scan angle in terms of beamwidths with respect to the off-axis position of the feed center-of-phase.

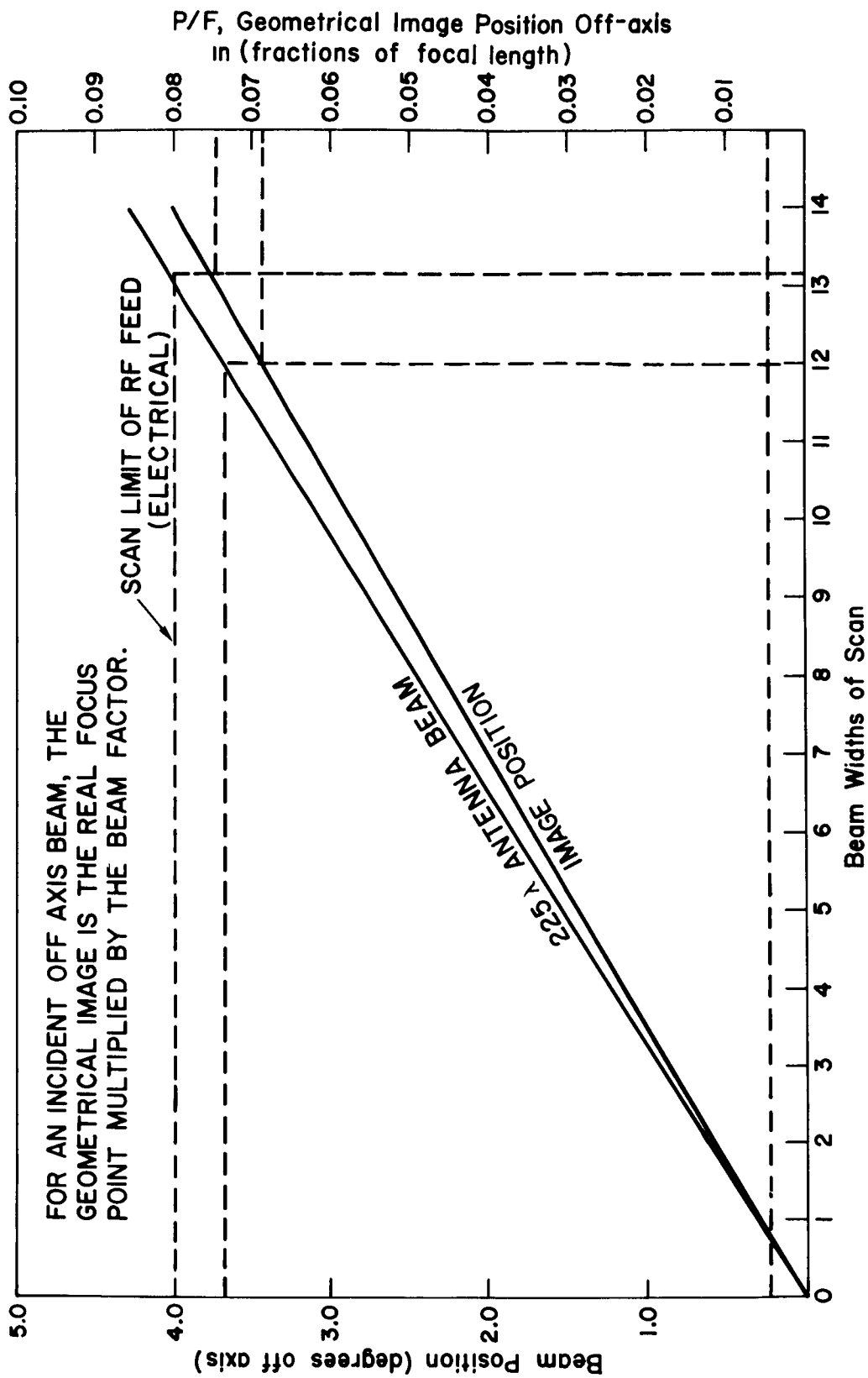


Figure 11-4. Beam widths of scan.

The data for scanning the secondary beam of a large aperture reflector antenna greater than a few beamwidths off the reflector axis were limited and questionable. To assess this area of technical uncertainty more carefully, it was necessary to consider all the variables concerned (i.e. illumination taper, diameter/frequency ratio, focal length/diameter ratio). Therefore, a computer program for the ATS-4 antenna system was established.

Using Figure 11-4 for a  $225-\lambda$  antenna reflector with an F/D ratio of 0.5, the relative position of the pattern for two adjacent stepped beams can be determined. The field patterns were computed assuming the total aperture was composed of N elements spaced  $\lambda/2$  across the aperture. This resulted in the summation

$$n = N$$

$$F = \sum_{n=1}^N A_n e^{j\phi_n};$$

$$n = 1$$

where  $A_n$  = amplitude of  $n^{\text{th}}$  radiating element with a given taper,

$$\text{and } \phi = KF \left[ \left( \frac{P^2}{2} \right) X^2 + \left( \frac{P}{4} - P^3 \right) X^3 \right],$$

where P = the angular displacement of the feed in radians, and

X =  $\pm$ limits of linear displacement from the parabolic axis, which is a function of the F/D ratio.

The patterns in Figure 11-5 represent the on-axis computed pattern, the first beam off-axis, and the pattern equivalent to that of the 12th beamwidth off-axis using the foregoing criteria. The validity of the computed field patterns was established by comparing the 12th beamwidth computed pattern with the measured pattern (see Figure 11-6). A 1/5-scale model was used to measure patterns. The desired scan of  $\pm 12$  beamwidths in one direction and  $\pm 6$  beamwidths in the orthogonal direction will be implemented using a hybrid configuration. The larger scan requirement will be accomplished using a digital, electronically scanned array. The array will consist of 32 horns which are excited in adjacent pairs to properly illuminate the edge of the reflector at the -20 db points of the primary feed patterns. To scan one step off-axis so that the adjacent secondary beam crosses over at or near the -1 db points, it is necessary to use one of the first pair of adjacent horns, thus forming another prime feed

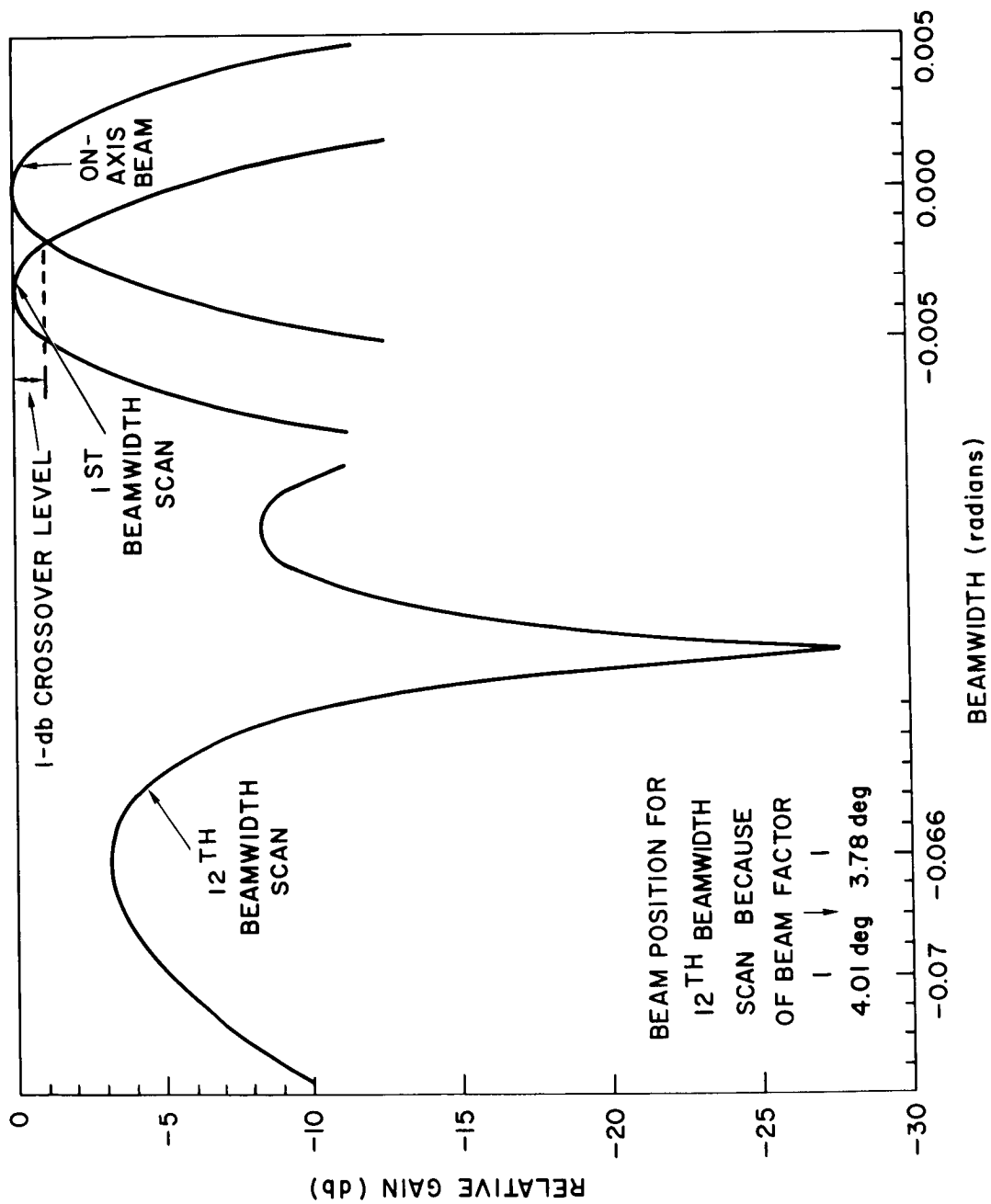


Figure 11-5. Beam crossover level (db) for 1st beamwidth scan & 12th beam for 30 foot parabolic reflector.

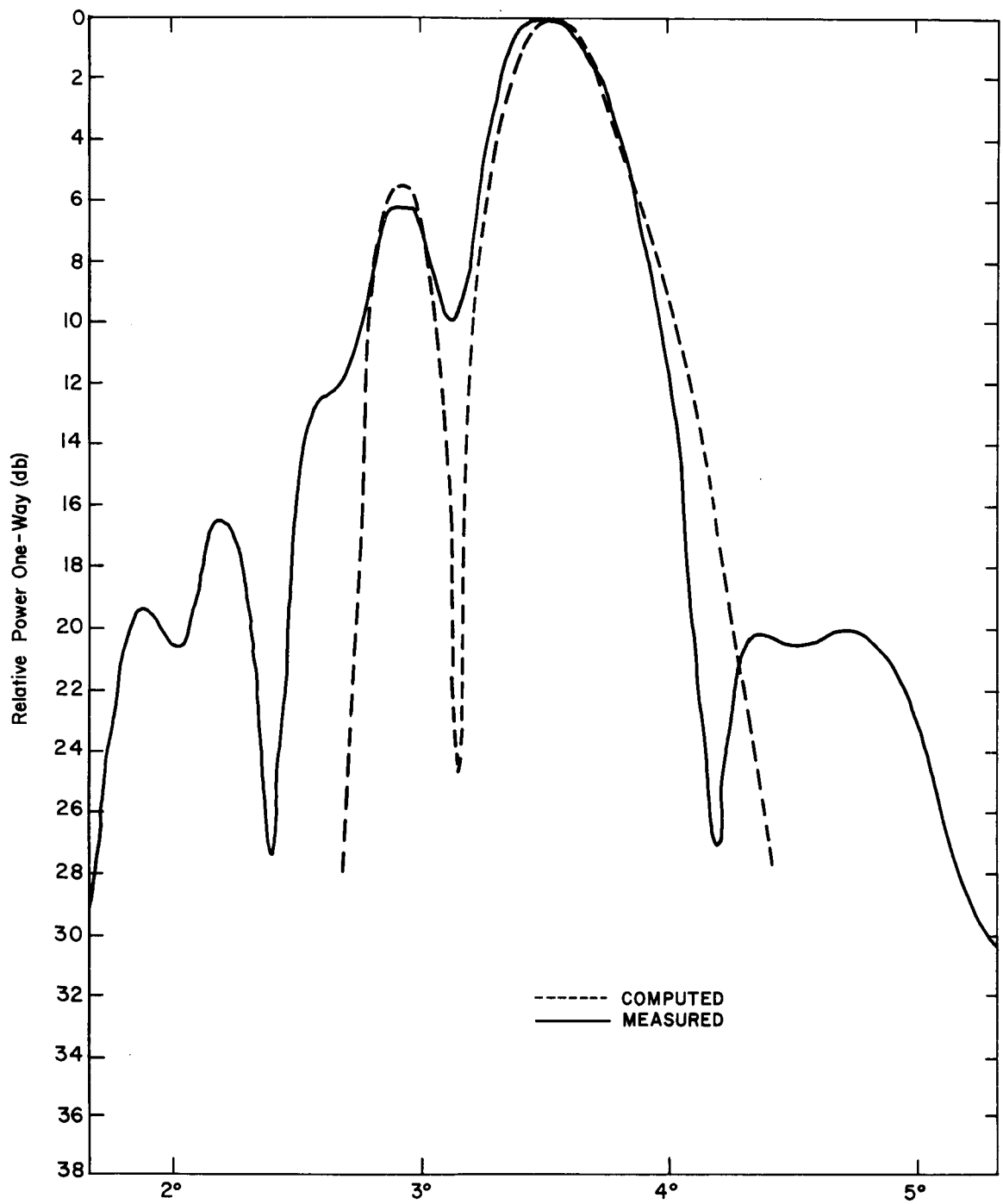


Figure 11-6. Computed and measured pattern comparison (12th beamwidth of scan).

array of two adjacent horns. This process of digitally stepping one horn at a time while maintaining two horns excited at one time continues through to the full scan of  $\pm 12$  beamwidths. Figure 11-7 shows this stepping technique. It should be noted that the central pair of horns are subdivided into a total of four subapertures. These are used in conjunction with a monopulse system in addition to forming part of the electronic digital scan for beams 15, 16, and 17 as shown in Figure 11-8. All switches and circulators are of the ferrite type requiring no holding or biasing power during RF operation. Where latching is used in the ferrite switches, the only switching power required is that which is necessary to place the ferrite device in either of two states. Characteristics of the ferrite devices intended for use in this system are listed in Table 11-1. To allow scanning the secondary beam  $\pm 6$  beamwidths in a North-South direction, a mechanical scan is provided. Figure 11-7 reflects the basic design technique and components required to physically move the feed system upon command. Basically, this mechanical drive system consists of two lead screws turned by a stepped motor-driven gear. The 32-element, electrically scanned array is attached to the two lead scanner screws through threaded sleeves, causing the entire array to be moved  $\pm 1/2$  foot (equivalent to  $\pm 6$  beamwidths) off the parabolic reflector axis. To determine the instantaneous position of the feed accurately, a digital shaft angle encoder is used in conjunction with the step motor. Using a standard 6-bit shaft angle encoder will be used with a 1-foot displacement. It is planned that the full 1-foot excursion of mechanical scanning will take 5 minutes or less.

#### UHF System (Monopulse and Command)

The UHF RF feed system will be located at the prime feed focus of the parabolic reflector. Since it will operate in a monopulse as well as in a command mode, it will consist of four linearly polarized cavity antennas. Two of these antennas will be located on each side of the X-band system as depicted in Figure 11-7. It is attached to the X-band scanning system and will be physically displaced from the parabolic reflector axis when X-band mechanical scan is used. A switch will be incorporated in the sum channel of the monopulse system and will allow a transponder to be connected for command and communications purposes. This system could also be used in transmitting telemetry data.

#### RF FEED SUPPORT CONSIDERATIONS

The interaction between the radiated energy from the RF feed and the feed support structure is an area requiring further study. Normally, the RF

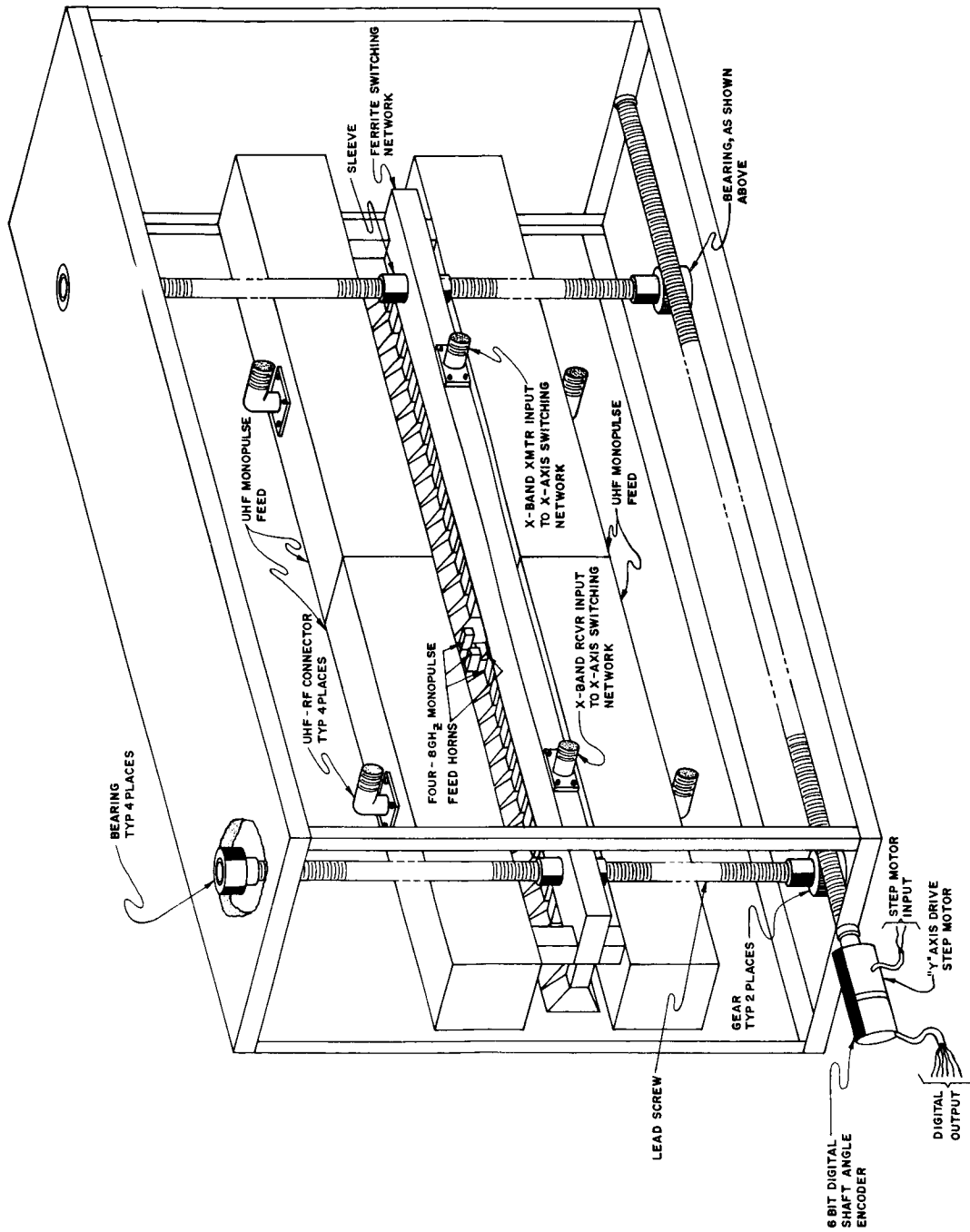


Figure 11-7. Hybrid X-band RF feed system.

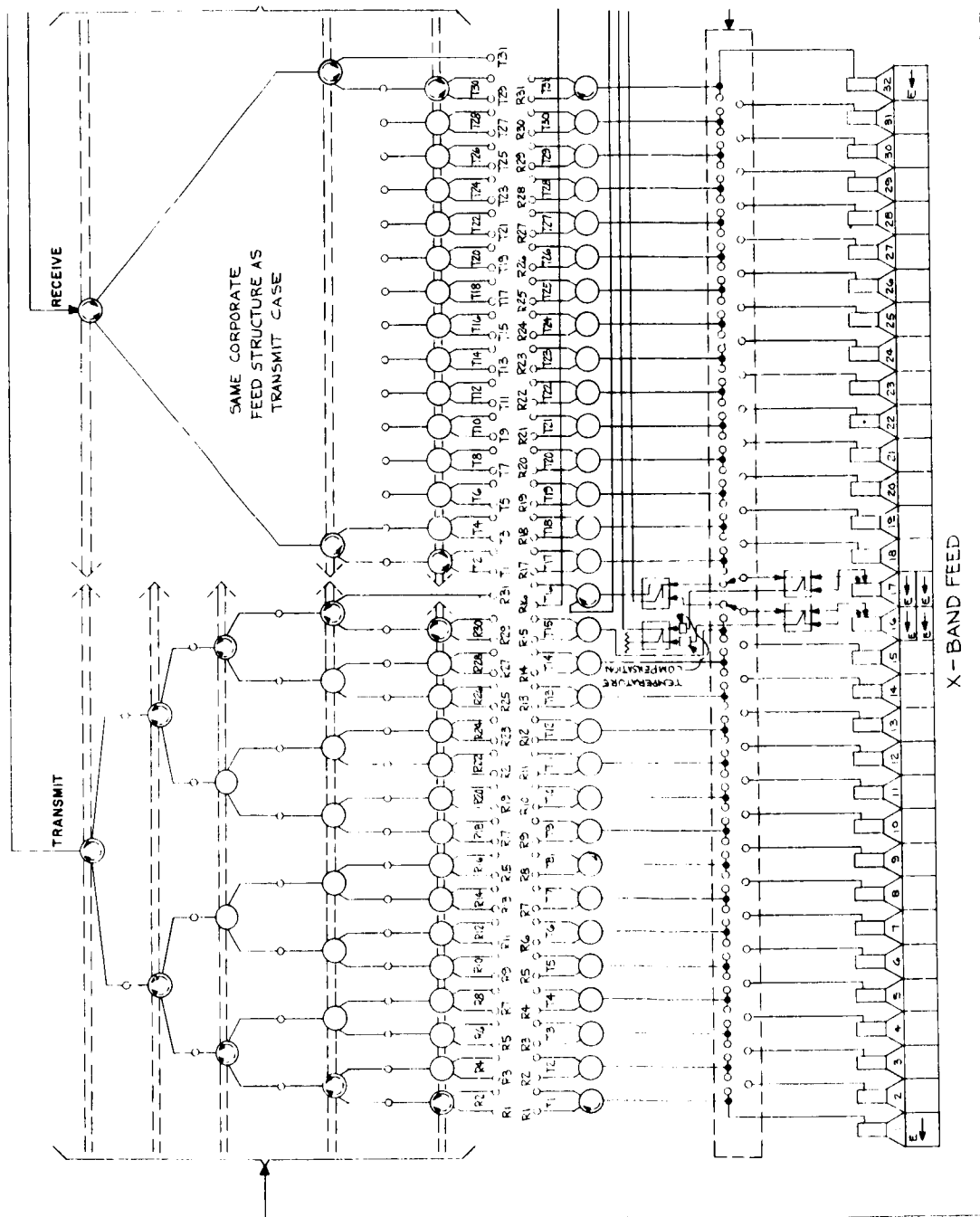


Figure 11-8. Monopulse and electronic digital scan system.

Table 11-1

Pulse-Latched Ferrite Switch Electrical Characteristics

Switch Type: AP 31 T

Frequency:  $7.3 \pm 0.73$  GHz (Xmtr) and

$8.0 \pm 0.8$  GHz (rcvr)

Insertion Loss:  $\leq 1.7$  db; 0.3 db/sw section

Isolation:  $\geq 25$  db

Power handling capability: 3 watts average

Switching time:  $\leq 20 \mu\text{sec}$

Switching rate:  $\leq 1$  KHz

Total switching energy/pole required from power supply:  $\leq 600$  microjoules

Driver supply voltage: 28 vdc  $\pm 2\%$

Trigger pulse req d:  $\pm 15$  volts nominal; 20 - sec pulse width; into 50 ohms

Driver supply current (worst case): Non-reciprocal single switching matrix

(SP 31 T) for one pulse  $\leq 750$  ma peak;

two switch matrices (transmit and receive)

simultaneously for one pulse  $\leq 1.5$  amp.

Nominal Impedance: 50 ohms

VSWR:  $\leq 1.25:1$

Phase shift (insertion phase) between adjacent switches:  $\pm 5$  degrees over

$25^{\circ}\text{C} \pm 10^{\circ}\text{C}$ .  $\pm 10$  degrees over  $-54^{\circ}\text{C}$  to  $65^{\circ}\text{C}$

feed support structures used in conjunction with a reflector are fixed so that a comparatively large angle is formed between the RF feed area and the intersection of the supports with the reflector. Under these conditions, the high level energy from the RF feed is not obstructed by the feed support when propagating toward the reflector surface. When the energy is reflected from the reflecting surface, it is intercepted by the feed supports resulting in a small area of energy blockage. Both analytical calculation and measured data are available which describe energy losses under these conditions.

Unfortunately, this information for system performance degradation does not exist for a configuration such as the ATS-4 reflector and RF feed system for the following reasons:

- a. The reflector must be folded for launching, allowing only a 6-foot to 8-foot-diameter circumference to attach the feed support into the 30-foot diameter reflector. Since the experiments package in the area of the RF feed is approximately 3 feet in diameter, the resulting feed support structure approaches a column of cylindrical configuration. Thus, the highest RF energy levels from the primary feed are intercepted by the feed supports in traveling toward the reflector and also on being reflected from the reflector.
- b. To allow relatively large scan angles, it is planned to use a higher-than-normal taper (-20 db energy level on the periphery of the reflector with the RF feed on-axis). Therefore, a higher-than-normal concentration of energy will be directed through the feed support.
- c. The X-band RF feed for the ATS-4 system is a scanning feed and therefore represents a variable interaction problem.
- d. Two widely spaced frequencies (X-band, and UHF) are being used, thus preventing the possibility of designing the feed support to accommodate one frequency (i. e. tuning).
- e. Monopulse performance degradation must be considered, particularly with respect to the difference mode slope and antenna bore-sight. Preliminary measurements recently made approximating the small-angle feed support structure problem have been made by Airborne Instruments Laboratory and General Electric. These incomplete and inadequate measurements only indicate that a greater system loss is encountered (1.5 db to 4 db loss for small angle feed supports as compared to 0.5 db to 1.0 db for wide-angle feed supports).

Because of the small feed support angle, multiple frequency operation, monopulse operation, higher primary feed energy tapers, and the scanning feed, it is planned that measurements are to be made using as near as possible the exact simulation to determine the extent of performance degradation. Configurations to be investigated will include metallic and dielectric tubular struts of various support configurations and also reinforced low dielectric materials formed into a cone housing.

## SYSTEM OPERATION

As a means for establishing the complete operational functions of the two RF systems (X-band and UHF) the following paragraphs will describe what may be typical events starting from the time at which a ground station initiates a command to point the large aperture antenna in its direction. Figure 11-9 is a functional block diagram of the two RF feed systems.

### UHF MONOPULSE

The UHF monopulse system (Figure 11-9) will provide a pointing error signal as a result of a transmission from a ground station to the spacecraft. The pointing error signal can be used to command the spacecraft to a zero error condition or it can be telemetered to the ground. For the zero error condition, the spacecraft axis will be aligned to pass through the ground station. Of prime importance in this system is that at UHF (and more specifically in the 400-MHz region) monopulse can reliably provide an error signal from a ground station  $\pm 9.5$  degrees off of the 30-foot-diameter reflector axis with a resulting pointing accuracy of 0.1 degree. This is an included angle of 19 degrees as compared to the angle of 17 degrees subtended by the earth's disk from the spacecraft at a synchronous altitude. Thus, it is possible to orient the spacecraft to the correction position even in the event that the initial programmed spacecraft orientation is in error. In addition, this system allows a re-orientation in the event that a new pointing is required within the 19-degree included angle. A switch is incorporated in the UHF system to allow a communications transponder to be placed in the system.

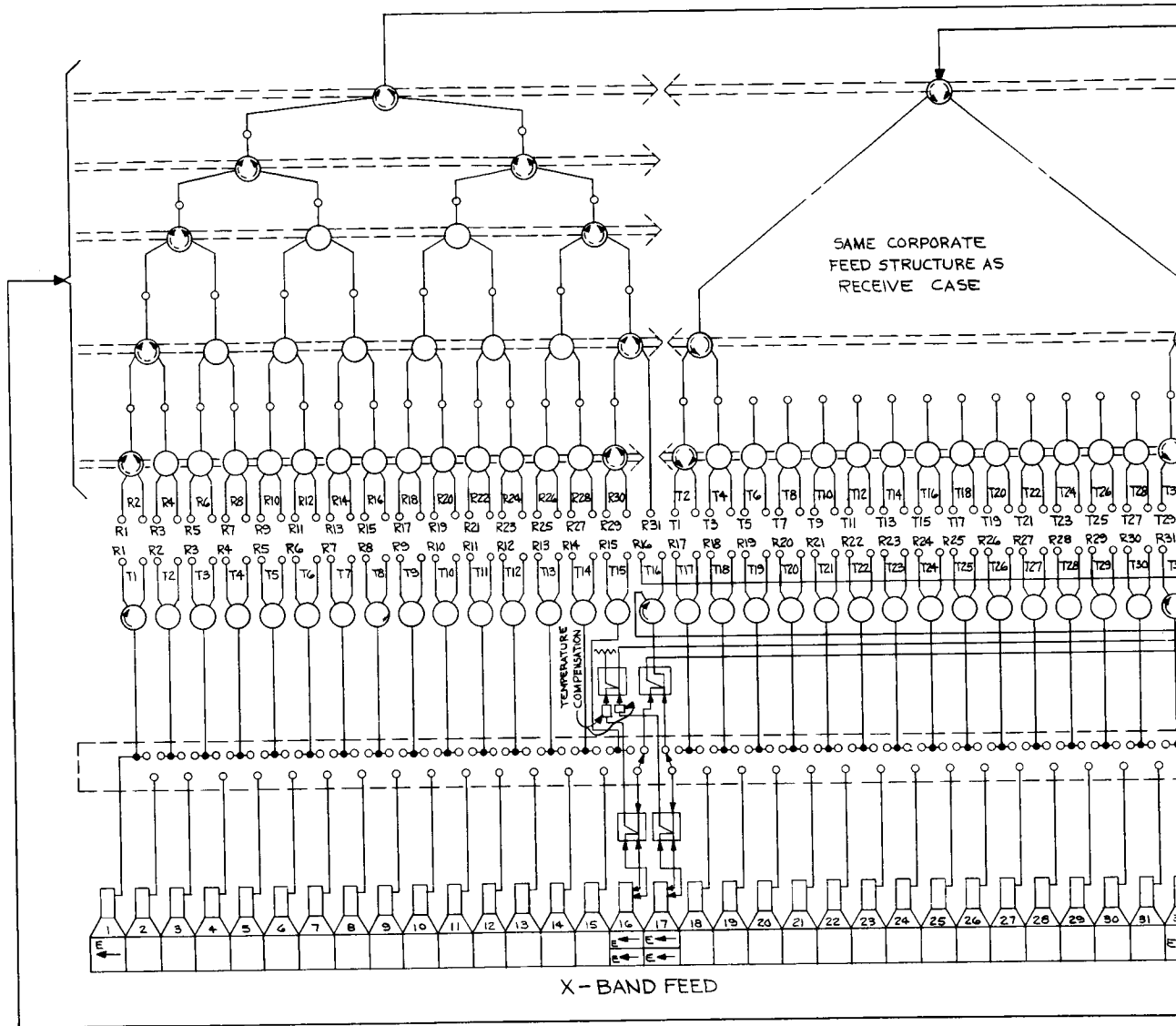
### X-BAND MONOPULSE AND SCANNING

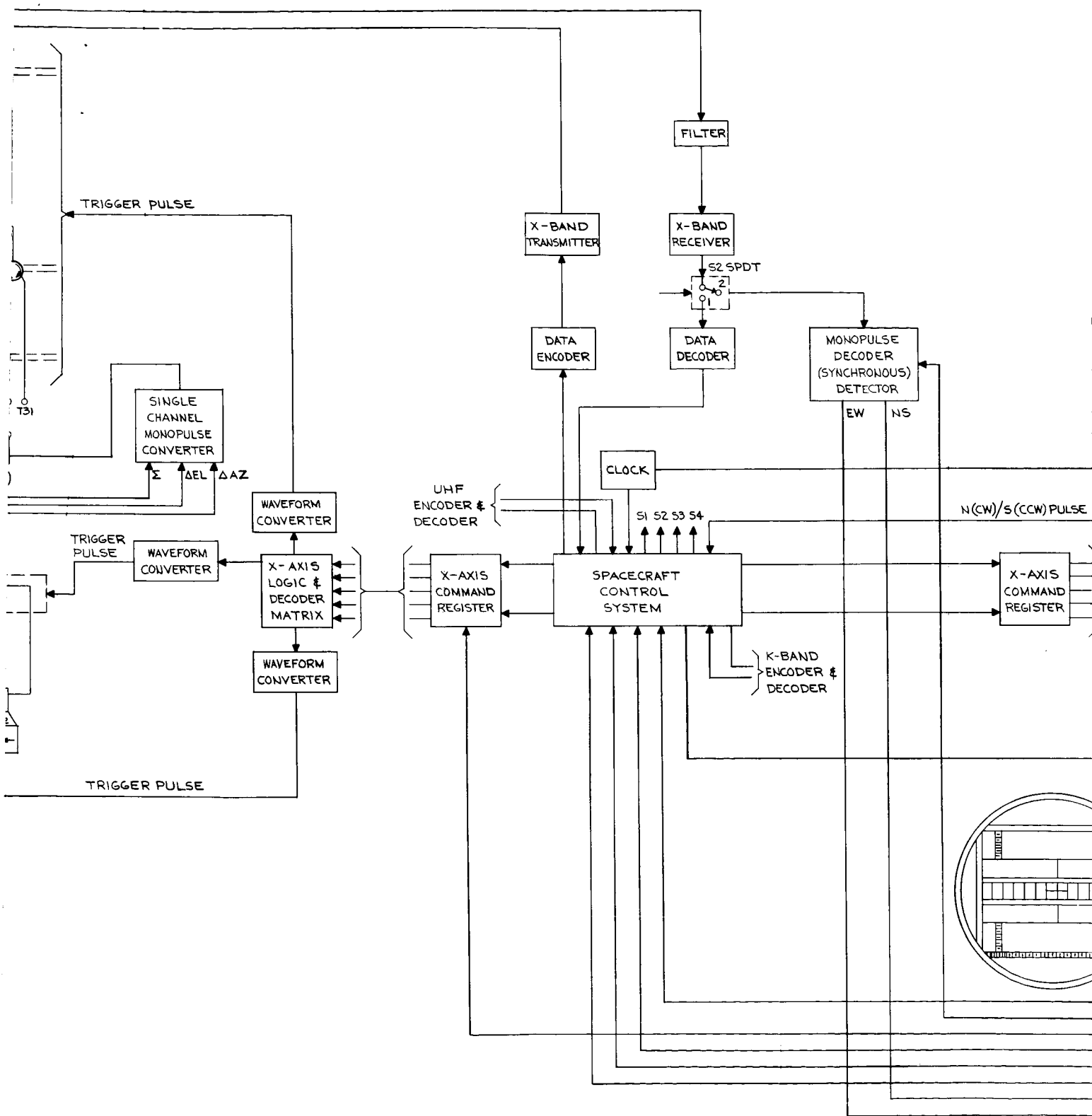
Once the spacecraft is pointing toward the specific ground station, an accuracy of 0.1 degree is achieved using the UHF monopulse system. The block diagram shows the switching arrangement to place the 3-GHz monopulse system in operation. This X-band monopulse is effective in providing error

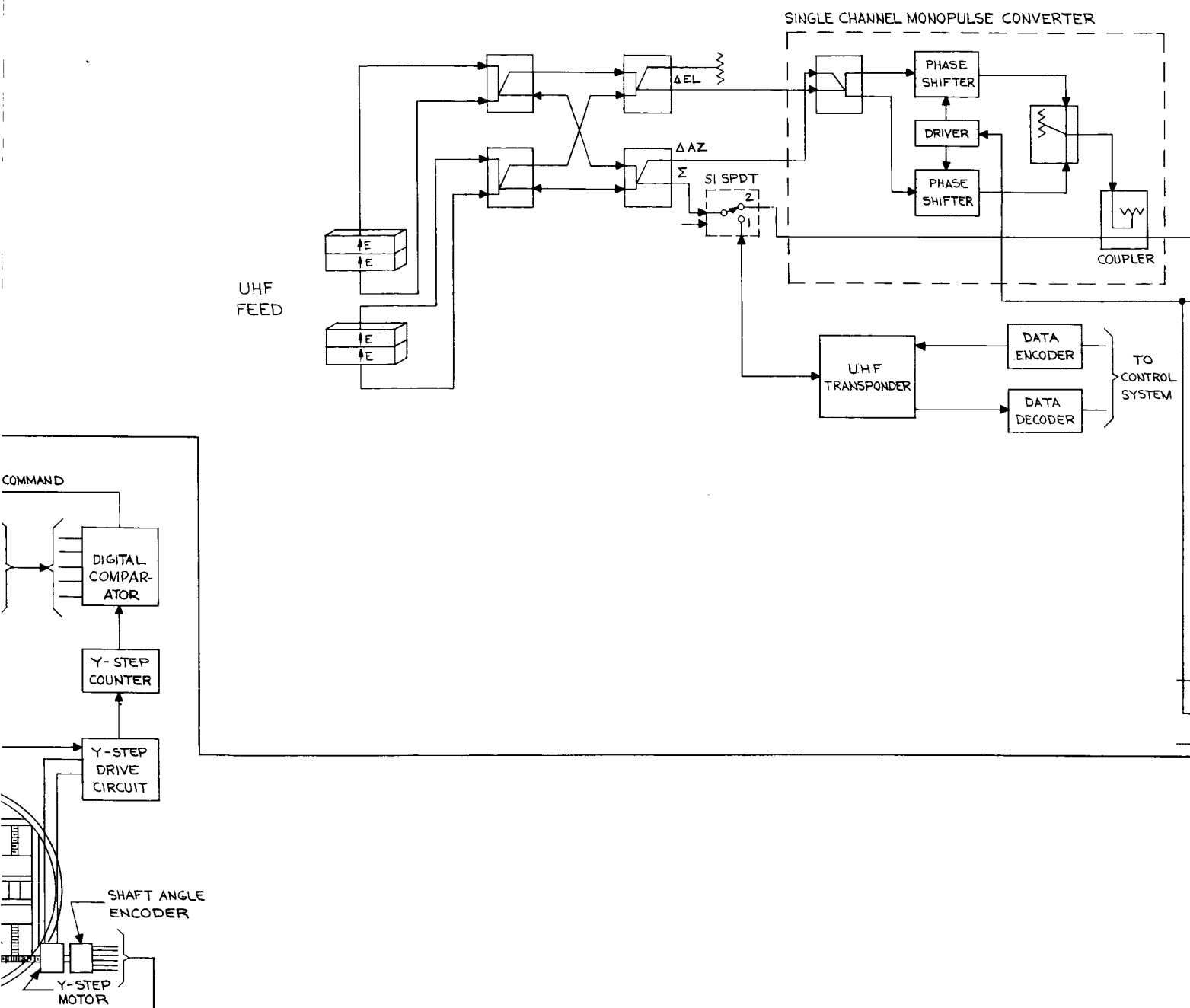
signals  $\pm 1/2$  degree off of the antenna boresight axis with a resulting pointing accuracy of approximately 0.01 degree. Note that the sum channel in the monopulse network is identical to the 16<sup>th</sup> beam of the scanning X-band feed. Referring to Figure 11-9 it will be seen that a switch is incorporated to place the sum channel in the monopulse network or the scanning X-band feed.

Upon command from the ground station, the X-band scanning system can be activated. Figure 11-8 shows the switching network for this system. This network allows simultaneous transmission and reception of energy on any two beams (except two adjacent beams which have approximately -1 db crossover levels) within the  $\pm 12$  beamwidth limit. To point a particular beam in the electronic scan mode, a command signal is initiated on the ground and received at the spacecraft. As shown in Figure 11-9, the command signal is received and sent through a decoder. This resulting signal is processed in the control system logic network where the properly coded output is sent either to the X or Y command register. The output from the command register is processed in a decoder matrix, which selects the proper switch position corresponding to the commanded beam position.

When considering communication between any two stations on the ground within  $\pm 12$  beamwidths, it is only necessary to redirect the spacecraft in yaw to align the electronic scan axis with the two ground stations. The mechanical scan allows the displacement of the electronic scan axis  $\pm 6$  beamwidths off the reflector axis and normal to the electronic scan axis. Moving ground satellite stations or aircraft may be tracked as follows. With the X-band monopulse tracking the moving ground station satellite station or aircraft, an error signal is presented to the X-band scan control system, and continuous communications can be realized. A summary of the spacecraft monopulse parameters used to arrive at the signal-to-noise ratio for the systems described is presented in Table 11-2.







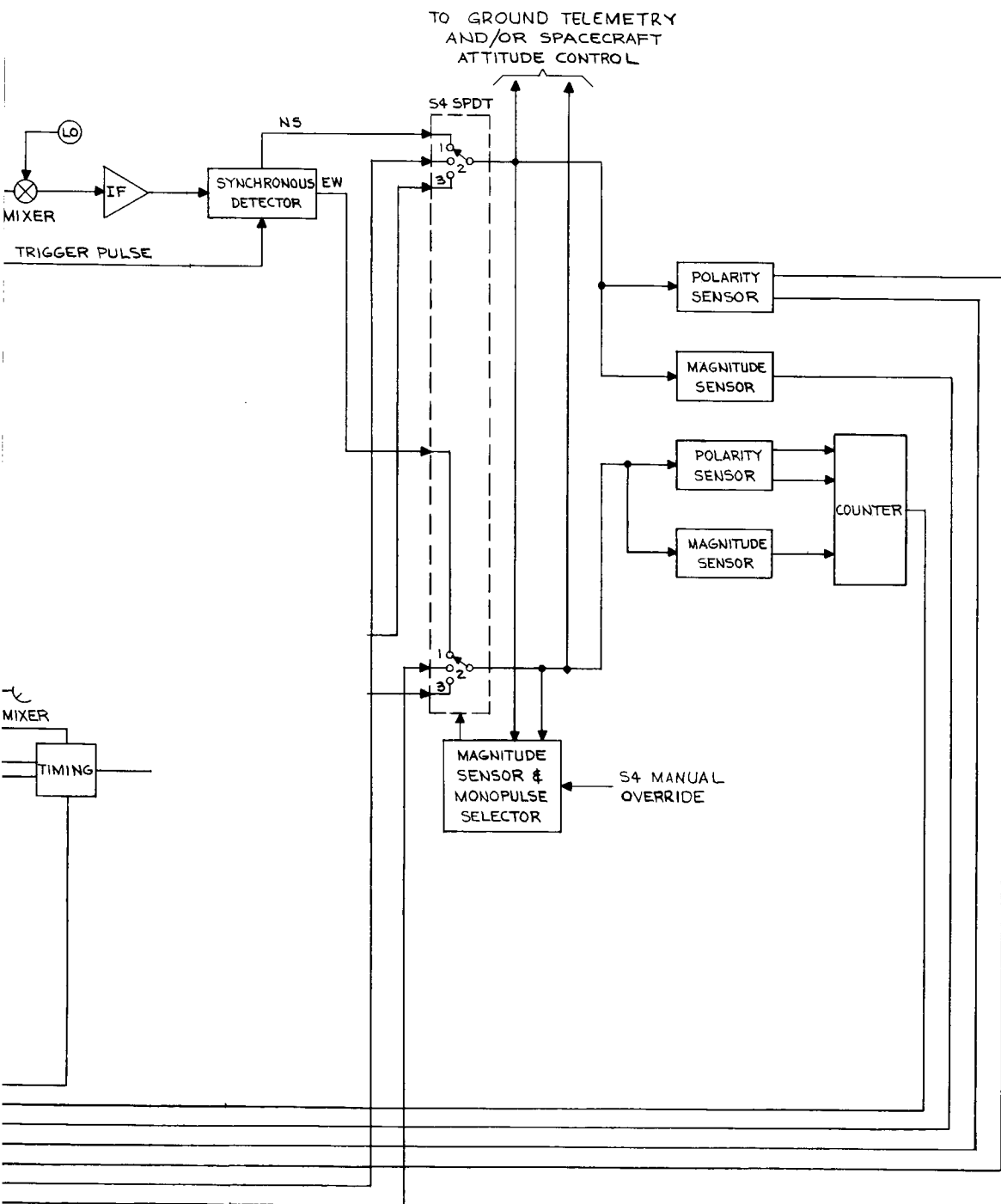


Figure 11-9. Antenna and RF system block diagram.

Table 11-2  
ATS-4 Spacecraft Monopulse Signal-to-Noise Ratio

Parameters (Nominal)	Frequency	
	0.4 GHz	8 GHz
$P_T$ = transmitter power output = 1 watt	0 dbw	0 dbw
$L_T$ = transmitter transmission line and component losses	-3 db	-3 db
$G_t$ = transmitter antenna gain (40-ft MOJAVE at 0.4 GHz & 8 GHz, 15-ft at 35 GHz)	31 db	58 db
ERP = net effective radiated power	28 dbw	55 dbw
$L_p$ = path loss	-176 db	-202 db
$L_{pa}$ = atmospheric attenuation	0 db	0 db
$P_r$ = power density at monopulse receiver antenna	-148 dbw	-147 dbw
$G_r$ = receiver antenna gain (30-ft at 0.4 GHz & 8 GHz, 8-ft at 35 GHz)	27 db	50 db
$L_R$ = receiver transmission line and component losses	-3 db	-4 db
S = receiver converter input signal	-124 dbw	-101 dbw
NF = receiver noise figure	8 db	10 db
B = receiver noise bandwidth (Hz) - 1 Hz		
K = Boltzmann Constant = $1.38 \times 10^{-23}$ watt/Hz		
T = earth temperature $\approx 290^\circ$ K ( $62^\circ$ F)		
KTb = noise seen by monopulse antenna	-174 dbw	-174 dbw
N = total system noise = KTB NF	-166 dbw	-164 dbw
S/N = signal to noise ratio	42 db	63 db

## SECTION 12

### COMMUNICATIONS SUBSYSTEMS

#### INTRODUCTION

Independent UHF and X-Band communications subsystems are proposed for the ATS-4 spacecraft. Operating frequencies, RF bandwidths, and CW power ratings for the two subsystems are summarized in Table 12-1.

Table 12-1  
Summary of Communications Subsystem Characteristics

Communications Subsystem	Receive Frequency	Transmit Frequency	Overall RF Bandwidth	CW Power Output
UHF	401 MHz	466 MHz	10 MHz	40 watts
X-Band	8.0 GHz	7.3 GHz	40 MHz	24 watts

Each subsystem would have essentially redundant wideband transponders of the frequency translation type, capable of either linear or hard-limiting operation. These subsystems would serve a dual purpose. They would assist in evaluating the deployment and subsequent performance of the large aperture antenna and they would also provide a means of exercising the technology of a three-axis stabilized high-gain antenna in synchronous orbit through a series of demonstration-type communications experiments involving small ground terminals, in-flight aircraft, and satellite-satellite links. The number and variety of signals which could be successfully relayed by transponders of the type proposed, together with the availability of the high-gain spacecraft antenna in synchronous orbit, would make practical many types of satellite operations heretofore difficult or impossible. In particular, wideband links to minimal ground terminals and satellite-satellite links will be feasible for the first time in the history of space communications. Several such experimental systems have been considered and are discussed in the section of this report dealing with ATS-4 experiments. It should be noted that those possible applica-

tions presuppose inclusion in the spacecraft of communications transponders of the type outlined below.

## UHF SUBSYSTEM

### DESCRIPTION OF SUBSYSTEM

A functional block diagram of the proposed ATS-4 UHF communications subsystem is given in Figure 12-1. Important characteristics are summarized in Table 12-2. The entire subsystem is redundant with the exception of a common preamplifier employed to avoid the 3 db penalty in receiving system sensitivity which would be incurred by using a hybrid divider immediately after the duplexer. After up-conversion from IF to 466 MHz, a hybrid combining network prior to power amplification allows either transponder to drive either output stage, ensuring maximum flexibility and dependability.

Both linear and hard-limiting modes of transponder operation are included, to accommodate the large number and variety of modulated signal types to be encountered in proposed applications and demonstrations of the ATS-4 system. For example, signals such as single-sideband modulated frequency-division-multiplexed voice channels and amplitude-modulated video signals require a linear transponder, whereas wideband frequency modulated or spread-spectrum signals would be handled most efficiently by a hard-limiting transponder. The choice of transponder, mode, and output stage would be controlled through the spacecraft C & TM subsystem.

### APPLICABLE TECHNOLOGY

The UHF communications subsystem proposed here is a rather straightforward extrapolation of state-of-the-art communications satellite technology to meet the requirements of the ATS-4 mission. The basic frequency-translation transponder design is, with the exception of 3 db bandwidth and dual-mode capability, very similar in concept to the VHF transponder built by Hughes for the ATS-B spacecraft under NASA-5-9593. Also, the ATS-4 UHF receive and transmit frequencies of 401 MHz and 466 MHz are identical to those of the IRLS Program, for which solid-state RF equipment is being developed by Motorola under NAS-5-10258.

These two existing programs serve to establish the general feasibility of the ATS-4 UHF communications subsystem proposed here, and in particular provide a basis for the weight, prime power, command and telemetry estimates

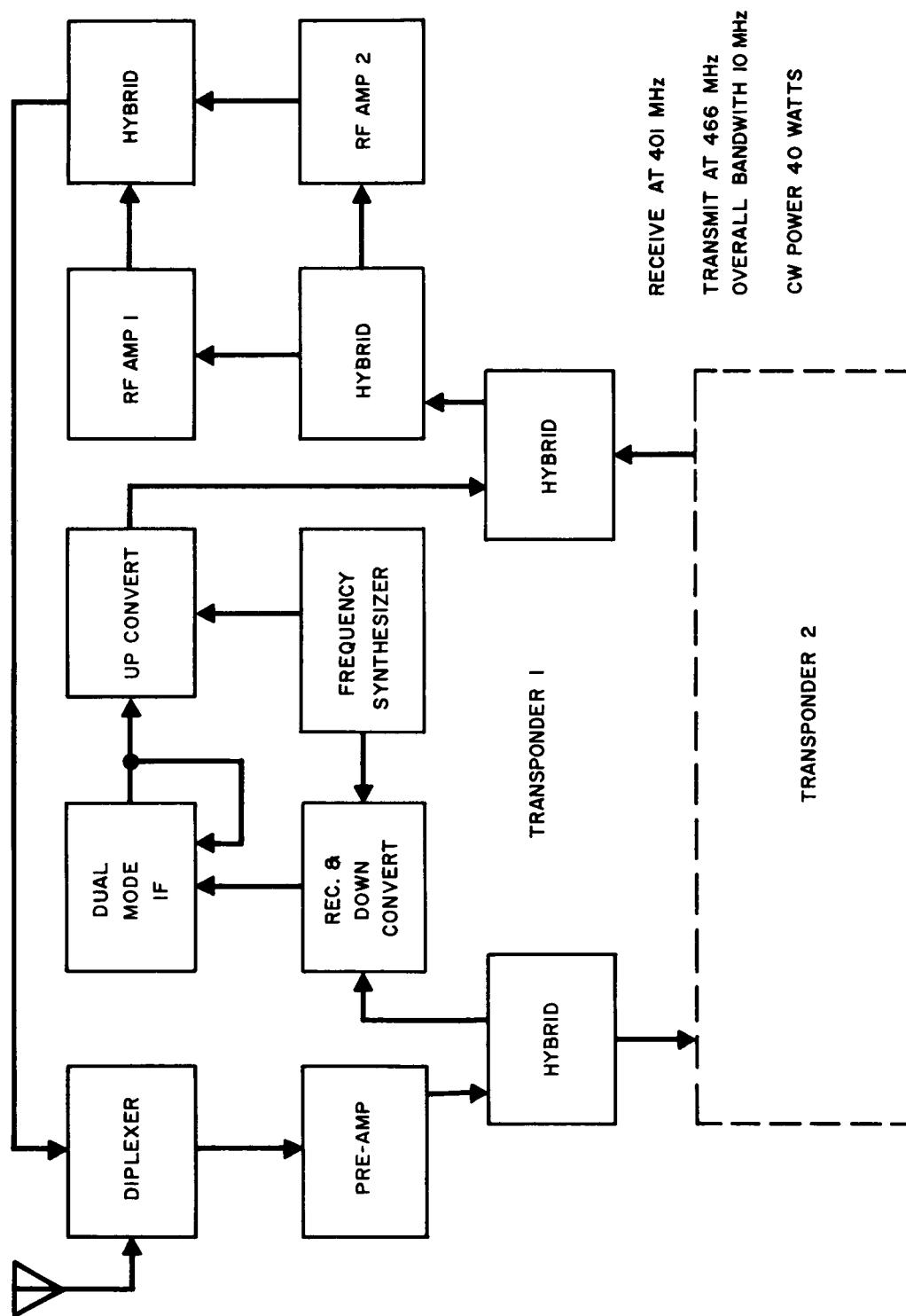


Figure 12-1. ATS-4 UHF communications subsystem.

given in Table 12-2.

Table 12-2  
Essential Characteristics of ATS-4 UHF Communications Subsystem

Receive center frequency	401.0 MHz
Transmit center frequency	466.0 MHz
3 db bandwidth (overall)	10 MHz
Receiver noise figure	3 db (Max)
IF frequency (tentative)	60 MHz
Modes of operation	(a) Linear (reduced power) (b) Hard-limiting
RF output stage	Redundant solid state
RF power output	40 watts (saturated)
Estimated weight	20 lb
Estimated prime power requirements	72 watts
Estimated command requirements	12 latching type relay commands
Estimated telemetry requirements	(a) 6 analog channels; 2 at 20 samples/sec min; 4 at 1 sample/sec max  (b) 12 1-bit digital channels; all at 1 sample/sec max

## X-BAND SUBSYSTEM

### DESCRIPTION OF SUBSYSTEM

A functional block diagram of the proposed ATS-4 X-Band communications subsystem is given in Figure 12-2. Important characteristics are summarized in Table 12-3. As with the UHF subsystem described above, the X-Band subsystem is redundant, with the exception of a common high performance front end. A further similarity is the capability of dual-mode operation. Important features peculiar to the X-Band communications subsystem are provision for transmission to earth of frequency-modulated video data originating on-board the ATS-4 spacecraft, via a wideband VCO operable through the transponder; provision for transmission of conventional narrowband spacecraft telemetry by angle-modulating a low-power beacon working into the transponder power stage; and a highly versatile TWT power amplification arrangement, in which either transponder can drive any one, any combination, or all of the four TWT's in parallel to develop output RF levels into the large-aperture antenna of 6, 12, 18, or 24 watts. This arrangement makes for a highly flexible and reliable output stage, and guarantees graceful degradation in the event of one or more TWT failures.

### APPLICABLE TECHNOLOGY

The subsystem proposed here is of essentially the same design as that used by Hughes in Comsat's "Bluebird" HS303A spacecraft. Apart from operating frequencies and bandwidth, the only critical differences are the dual-mode capability and inclusion of the wideband VCO for transmission of local video. HS303A system summary documents served as a basis for the weight, prime power, telemetry and command estimates given in Table 12-3.



Table 12-3  
Essential Characteristics of ATS-4 X-Band Communications Subsystem

Receive center frequency	8.0 GHz
Transmit center frequency	7.3 GHz
3 db bandwidth (overall)	40 MHz
Beacon frequency	7.2 GHz
Receiver noise figure	7 db (Max)
Type repeater	Single conversion
Modes of operation	(a) Linear (reduced power) (b) Hard-limiting
RF output type	4 switchable TWT's in parallel
RF output power	6, 12, 18, or 24 watts
Estimated weight	40 lb
Estimated prime power requirements	80 watts (Max) (depends on RF power output level selected)
Estimated command requirements	22 latching type relay com- mands
Estimated telemetry requirements	(a) 12 analog channels; 2 at 20 samples/sec min; 10 at 1 sample/sec max  (b) 22 1-bit digital channels; all at 1 sample/sec max

## SECTION 13

### CONTROLS

#### INTRODUCTION

In this section, a description of the spin-control system used during the transfer orbit and for the three-axis stabilization system used while in synchronous orbit is given. After the performance requirements are stated, the complete sequence beginning with separation from the Centaur launch vehicle to final operational stabilization in orbit is given. A more detailed description of the calculations and the limiting performance criteria can be found in the subsequent paragraphs.

The control-systems sequence of operation cover three distinct phases:

1. Spinning body control
2. Acquisition control
3. Operational control

For operational control, it is required to stabilize the spacecraft in all three axes to 0.1 degrees and to slew the entire spacecraft to any desired point within the earth's disk at slew rates up to 1 degree per minute. It is required to maintain stabilization to these axes during stationkeeping maneuvers. One can readily recognize the difficulties in detailed design when the dynamics of the spacecraft structure are taken into account. Although no doubt exists as to the feasibility of designing such a control system in this first design approach, considerable design ingenuity will be required to achieve spacecraft dynamics compatible with stable control operation.

Because of the use of the TE 364 solid propellant kick stage, it is necessary to spin the spacecraft during burn of the final injection phase. As stated in Section 9, the exact orientation of the spin vector is determined by the requirement to eliminate the inclination between the orbital and equatorial planes so as to inject the spacecraft in a true geosynchronous equatorial orbit.

Following separation from the Centaur launch vehicle, after its second burn the spacecraft is still in a folded condition with the TE 364 and its adapter attached. A number of solid-propellant spin rockets will spin it to a rate of 60 rpm. Because of the unfavorable moment ratio of the spacecraft in the

folded condition, active nutation damping is required. This is accomplished with one axial thruster properly phased and synchronized throughout the time that the spacecraft is in the transfer orbit; during this time attitude measurements are made to determine precisely the orientation of the spacecraft spin vector in space. Then the spacecraft is precessed to achieve vernier correction of the spacecraft attitude prior to apogee motor firing. Spacecraft attitude is measured using the Syncom and ATS-B type sun and RF polarization sensors. If SCADS is a successful experiment, this will provide additional backup data.

The sun sensor utilizes a number of fan-shaped viewing beams. As the image of the sun is viewed successively when the spacecraft rotates about its axis, a series of pulses are generated. By relating the geometry of the sun line, spacecraft axis, the angles between the fan-shaped viewing beams, and the time interval between pulses, the spin-axis orientation with respect to the sun line can be established. The fan-beam concept is shown in Figure 13-1. The sun-sensor and the RF-polarization measurements in combination uniquely define the spacecraft attitude in space.

SCADS like the sun sensor utilizes a narrow fan-shaped viewing beam. As the spacecraft spins, stars are successively viewed by the beam. The impulses generated as stars are viewed are telemetered to the ground, where they are compared in a computer program to a star map stored in the computer memory. The impulse time relation will correlate with the star map for a unique spacecraft-attitude determination. It will thus provide 100-percent redundancy to the two prime sensors. Successful performance of SCADS on the ATS-C flights could result in its becoming the preferred choice over the sun sensors and RF sensor, because of the much higher accuracy provided by the SCADS. Another sensor is needed to provide synchronization of the jets for nutation damping. This will be accomplished with an accelerometer of the type flown before. A summary of the control characteristics is given below:

Axial thrust - 5 pounds at 2.4 feet

Spin rate - 60 RPM

Jet "on" time - 0.2 second

Axial inertia - 390 slug-ft<sup>2</sup>

Inertia ratio - 0.13

Precession increment - 0.053 degree

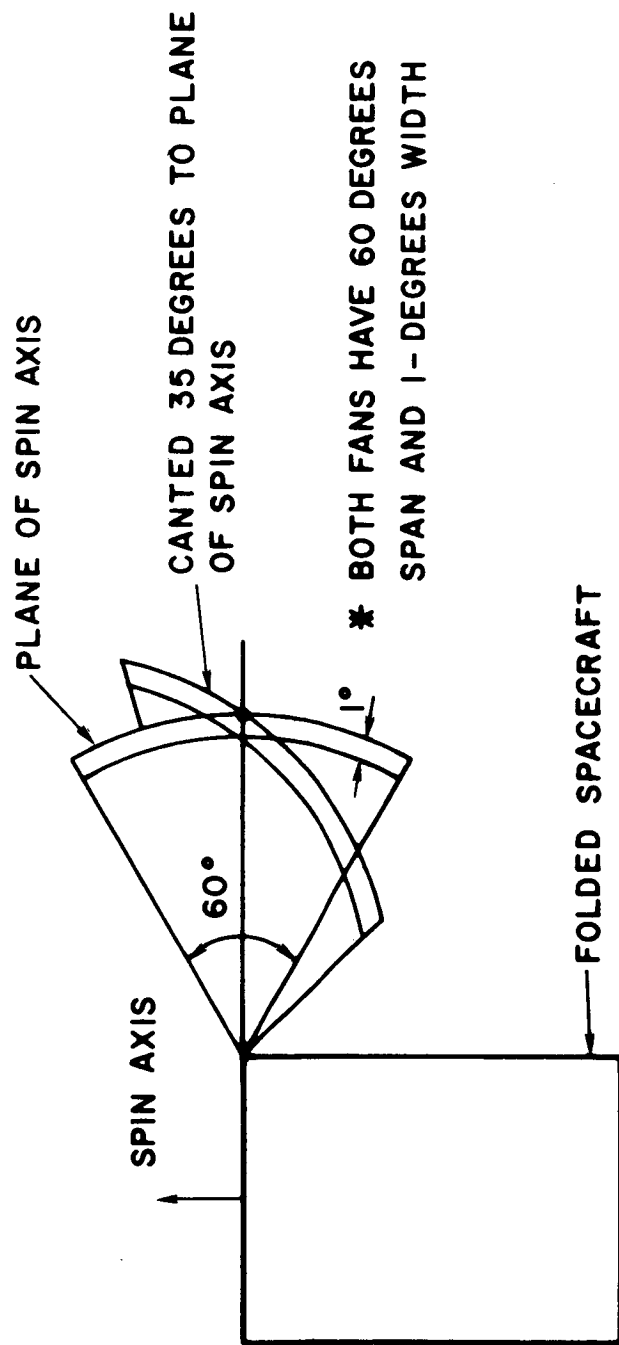


Figure 13-1. Syncom type sun sensor.

Precession rate - 3.17 degrees/min

Nutation increment - 0.053 degree

Nutation damping rate - 2.75 degrees/min

Cone-angle threshold - 0.2 degree

Fuel (damping or precession) - 19 pounds sec/degree

Coarse spin-axis measurement - 1.5 degrees

Fine spin-axis measurement - 0.1 degree.

Following burnout of the TE 364 motor, the spacecraft is precessed to the required attitude; axial thrust is applied by means of two axial hydrazine thrusters. This accomplishes vernier correction of the orbit inclination and eccentricity. The spacecraft is then despun to approximately 1 degree per second by yo-yo. The spent-rocket casing and adapter sections are then separated. As stated before, failure of the separation mechanism does not render the following sequence inoperative.

The remaining sequence is explained by means of Figure 13-2. Although the spin axis is shown perpendicular to the orbital plane, this is not at present a strict requirement but one can expect that it will be in this approximate configuration. The resistance gas system is turned on at this point and the sun sensors are activated to acquire the sun. The sensors have a large field of view so that orientation from any arbitrary position is possible. The sensors are of the analog-null type. The same principle as was used on OGO can be employed. Once the roll axis points toward the sun, the gas system keeps it pointing in this direction. By command, the control system is now turned off and deployment of the dish is activated. After deployment the control system is reactivated, stabilization to the sun is reestablished and a roll of 12 degrees per minute is introduced. Inspecting the figure one sees that the yaw axis will move in a plane normal to the figure. As the spacecraft continues in orbital flight, the yaw axis which is coincident with the RF pointing axis will eventually start sweeping across the earth. The spacecraft is then ready to be switched to the earth acquisition mode.

There are three sensors which can be used for this mode. The primary sensor is a double-mirror OGO-type horizon sensor. The narrow field of view simply sweeps over a 34-degree angle sweeping in one plane across the earth as shown in Figure 13-3. With an appropriate mirror arrangement, a sweep in

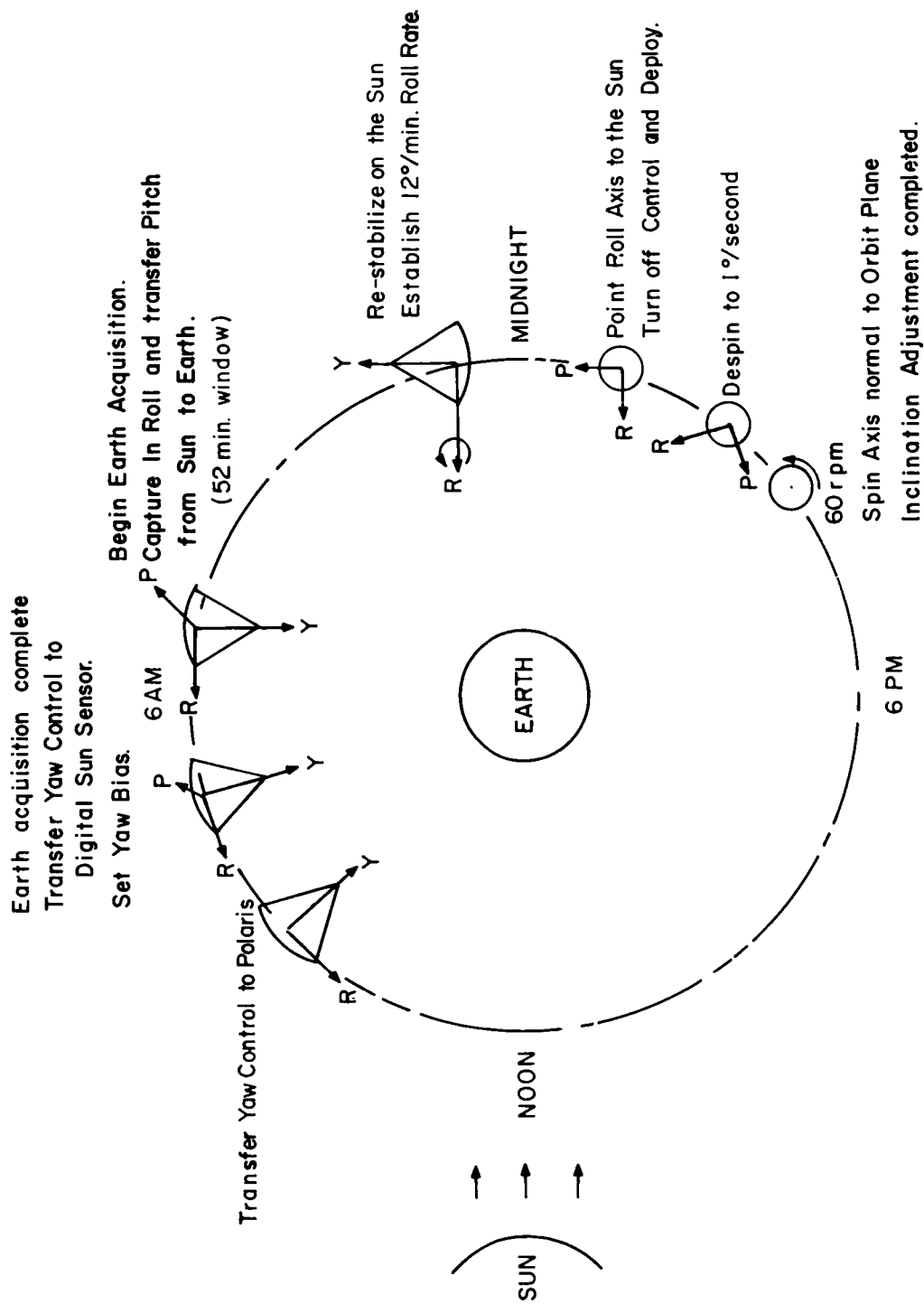


Figure 13-2. ATS-4 attitude control acquisition sequence.

EARTH  
SENSOR

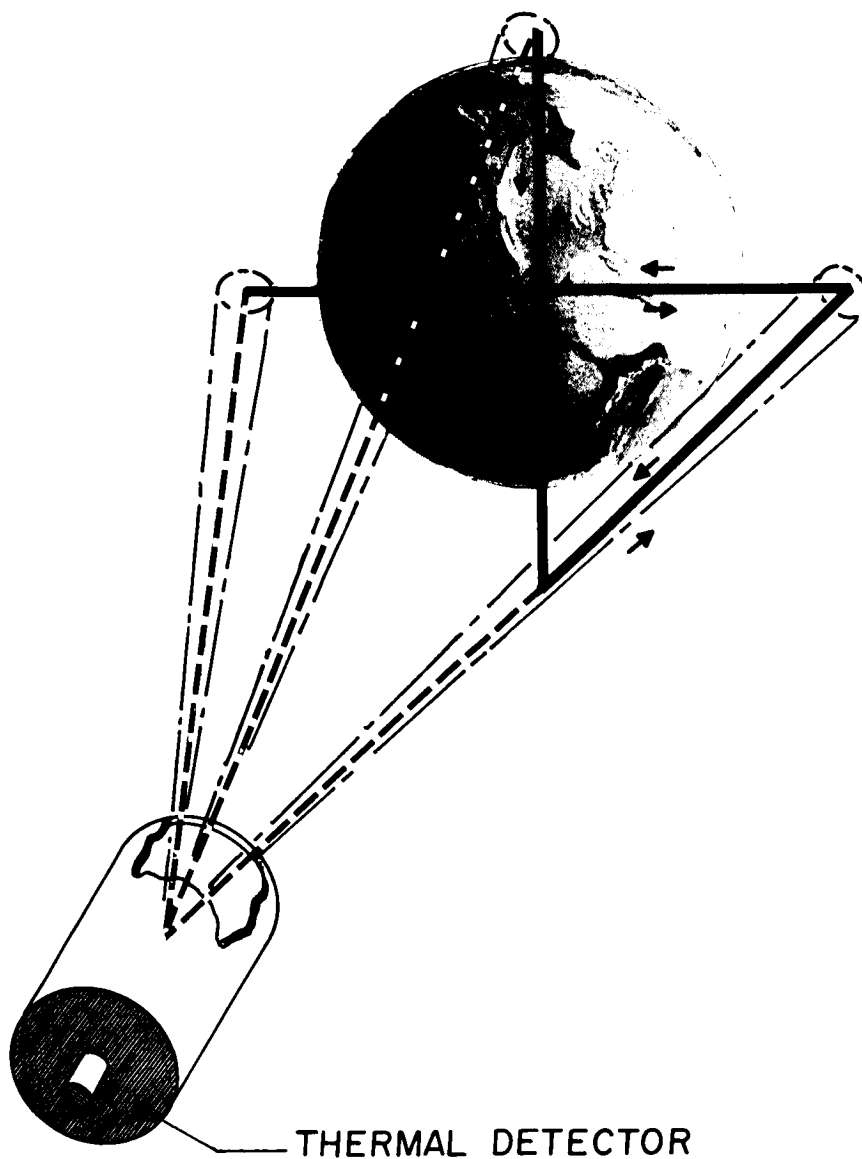


Figure 13-3. Earth sensor field of view.

a plane normal to the one just described is implemented. The principle is indicated on the same figure. Of course, the spectra-sensitivity of the horizon scanner is selected so that day-and-night operation is possible. With these two error signals, the yaw axis can be pointed toward the center of the earth uniquely. This requires that roll control is deactivated from the sun-pointing mode. As stated before, a monopulse RF error detector is being included and the interferometer is proposed as an experiment. Either one of the two outputs can be used for error sensing. The monopulse would, of course, point the RF axis in the direction of the ground station while the earth horizon sensors would point towards the center of the earth. However, earth acquisition is possible by either technique. The interferometer attitude data require that calculations are performed on the ground and appropriate commands given to the spacecraft.

With sun-pointing control turned off, it is necessary to point the pitch axis in the direction normal to the orbital plane. It is proposed to make use of Polaris to accomplish this. The choice of Polaris has the advantage that its spectral radiance can easily be distinguished from its neighbors, so that Polaris is by far the brightest star within a large spherical angle. Secondly, it lies almost due north so that an axis at nearly 90 degrees to the orbital plane can be sensed. The field of view is shown in Figure 13-4. Because of the narrow angle of 4 degrees in the pitch-roll plane it is necessary to bring Polaris within the field of view. This is accomplished by injecting a bias in an additional digital sun sensor by command. A digital sun sensor is proposed because of the achievable high accuracy over the  $\pm 40$ -degree acceptance angle. The 25-degree fan-type field of view of the tracker is necessary to stay locked during slew maneuvers when in operational control.

With the tracker activated and biased with an 0.83-degree orbital rate sinusoid, the spacecraft will point due north. The electronic bias is required since Polaris is 0.83 degree off the celestial North Pole. For all the maneuvers described so far, the gas system is used exclusively. For rate control it is necessary to include a 3-gyro rate package which can be deactivated when operation control in the spacecraft has been accomplished. Should control be lost at any time, it can readily be reactivated and the entire sequence repeated. A separate single gyro to be operated in conjunction with the digital yaw sun sensor is proposed as a yaw inertial hold to provide redundancy against failure in the Polaris tracker. It can readily be seen that a yaw inertial quality gyro with sun-sensor update will accomplish this although at lower accuracy than a Polaris tracker would provide.

The spacecraft is now ready to assume operational control so that the three momentum wheels can be turned on. Slewing of the spacecraft can be

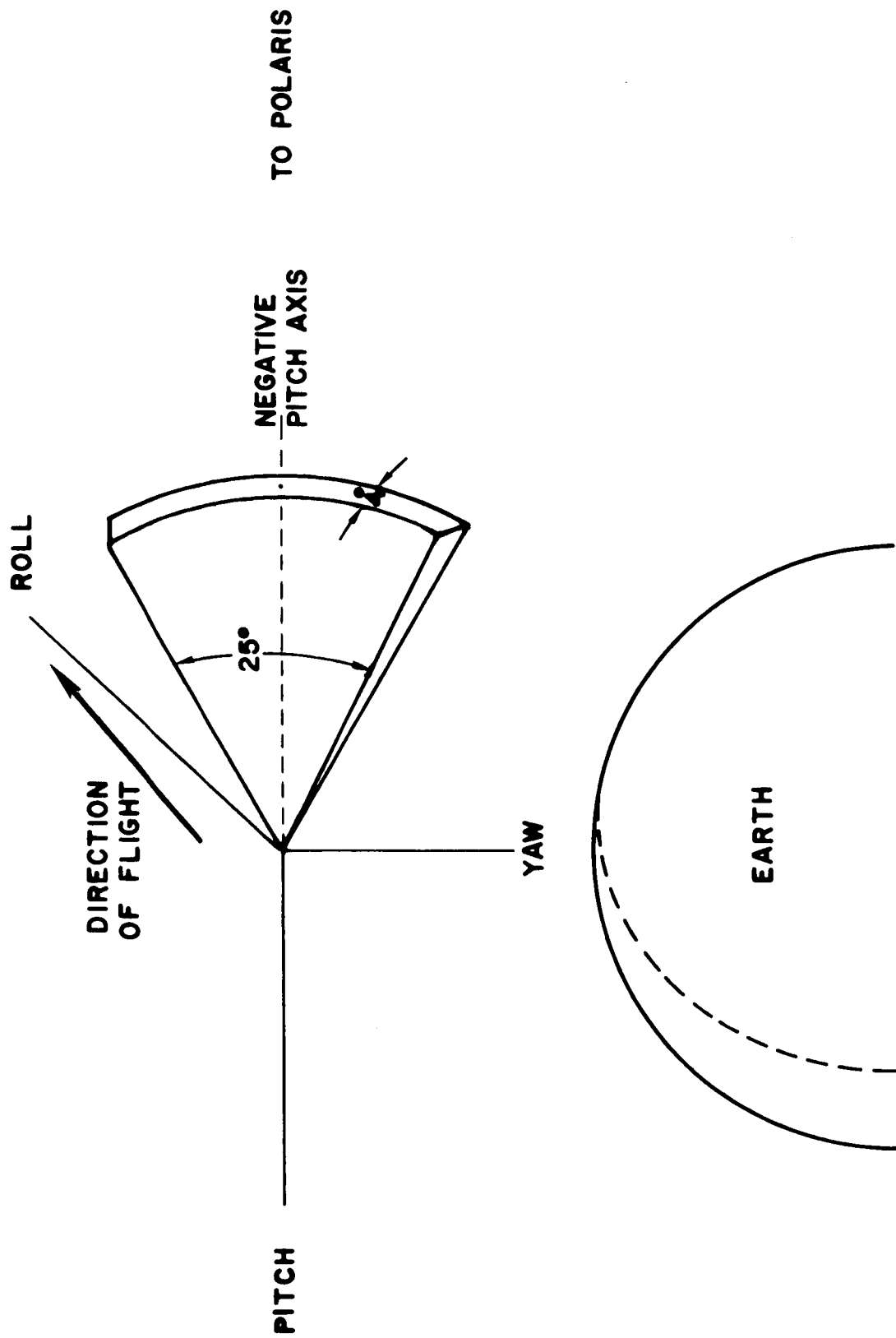


Figure 13-4. Polaris tracker field of view.

commanded and the control system will operate on the flywheel control exclusively, using gas only for momentum dumping. Either the earth horizon sensors with the Polaris tracker or the monopulse system with the Polaris tracker can be used for error sensing.

It is interesting to note that a high degree of redundancy is provided. The vehicle, after separation from the Centaur, uses multiple spinup rockets and two axial hydrazine thrusters, one of which would suffice to provide successful operation for spin-axis control and active damping. The accelerometer used for nutation sensing is a simple device; no redundancy is planned. Redundancy in the sensors exists between the sun sensor and SCADS and between the RF polarization sensor and SCADS. The gas system is being sized so that if one or both yo-yo despin devices should fail, despin could be obtained by gas thrusters. During the sun-acquisition mode, no redundancy is planned for the sun sensor and gyro rate sensors because of the extreme simplicity of these devices. The gas jets, as stated before, are arranged in such a manner that a simple jet failure would be compensated by the ones remaining. For the earth acquisition mode, the monopulse error detector provides redundancy against failure of the earth-horizon detectors; the gyro compass is redundant against failure of the Polaris tracker. Proposed for an experimental mode is a gravity-gradient rod with tip mass mounted in a gimbaled configuration; this configuration provides full redundancy for the gas system once the spacecraft is under operational control.

## GENERAL DESCRIPTION

The spacecraft attitude-control mission begins at the time of separation from the launch vehicle.

The requirements placed upon the spinning body control during the transfer ellipse and the initial orbit corrections are active nutation damping, spin axis precession, and measurement of the spin-axis orientation. After injection into a near-synchronous orbit and the initial orbit correction, the spacecraft is despun and the acquisition sequence shown in Figure 13-2 begins. This sequence begins with the alignment of the spacecraft roll axis with the sun line and makes possible the utilization of simple earth search and Polaris acquisition maneuvers. The acquisition control utilizes reaction jets operated in a pulse-modulation fashion. For the primary operational control, a wheel-jet hybrid system has been chosen. In case of wheel failure, a jet-only backup control capability exists.

A block diagram of the acquisition and operation control is given in Figure 13-5. The control electronics for the acquisition control utilizes linear circuitry and the operational control uses a digital central signal processor time-shared between the three axes with pulse-width modulation control of the momentum wheels used to eliminate the need for linear power amplifiers and digital-to-analog converters.

The weights and inertias used in these calculations were assumed values based on an earlier configuration. The latest numbers are given in a previous section. The change in specific numbers do not significantly affect the conclusions.

### SPINNING BODY CONTROL

Spinning body control is used during the transfer ellipse and initial synchronous orbit corrections. Control is obtained from one axial thruster (two are carried for redundancy) using the techniques pioneered on Syncom and used on ATS D&E. The requirements placed upon the control are active nutation damping, spin-axis precession, and spin-axis orientation measurements. A summary of the control characteristics is given in the Introduction.

ATS-4 will use axial synchronized jet pulses, one pulse per revolution, to precess the spin axis. As shown in Figure 13-6, the nutation cone angle increases and decreases in a periodic fashion. Thus the existence of the initial coning does not complicate spin-axis maneuvers. Precession control will utilize the techniques pioneered by Syncom. If a ground-station synchronizer and the command-system execute-tone command are used, telemetry of the sun pulses used for jet synchronization and rhumb line precession will require a wide-band link (suitable for passing 2.8-millisecond pulses). This telemetry requirement could be eliminated by using a spacecraft-carried synchronizer and a digital command word to set the constant sun-sensor angle required for rhumb-line precession.

Because of the inertia ratio (0.13), passive dampers cannot be used to remove transverse body rates. Therefore, as on ATS D&E, axial-jet pulses synchronized with the body-sensed nutation frequency will be used to remove the transverse momentum. Figure 13-7 illustrates the operation of the active nutation damping control. Each jet pulse reduces the transverse momentum by  $\Delta H_T$  corresponding to a cone-angle reduction of  $\Delta \theta_n$ ; between jet pulses, the spin axis rotates 54 degrees about the momentum vector. The shift in the inertial orientation of the momentum vector, " $\alpha$ ", is periodic and for the ATS-4 nominal parameters has a peak value of 0.116 degree. Thus active nutation damping does not appreciably affect the inertial orientation of the spinning body.

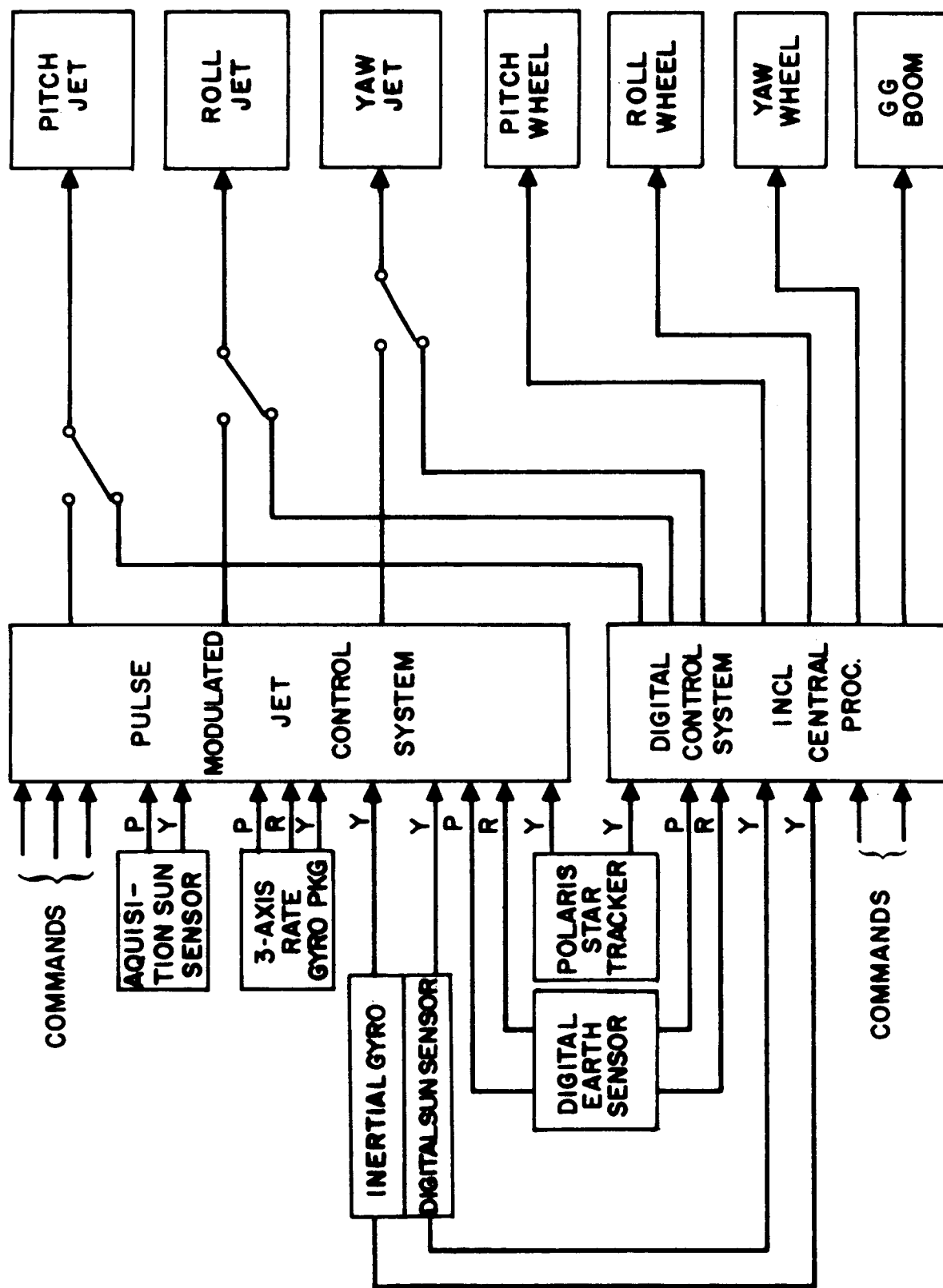


Figure 13-5. ATS-4 control system concept.

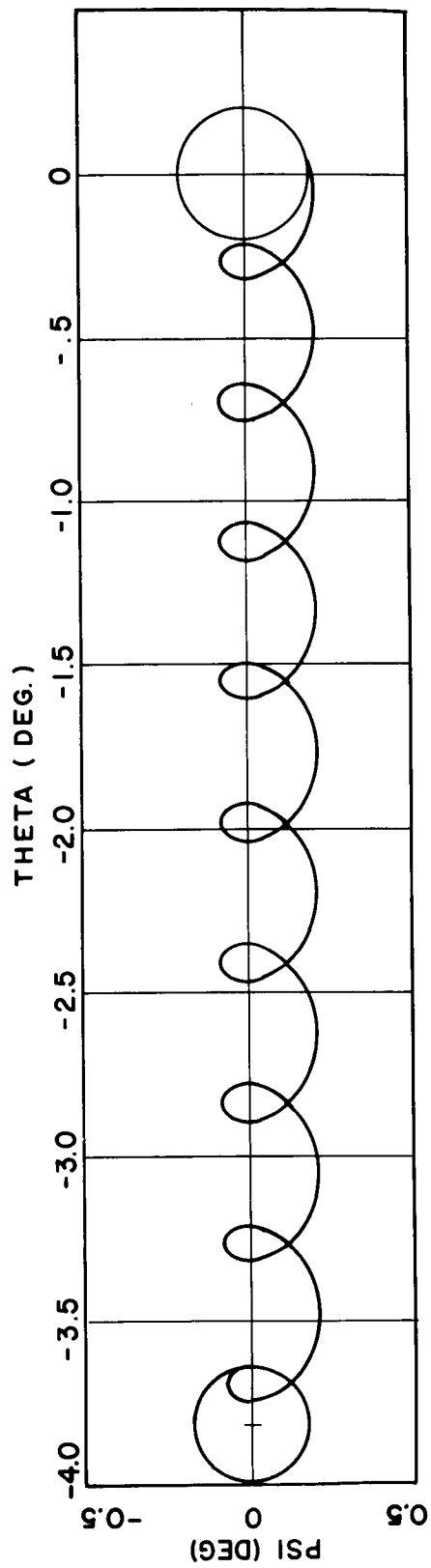


Figure 13-6. Spin-axis precession with nutation.

$\omega_p$  = Spin-axis free precession frequency

$\omega_n$  = Body-sensed nutation frequency

$\omega_o$  = Spin rate

$\sigma$  = Inertia ratio (0.13)

$\omega_p = \sigma \omega_o, \omega_n = (1-\sigma) \omega_o, \Delta\theta_p = \omega_p (2\pi/\omega_n)$

$\Delta\theta_p = \left(\frac{\sigma}{1-\sigma}\right) (2\pi)$  Radians per nutation cycle

$\Delta\theta_p = \frac{0.13}{0.87} (360^\circ) = 54^\circ$

$\alpha(\eta)$  = Momentum vector precession angle after  $\eta$  damping impulses

$\Delta\theta_n$  = Nutation damping increment

$|\alpha| = \Delta\theta_N \left| \sin\left(\eta \Delta\theta_p/2\right) / \sin\left(\Delta\theta_p/2\right) \right|$

$|\alpha|_{\max} = 0.116^\circ$

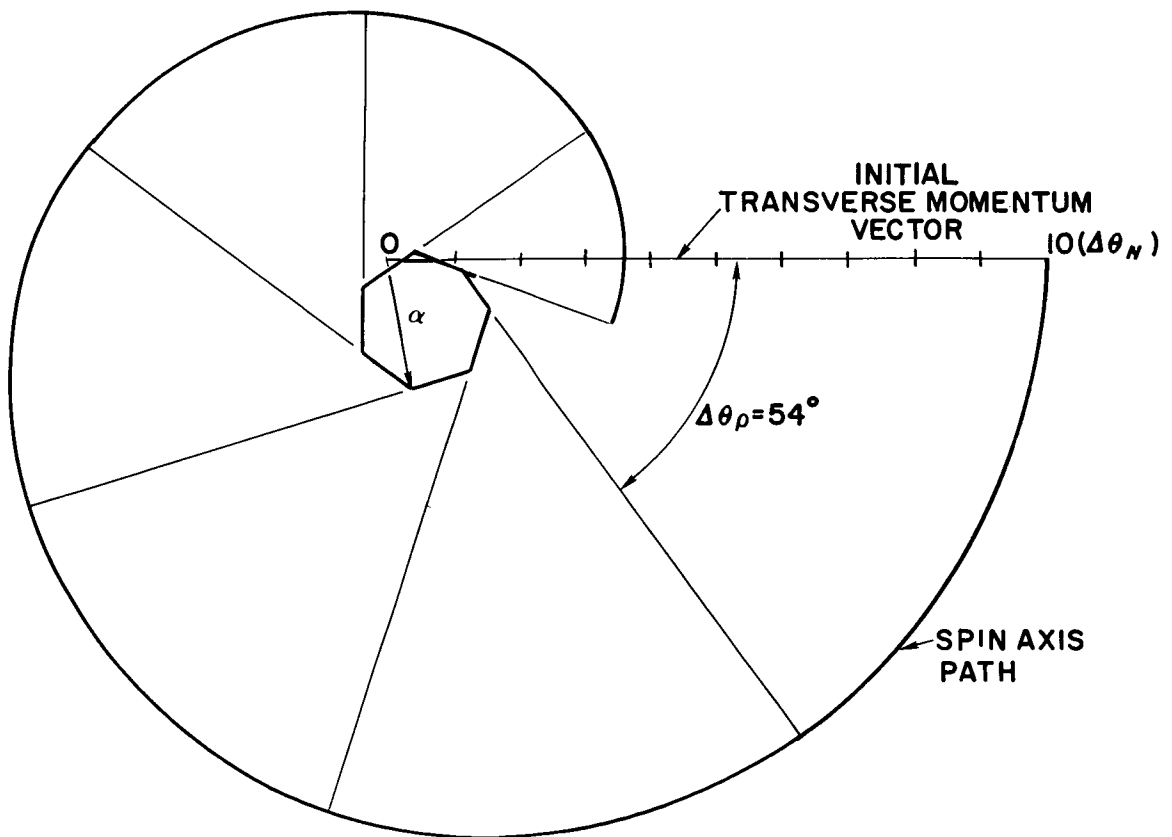


Figure 13-7. Active nutation damping.

For spinning body control the spin axis attitude is measured in two ways. For a coarse measurement ( $\pm 1.5$  degrees), a "Syncom"-type sun sensor is used for determining the angle between the spin axis and sun line, with ground measurement of the incoming RF polarization to determine the rotation of the spin axis about the ground-station-spacecraft line of sight. For a fine measurement ( $\pm 0.1$  degree) SCADS, using the spacecraft spin rate, may be used. SCADS is a star-field mapper that periodically scans a portion of the sky with a slit; the time between observed stars is used to calculate the spin-axis attitude. A detailed description of SCADS appears in Section 20C.

For active nutation damping of a spinning body, the transverse body rate must be sensed in order to synchronize the jet pulses by ground command. The cone-angle threshold is proportional to the minimum transverse rate that can be sensed. For the nominal ATS-4 parameters a 0.2-degree threshold requires sensing a transverse body rate of 0.154 degree/sec. This could be done with one of the body-rate gyros; however, the alignment required to prevent spin-rate coupling is quite severe. Since the transverse rate is varying sinusoidally, an angular accelerometer could also be used; and since the spin rate is nearly constant, there will be little coupling. The acceleration that must be sensed for a 0.2-degree threshold is 0.84 degree/sec<sup>2</sup>. An accelerometer seems to be the preferred approach.

## ACQUISITION CONTROL

After vehicle injection into a near-synchronous orbit, initial orbit corrections, and despin, the acquisition sequence begins. This sequence begins with the alignment of the spacecraft roll axis with the sun line and sequential acquisition of the earth (roll/pitch) and Polaris (yaw reference). The final mode for the acquisition control is a 3-axis stabilized earth-pointing mode. The in-house study investigated this control mode in detail. The work has shown that a pulse-modulated reaction jet control can fulfill the acquisition control requirements as well as provide some backup operational control capability. The acquisition control torque levels are given below:

Roll torque - 0.12 ft-lb (10 degrees/min<sup>2</sup>)  
Pitch torque - 0.077 ft-lb (10 degrees/min<sup>2</sup>)  
Yaw torque - 0.04 ft-lb (5 degrees/min<sup>2</sup>).

The accelerations given are for the antenna in the deployed condition. Deployment will take place while the roll axis is pointing at the sun. Pulse-modulated reaction jets provide very low fuel consumption while limit cycling. Consumption of 6,900 ft-lb sec (10 pounds of fuel) will provide for acquisition plus one year of backup operational control.

The spacecraft acquisition and deployment sequence as shown in Figure 13-2 is

1. Despin (rockets or yo-yo) down to 1 degree/sec body rates.
2. Lock the roll axis on the sun line, i. e., control pitch and yaw position and roll rate - fully folded.
3. Switch off control, and deploy solar paddles and reflector.
4. Restabilize on the sun line.
5. Acquire the local vertical. Roll around the sun line to acquire the earth; transfer roll and pitch control to the earth.
6. Switch yaw control to the digital yaw sensor; bias this sensor to acquire Polaris; transfer yaw control to Polaris.

One of the primary reasons for considering an all-jet system is that the same actuator can be used for control from sun-line acquisition through earth acquisition and local vertical pointing, thereby simplifying the system. This requires sufficient thrust to acquire the sun and earth in a reasonable time as well as a small impulse for control during the local vertical pointing limit cycle. Early investigation showed that with the jet controller used, the minimum impulse (limited by jet "on" time) could be easily set. For this reason it was decided to use as high a thrust level as possible. To keep the system simple, it was decided that only a single thrust level would be used if possible. The maximum jet size, therefore, is limited by the maximum specified acceleration the reflector can sustain in the deployed condition. These accelerations and thrust levels are shown in Table 13-1.

Table 13-1

Acceleration, Torque, and Thrust/Jet Levels

	Acceleration (deg/min <sup>2</sup> )	Torque (lb-ft)	Thrust/jet (lb)
Roll	10	0.12	0.03
Pitch	10	0.077	0.02
Yaw	5	0.04	0.005

The inertias used to derive Table 13-1 are shown in Table 13-2.

Table 13-2

Nominal Values of Spacecraft Inertias (slug-ft<sup>2</sup>)  
(Not including gravity gradient boom)

Without adapter; nothing deployed

Roll	1686 slug-ft <sup>2</sup>
Pitch	1686 slug-ft <sup>2</sup>
Yaw	274 slug-ft <sup>2</sup>

Everything deployed (orbit condition)

Roll	2686 slug-ft <sup>2</sup>	paddles parallel to roll axis
	2722 slug-ft <sup>2</sup>	paddles parallel to yaw axis
Pitch	1617 slug-ft <sup>2</sup>	
Yaw	1846 slug-ft <sup>2</sup>	paddles parallel to roll axis
	1810 slug-ft <sup>2</sup>	paddles parallel to yaw axis

Paddles only (per paddle)

Roll	537 slug-ft <sup>2</sup>	paddles parallel to roll axis
	555 slug-ft <sup>2</sup>	paddles parallel to yaw axis
Pitch	35 slug-ft <sup>2</sup>	
Yaw	540 slug-ft <sup>2</sup>	paddles parallel to roll axis
	522 slug-ft <sup>2</sup>	paddles parallel to yaw axis

The operation of the jet controller (Figure 13-8) has been covered in the literature. For large signal operation (acquisition), the operation is identical to a standard relay controller. For small-signal operation, near the dead zone of the controller, the minimum pulse put out by the system is controlled by the lag in the feedback. The use of this lag feedback allows a much smaller minimum on time than could be set by a gyro-determined switching line. This minimum on time can be set to the minimum on time of the jets. In the absence of disturbance torques, these minimum impulses insure very low rate limit cycles and low gas consumption.

Figure 13-9 shows the ATS-4 body-fixed coordinate system.

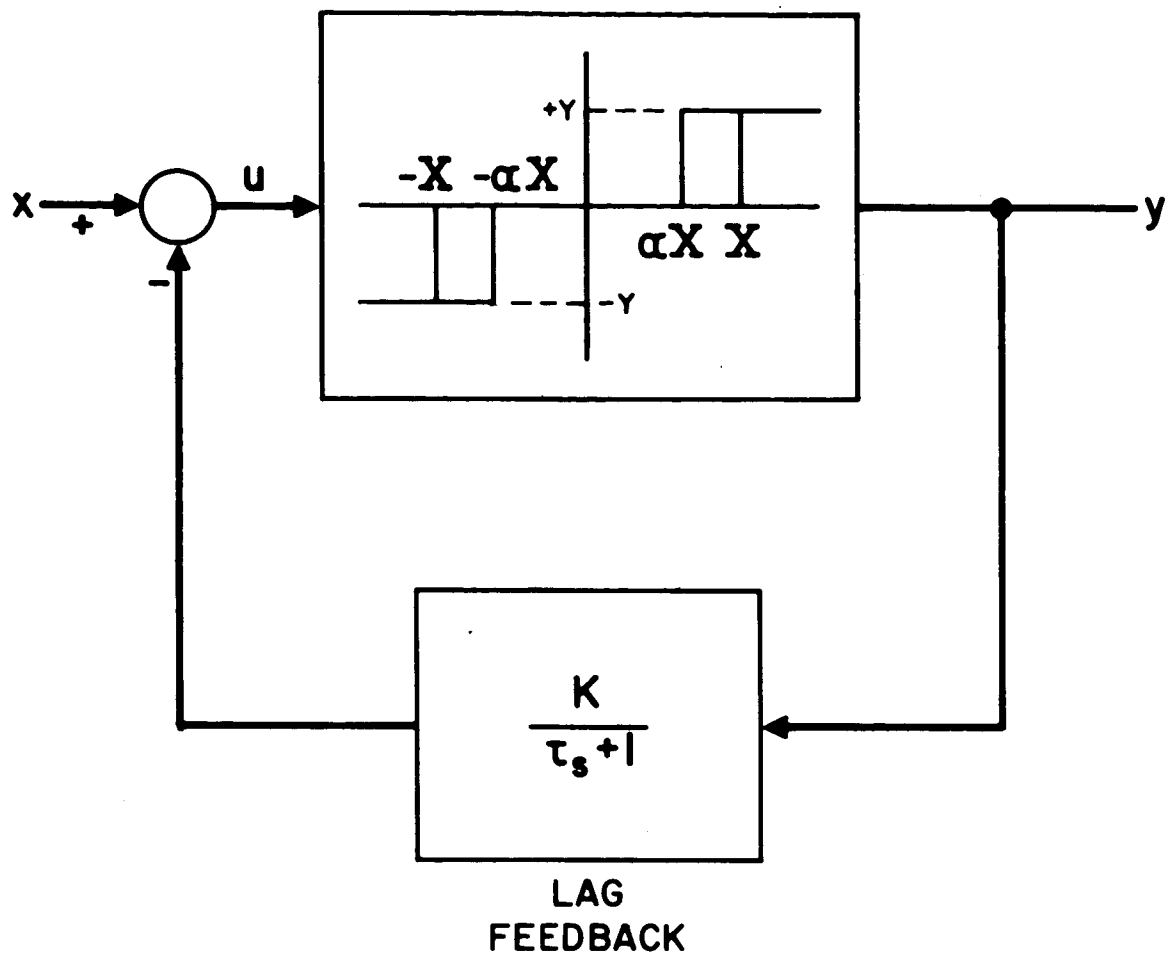


Figure 13-8. Jet controller.

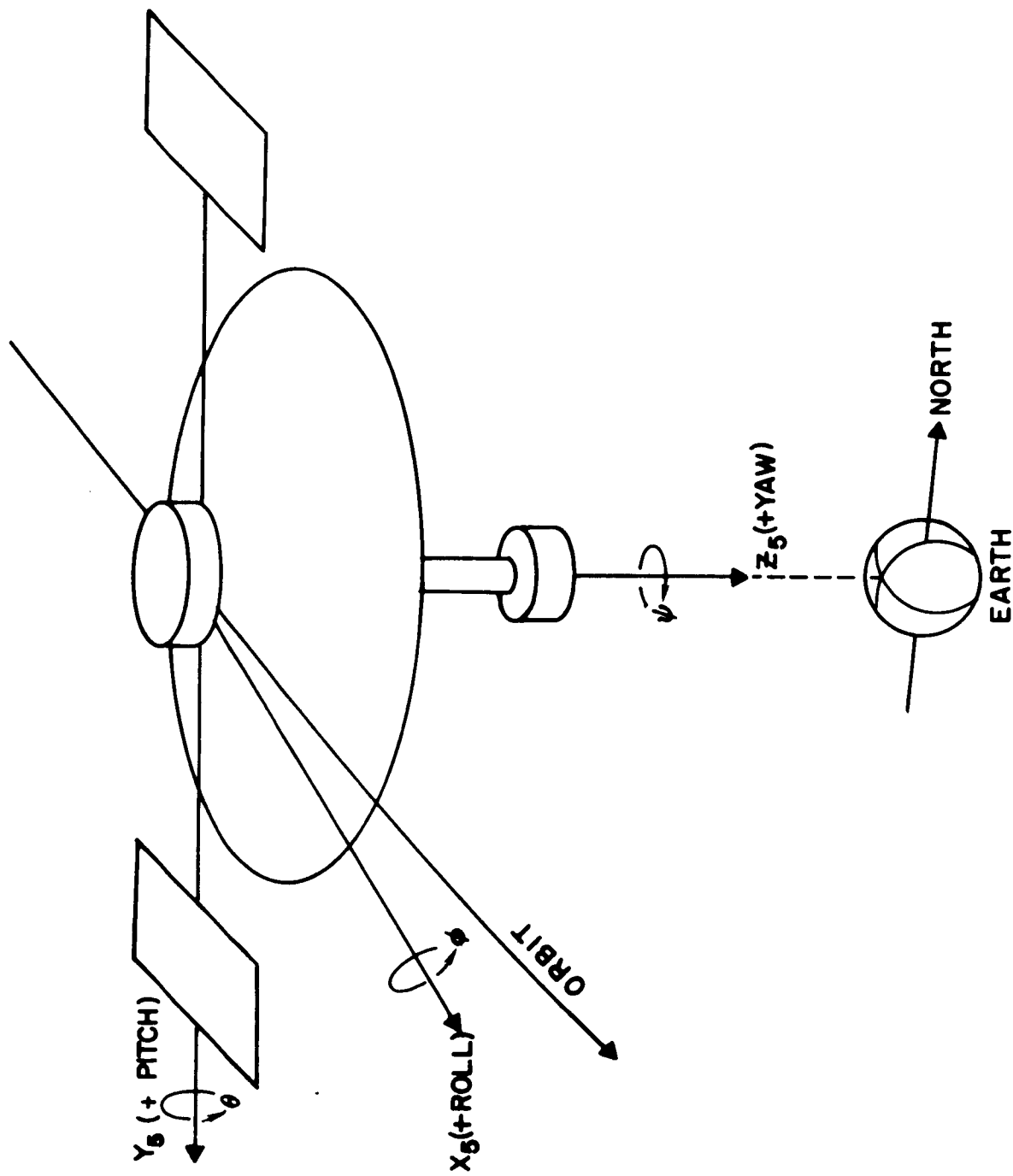


Figure 13-9. ATS-4 body-fixed coordinate system.

## SUN-LINE ACQUISITION

Following despin, the roll axis is to be locked on the sun line to give pitch and yaw control in position. Roll rate is to be controlled by a rate gyro. The body rates at the start of this acquisition sequence are expected to be 1 degree/sec or less, in all three axes. It may be necessary to use the acquisition system in a rate mode to get down to these rate specifications.

1. Accuracy:  $\pm 1.5$ -degree limit cycle in pitch and yaw, 0.021 degree/sec roll rate.
2. Stability: stable limit after acquiring sun line from any angle at initial rates of 1 degree/sec.
3. Response Time: acquire the sun line within one-half hour after despin.

The acquisition sun sensor is a relatively coarse analog sensor. A threshold of  $\pm 0.5$  degree and linear (10 percent) range of  $\pm 30$  degrees is sufficient. The three-axis rate-gyro package is specified to have a signal-to-noise ratio of 1:1 at 0.01 degree/sec. These sensors are state-of-the-art.

The block diagram for the pulse-modulated jet system including sun mode, earth-acquisition mode, and earth-pointing mode is shown in Figure 13-10.

The three control loops were simulated on the analog computer on a single-axis basis. With the aid of these simulations the control laws and system parameters were determined. These parameters and control laws were then used in a three-axis program on the digital computer. This program took dynamic coupling into account.

Since the primary function in this mode is large-scale acquisition, the system linear range is set low; thus, operation is essentially bang-bang. The controller is set to saturate at 5 degrees (Figure 13-11).

$$5^\circ K_S = KY. \quad (1)$$

Below the saturation level the controller operation is quasi-linear (Reference 1). Assuming operation at low rates (below the rate-gyro threshold) the open loop transfer function in this small linear range is

$$K_S \left( \frac{1}{KY} \right) \left( \frac{\tau_S + 1}{\frac{\tau_X S}{KY} + 1} \right) \frac{T}{JS^2}. \quad (2)$$

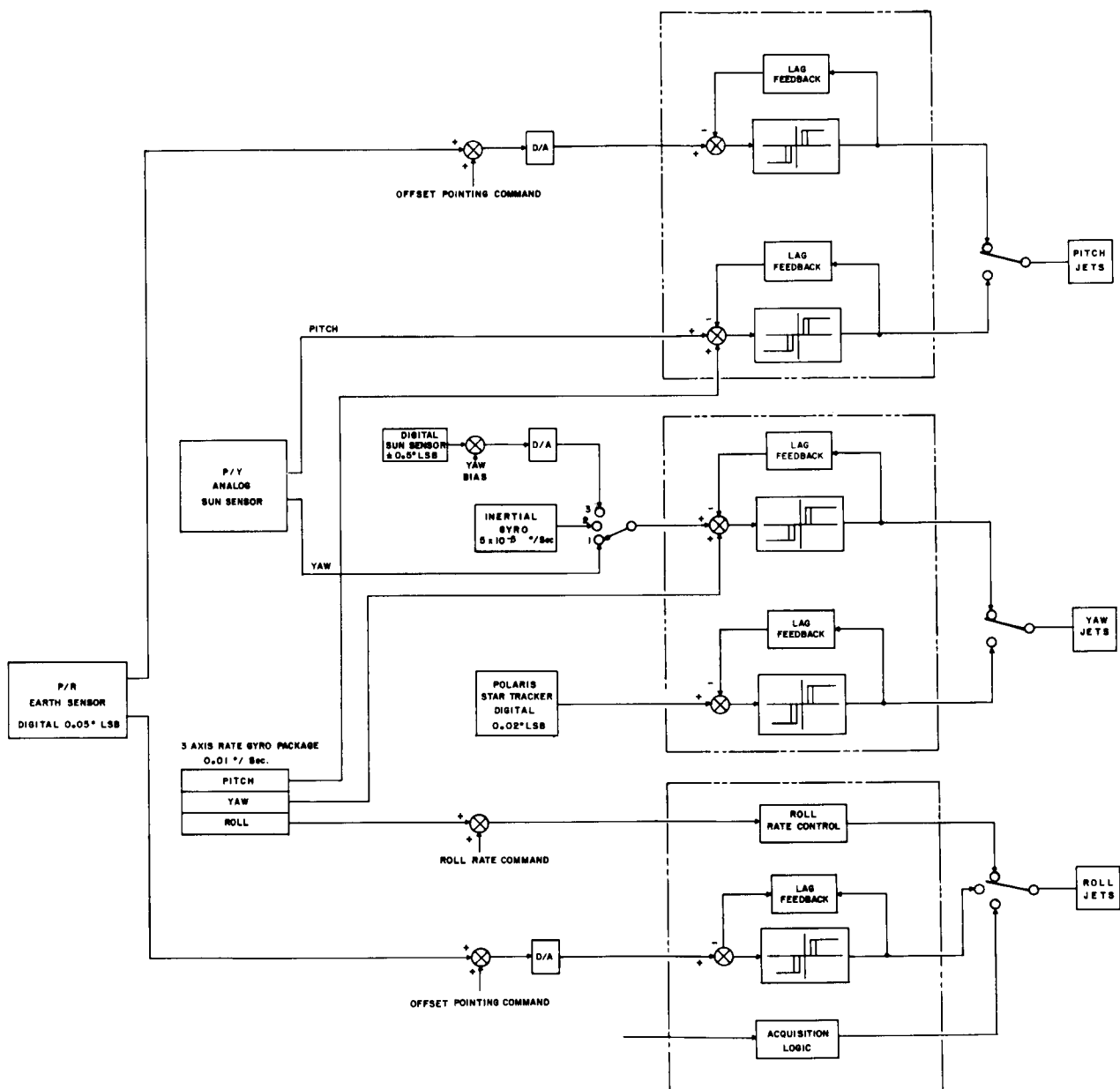


Figure 13-10. Pulse-modulated system block diagram.

The open-loop gain is essentially determined by Equation 1. Neglecting the lag in the controller, the characteristic equation in this linear range is

$$S^2 + K_{OL} \tau S + K_{OL} \quad (3)$$

where  $K_{OL}$  = open-loop gain  $\text{-sec}^{-2}$ . In this case for pitch

$$\begin{aligned} K_{OL} &= \left( \frac{1}{50} \right) (57.3) \left( 4.57 \times 10^{-5} \frac{\text{rad}}{\text{sec}^2} \right) \\ &= 5.23 \times 10^{-4} \text{ sec}^{-2}. \end{aligned} \quad (4)$$

For a  $\xi$  of 0.7 the required  $\tau$  is

$$\begin{aligned} \tau &= \frac{2\xi}{\sqrt{K_{OL}}} \\ &= \frac{2(0.7)}{\sqrt{5.23 \times 10^{-4}}} = 61 \text{ sec.} \end{aligned} \quad (5)$$

For large-signal operation, the gyro gain determines the switching line in the phase plane.

The roll loop in the sun-pointing mode is a simple rate-control loop (Figure 13-11).

Table 13-3 is a summary of the loop parameters chosen. These were chosen and verified as acceptable with the aid of single-axis analog simulations.

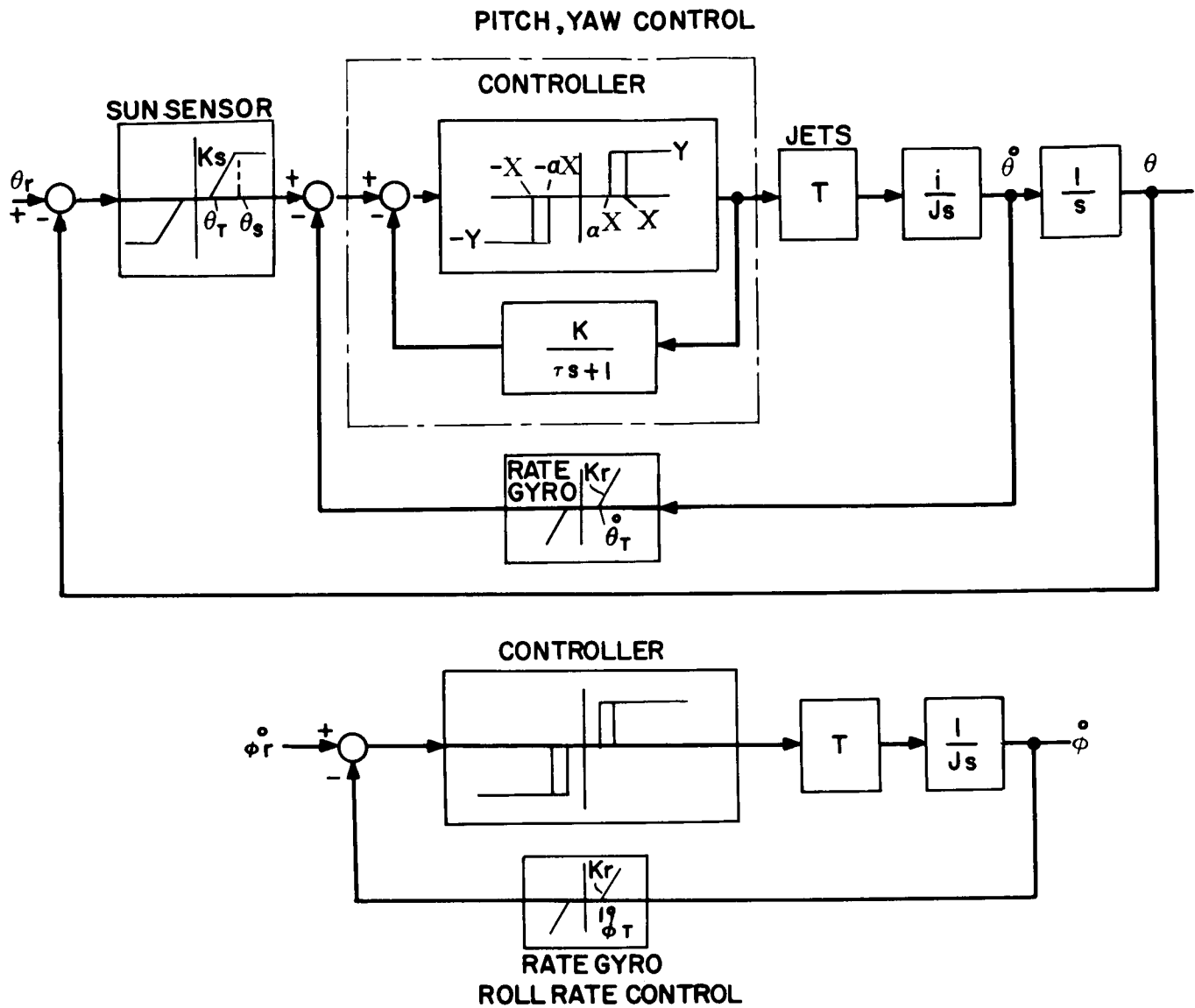


Figure 13-11. Sun-mode block diagram.

Table 13-3

## Sun-Mode Control-System Parameters

	Pitch	Roll	Yaw
$K_S$	2 V/deg	-	2 V/deg
$K_R$	60 V/deg/sec	60 V/deg/sec	60 V/deg/sec
X	1 V	-	1 V
$\alpha$	0.9	-	0.9
KY	10 V	-	10 V
$\tau$	61 sec	-	33.4 sec
Min. "on" Time	0.61 sec		0.334 sec
Jet Torque	0.077 lb-ft	0.115 lb-ft	0.04 lb-ft
Inertia	1686 slug-ft <sup>2</sup>	1686 slug-ft <sup>2</sup>	274 slug-ft <sup>2</sup>
Acceleration	$4.57 \times 10^{-4}$ rad/sec <sup>2</sup> 9.4 deg/min <sup>2</sup>	$6.83 \times 10^{-5}$ rad/sec <sup>2</sup> 14.1 deg/min <sup>2</sup>	$14.6 \times 10^{-4}$ rad/sec <sup>2</sup> 30.1 deg/min <sup>2</sup>

With the parameters determined on a single-axis basis, the three-axis equations of motion and control laws were put on the digital computer to determine acquisition times and fuel (Reference 2).

Table 13-4 is a comparison of acquisition times and fuel required using a full sine sensor and limited sensor ( $\pm 30$  degrees). The initial conditions used for this acquisition sequence were 1 degree/sec body rates in all three axes, and the sun line aligned with the body yaw axis. Acquisition is defined as the state in which all body rates are zero and the roll axis is aligned with the sun line.

Table 13-4

## Sun-Line Acquisition

	Full Sensor	Saturated Sensor
All body rates (+)		
Acquisition time (min)	11.4	10.65
Acquisition fuel (lb-ft-sec)	106.0	84.6
Utilization ratio (R)	2.52	2.01
Performance criterion ( $\Phi$ )	28.8	21.4
Pitch rate (-)		
Acquisition time (min)	12.25	10.4
Acquisition fuel (lb-ft-sec)	115.2	101.7
Utilization ratio (R)	2.74	2.42
Performance criterion ( $\Phi$ )	33.6	25.2

The utilization ratio (R) and performance criterion ( $\Phi$ ) are defined in Reference 3.

$$R = \frac{\text{Fuel used to acquire (ft-lb-sec)}}{\text{Initial momentum of spacecraft (ft-lb-sec)}}$$

$$\Phi = t_a \times R,$$

where  $t_a$  = acquisition time.

The reduction in acquisition fuel achieved by use of a saturated sun sensor was anticipated. Single-axis simulations demonstrated that with the proper parameters there could be periods in the acquisition sequence in which the spacecraft "coasts" and therefore does not require fuel. Table 13-4 does show that the time specifications for acquisition can be met using jets sized for operation in the fully deployed mode. Thus the same size jets may be used for acquisition and fine pointing.

The fuel and time shown in Table 13-4 can undoubtedly be reduced by optimization techniques. However, with a four-foot arm on each jet and a specific impulse of 175 sec (heated ammonia), the weight of fuel for acquisition (from these initial conditions) is less than 0.2 pound.

Figure 13-12 is a plot of successive projections of the body-roll axis on the inertial pitch-yaw plane.

If reacquisition of the sun line is necessary after deployment, the control accelerations will be much smaller. However, initial rates should also be much smaller. Table 13-5 shows reacquisition time and fuel requirements with the sun line in line with the yaw axis and zero rates around all axes.

Table 13-5

Reacquisition - Sun Mode

Time (min)	4.34
Fuel (lb-ft-sec)	19.3

Limit cycle operation in this mode is not critical with respect to fuel use, since earth acquisition follows soon after sun acquisition. The amplitude of the pitch limit cycle is important—too large a limit cycle amplitude reduces the window for earth acquisition. With the parameters of Table 13-3 and sensor

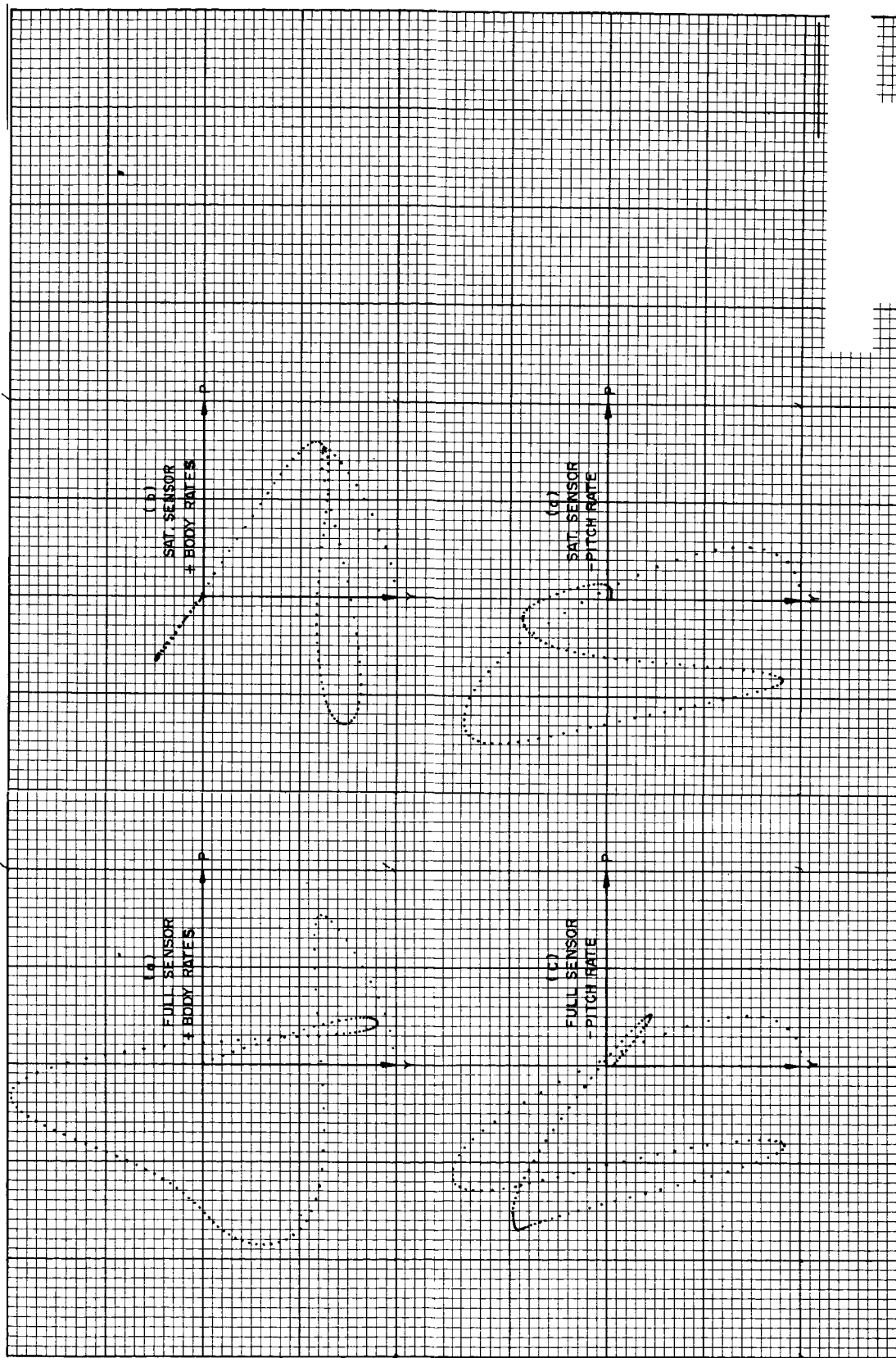


Figure 13-12. Direction cosines of body roll axis on  $P/Y$  plane.

thresholds of  $\pm 1.2$  degrees (sun sensor) and 0.04 degree/sec (rate gyro) the analog computer results showed limit cycle amplitudes of  $\pm 1.6$  degrees. Thus, with 0.01 degree/sec gyros and 0.5 degree sun sensors, the limit cycle could easily be kept below  $\pm 1.5$  degrees.

With the lag feedback providing rate information in the controller linear range, the threshold of the rate gyro could be opened. This could be used to prevent the jets from firing on gyro noise.

## EARTH ACQUISITION

Once the spacecraft is in the sun mode (roll axis pointed toward the sun) and fully deployed, it is sent a roll-rate command. In the sequence depicted in Figure 13-2, this would occur about 5:00 a.m. As it rolls around the sun line the earth sensor will (at some time) automatically scan the earth. During this period earth acquisition must take place.

The window or time available for earth acquisition is determined by the size of the earth's disk and orbital rate. From synchronous altitude the earth's disk subtends an angle of 17 degrees. With a 15 degrees/hr orbital rate the nominal viewing time is 68 minutes. However, this time is reduced by two factors:

1. Minimum chord required by the earth sensor: 0.5 degree.
2. Dead zone in pitch (sun mode): +1.5 degrees.

Since these quantities subtract on both edges of the earth, the effective earth width is 13 degrees and the viewing time 52 minutes. See Figure 13-13.

The rate at which the spacecraft is commanded to roll around the sun line is constrained by two factors:

1. The maximum rate is determined by the jet size. If the rate is too high, the jets will be unable to stop the spacecraft during the time the earth is in view of the sensor. For the jet size chosen, this maximum rate is 0.308 degree/sec. With this initial rate, the jets would be able to stop the spacecraft in 17 degrees.
2. The minimum rate is determined by the previously mentioned acquisition window. In the worst case the spacecraft would roll 360 degrees before the acquisition sequence could begin. If the

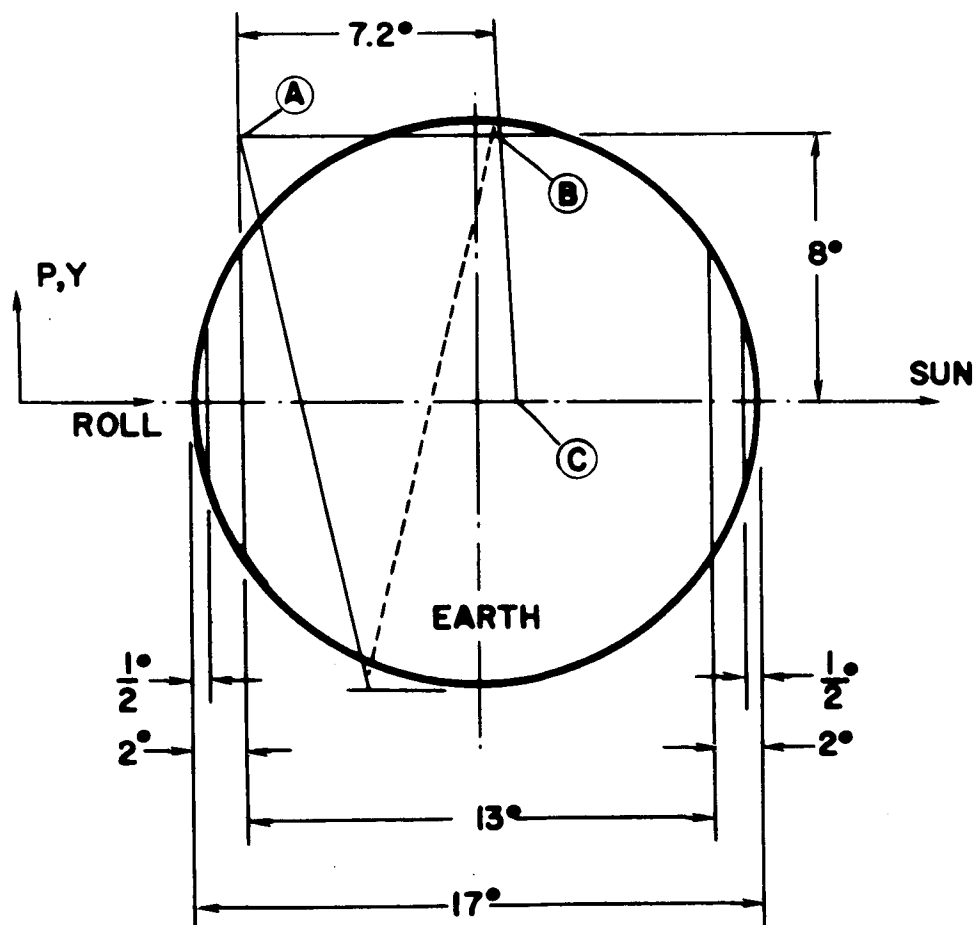


Figure 13-13. Local vertical acquisition.

roll rate were 0.115 degree/sec, all 13 degrees of the available earth would be used before acquisition could start. (See A to B in Figure 13-13.)

The roll rate chosen is 0.21 degree/sec. With this initial rate the jets will stop the spacecraft in 8 degrees of roll. The distance traversed across the earth's disk while the spacecraft is rolling 360 degrees is 7.2 degrees of an allowable 13 degrees.

There are at least three possible sequences which can be used to acquire the local vertical from the initial roll rate:

1. At the proper time, switch to the fine roll control and acquire the earth in roll single axis. Switch to fine pitch control and acquire in pitch.
2. At the proper time, switch to roll and pitch fine control and acquire both axes simultaneously.
3. At the proper time, switch proper jet on to stop spacecraft at approximately zero roll error (open loop). Switch roll and pitch to fine control.

These three sequences were compared with the aid of the analog computer. The comparison is shown in Table 13-6. Sequence 3 has been chosen as the most desirable from the time and fuel aspects. In summary, the earth acquisition sequence is as follows:

1. Roll around the sun line at -0.21 degree/sec.
2. At +8.0-degrees roll error (point B, Figure 13-8), turn on jet to reduce rate to zero (point C, Figure 13-13).
3. Switch roll control to fine pointing mode.
4. Switch pitch control to fine pointing mode.
5. Switch yaw control from the analog sun sensor to the digital sun sensor (Figure 13-2).
6. Bias digital sun sensor to acquire Polaris.
7. Switch yaw control from sun to Polaris.

Table 13-6

## Sequence Comparison

	Time (Min) Acquire Margin	Angle Across Acquire	Earth Margin	Overshoot (Degrees)	Fuel (ft-lb-sec)	Initial Conditions
1. Acquire roll and pitch single axis*	40	12	10.0 deg	3.0 deg	Roll 8.0 Pitch 0.5	21.8 0 deg 0.21 deg/sec 6.4 2.3 deg 0 deg/sec
2. Acquire roll and pitch simultane- ously*	35	17	8.8 deg	4.2 deg	Roll 8.0 Pitch 0.25	21.8 0 deg 0.21 deg/sec 4.3 <1.0 deg 0 deg/sec
3. Decelerate to 0, 0 & acquire roll and pitch single axis.	32	20	8.0 deg	5.0 deg	Roll ~0 Pitch 0.25	8.6 +8.0 deg -0.21 deg/sec 4.3 1.0 deg 0 deg/sec

\* Acquisition defined as time when rate is below  
0.005 degree/sec and position is below 0.5 degree.

## LOCAL VERTICAL POINTING

Following earth acquisition, the primary operational mode of the spacecraft will use reaction wheels. Jets will be used for dumping the wheels. However, the reaction jet system must be able to function (at least for a limited time) as a backup system.

### Specifications:

Accuracy:  $\pm 0.1$ -degree steady-state pointing error.  $\pm 0.5$ -degree dynamic error, i.e., maximum following error for ramp or sinusoidal input; maximum offset during stationkeeping disturbance.

Stability: Stable, low-rate limit cycle.

Response Time: Horizon-to-horizon slew (17 degrees) and settle within one-half hour.

Bandwidth: Track a low-altitude earth satellite with above stated dynamic error. Sufficiently high to maintain accuracy in presence of environmental disturbance torques. Minimize to refrain from exciting structural resonance.

Offset Point:  $\pm 8.5$  degrees in roll and pitch (i.e., anywhere on earth's disk).

### Sensors

Roll/pitch earth sensor - IR, time-shared detectors

Accuracy (LSB) -  $\pm 0.05$  degree  
Linear Range -  $\pm 9.0$  degrees

Polaris yaw sensor

Accuracy -  $\pm 0.02$  degree  
Field of view - 25-degree cone  
(Allows  $\pm 8.5$ -degree offset in roll and pitch with margin for overshoot)  
Linear Range -  $\pm 1$  degrees

Digital sun sensor (alternate yaw)

Accuracy           -  $\pm 0.5$  degree  
 Linear Range      -  $\pm 45$  degrees

Inertial gyro (inertial yaw hold)

Average drift -  $5 \times 10^{-5}$  degrees/sec.

The basic control loop used for fine pointing in all three axes is shown in Figure 13-14. Position information is obtained from the sensor listed above. Lead is obtained from the lag feedback (pseudo-rate) around the jet control relay. When the input voltage to the controller is less than required to saturate it the controller will operate in its pulsing or quasi-linear range. In this range the transfer function of the controller is approximately

$$\frac{1}{K} \left( \frac{\tau S + 1}{\left( \frac{\tau}{KK_1} \right) (S + 1)} \right), \quad (6)$$

where  $KK_1$  is the open loop gain of the controller loop and is much greater than one. From Figure 13-14 the open loop transfer function is

$$OLTF = \frac{K_{OL}}{S^2} \left( \frac{\tau S + 1}{\left( \frac{\tau}{KK_1} \right) (S + 1)} \right), \quad (7)$$

where  $K_{OL} = \frac{K_E}{K} \frac{(T/Y)}{J}$ .

Neglecting the controller lag, the closed loop transfer function is

$$CLTF = \frac{K_{OL} (\tau S + 1)}{S^2 + K_{OL} \tau S + K_{OL}}. \quad (8)$$

The characteristic equation is that of a second-order system where

$$\begin{aligned} K_{OL} &= \omega_n^2 \\ K_{OL} \tau &= 2\xi \omega_n \\ \tau &= \frac{2\xi}{\omega_n}, \end{aligned} \quad (9)$$

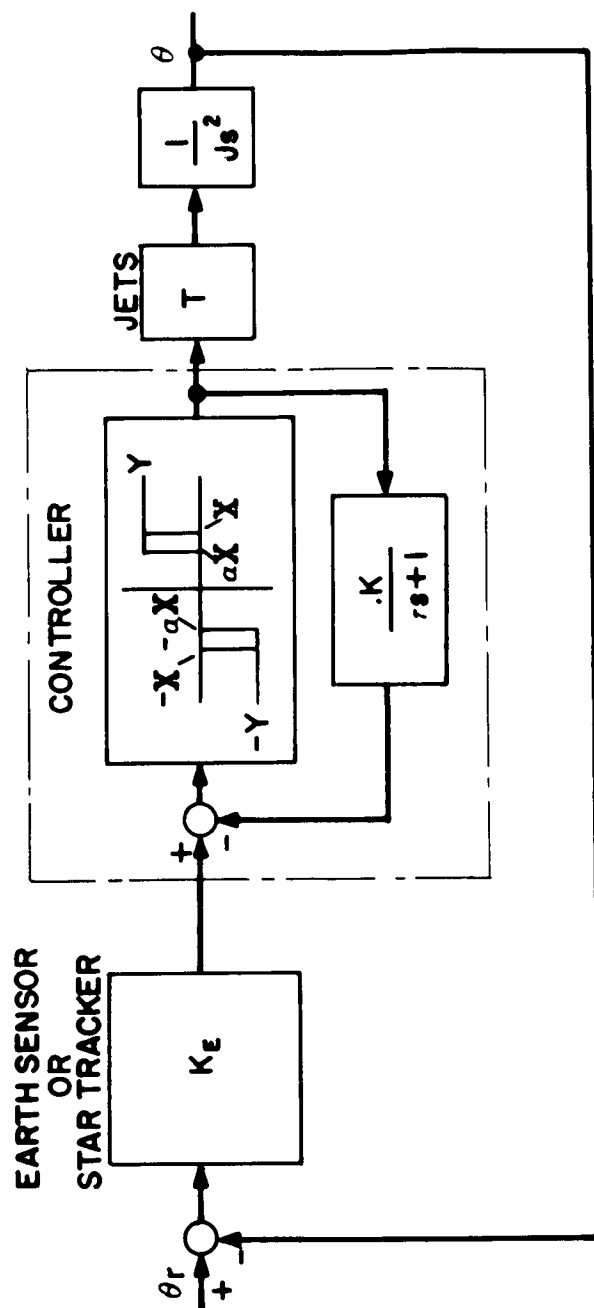


Figure 13-14. Basic control loop for all three axes earth pointing mode.

Where  $K_{OL}$  and  $\tau$  determine bandwidth and damping.

In roll and pitch the bandwidth is determined primarily by the solar-pressure torques. Since these are basically type-two systems, a constant torque disturbance (e.g., solar pressure) which is an acceleration input results in a steady-state offset. The bandwidth must be sufficiently high to insure that this offset is low. The offset is

$$\theta_{\epsilon} = \frac{T_D/J}{K_{OL}}, \quad (10)$$

where  $\theta_{\epsilon}$  = offset - radians

$T_D$  = disturbance torque - lb-ft.

It has been estimated that  $10^{-4}$  lb-ft is a reasonable maximum for solar pressure in pitch and roll. Allowing an offset of 0.01 degree (0.000174 rad), the open-loop gains are:

$$\begin{aligned} \text{Pitch } K_{OL} &= 3.56 \times 10^{-4} \text{ sec}^{-2} \\ \text{Roll } K_{OL} &= 2.11 \times 10^{-4} \text{ sec}^{-2}. \end{aligned} \quad (11)$$

Use the higher of these two for both pitch and roll. For a  $\xi$  of 0.7 the time constant in the lag feedback is

$$\tau = \frac{2\xi}{\omega_n} = \frac{2(0.7)}{\sqrt{3.56 \times 10^{-2}}} = 75 \text{ sec.} \quad (12)$$

The equation for the minimum on-time (m.o.t.) of the jets as determined by the controller is

$$\text{m.o.t.} \cong \frac{\tau(1-\alpha)X}{KY} \quad \text{for} \quad \frac{(1-\alpha)X}{KY} \ll 1. \quad (13)$$

A reasonable m.o.t. for the type of resistance jet being considered is 0.1 sec. With this m.o.t. the following system parameters satisfy the control loop requirements:

$K_E$	12.8 V/deg
$KY$	100 V
$\alpha$	0.73
$X$	0.5 V

Offset pointing will be accomplished by commanding 1-degree/min ramps into pitch and roll. A horizon-to-horizon slew would take 17 minutes allowing 13 minutes for settling. Figure 13-15 is an analog-computer record showing this type of ramp response in roll. The system does settle within the 13 minutes allowed. The maximum following error, even during the transient, is less than the 0.5 degree specification.

In yaw the bandwidth is determined by the coupling torque which results from a 1-degree/min slew in pitch and roll. This occurs during an offset-point command. This torque is of the same order of magnitude as the solar-pressure torques in pitch and roll. However, since it is during a slew command, the required dynamic error is 0.5 degree. Allowing a  $0.4\text{-degree}$  offset due to this torque disturbance, the required  $K_{OL}$  is  $0.0775 \times 10^{-4} \text{ sec}^{-2}$ .

The time constant required for  $\xi = 0.7$  is 503 sec. The remaining parameters, assuming an m.o.t. of 0.1 sec, are:

$K_E$	12.8 V/deg
KY	2300 V
$\alpha$	0.04
X	0.5 V

Bode plots of the three loops are shown in Figure 13-16.

A backup mode will be available for yaw control. This mode will use a digital sun sensor in conjunction with an inertial gyro for sensors. See Figure 13-10. The mode operation will be as shown in Figure 13-17. The gyro will be used during the noon and midnight passes. The specified drift rate for the gyro is  $5 \times 10^{-5} \text{ deg/sec}$  for a six-hour hold; this represents an error of about 1.1 degree. The sun sensor with a specified threshold of 0.5 degree will have a comparable accuracy. This backup system has an accuracy comparable to that of the sun-mode pointing. An RF attitude sensor is being considered as part of the experimental package for this spacecraft. This sensor could be used as a backup sensor for the earth sensor in the fine-pointing mode.

The frequency response required for tracking a low altitude satellite is about 0.00116 rad/sec (90 min period). Figure 13-16 shows that this is well within the specified bandwidth for the roll and pitch loops.

### Disturbances

Besides the solar pressure and coupling torques used to determine system bandwidth, other disturbances have been considered.

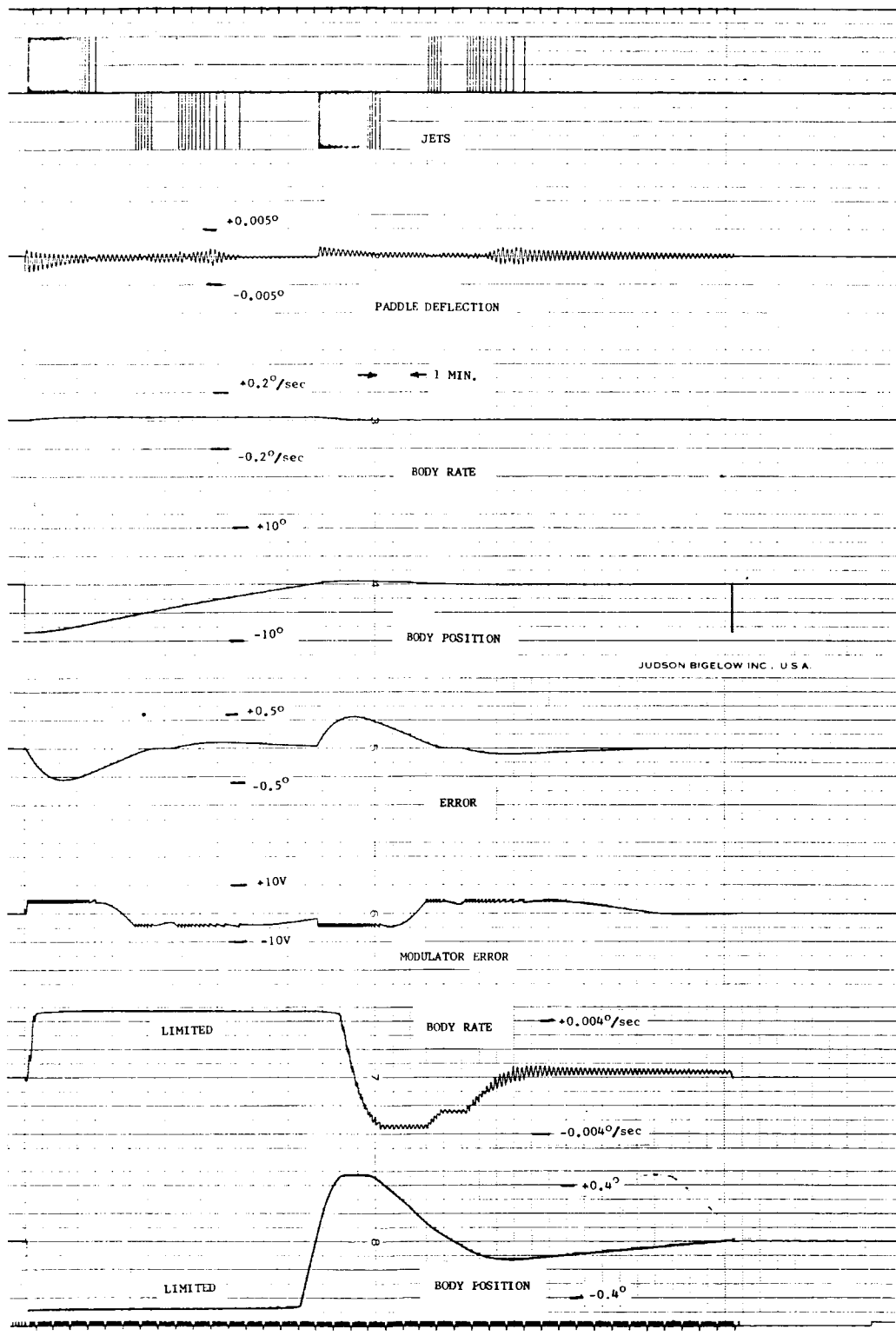


Figure 13-15. Ramp response.

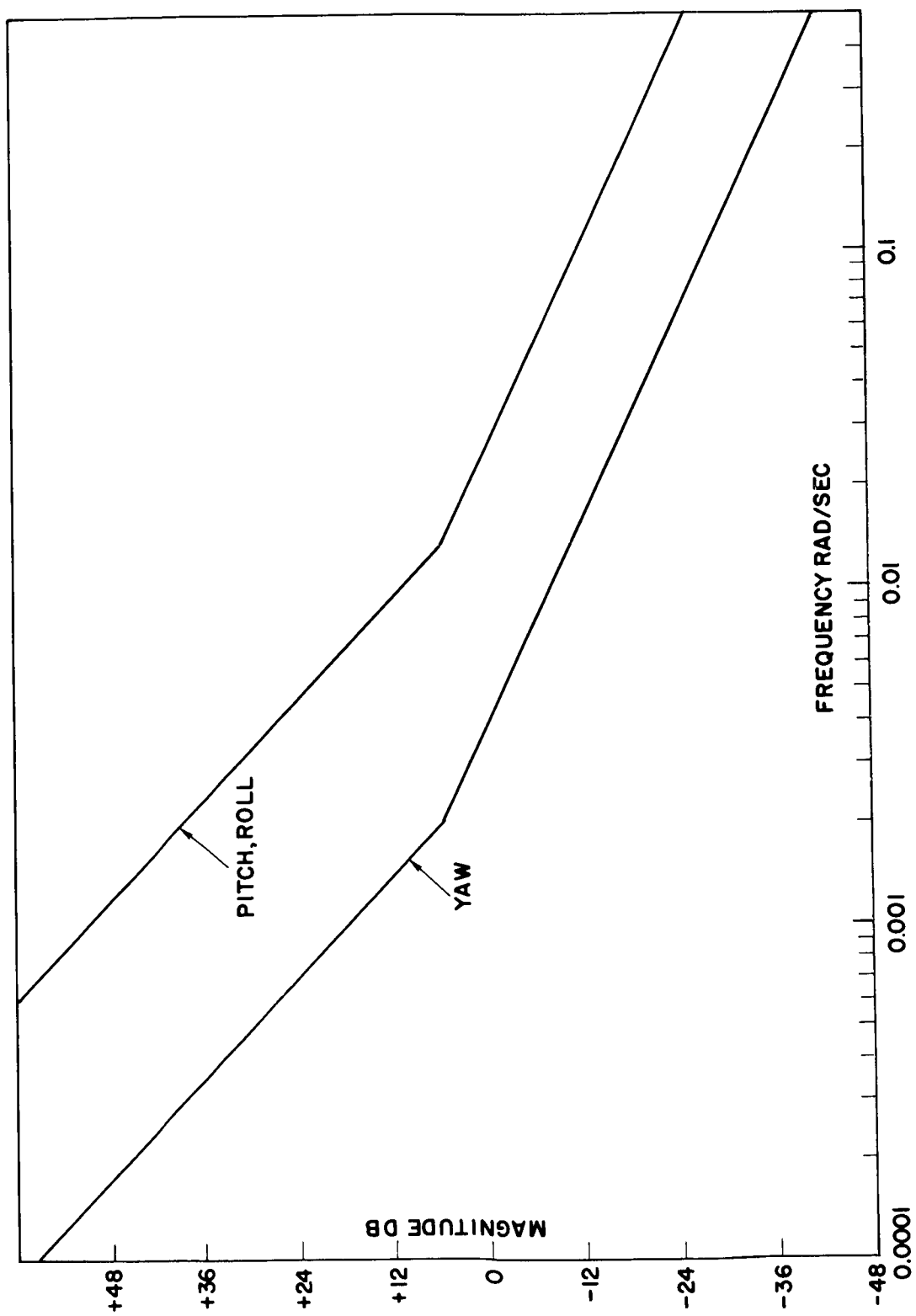


Figure 13-16. Earth pointing mode plot.

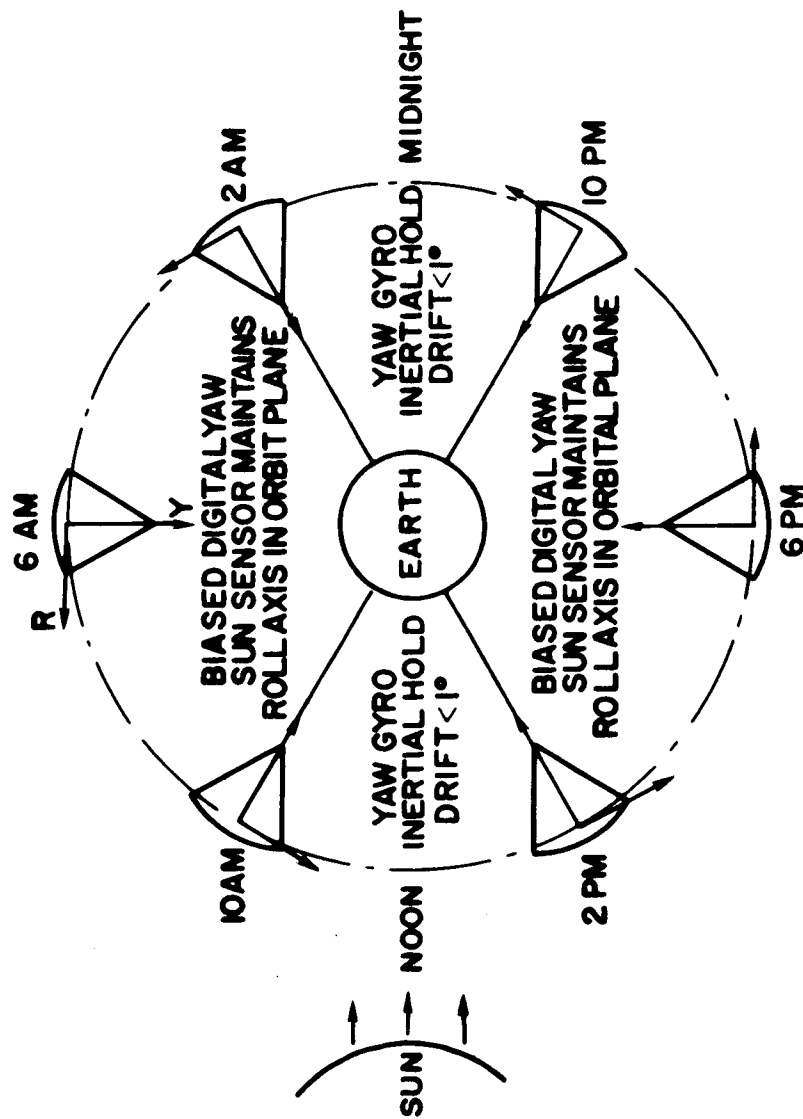


Figure 13-17. Sun-sensor/gyro-backup yaw control.

At the present time the total amount of fuel weight expected is about 30 to 40 pounds. This compares with a total spacecraft weight of approximately 1,300 pounds. Since the fuel weight is small and fuel sloshing can be minimized with proper tank and baffle design, it was decided to neglect fuel sloshing effects at this time.

Single degree of freedom solar paddle bending was simulated with the spacecraft to determine the effects on the system. A paddle natural frequency of 0.1 Hz and damping ratios ( $\xi$ ) around 0.005 were investigated. Some interaction was noticed, especially during rapid changes in position. The maximum deflection of the paddle was always less than 1 degree (Figure 13-15). The effect on the body position was not great; body position remained within the  $\pm 0.1$ -degree error band at all times. The assumed damping ratio of 0.005 may have been high. There is some information indicating that material damping at these frequencies is effectively zero. This problem is being investigated with the objective of raising  $\xi$  by some means if it is found to be extremely low. If the natural frequency is raised, this vibration becomes less of a problem. The root locus plot of the linear model of this system remains entirely in the left half plane indicating a stable system. However, since the model used to date has been simplified, asymptotic stability cannot be assumed at this time.

Another possibility that may be encountered is a steady-state jet-pulsing at the natural frequency of the solar paddles. This could occur for a particular level of disturbance torque. For a linear system with adequate damping this presents no problem; however, for lightly damped solar paddles and a non-linear control system this may present a problem. The problem is being considered.

### Fuel consumption

In a long-life mission with fine pointing requirements one of the primary concerns is fuel consumption.

The momentum required to compensate for the solar pressure disturbance is the integral of the absolute value of the disturbance torque. The solar-pressure torque for both pitch and roll has been assumed to be sinusoidal with a maximum value of  $10^{-4}$  ft-lb in both axes. The period for the pitch disturbance is orbital period. The period for the roll disturbance is one year.

$$\begin{aligned}\frac{\text{Momentum}}{\text{Period}} &= \int_0^P |T_{\text{DIS}}| dt \\ &= 2 \int_0^{P/2} (T_D \sin \omega t) dt \\ &= \frac{4T_D}{\omega},\end{aligned}$$

where  $T_D$  = Peak torque (lb-ft)

$\omega$  = Frequency of disturbance ( $\text{sec}^{-1}$ ).

For one year the fuel required for both pitch and roll is 4000 lb-ft-sec.

The fuel required for sun line and local vertical acquisition has been determined. See previous sections. The momentum per pitch slew is 0.94 ft-lb-sec. For a roll slew it is 1.58 ft-lb-sec. Assuming one pitch and one roll slew per day the total momentum required for one year is 921 ft-lb-sec. The single yaw slew to acquire Polaris requires a negligible amount of fuel compared to the above.

The coupling torque on the yaw axis due to a pitch/roll slew (1 degree/min) is about  $10^{-4}$  lb-ft. This represents about 0.1 ft-lb-sec per slew. For one slew per day for a year it is 36.5 ft-lb.

Tracking a low-altitude earth satellite is essentially a sinusoidal input to the system. The momentum required per orbit of the low altitude satellite is:

$$\begin{aligned}H &= 4A\omega J \text{ ft-lb-sec,} \\ \text{where } A &= \text{Peak of sin wave (radians)} \\ \omega &= \text{Orbital frequency (rad/sec)} \\ J &= \text{Spacecraft inertia (ATS-4) (slug-ft}^2\text{)}.\end{aligned}$$

For a low orbit  $A$  and  $\omega$  are 8.5 degrees and  $2\pi/5400$ , respectively, and  $H$  is 1.89 ft-lb-sec. Tracking for two 30-day periods would require 1806 ft-lb-sec.

The fuel requirements for one year of operation are summarized in Table 13-7.

Table 13-7

## Gas Consumption (ft-lb-sec)

	Pitch	Yaw	Roll
Sun acquisition	41.6	17.3	42.8
Sun reacquisition	19.3	-	-
Earth acquisition	4.5	-	9
Solar pressure	2000	-	2000
Offset point slew	343	36.5	577
Satellite tracking	-	-	1806

The total amount of fuel required as listed in this table is about 6900 ft-lb-sec for one year of operation. Each jet will have about a four-foot arm. The specific impulse of heated ammonia is expected to be about 175 seconds. This represents about 10 pounds of fuel (without margin). For a two-year mission with gas jets this would be about 20 pounds. An investigation showed that if rotatable solar paddles were used this fuel consumption number could easily be increased by 60 percent. This is a good reason to specify a fixed solar array.

Stationkeeping

The location of the jets is shown in Figure 13-18. East-west station-keeping may be carried out by firing jets 2 and 4. At least two methods are available for carrying out stationkeeping requirements. If stationkeeping jet 2 is fired with the C.M. about 2 feet below the jet, the spacecraft will experience a disturbance torque of 0.03 ft-lb that must be accounted for by the pitch control system. This high torque will cause a high duty cycle, high pulse rate from the pitch jet. With a bias applied simultaneously to the control system, the offset error could be kept at less than 0.5 degree. A preferable method would be to size the stationkeeping jet so that it balances the pitch jet around the C.M. Simultaneous firing of these two puts the thrust vector through the C.M. In this case the pitch control system need only take care of the resultant imbalances.

OPERATIONAL CONTROL

The operational (on station) requirements are summarized below:

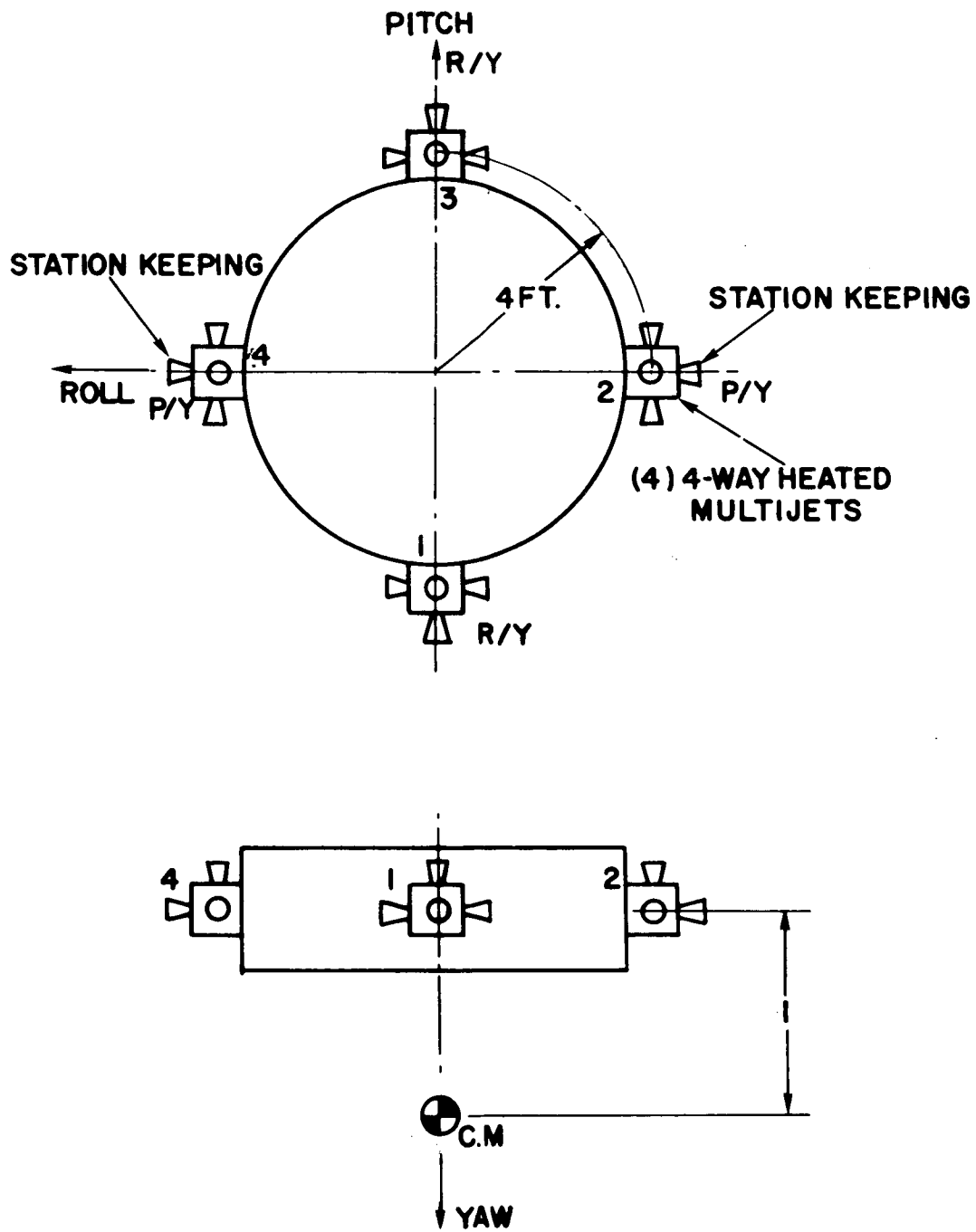


Figure 13-18. Thruster utilization.

Steady-state pointing	±0.1 degree
Offset range	±8.5 degrees
Horizon-to-horizon slew (17 degrees)	30 min
Sinusoidal input	
Peak value	±8.5 degrees
Frequency	0.07 rad/min
Peak error	±0.5 degree
Ramp input	
Maximum rate	1 degree/min
Steady-state error	0.5 degree.

Although our study showed that the pulse-modulated reaction-jet control could possibly fulfill the operational control requirements, a wheel-jet hybrid control similar to the Nimbus and OGO control systems is specified as the operational control for the following reasons:

The system is less sensitive to sensor noise.

The system is less sensitive to structural vibrations and disturbances.

There are smaller orbital stationkeeping disturbances.

Gas consumption is less dependent on the operational program.

The system is adaptable to a gimbaled gravity-gradient boom experiment.

There is approximately equal weight tradeoff for a two-year mission.

The wheels required, based on a nominal  $10^{-4}$  ft-lb solar pressure torque, are similar to the OAO fine wheels (2 ft-lb-seconds momentum storage and 0.04 ft-lb torque). Also our study has shown that the control system bandwidths can be kept below 0.10 radians per second by using proportional plus integral control implemented through a time-shared digital controller.

## SENSORS

The primary sensors for three-axis earth-pointing control will be a gimbaled infrared earth scanner for roll/pitch and an electronically scanned star tracker for the yaw reference (Polaris).

Star trackers using no moving parts have been developed with the following demonstrated performance capability:

Field of view: 8 degrees diameter

Accuracy: 10 arc/seconds with a +3-magnitude star

Error gradient: 300 mv per arc/minute.

The Polaris tracker requirements in these areas are as follows:

Field of view: 4 degrees by 25 degrees, or 25 degrees diameter

Accuracy: 1 arc/minute

Error gradient: 100 mv per arc/minute.

There is a direct linear tradeoff between field of view and accuracy. The Polaris tracker requires three times the field of view, but can tolerate accuracy six times poorer. The larger field of view of the Polaris tracker requires a reduction in the error gradient to maintain the same limiting output voltage levels. The reduction of the gradient by a factor of three is again consistent with the reduced accuracy requirement. No problems are anticipated in adapting existing star-tracker technology and capabilities to the Polaris tracker requirements.

Horizon scanners which utilize mechanical scanning principles, such as rotating prisms, vibrating mirrors, etc., have been developed to the point where 1/4-degree accuracy has been achieved on a regular basis in actual flights. This level of accuracy can be obtained over various altitude conditions and over appreciable linear ranges. At least two companies have already supplied such instruments, and several others are capable of supplying them. The requirements of ATS-4 are such that a satisfactory horizon scanner can be developed from presently known principles, with no advance in the state of the art. The two main requirements are:

1. Accuracy  $\pm 0.1$  percent
2. Offset capability  $\pm 8.5$  degrees in each axis

These apparently difficult requirements are mitigated by the following factors:

1. Altitude is fixed at synchronous with eccentricity only 0.022.
2. Outputs need be updated only once every two seconds; this is a very long time constant in terms of horizon scanners.

In addition to these two factors, certain solutions of requirement 2 automatically make requirement 1 easier to meet. This comes about as follows: Assume that the sensor is gimballed to provide for the 8.5-degree offset requirement. This would not only allow offset, but it would mean that the sensor needs high accuracy only at sensor null. The linear range needed is very, very small (determined only by the null of the gimbal servo loop). Actually, it is not necessary to gimbal the entire sensor. Only the optical axis need be gimballed. This can be done with mirrors, prisms, or other means. By combining these known principles of horizon scanner design, an ATS-4 scanner could be developed in a reasonably short period of time, with a very high probability of success.

Other ATS - 4 sensors, not required for normal three-axis earth pointing, are:

Acquisition Sun Sensor - Four linear null detectors plus an array of logic cells to provide two-axis inertial orientation toward the sun. The sensor will have a spherical field of view and  $\pm 0.5$ -degree accuracy at null.

Digital Sun Sensor - A slit-type sensor to provide yaw control for Polaris acquisition. The sensor will have a linear range of  $\pm 40$  degrees with an accuracy of  $\pm 0.75$  degrees and sensitivity sufficient to operate at sun incident angles as low as 30 degrees. A digital command word will provide the appropriate bias, determined by time of day and time of year, to place the spacecraft roll axis within  $\pm 1.5$  degree of the equatorial plane.

Body Rate Sensors - A three-axis package is required for rate control and damping during the acquisition sequence. The required minimum commandable rate is 0.2 degree/sec with a threshold of 0.02 degree/sec.

Inertial Gyro - Yaw control to within  $\pm 3$  degrees is required for efficient solar-array operation and station-keeping thrusting. Yaw control as a backup to the Polaris sensor can be obtained to this accuracy over 67 percent of the orbit, using the biased digital sun sensor. Yaw control during  $\pm 2$  hours of local noon and midnight would degenerate to just a rate limit of less than 0.02 degree/sec as maintained by the yaw body gyro; a yaw reacquisition would occur twice a day. Yaw control to within  $\pm 3$  degrees over the complete orbit

can be obtained by adding a yaw gyro of medium inertial quality (average drift  $5 \times 10^{-5}$  degrees/sec).

## SUMMARY OUTLINE

### Mission Requirements

#### Spinning-body control

Active-nutation damping threshold (cone angle)	0.2 degree
Spin-axis reorientation accuracy	±1.5 degree
Fuel (precession and damping)	19 ft-lb-sec/degree

#### Acquisition Control

##### Sun-line acquisition

Initial body rates	±1 degree/sec
Steady-state yaw/pitch error	±1 degree
Steady-state roll rate	±0.05 degree/sec
Time to acquire	10 min
Fuel to acquire	100 ft-lb-sec

##### Local vertical acquisition

Initial roll rate	0.2 degree/sec
Steady-state roll-pitch error	±0.5 degree
Time to acquire (max)	30 min
Fuel to acquire	30 ft-lb-sec

##### Polaris acquisition

Sun sensor bias (max)	38 degrees
Steady-state yaw error	±0.5 degree
Time to acquire (max)	6 min
Fuel to acquire (max)	18 ft-lb-sec

##### Stationkeeping disturbance

Disturbance torque	0.003 ft-lb
Attitude error	±0.5 degree

## Operational control

### Static pointing

Steady-state error	$\pm 0.1$ degree
Off-vertical range	$\pm 8.5$ degrees
Horizon-to-horizon (17 degrees) maneuver	30 min

### Sinusoidal input

Peak value	$\pm 8.5$ degrees
Frequency	0.07 rad/min
Peak error	$\pm 0.5$ degree

### Ramp input

Maximum rate	1 degree/min
Steady-state error	0.5 degree

### Stationkeeping disturbance

Peak value	0.75 ft-lb-sec
Duration (max)	250 sec
Peak error	$\pm 0.5$ degree
Settling time	10 min

## Sensor requirements

### Roll/pitch earth sensor

Accuracy	$\pm 0.05$ degree
Offset range	$\pm 8.5$ degrees

### Polaris yaw sensor

Accuracy	$\pm 0.02$ degree
Field of view	25 degrees x 4 degrees
Linear range	$\pm 1$ degree

### Digital yaw sun sensor

Accuracy	$\pm 0.75$ degree
Linear range	$\pm 40$ degrees

### Acquisition sun sensors

Accuracy	$\pm 0.5$ degree
Field of view	spherical

### Spinning-body sensors

Sun sensor (2 axes)	$\pm 0.5$ degree
RF polarization angle	$\pm 1$ degree
Star field mapper (3 axes)	$\pm 0.1$ degree
Accelerometer range	0.84-42 degrees/sec <sup>2</sup>

### Body-rate gyros

Threshold	0.02 degree/sec
Commanded rate	0.2 degree/sec

### Inertial yaw gyro

Average drift	$5 \times 10^{-5}$ degree/sec
Duration of inertial hold	4 hours
Maximum yaw-error increase	$\pm 1$ degree

## Control Concepts

Synchronized axial jet pulses - 12-ft lb, 0.2-second pulses used to control the spinning body.

Pulse modulated jets - Used in the acquisition control to provide the torque for sun acquisition, operational control.

Wheel-jet hybrid - Used with the digital operational control system to provide momentum control for the operational mission requirements.

## Control-system design guidelines

Reaction jet thrusters - Use one set of thrusters for both attitude control and stationkeeping Use the thrust level for sun acquisition, local vertical acquisition, and backup operational control.

Three-axis time-shared digital controller - Used to obtain high-accuracy processing of command and error signals and to generate low-frequency compensating networks.

Control system bandwidth - Minimize to prevent control-system/structure resonance.

## REFERENCES

1. Schramm, Robert: Analysis of a Pulse Modulator. Stabilization and Control Branch Report No. 146, Aug. 1966
2. Frisch, Harold P.: Quaternion Representation of the Dynamic Equations Describing the ATS-4 Acquisition Study. Stabilization and Control Branch Report No. 145, Aug. 1966
3. Sahroff, A., Farrenkopf, R., Frew, A., and Gran, M.: Investigation of the Acquisition Problem in Satellite Attitude Control. Tech Report AFFDL-TR-65-115, Research and Technology Division, Air Force Systems Command, Wright-Patterson Air Force Base, Ohio, Dec. 1965

## SECTION 14

### PROPULSION SYSTEMS

#### A. PROPULSION SYSTEMS ANALYSIS

##### PROPULSION SYSTEM SELECTION AND ANALYSIS

Previous sections of this report have described the launch sequence, the orbit correction maneuvers, and the east-west station keeping requirements. The launch vehicle, spinup rockets, and apogee kick motor have been selected. Now, the remaining spacecraft propulsion requirements must be provided.

During the launch phase, a propulsion system must provide for the following spacecraft maneuvers: nutation damping, spin axis precession, and eccentricity and inclination removal. A vernier propulsion system, moreover, is required to provide for initial spacecraft stabilization, momentum dump for the attitude control wheels, east-west station keeping for 2 years, and back-up for the primary attitude control system for 1 year of operation.

The following constraints have been placed on the auxiliary propulsion system:

- a. The attitude control system requires a torque of approximately 12 ft-lb about the plane perpendicular to the spin axis (i. e. thrust parallel to the spin axis) during the launch phase.
- b. The thrust for removal of eccentricity and inclination should be as high as possible to keep the pulse time to a minimum.
- c. The attitude control system torque requirements for the vernier propulsion system are
  - (1) Roll: 0.12 ft-lb
  - (2) Pitch: 0.08 ft-lb
  - (3) Yaw: 0.04 ft-lb
- d. The propulsion system is to provide a one year back-up for the primary attitude control system. This capability should be maintained even with one thruster module inoperative.

- e. The jets cannot be located at the spacecraft center of mass.

The first constraint calls for a combination of either a high thrust on a short moment arm or a low thrust on a long moment arm. The second constraint dictates the high thrust, short moment arm design. Space allocation, however, dictates a long moment arm to avoid jet impingement problems. A thrust level of 5 pounds with a 2.4 foot moment arm has been selected as a compromise for these requirements. The third and fourth constraints dictate thrust levels between 0 and 60 millipounds. The 5 pound propulsion jets cannot be used for any of these functions. Figure 14-1 shows the jet locations with the chosen thrust sizes. The method of sizing the thrust levels is presented later in this section.

A hydrazine system has been chosen to provide the 5 pound thrust requirements during the launch phase, and an ammonia thermal storage resistance jet system has been selected to satisfy the vernier propulsion needs.

The hydrazine ( $N_2H_4$ ) system, which is described in Section 14-B provides a number of advantages over a hydrogen peroxide ( $H_2O_2$ ) system. Hydrazine requires less handling and storage care. Peroxide propellant reacts to some extent with almost every substance. When  $H_2O_2$  becomes contaminated, it will decompose. Contamination may continue to the point where an explosion occurs. As might be inferred from the contamination aspects,  $H_2O_2$  presents more component material compatibility problems than  $N_2H_4$ . Hydrazine gives better performance than the hydrogen peroxide. Steady state specific impulse of  $N_2H_4$  is approximately 235 seconds, while that of  $H_2O_2$  is about 150 seconds. Hydrazine, then, in addition to being more reliable than hydrogen peroxide, will provide a savings in system weight. Hydrazine systems are scheduled to fly on a number of spacecraft and should be a reliable flight proven system, representing the state-of-the-art, for the ATS-4 launch date.

The thermal storage resistance jets, which are described in detail in Section 14-B provide considerable savings in fuel consumption over a cold gas system. The specific impulse of the ammonia ranges from about 100 to 260 seconds, depending on power input. Compare this to nitrogen, for example, with a specific impulse of about 47 seconds. Moreover, the tankage weight of the ammonia feed system is considerably less than that of a nitrogen system.

Both ion and radioisotope engines are capable of satisfying the vernier propulsion requirements. Ion engines were eliminated from consideration because of the large power requirement associated with the selected thrust level of the jets. Radioisotope thruster development has not progressed to the point where they could be logically considered for ATS-4.

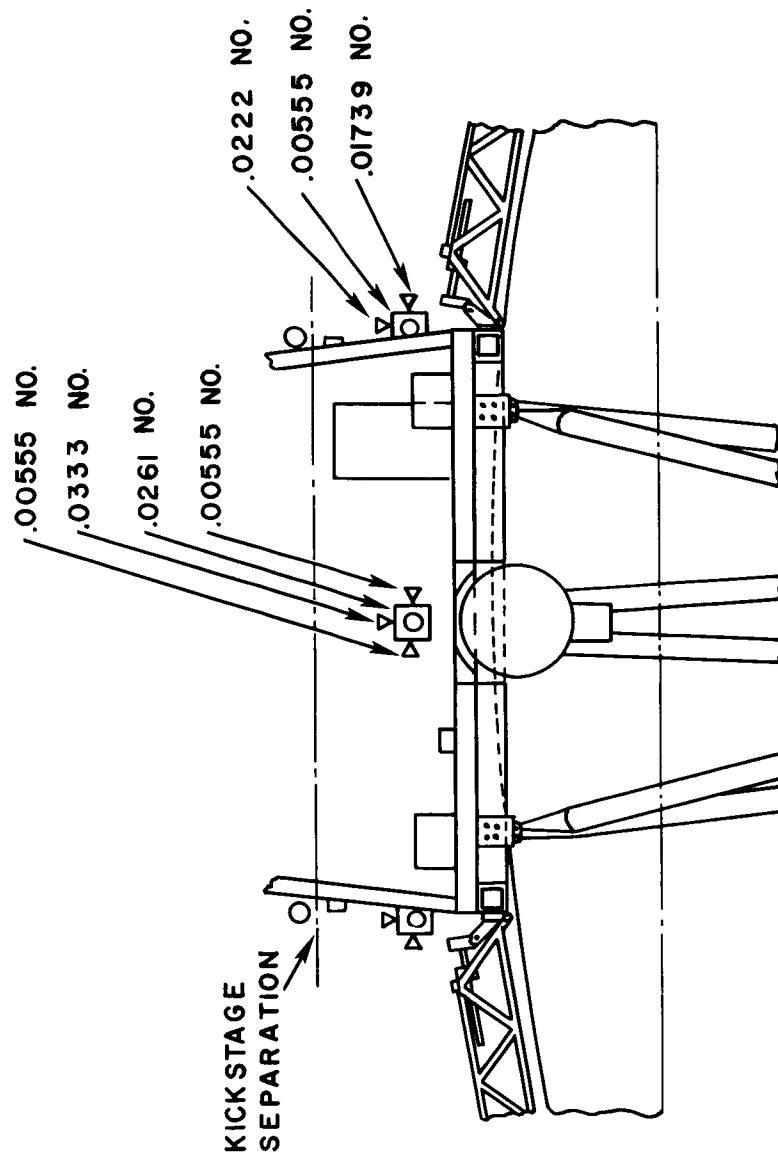


Figure 14-1. Resistance jet locations and thrust sizes.

A low thermal inertia resistance jet is being used experimentally in ATS-B. Power is turned on and a short propellant pulse takes advantage of the system's quick heat up. The specific impulse involved here is dependent on the peak power input to the thruster. The thermal storage resistance thruster was chosen over the low thermal inertia type because it requires a lower peak power input for the same specific impulse.

A thermal storage resistance jet is being flown this year by the Naval Research Lab. This type of system should be flight qualified before ATS-4 is launched. The operation of the system for ATS-4 will provide advanced technology in trading off power input with propellant usage.

It is explained in Section 14-B that a standby power input to the thruster heaters is recommended for the resistance jets. The planned ATS-4 operation mode is to provide a standby power input of 5 watts to each thruster module. The total standby power is about 30 watts, including feed system, telemetry, and power conditioner requirements. All inertia wheel momentum dump will be done with no additional power input. Every 10 to 11 days, the station keeping thruster module will receive an additional 30 watts for two 2-hour periods, 12 hours apart. This will conserve propellant as well as demonstrate the resistance jet capability of providing  $I_{sp} > 200$  seconds. In the event of an attitude control system failure, the resistance jets would take up this function. Three of the thruster modules would be used. The power saved from the primary attitude control system would be added to these three modules, providing an increase in operating temperature thereby decreasing propellant consumption.

Table 14-1 indicates the resistance jet ammonia propellant consumption and weight breakdown. The specific impulses shown are based on Figure 14-7 and the power inputs previously specified. Enough propellant is provided to accomplish items 1, 2, and 3 in Table 14-1, and at least 6 months of the 1 year backup for the attitude control system (i. e. with all the thruster heaters inoperative).

The propellant and weight analyses of the hydrazine system are presented in Table 14-2. The propellant weight for various functions differs from that presented in Section 14-B in that Table 14-2 is based on updated launch error analyses. Since the total propellant requirement has not changed significantly, the tankage and component weights are the same as those presented in Section 14-B. The power requirements for this system are given in Table 14-6 of Section 14-B.

Table 14-1

## Ammonia Propellant Use and System Weight

	Total Impulse (lb-sec)	Assumed Average Specific Impulse (sec)	Propellant Weight (lb)
* 1. East-West Station Keeping for Two Years ( $\Delta V = 50$ ft/sec)	2174	200	10.9
* 2. Initial Orbit Corrections ( $\Delta V = 50$ ft/sec)	2174	200	10.9
**3. Primary Attitude Control System Requirement	181	140	1.3
**4. One year backup for Primary Attitude Control System	1763	160	11.0
Total Propellant Extra fuel to account for possible thruster failures or spacecraft heater power failures.			34.1
Hardware Weight			22.9
			46.0
Total System Weight			103.0

\* Based on simultaneous radial and tangential thrusting to provide thrust through center of mass.

\*\* Based on Jet locations shown in Figure 14-1 and information obtained from Stabilization & Control Branch.

Table 14-2

## Hydrazine Propellant Use and System Weight

Function (all error quantities based on trade-off studies in previous sections)	Duty Cycle Time on Time off	Total Time	Firing Time (sec)	No. of Thrusters Used	Assumed I <sub>sp</sub> (sec)	Propellant Wt. (lb)	Approximate No. of Pulses
1. Damp out Residual Spinup Rates (4.24 degrees per second)	$1/3 = \frac{.18126}{.5435}$	59.1 sec	19.7	1	215	0.5	108
2. Spin Axis Precession (12.8 due to spinup)	$1/6 = \frac{.1812}{1.087}$	274.8 sec	45.8	1	225	1.0	253
3. Active damping to 2nd Apogee (Assuming 1 degree per hour)*	$1/6 = \frac{.1812}{1.087}$	15 3/4 hr	59.0	1	125	2.4	326
4. 2nd Spin Axis Precession (Assuming 1/4 of #2)	$1/6 = \frac{.1812}{1.087}$	68.7 sec	11.5	1	215	0.3	63
5. Damp Out Transverse Rates After Firing of Kick Motor (6.1 degrees per second)	1/3	63.3 sec	21.1	1	215	0.5	117
6. Active Damping After Kick Stage Firing (Assume 1 degree per hour)	1/6	48 hr	163.0	1	125	6.5	905
7. Precession to remove inclination (Maximum of 110 percent)	1/6	2460 sec	376	1	230	8.2	208
8. Inclination Removal ( $\Delta V = 85.0$ ft/sec)	Steady Firing	525 sec	525	2	235	22.3	1
9. Precession to remove eccentricity (90 degrees)	1/6	1632 sec	306	1	230	6.6	169
10. Eccentricity Removal ( $\Delta V = 87.5$ ft/sec)	Steady Firing	479 sec	479	2	235	19.7	1
Total						78.0	
15% Contingency Factor						11.7	
Tankage & Hardware Weight						22.9	
Total System Weight						112.6	

\* Information obtained from Stabilization &amp; Control Branch

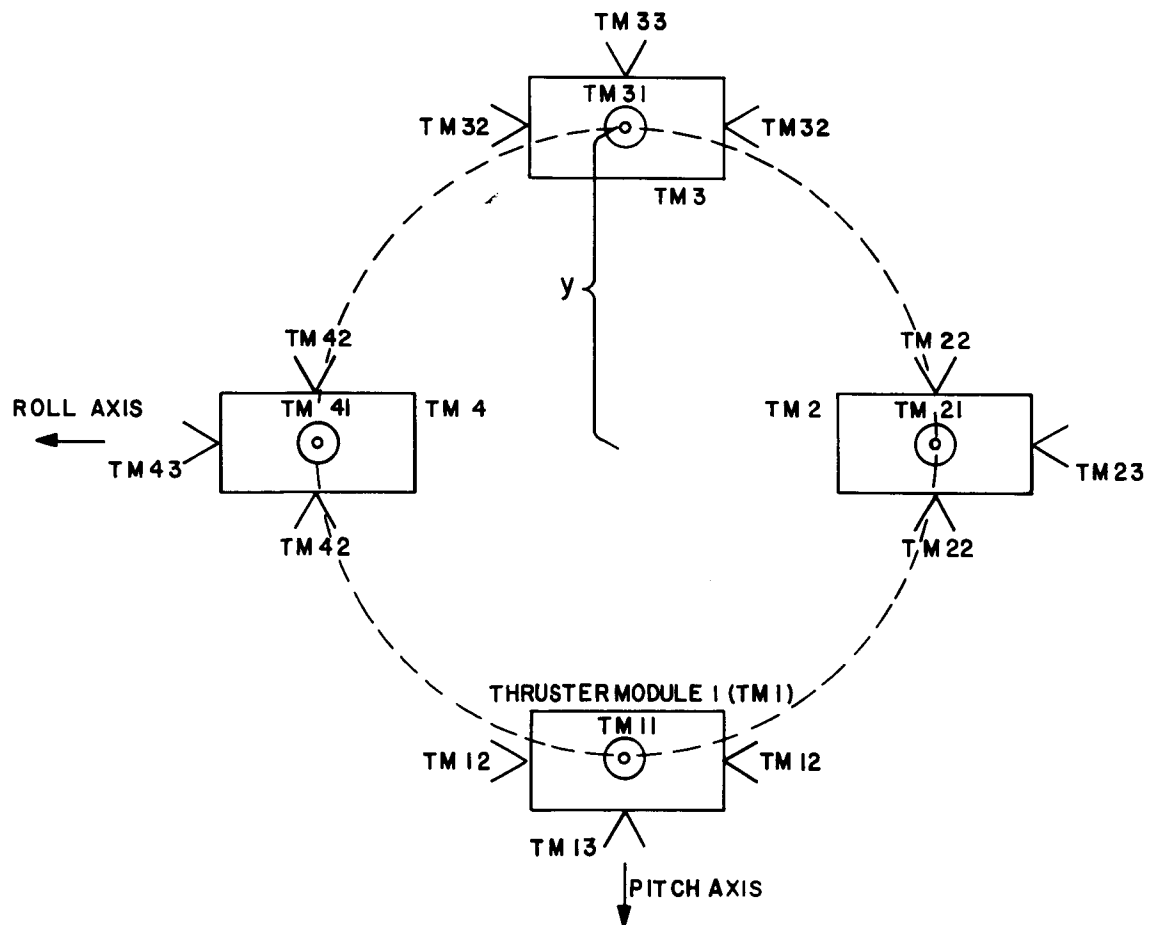


Figure 14-2. View of thruster jet locations looking down yaw axis.

## SIZING AND FUNCTIONS OF VERNIER PROPULSION JETS

The vernier propulsion system must satisfy the following requirements: roll torque of 0.12 ft-lb, pitch torque of 0.08 ft-lb, yaw torque of 0.04 ft-lb, back up for the primary attitude control system with one thruster module inoperative, and resultant vector for E-W station keeping passing through the CM of the spacecraft.

All the thruster jets are located in the same plane, perpendicular to the yaw axis. Figure 14-2 is a simplified view of the thrusters, looking down the yaw axis. Let Y be the perpendicular distance from the yaw axis to the thrust vectors, not passing through the yaw axis. Let X be the distance from the plane of the thrusters to the CM. Symmetry dictates that modules 1 and 3 and modules 2 and 4 have the same thrust levels.

Referring to the nomenclature shown in Figure 14-2, the following equations apply:

Roll Requirement:

$$(TM11) \ Y = 0.12 \quad (1)$$

Roll Requirement With One Module Inoperative:

$$(TM13) \ X = 0.12 \quad (1a)$$

Pitch Requirement:

$$(TM21) \ Y = 0.08 \quad (2)$$

Pitch Requirement with One Module Inoperative:

$$(TM23) \ X = 0.08 \quad (2a)$$

Yaw Requirement:

$$2 (TM22) \ Y = 0.04 \quad (3)$$

$$2 (TM12) \ Y = 0.04 \quad (3a)$$

Station Keeping Through CM:

$$(TM11) \ Y = (TM13) \ X \quad (4)$$

On the spacecraft configuration selected for ATS-4,  $Y = 3.6$  ft and  $X = 4.6$  ft. Solving equations 1 through 4 gives the following thrust levels:

$$TM11 = 0.0333 \text{ lb}$$

$$TM12 = 0.00555 \text{ lb}$$

$$TM13 = 0.0261 \text{ lb}$$

$$TM21 = 0.0222 \text{ lb}$$

$$TM22 = 0.00555 \text{ lb}$$

$$TM23 = 0.01739 \text{ lb}$$

Table 14-3 gives the various propulsion functions of each thruster.

## TELEMETRY AND COMMAND REQUIREMENTS

The two hydrazine thrusters will require a total of 14 data channels. The parameters to be telemetered are specified in Table 14-4. The measurements specified are the minimum that would allow performance evaluation and trouble monitoring. The output from the respective transducers will be signal conditioned to the required 5 volt full scale level to meet the spacecraft telemetry interface requirements. The design and fabrication of the signal conditioners will be straightforward, requiring a minimum of circuit design effort. Physical packaging will depend on the space, weight, and location allocated by the spacecraft.

The hydrazine thrusters will be operating in a pulse mode, either as a pair or singly, controlled by the on-board logic/command system. The duty cycle will vary with thrusting function and the pulse duration will be less than one second for most functions. This means that all 14 channels should be sampled in a fixed sequence, if possible to the exclusion of all other spacecraft telemetry, to acquire as much as possible of the transient or short duration (less than one second) signals.

The proposed telemetry data transmission rate prior to spacecraft deployment is 40 samples per second (owing to antenna pattern deficiency). Even with the exclusion of all other spacecraft telemetry, the greatest sample rate which could be obtained from the 14 channels is three per second. A pulse of less than 0.3 seconds duration could be completely undetected by the telemetry system. Thus, the proposed 40 samples-per-second system is inadequate for the required hydrazine telemetry.

Table 14-3

## Vernier Propulsion System Utilization

Thruster Jet Number	TM11	TM12	TM13	TM21	TM22	TM23	TM31	TM32	TM33	TM41	TM42	TM43
Jet Thrust Level (lb) x 10 <sup>2</sup>	3.33	.555	2.61	2.22	.555	1.739	3.33	.555	2.61	2.22	.555	1.739
Station Keeping	*		*									
+ Roll Torque			**				*					
- Roll Torque	*								**			
+ Pitch Torque				*								**
- Pitch Torque						**				*		
Yaw Torque (Couple)		**			*			**			*	

\* Signifies the jets which would be used with all four modules operative.

\*\* Signifies the jets which would be used if the \* jets had failed.

Table 14-4

## Telemetry Requirements for ATS-4 Hydrazine System

<u>Telemetry Requirements</u>	<u>No. of Measurements</u>
Thrust Measurement	2
Chamber Pressure	2
Temperature (2 in combustion chamber & 1 in feed tube)	6
Hydrazine Pressure	2
Nitrogen Tank Pressure	2
Total	<u>14</u>

Table 14-5

## Telemetry Requirements for ATS-4 Ammonia Resistance Jet System

<u>Telemetry Requirements</u>	<u>No. of Measurements</u>
Storage tank pressure	1
Storage tank temperature	1
Plenum tank pressure	1
Plenum tank temperature	1
Propellant flow rate	1
Voltage input to thruster heaters	4
Current drawn by thruster heaters	4
Thruster core temperature	4
Pressure at thruster inlet	16
Cumulative number of pulses from each jet	<u>16</u>
Total	49

It appears that if 40 samples per second becomes the actual spacecraft sampling rate, some compromise hydrazine telemetry requirements will have to be proposed. These compromises will have to be made when information becomes available as to the maximum telemetry sampling rate allotted to the hydrazine system.

The command system for the hydrazine thrusters will consist of six on-off commands. The first command will be the opening of propellant and pressure equalizing gas tanks to the feed manifolds. This command can be programmed into the launch phase spacecraft command system. The second command is an emergency command to close off the propellant feedline and will be a manual keyboard command. Both of these commands will be "on" commands only. In addition to these, it is desirable that two sets of thruster on-off ground command capability be provided to override the on-board spacecraft command system.

The ammonia resistance jet system requires a total of 49 channels (see Section 14-B for a description of the system). The parameters to be measured are listed in Table 14-5. Again, it may become necessary to make compromises if this requirement is beyond the telemetry system capabilities.

Operation of the thrusters for both inertia wheel momentum dump and east-west station keeping will be at pulses ranging from 15 seconds to 4 minutes. Two measurements per second would be adequate for data evaluation. On the basis of preliminary telemetry system information, it appears that this requirement should be within the capabilities of the spacecraft telemetry system.

If the thrusters are pressed into the back-up attitude control use, however, pulses of the order of .25 seconds with a 50% duty cycle may be required. A considerable increase in the sampling rate would be required to obtain meaningful data.

The command system will be employed to turn on the primary power to the four power conditioners shortly before the spacecraft reaches the synchronous altitude. The power to the thrusters will be gradually stepped up to the normal operating power ( $\approx 5$  watts each). The power conditioner will have the capability of supplying higher power levels to the thrusters (for station keeping operation) via ground command. The pulsing of the thrusters under normal conditions will be controlled by the on-board stabilization and control logic system. The on-board system will also pulse the thrusters in the event they are called upon to perform as back-up attitude control thrusters. In this event, the power input to the thruster heaters will be increased by an amount that

would be freed from the primary control system. This switchover will be done via ground command, through the power conditioner.

Only during the less frequent station keeping operation (once every ten to eleven days) will the jets (pre-selected) be pulsed via ground command. Power to the station keeping thruster will be increased to the selected operating level (approximately 35 watts) via ground command through the power conditioner, approximately two hours before thrusting. Since the required ground control of the thrusters is not extensive, a pre-programmed automatic command probably will not be necessary, and all commands can be executed via the manual key board system. Although the thrusters will usually be commanded by the spacecraft stabilization and control logic system, there will be provisions for ground command take-over of the thrusters in an emergency.

## **B. PROPULSION HARDWARE DESCRIPTION**

### **ATS-4 APOGEE KICK MOTOR DESCRIPTION**

One of the constraints placed on the in-house ATS-4 design study was that some version of the Thiokol Chemical Corporation TE-M-364 solid propellant motor be used for synchronous orbit injection of the ATS-4 spacecraft. This motor was originally designed to be the retro propulsion system for the Surveyor program. It has since been chosen, however, by the Boeing Company for use with the Burner II upper stage and was chosen by NASA as the third stage propulsion system for the Improved Delta launch vehicle. The motor has been flown successfully in both the Surveyor and Burner II programs and is scheduled to be flown on the Delta vehicle in 1967. A further ATS-4 study constraint is to use the Delta version of the motor. The performance of the TE-M-364 motor is classified. The unclassified data pertaining to the motor is listed in Table 14-6. Figure 14-3 is a drawing of the TE-M-364 motor. The motor proposed for ATS-4 has ballistic components identical to the drawing and also has a flange attached about the periphery of the case for mounting. Insulation inside the case holds the external case temperature to a minimum during firing. These two features apply to the Delta version only.

### **SPIN-UP ROCKET DESCRIPTION**

The Atlantic Research Corporation MARC 6A1 1-KS-210 solid propellant motor is proposed for ATS-4 spinup. Four of these motors are needed to spin-up the spacecraft to the desired spin rate. The physical characteristics of the MARC 6 A1 1-KS-210 rocket motor are listed in Table 14-7. Figure 14-4 is a drawing of the MARC 6 A1 1-KS-210 motor.

Table 14-6

TE-M-364 Characteristics

Case Weight - 140 pounds

Propellant Weight - 1440 pounds

Expansion Ratio - 53:1

Combustion Chamber - Spherical

Case Material - Steel (Titanium Case Under Development)

Propellant - Composite cast-in-case  
Minuteman 1st Stage Type  
With Aluminum (TP-H-3062)

Total Impulse Variation -  $\pm 0.6$  percent (3 )

Table 14-7

MARC 6A1 1-KS-210 Characteristics (vacuum)

Burn time @ 70° F	-	1.077 sec
Action time	-	1.501 sec
Average Thrust	-	206 lb
Average Pressure	-	1046 psia
Total Impulse	-	222 lb-sec
Specific Impulse	-	218 sec
Burning Rate	-	0.367 in/sec
Loaded Weight	-	3.38 lb
Expend Weight	-	2.32 lb
Length	-	10.2 in
Diameter (maximum)	-	3.062 in
Igniter	-	two parallel squibs
Firing Current	-	3.0 amp
Maximum no-fire current	-	0.2 amp
Resistance	-	0.35 - 0.65 ohm

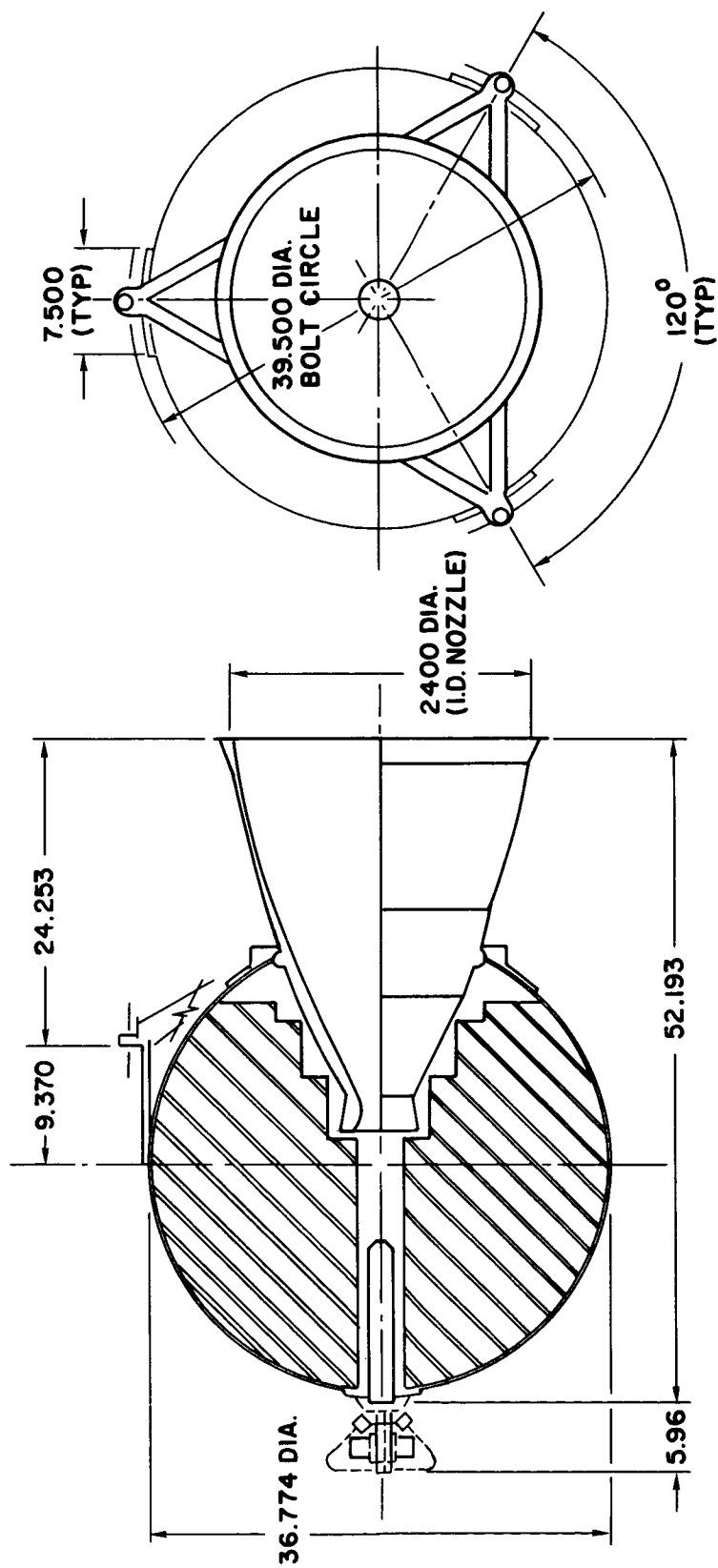


Figure 14-3. ATS-4 type TE-M-364 solid propellant apogee motor.

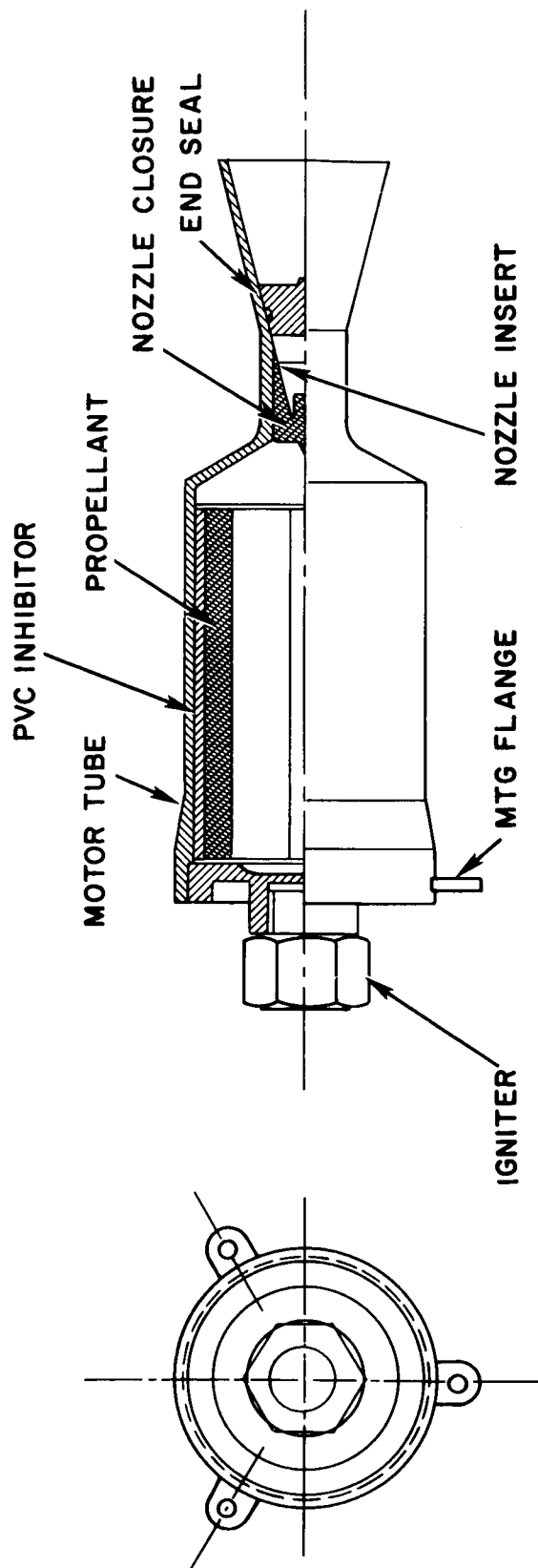


Figure 14-4. Atlantic Research Corporation solid propellant motor MARC 6A1 1-KS-210.

## HYDRAZINE SYSTEM FOR ATS-4

The propulsive elements for the station seeking system proposed for ATS-4 are a pair of 5 pound thrust engines using monohydrazine propellant and a spontaneous catalyst bed. The system is designed so that propellant and nitrogen ( $N_2$ ) usage will not cause an unbalance of the spacecraft. This is accomplished by a manifolded dual feed tankage setup. The interconnecting manifolds maintain pressure and propellant equalization.

The expulsion of the propellant from the tanks is dependent upon  $N_2$  pressure and the centrifugal force generated by the spinning spacecraft. The propellant lines to the engines from the propellant tanks are located on the outer periphery to take advantage of this force.

The proposed system as shown in Figure 14-5 is based on requirements indicated in Table 14-8. An overall envelope size is not shown because components will probably be located in each of the four quadrants of the spacecraft. However, the largest component sizes are indicated.

Table 14-9 presents the required component weights. In addition, the total loaded system weight is included.

Power requirements are outlined in Table 14-10. The solenoid valve power requirements shown is the power needed to instantaneously open them and hold them open. The power shown for the explosive valves is the total for the three valves.

## THERMAL STORAGE RESISTANCE JET SYSTEM

As discussed in Section 14-A, a thermal storage resistance multi-jet system using ammonia as the propellant has been chosen to provide for the low thrust station keeping and attitude control requirements. In addition to station keeping and momentum dump for the attitude control system wheels, this system provides for station acquisition and a complete back-up in the event of the primary attitude control system failing.

Figure 14-6 shows the essential features of a typical resistance jet. The overall length is about 5 inches with approximately a 3 inch diameter. The thruster module weighs less than 1.5 pounds. The thruster assembly consists of a body with up to five nozzles in its outer shell, a heater subassembly consisting of a resistance wire wound on an electrical insulator, and heat shielding fabricated from layers of thin metallic foil separated by minimum contact support wires.

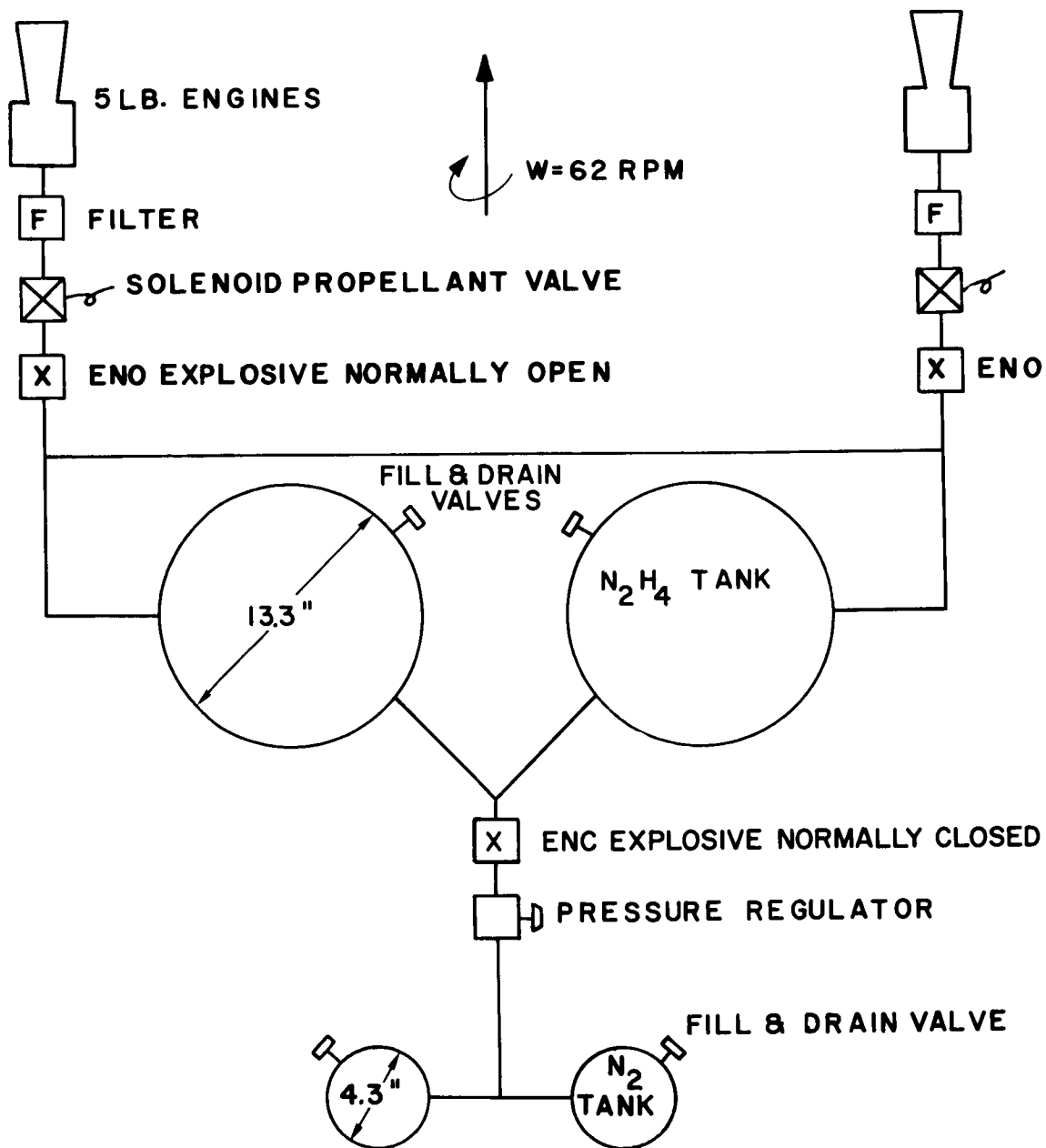


Figure 14-5. Hydrazine station seeking system for ATS-4.

Table 14-8

## Five Pound Hydrazine Propellant Use

Function	Duty Cycle Time-on Time-off	Total Time	Firing Time (sec)	No. of Thrusters Used	Assumed I <sub>sp</sub>	Propellant Wt. (lb)	No. of Pulses
1. Damp Out Residual Spin-up Rates	$1/3 = \frac{.18126}{.5435}$	59.1 sec	19.7	1	215	0.5	110
2. Spin Axis Precession (10 degrees due to spinup)	$1/6 = \frac{.1812}{1.087}$	210.0 sec	35.0	1	225	0.8	210
3. Active Damping to 2nd Apogee 1/6 duty cycle for a total of 3.5 sec firing every hour	$1/6 = \frac{.1812}{1.087}$	15 3/4 hr	55.0	1	125	2.2	332
4. 2nd Spin Axis Precession	$1/6 = \frac{.1812}{1.087}$	53.0 sec	9.0	1	215	0.2	53
5. Damp out transverse rates (After firing kick motor)	$1/3 = \frac{.1812}{.5435}$	63.3 sec	21.1	1	215	0.5	120
6. Active damping after kick stage firing - 1/6 duty cycle for a total of 3.5 sec firing every hour	$1/6 = \frac{.1812}{1.087}$	48 hr	163	1	125	6.7	905
7. Precession to remove inclination (110 degrees)	1/6 (will be longer pulse than 4)	2100 sec	350.0	1	230	7.6	2100
8. Inclination Removal	Steady firing	492 sec	492.0	2	235	20.9	1
9. Precession to remove eccentricity	1/6 (Same as 7)	1700 sec	284.0	1	230	6.2	1700
10. Removal of Eccentricity	Steady Firing	615 sec	615.0	2	235	26.2	1
TOTAL +15%						71.8 10.8 <u>82.6</u>	

Table 14-9

## ATS-4 Hydrazine System Weight Breakdown

Component	Weight (lb)	No. of Components	Total Weight (lb)
5 lb Reactors	1.75	2	3.50
Filters	1.0	2	2.00
Solenoid Valves	0.50	2	1.00
N <sub>2</sub> H <sub>4</sub> Tanks	4.55	2	9.10
Explosive Valves	0.25	2	0.50
Dual Series Press. Reg.	1.90	1	1.90
N <sub>2</sub> Tanks	1.00	2	2.00
Fill & Drain Valves	0.15	4	0.60
Thruster Lines	2.00		2.00
Total Dry Weight			22.60
N <sub>2</sub> Weight			0.23
N <sub>2</sub> H <sub>4</sub> Weight			82.60
Total System Weight			105.43

Table 14-10

## Power Requirements

- 2 Solenoid Valves - 5 watts to instantaneously open (each)  
2 watts to hold open (each)
- 3 Explosive Valves - 15 watts (5 watts each)

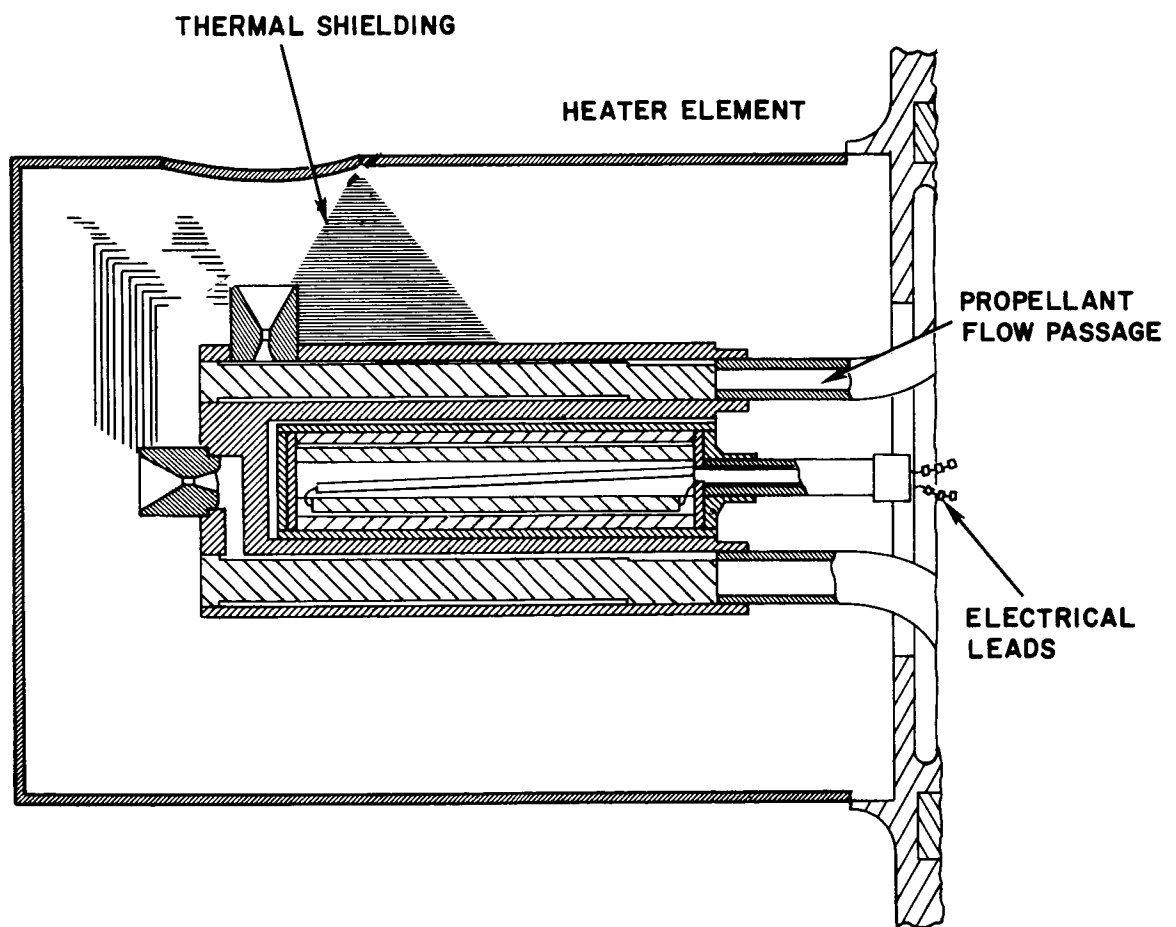


Figure 14-6. Typical thermal storage resistance multi-jet.

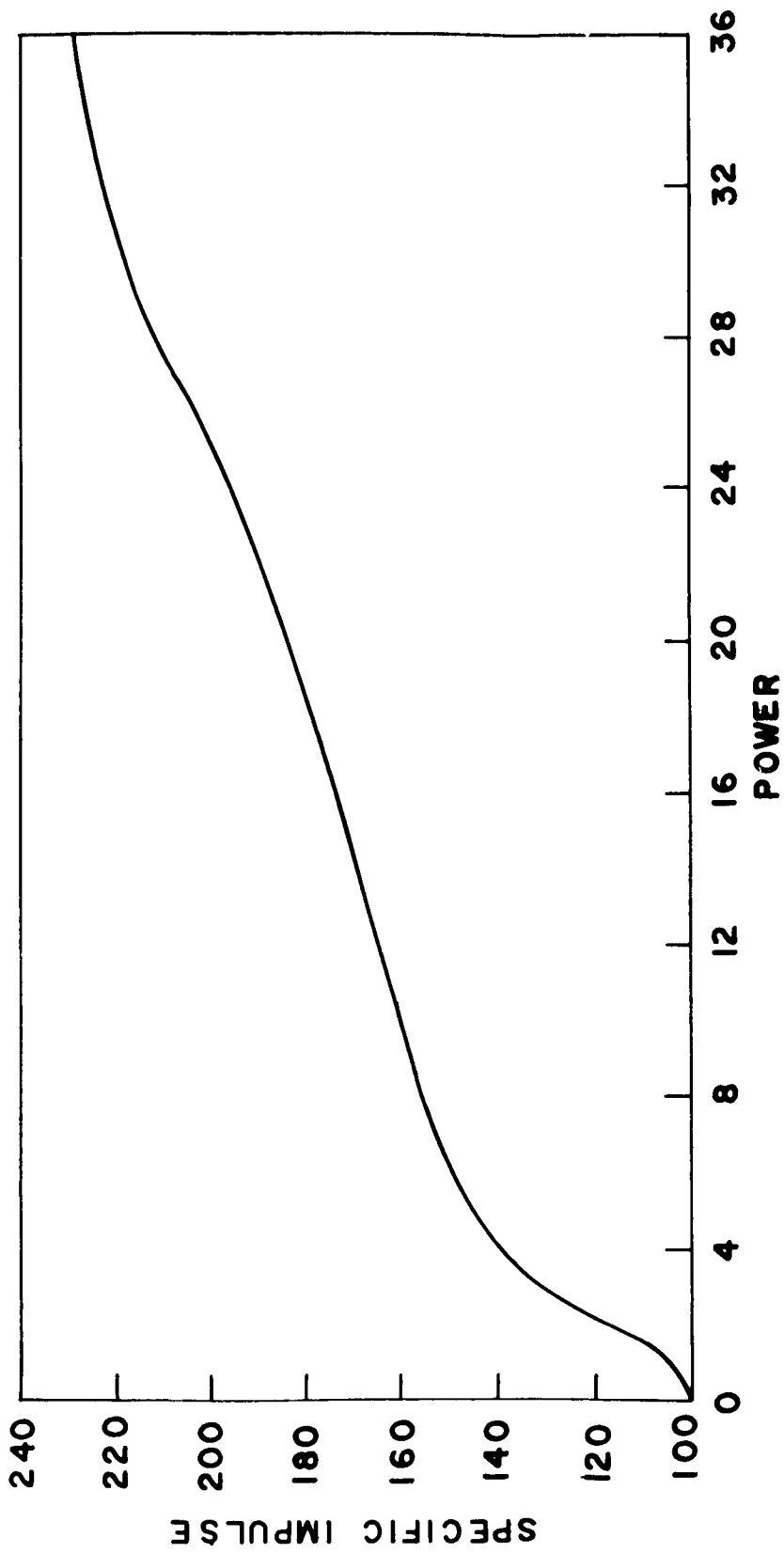


Figure 14-7. Estimated short pulse specific impulse vs power input for a thermal storage resistance jet.

The purpose of the resistance jet is to increase the specific impulse of the gas by the addition of heat. As the propellant passes through the thruster body, it is heated up to operating temperature by its contact with the hot flow passage. This hot surface receives its heat from the heater unit which is installed in the center of the thruster body.

The heater cartridge consists of a high temperature resistance wire wound on a grooved insulating mandrel and contained within a cylindrical sheath. Pneumatically impacted filler material separates the wound filament wire from the sheath. Although other combinations of materials are still being investigated, present studies indicate that platinum wire wound on a magnesia core impacted with a boron nitride fill provides the most reliable heater element.

The spacecraft power system will operate at a nominal 28 volts. Heating elements now in existence operate on approximately 13 volts and 2 amps (no successful 28 volt heater has been developed). This means that power conditioning will be needed to provide the proper voltage and current to the thruster heater. An in-house study has been initiated to develop this item. Present information indicates that power conditioner efficiency of 90 percent can be obtained.

The resistance jet can be operated at temperatures up to 2000°F. This presents a problem of cutting down on the heat conduction and radiation losses. The thermal shielding in the thruster module has been incorporated for this purpose. Considerable work has been done to optimize the number and type of shields. The desirable characteristics of the shielding material are low emissivity, poor heat conductivity, light weight, non-reactive with ammonia, and a minimum of fabrication problems. Nichrome V appears to be the best compromise material at this time. The shielding consists of 30 to 40 layers of metallic foil (0.001 in to 0.003 in thick) separated by 0.01- to 0.02 inch diameter wire. Again Nichrome V appears to be the best choice for the spacer wires separating material.

The operational flexibility which enables the resistance jet to be pulsed at temperatures up to 2000°F presents the option of trading off  $I_{sp}$  and power input. Figure 14-7 shows an estimate of the resistance jet  $I_{sp}$  to power input for short pulses. This curve is based on test data from existing thrusters together with estimates of design improvements now being incorporated.

Jet nozzle throat sizes and contours are designed for a particular operating condition. The thrust level of the jets is dependent on the nozzle design and both the final temperature and pressure of the gas. Existing designs range from about 5 to 60 millipounds thrust with supply pressures ranging from less than 1 up to approximately 5 atmospheres. The gas temperature will depend on the power input to the heater. The relationships between thrust, power input, and supply

pressure will have to be determined when the thruster design is finalized.

At this time, insufficient data is available on the cycling life of heater assemblies. Long life operation at approximately 2000°F has been demonstrated. The reliability of a heating element being cycled a large number of times from ambient temperature up to 2000°F is questionable at this time. It may well be that some minimum standby temperature (power input) will be necessary to perform cycling to high temperature operation. For this reason, a standby power input of 5 watts is recommended for each thruster module. It is probable that this quantity may be significantly reduced as test data becomes available and as heater assembly development continues.

The thrust level of the resistance jets takes a finite amount of time to build up to the full thrust level. Tests run at GSFC show that it takes approximately 0.1 second to reach approximately 95 percent of full thrust. It also requires a finite time for the thrust level to decay from full thrust down to zero. The build up and decay time will be dependent on the solenoid reaction time as well as the volume of propellant between the solenoid and the thruster nozzle. The ATS-4 feed system should provide better reaction characteristics than the system now being used in tests at GSFC.

In order to obtain a high degree of accuracy in predicting thrust levels of the resistance jets, a constant pressure zero gravity storage and feed system is used to provide the ammonia propellant for the thrusters. The system chosen for this application is shown schematically in Figure 14-8. The titanium storage tank shown is approximately 17.7 inches in diameter with a 7.6 inch regulator assembly attached to one end. Fully loaded, the tank can hold 57 pounds of ammonia. The ammonia in the storage tank is maintained at the saturation pressure (up to a maximum of about 200 psia) corresponding to the local environmental temperature. Including the fuel, the maximum weight for this subsystem would be 87 pounds.

The regulator assembly attached to the tank provides vapor flow at a regulated pressure within 1 percent of a preselected value (between 1 and 5 atmospheres). This regulator satisfies the zero gravity requirement: vapor flow output with either liquid or vapor flow from the storage tank.

Propellant flow into the resistance jet is accomplished by applying a signal to the solenoid valve adjacent to the thruster. As the gas leaves the plenum tank the pressure in both the plenum and preplenum drops. The pressure drop in the preplenum closes the pressure switch which opens the valve providing a pulse of liquid or vaporous ammonia from the storage tank into the preplenum. Any necessary vaporization takes place in the preplenum. In the

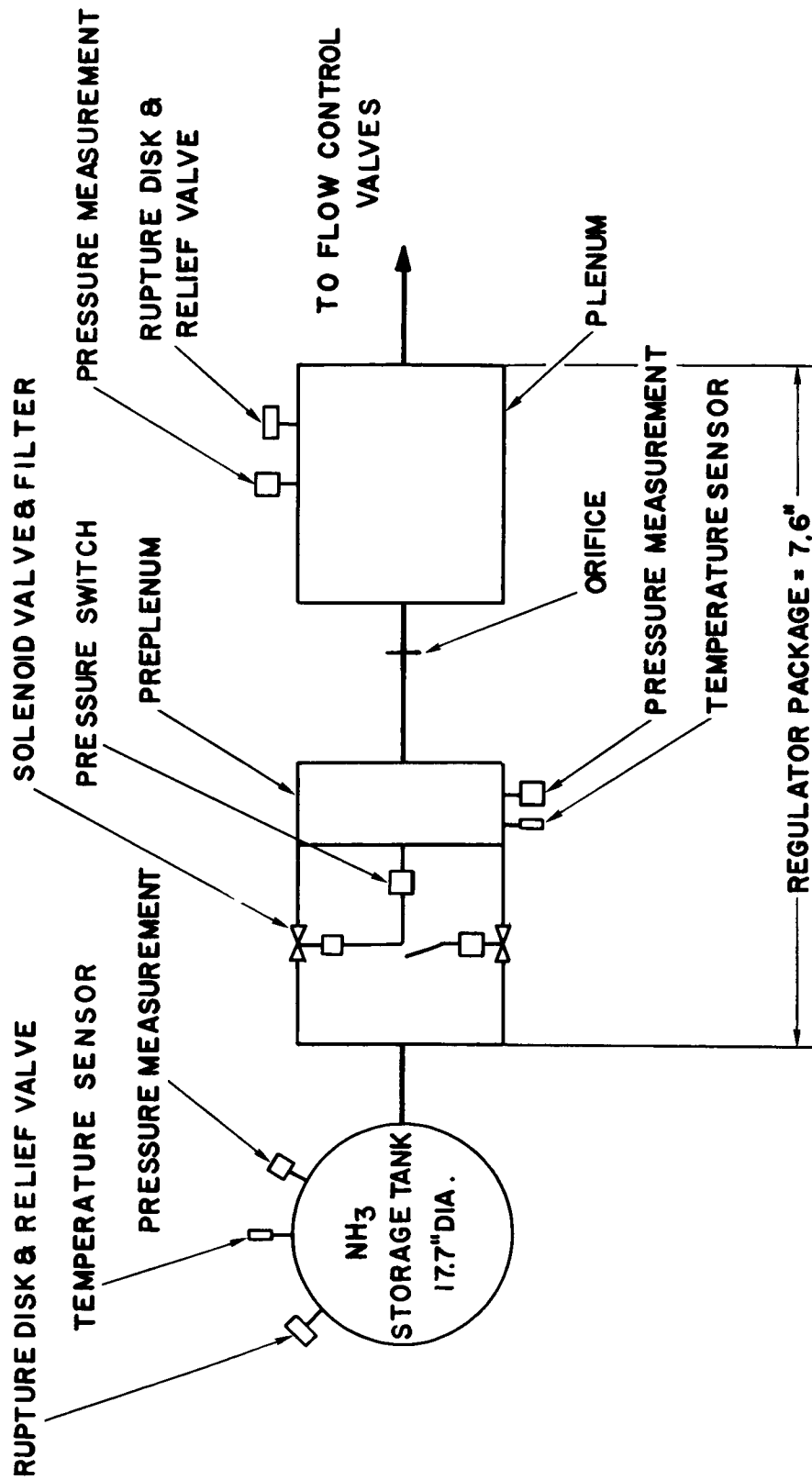


Figure 14-8. Ammonia feed system schematic diagram.

present design, the heat for ammonia vaporization is available from the regulator components and the higher temperature storage tank. The vapor then flows through an orifice which eliminates dead band and overshoot conditions in maintaining the plenum pressure with 1 percent of the preselected value.

For system reliability, the regulator assembly is equipped with a filter, a rupture disk and relief valve assembly, and a redundant pressure switch and solenoid valve. The storage tank also contains a rupture disk and relief valve assembly.

The ammonia feed and storage system has not been sized specifically for ATS-4 applications. A GSFC in-house test program in the next few months will be using a tank sized for 57 pounds of ammonia. In order to change the tank size, a new design may be required to facilitate manufacture. The weight of this system is only a weak function of tank size. The flow regulator assembly is the same size no matter how large a tank is used. For example, the tank weight savings in a redesign for 40 pounds of fuel would be of the order of 1.0 to 1.5 lb. On this basis, it is believed that any tank redesign weight savings would be outweighed by the problems and cost involved.

The total weight of this system is 103 pounds. This includes 57 pounds of propellant, 10 pounds for four power conditioners, 6 pounds for the four thrusters, and 30 pounds for the storage and feed system.

## SECTION 15

### ATS-4 THERMAL DESIGN

#### INTRODUCTION

The thermal analysis of the ATS-4 was divided into three parts: the 30-foot antenna, the antenna feed, and the adapter section. Most of the work was concentrated on the antenna, since this appears to be the most critical item.

There are two major thermal problems associated with the antenna. The first is the temperature excursions the antenna will experience during an orbit. Repeated thermal cycling induces thermal stresses in materials which could result in failure. The second, and probably more severe, problem is thermal gradients which produce distortions in the antenna.

#### TEMPERATURE EXCURSION OF ATS-4 ANTENNA

To assess the temperature excursions, computer runs were made using the transient heat-transfer program at Goddard. For this analysis the antenna was assumed to be made of aluminum and to weigh 200 pounds. Initially, the antenna was assumed to be continuous, i. e., with no holes cut out. Then, it was assumed to be 80-percent transparent. For the transparent cases the antenna was assumed to be composed of aluminum rods or of honeycomb having a 1-inch-by-1-inch cross section. The rods were allowed to absorb solar energy on the top and bottom faces only. This was done since absorption by the edges would require complete mechanical design details of the antenna and a complete analysis of the shading on the edges. Neither of these could be obtained in the allotted time. The orbit selected placed the sun at one of the equinoxes. This would be the most severe orbit, since the antenna would spend approximately one hour in the earth's shadow. The analysis and results are summarized in Table 15-1, and complete temperature-time history is plotted in Figure 15-1.

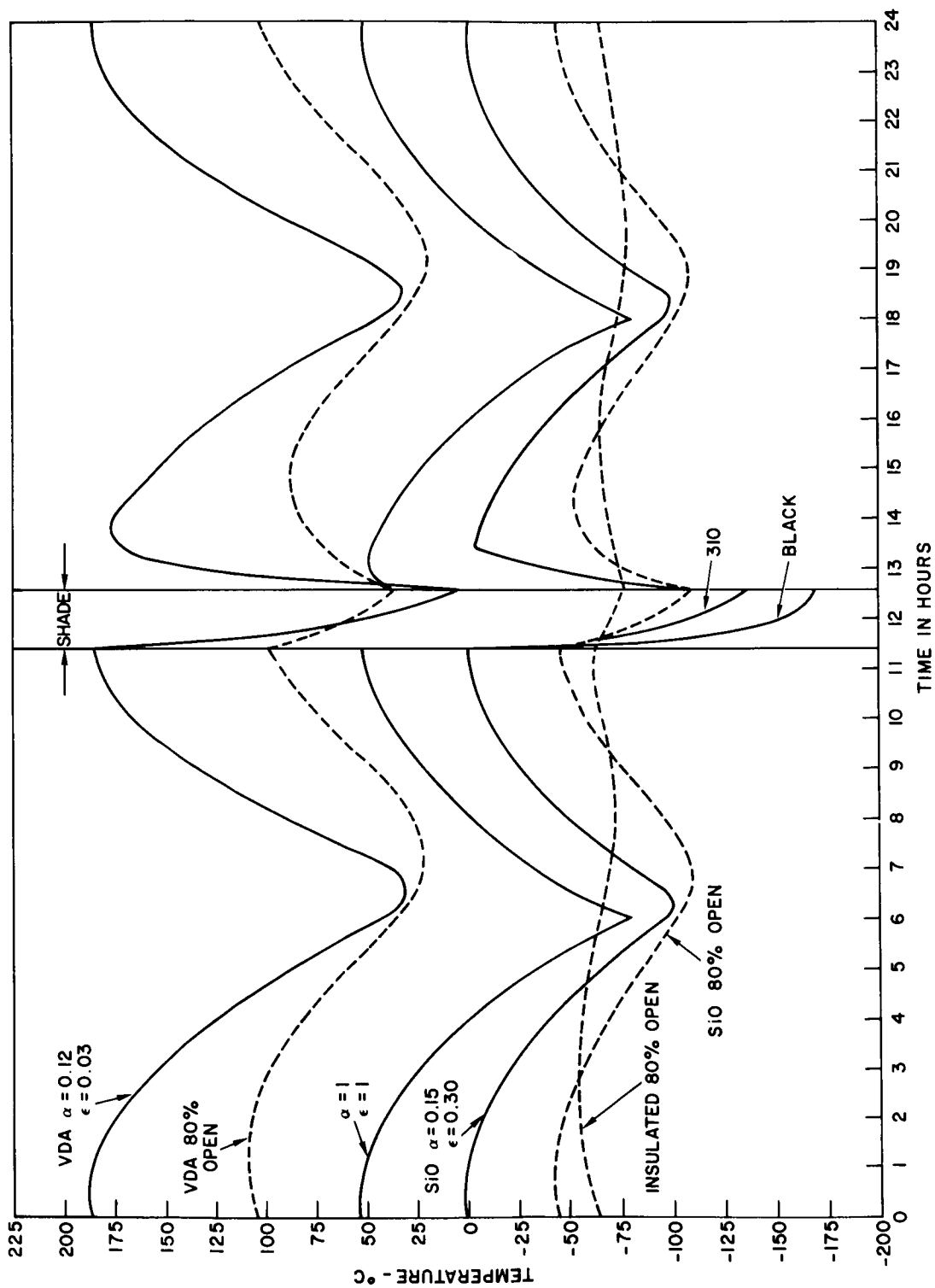


Figure 15-1. ATS-4 mean antenna temperature vs. time.

Table 15-1

## Temperature Excursion of ATS-4 Antenna

Material	Weight (Pounds)	Thermal Coating	$\alpha$	$\epsilon$	Percent Open	Maximum $\Delta T^{\circ}\text{C}$
Aluminum	200	Black	1	1	0	222
"	"	VDA	0.12	0.03	0	182
"	"	SiO	0.15	0.30	0	133
"	"	VDA	0.12	0.03	80	36
"	"	SiO	0.15	0.30	80	65
"	"	Insulation (Mylar out)	-	-	80	20

To reduce temperature excursions, the thermal coatings should be such as to run the antenna cold, and also have low absolute values of absorptivity ( $\alpha$ ) and emissivity ( $\epsilon$ ) to increase the time constant. Insulation reduces the temperature excursion by effectively increasing the time constant of the antenna. Although this seems to be the best solution from the thermal standpoint, there are some practical problems in using insulation. First, there is the problem of applying the insulation over the relatively complicated structure of the antenna. Any openings or sharp bends tend to negate the properties of the insulation by providing heat leaks. Second, there is the problem of handling. Squeezing the layers of insulation together either through handling or folding of the antenna may also provide heat leaks through the insulation.

#### TEMPERATURE GRADIENTS - COMPARISON OF PETAL FRAMES

Temperature gradients will occur across the antenna and normal to the antenna surface. To determine the gradients normal to the surface, it was assumed that the antenna will be made of square rods. Three types of rods were investigated: hollow, honeycomb, and styrofoam covered with aluminum. All rods had a 1-inch-by-1-inch cross section and were sized such that each

had a density of 4.64 lbs/ft<sup>3</sup>. The surface was assumed to be coated with SiO since, excluding the insulation, this coating results in minimum temperature excursions. An orbit was assumed such that the sun would move around the rod in 24 hours illuminating each side of the square rod equally. The results are summarized in Table 15-2. The temperature difference between the top and bottom faces is shown plotted in Figure 15-2 as a function of time.

Table 15-2

Comparison of 1-Inch x 1-Inch Cross Section Petal Frames

Material	Density <sub>3</sub> (Lbs/Ft <sup>3</sup> )	Coating	$\alpha$	$\epsilon$	Maximum Gradient °F
Aluminum (Hollow)	4.64	SiO	0.15	0.30	4.6
Aluminum (Honeycomb)	4.64	SiO	0.15	0.30	9.8
Styrofoam (Aluminum Plated)	4.64	SiO	0.15	0.30	13.6

Of the three frames compared, the hollow frame is obviously superior thermally. However, this is not the complete solution since the temperature gradient must be interpreted in terms of thermal deflections before final selection of a petal frame. For example, the honeycomb may deflect less than the hollow frame although the temperature gradient is twice as great. Although a solid aluminum rod probably would have a smaller gradient, it was not included in this comparison since it was decided to keep both dimensions and weight constant.

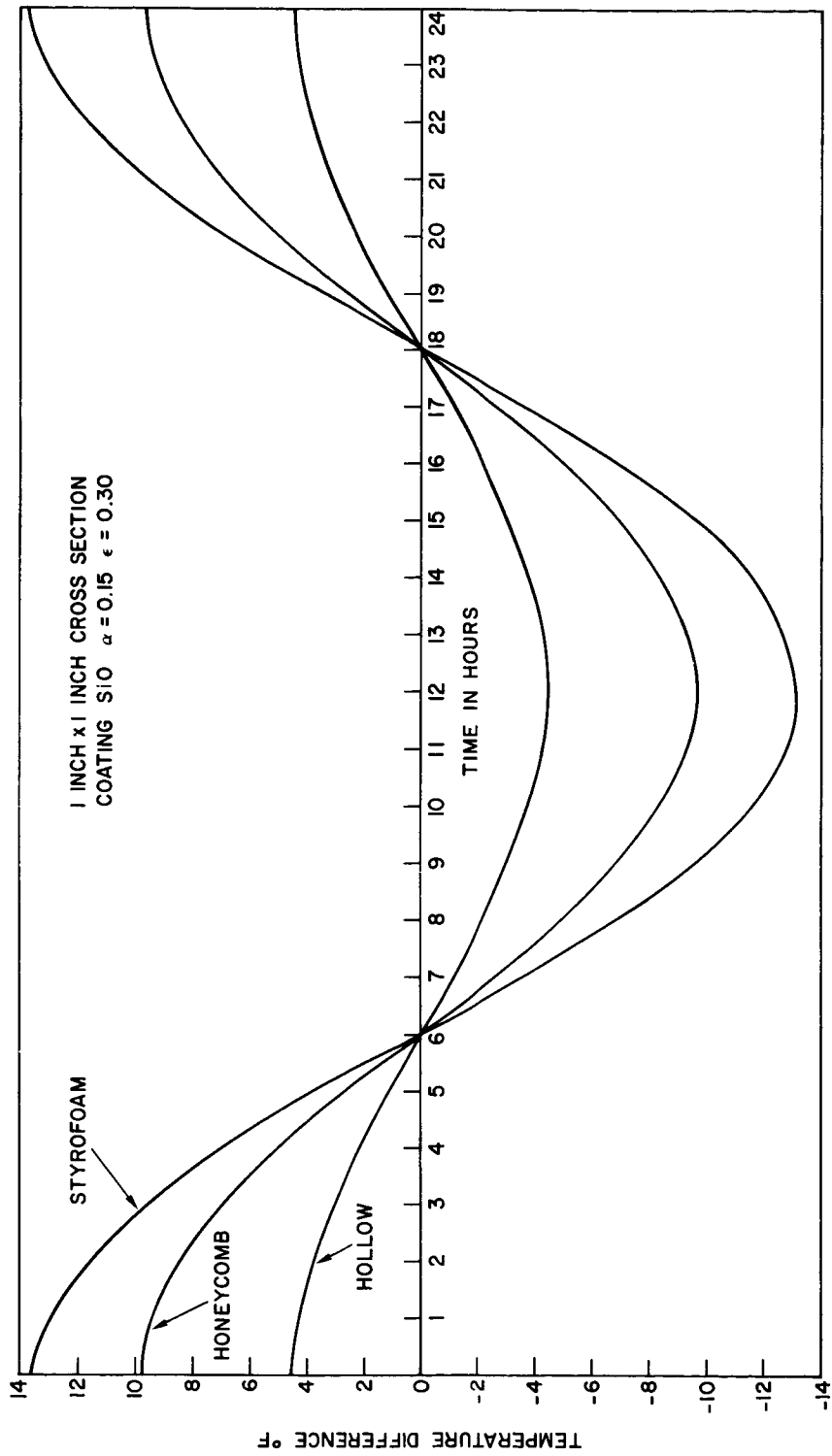


Figure 15-2. Comparison of petal frames.

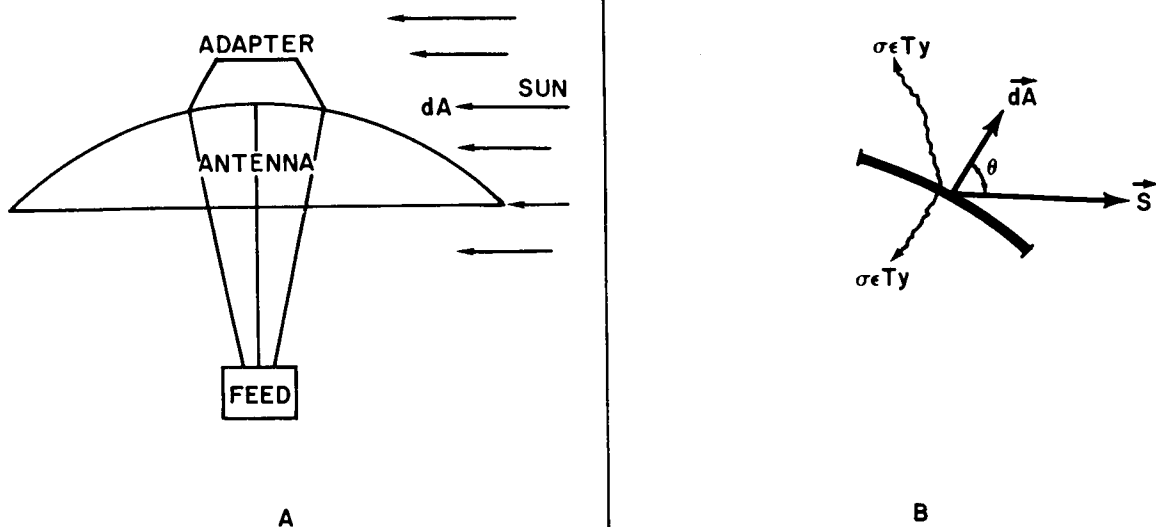


Figure 15-3. Thermal model for temperature gradients.

### GRADIENTS ACROSS ANTENNA

The largest temperature gradients in the antenna occur in the radial direction rather than normal to the surface. To assess these temperature gradients, the simplified thermal model shown in Figure 15-3 was assumed. Figure 15-3A shows the entire antenna while Figure 15-3B shows an elemental area  $dA$  with the thermal fluxes involved. Radiation interchange between elements was neglected since less than 5% of the energy radiated from the concave side and none of the energy radiated from the convex side impinges on the antenna. Conduction between elements was also neglected since this depends on material and thickness of the antenna petals, neither of which is known. Conduction along a thin rod of the dimensions assumed would be small compared to radiation from the rod surface. The antenna was assumed to be at equilibrium with its environment at two positions in orbit; (1) with the sun shining down the yaw axis, and (2) six hours later when the sun is at 90 degrees to the

yaw axis. This assumption is very nearly true for the sun along the yaw axis, but is relatively poor for the 90-degree case as will be shown later. However, because of its small thermal mass, the mesh will be very close to equilibrium in both cases. With the above assumptions and referring to Figure 15-3B, the equation for the thermal balance on an elemental area of the antenna is

$$\alpha \vec{S} \cdot \vec{dA} = 2 \sigma \epsilon T^4 \quad (1)$$

where

$\alpha$  = absorptivity

$\vec{S}$  = solar vector with magnitude equal to the solar constant (442 Btu/hr. ft<sup>2</sup>)

$\vec{dA}$  = unit vector normal to elemental area dA

$\sigma$  = Stefan-Boltzmann constant ( $0.1714 \times 10^{-8}$  / hr. ft<sup>2</sup> °R<sup>4</sup>)

$\epsilon$  = emissivity

$T$  = absolute temperature (°R)

2. = constant to denote radiation from both sides.

By performing the dot product, Equation 1 reduces to

$$\alpha S \cos \theta = 2 \sigma \epsilon T^4, \quad (2)$$

where:

$\theta$  = angle between normal vector ( $\vec{dA}$ ) and solar vector ( $\vec{S}$ ).

The lefthand side of Equation 2 was modified by the transmittance of the antenna for any energy which must pass through one side of the antenna before being absorbed by an elemental area. A transmittance of 80 percent was assumed for this analysis. Equation 2 was programmed on the IBM 7094 to solve for temperature as a function of solar position and any position of the antenna. A number of computer runs were made for the two orbital positions mentioned above and for a number of thermal coatings. The results of this analysis are summarized in Table 15-3 and plots of the isotherms are shown in Figures 15-4 through 15-11.

Table 15-3

## Temperature Gradients Across Antenna

Coating	$\alpha$	$\epsilon$	Transmittance	Solar Position in Degrees From Yaw Axis	$\Delta T^{\circ}\text{C}$
Black	1	1	80%	0	9.5
Black	1	1	80%	90	134.0
White	0.30	0.87	80%	0	7.0
White	0.30	0.87	80%	90	103.0
VDA	0.12	0.03	80%	0	15.0
VDA	0.12	0.03	80%	90	190.0
SiO	0.15	0.30	80%	0	8.0
SiO	0.15	0.30	80%	90	112.0

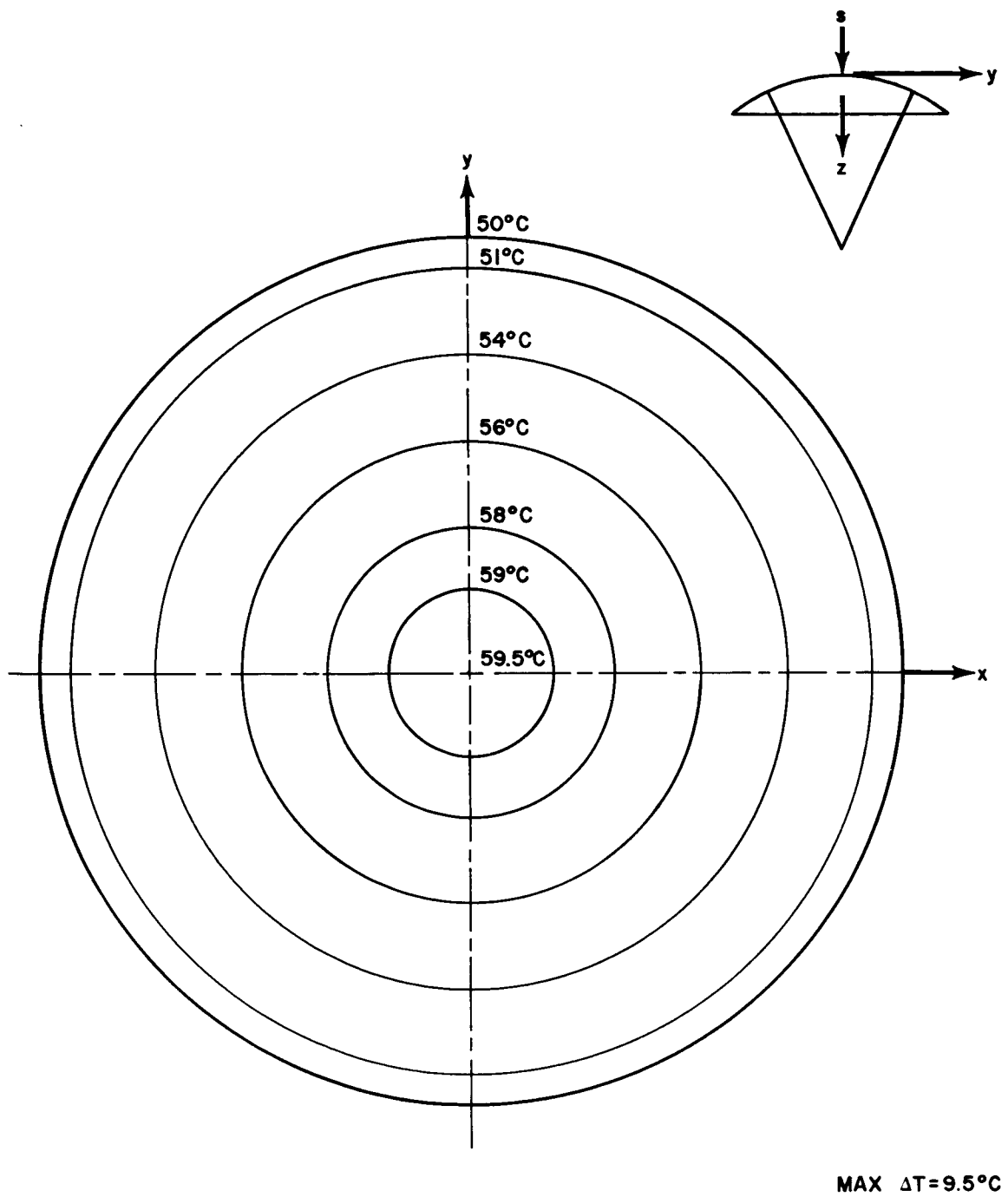


Figure 15-4. Isotherms on antenna; black coating; 0-degree case.

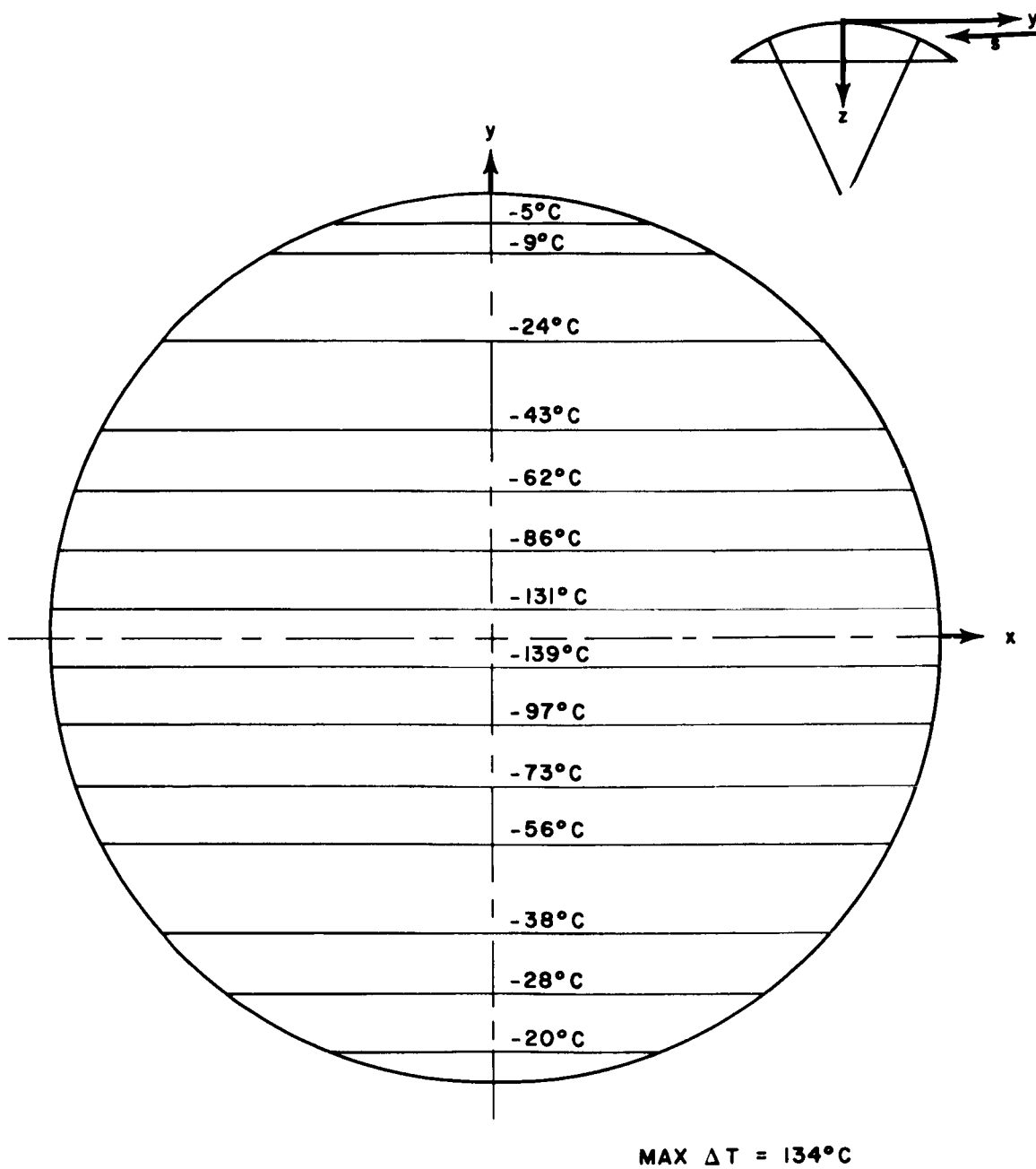


Figure 15-5. Isotherms on antenna; black coating; 90-degree case.

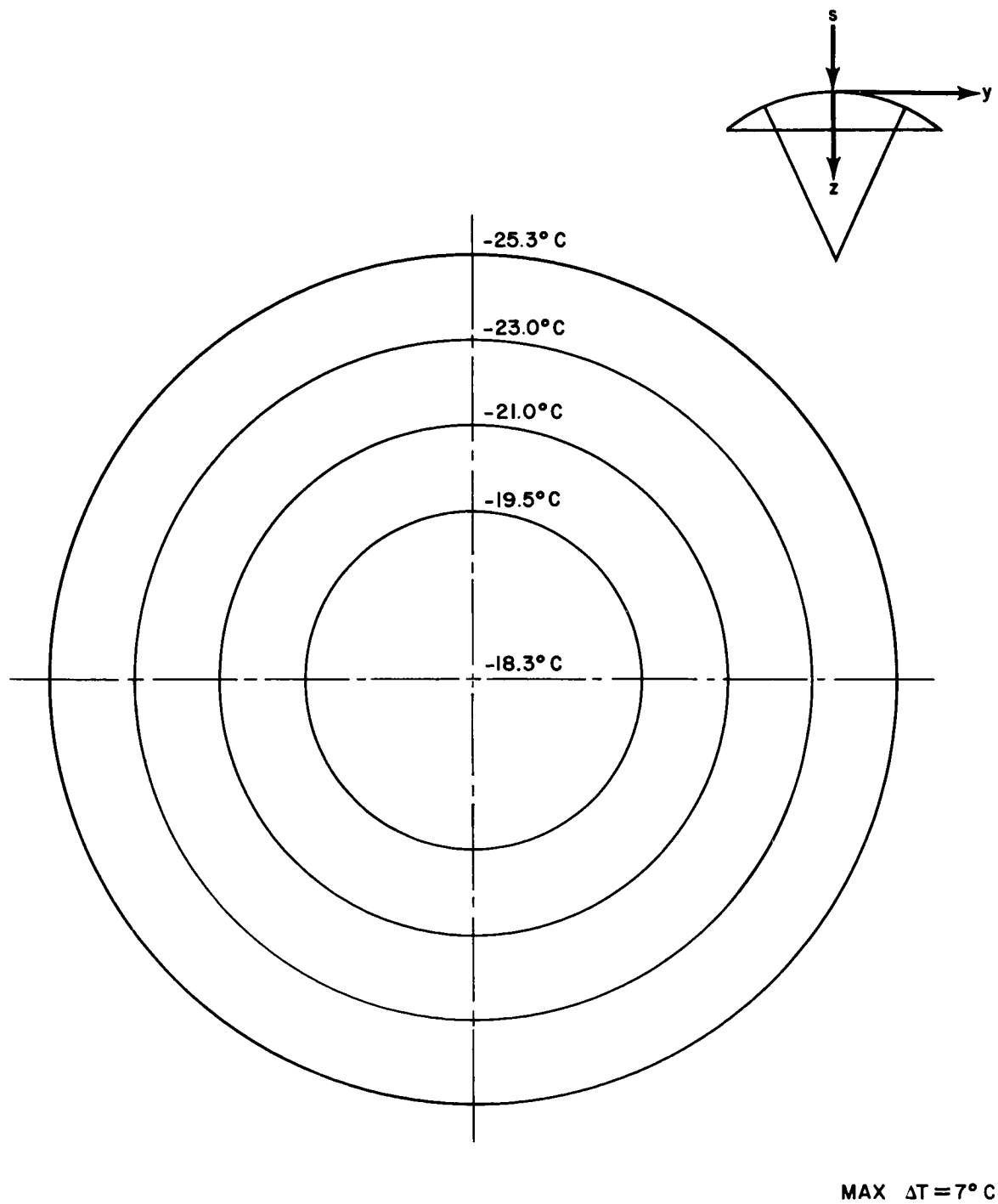
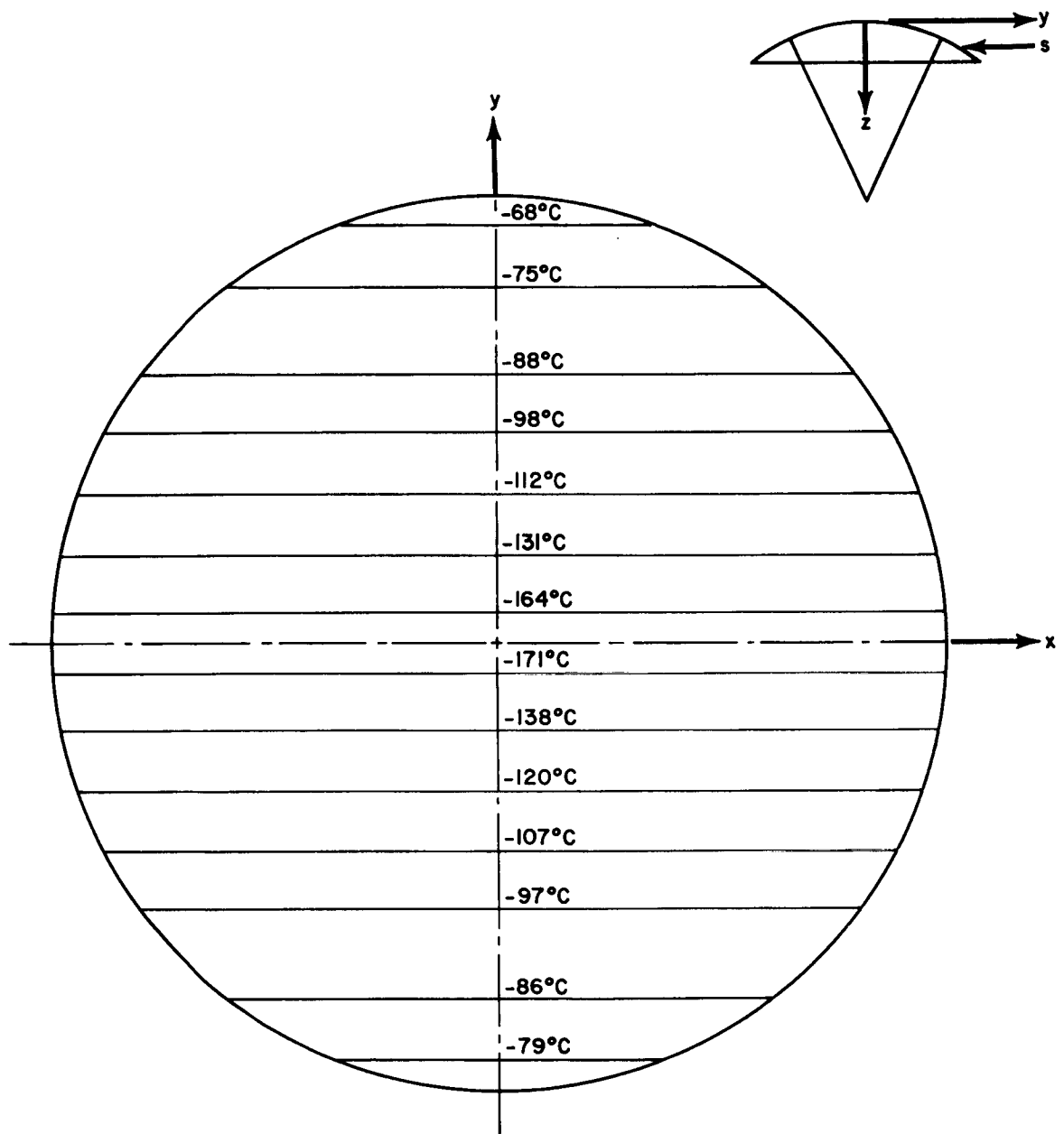


Figure 15-6. Isotherms on antenna; white coating; 0-degree case.



MAX  $\Delta T = 103^\circ$

Figure 15-7. Isotherms on antenna; white coating; 90-degree case.

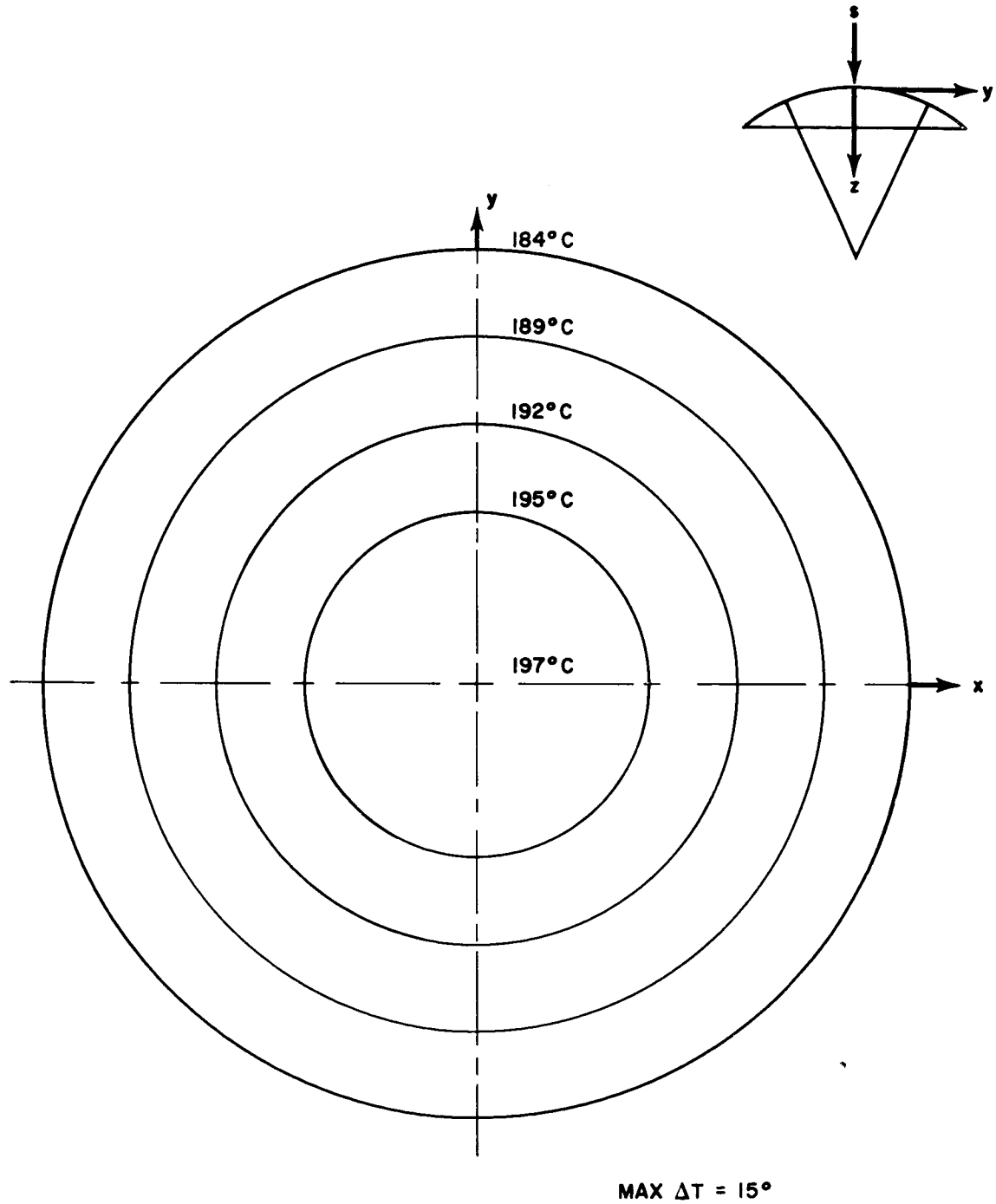
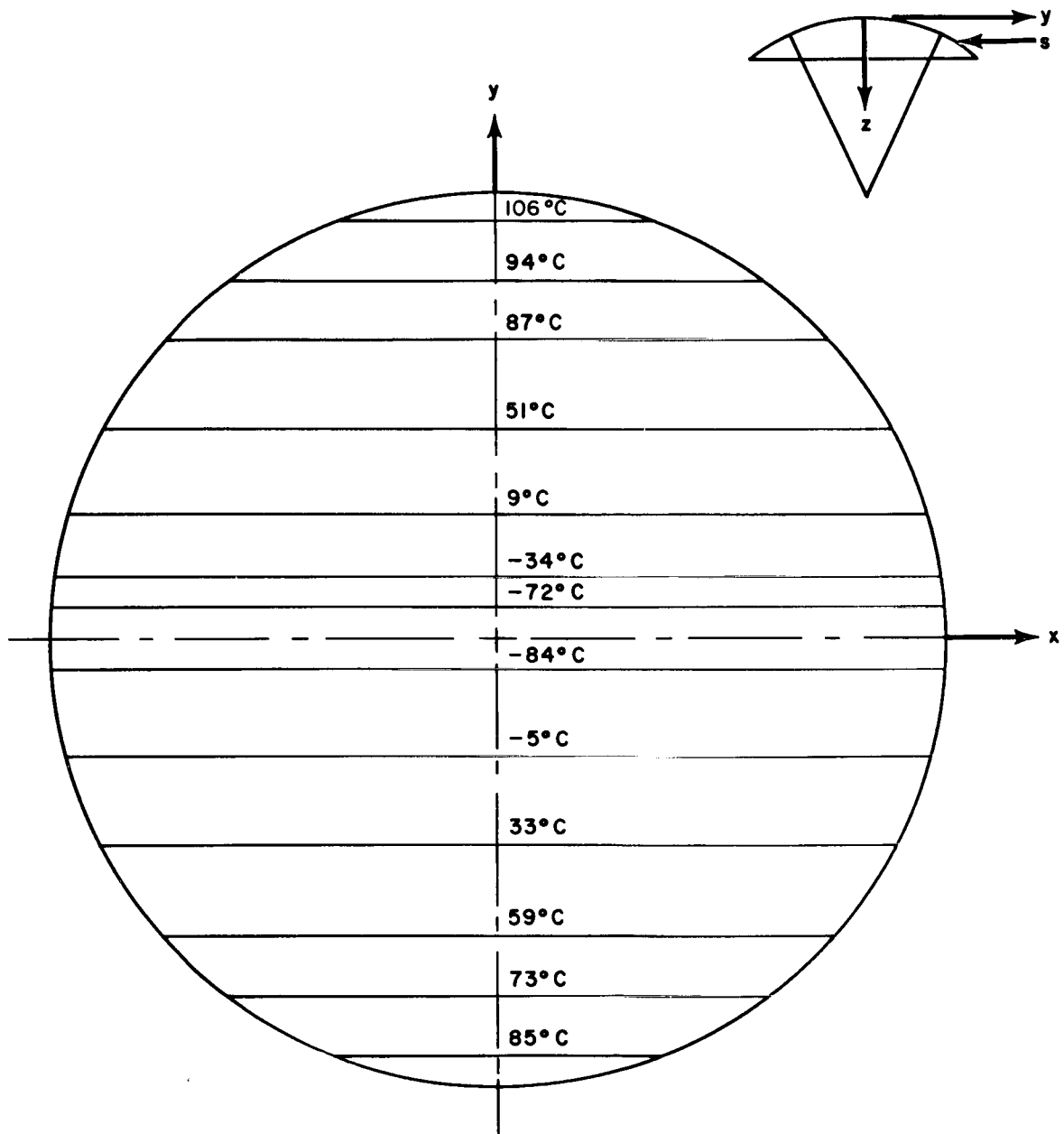


Figure 15-8. Isotherms on antenna; VDA coating; 0-degree case.



MAX  $\Delta T = 190^{\circ}\text{C}$

Figure 15-9. Isotherms on antenna; VDA coating; 90-degree case.

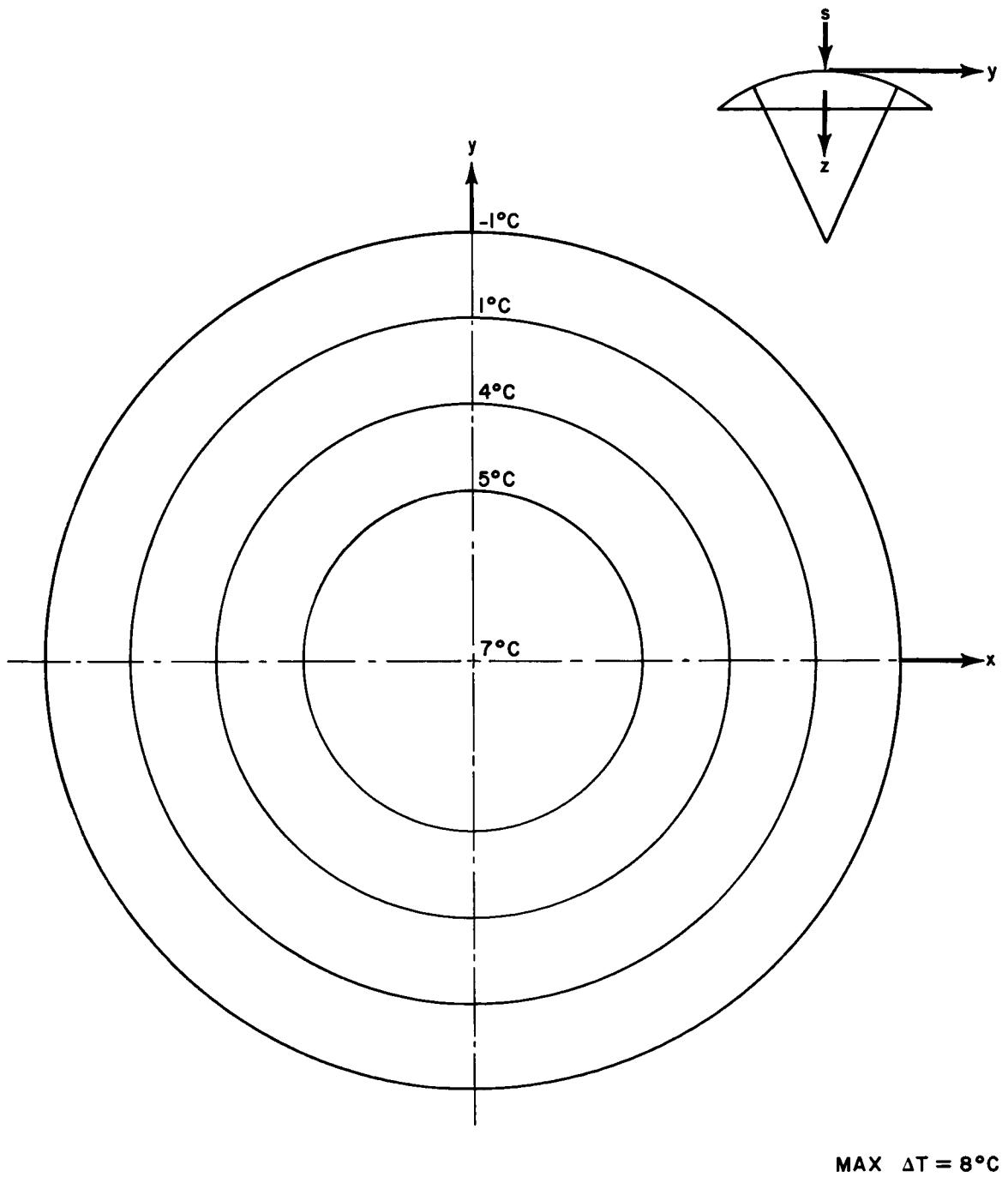


Figure 15-10. Isotherms on antenna; SiO coating; 0-degree case.

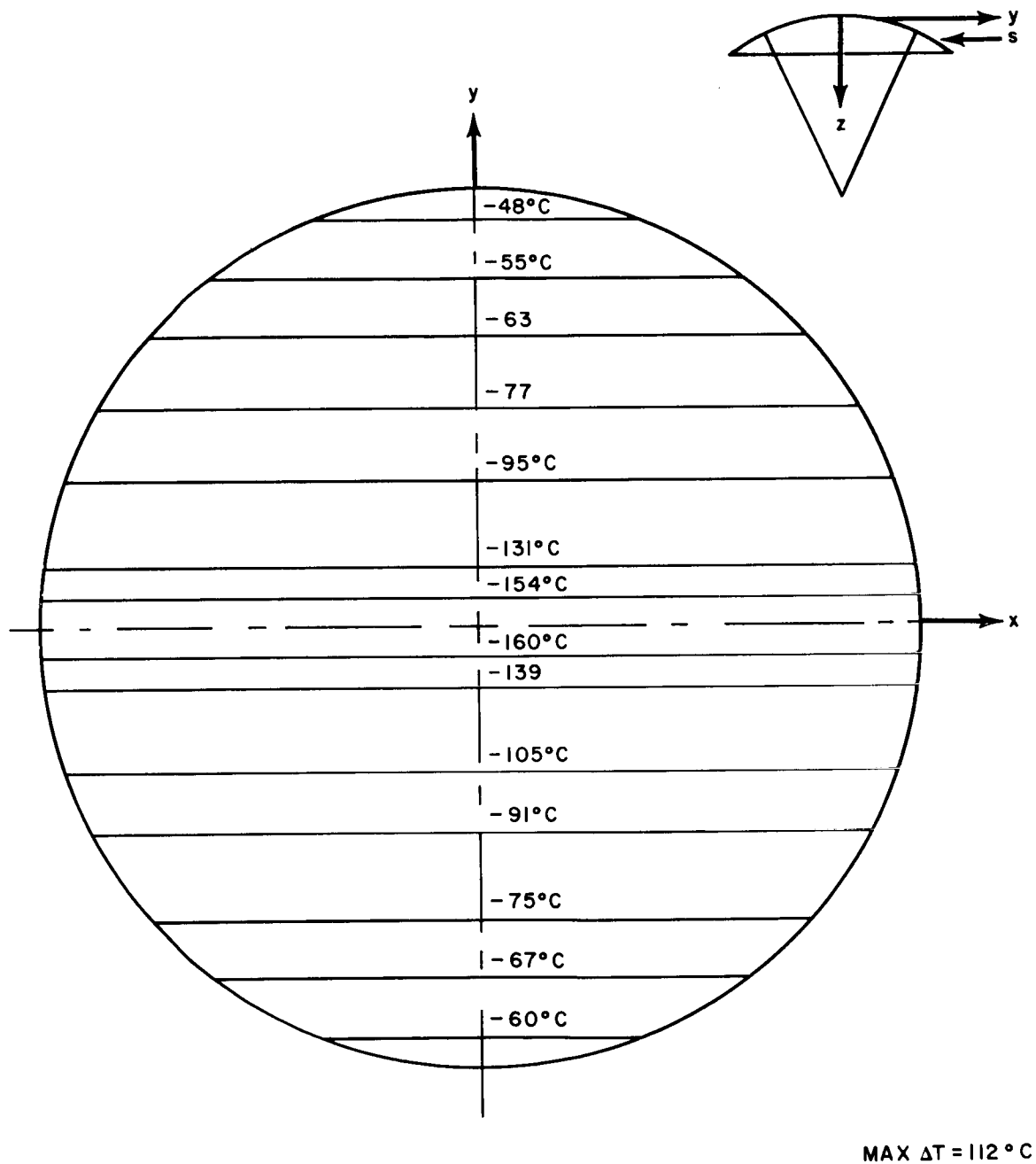


Figure 15-11. Isotherms on antenna; SiO coating; 90-degree case.

## DISCUSSION OF RESULTS

An examination of Figures 15-4 through 15-11 shows that gradients are smallest when the antenna is forced to run cold. These results are compatible with Figure 15-1 which shows that thermal excursions are also decreased when the antenna is cold. Hence, maintaining cold temperatures seems to be the direction to proceed to minimize both the temperature excursion and temperature gradient. The temperature gradients are large but again they must be interpreted in terms of deflections before one can assess the severity of the problem.

As to the validity of the gradient calculations, it is pointed out that the antenna was assumed to be in an equilibrium condition at both positions in orbit. The change of temperature with respect to time is a function of the absolute values of  $\alpha$  and  $\epsilon$ . The black and white coatings would have the shortest time constant and would therefore be closer to equilibrium conditions than the VDA and SiO coatings. The insulated antenna would have still a longer time constant. For this reason, an insulated antenna was not included in this analysis.

To evaluate the effect of the "thermal lag," consider the x-axis of Figures 15-10 and 15-11. If a honeycomb rod were placed on the antenna beneath this axis, the sun would move around the rod just as was assumed for the comparison of petal frames in Figure 15-2. Since the thermal coating assumed in Figure 15-2 is identical with that of Figures 15-10 and 15-11, the temperature at time zero in Figure 15-2 could be compared to the temperature along the x-axis in Figure 15-10, and the temperature at 6 hours in Figure 15-2 could be compared with the temperature along the x-axis in Figure 15-11. The temperature for the honeycomb petal frame in Figure 15-2 at time zero is  $6^{\circ}\text{C}^*$  ( $7^{\circ}\text{C}$  to  $-1^{\circ}\text{C}$  in Figure 15-10) and  $-107^{\circ}\text{C}^*$  at 6 hours ( $\sim 160^{\circ}\text{C}$  in Figure 15-11). Therefore, it can be seen that at time zero (i.e., sun along the yaw axis) the antenna is very close to its equilibrium temperature, while 6 hours later (i.e., sun  $90^{\circ}$  to yaw axis) temperature may be as much as  $50^{\circ}\text{C}$  away from equilibrium.

\* These temperatures are not plotted in Figure 15-2 but were obtained from the computer run which was used to plot Figure 15-2.

The benefits of an insulated antenna, although no analysis is shown, can be deduced from the above discussion. The disadvantages of insulation have been stated elsewhere and will not be repeated. To determine if the temperature gradients can be reduced to acceptable limits without the use of insulation, a much more detailed analysis must be performed. Before such analysis could begin, the following design information would have to be furnished:

1. Materials
2. Complete design of antenna including
  - a. Physical dimensions: thickness, hole size, hole pattern, etc.
  - b. Size and method of attachment of antenna support trusses
  - c. Size and method of attachment of adapter section
  - d. Size, material, and method of attachment of antenna feed support
  - e. Size and number of solar paddles
  - f. Power dissipation in any of the above.

With the above information at hand the detailed thermal analysis would consist of

1. A suitable thermal model with enough isothermal nodes to adequately describe the thermal gradients,
2. Conductances throughout the antenna and the antenna subassemblies (i.e., adapter, trusses, feed supports, etc.),
3. Solar radiation inputs including all blockages,
4. Computer runs to determine transient temperature distribution over the antenna as a function of time or position in orbit, and
5. Optimization of thermal coatings.

Items 1, 2, and 5 are standard in the thermal design of any spacecraft. Item 4 could be carried out on the existing heat transfer program at Goddard provided that the thermal model does not require a prohibitive number of nodes.

Determining the blockage mentioned in Item 3 appears to be the most critical item. Although blockage has been investigated in the past, the problem has never been as severe as in the ATS-4 antenna. Not only must blockage of the solar paddles, the adapter section, feed, and feed supports be considered, but also blockage of the supporting trusses and of the antenna itself. The importance of accurate determination of thermal inputs cannot be overemphasized. It is also important to note that the analysis outlined above should be

carried out for orbits other than the maximum shade orbit to insure that maximum gradients have been computed.

#### ATS-4 FEED AND FEED SUPPORT

A two-node transient analysis on the antenna feed was carried out and the results are shown in Figure 15-12. The internal components were assumed to weigh 254 lbs and the external cover 40 lbs. An average power dissipation of 92.4 watts was assumed. The purpose of the analysis was to determine if a passive system of thermal control was feasible. Although the internal temperature varied through only about 10°C, it must be noted, first, that this is mean internal temperature and the components will fluctuate around this mean; second, if the power is shut off for any length of time, the temperature will drop by about 35°C. Hence, it would be advisable to control temperature by an active system such as louvers.

Temperature gradients in the feed supports could deflect the feed. Although the supports are not yet designed, some analysis was performed on three-inch-diameter aluminum tubes. Wrapping the tubes with insulation and thermally decoupling the tubes from the antenna and feed, forces the tubes to run at almost uniform temperature and hence does not appear to be too severe a problem.

#### ADAPTER SECTION

Transient analysis on the adapter section during firing of the kick motor was performed. Because of the large mass of the kick motor and hence the long time constant, it appears that thermally isolating the motor from the components in the adapter section should not present a problem. Since the temperature of the components must be kept within relatively narrow limits and because of the rather large power dissipation, it appears that a louver system or some other active thermal control is required for the adapter section. Whether or not the kick motor is released after firing does not appear to be a thermal problem, since an active thermal control should be able to handle the problem either way.

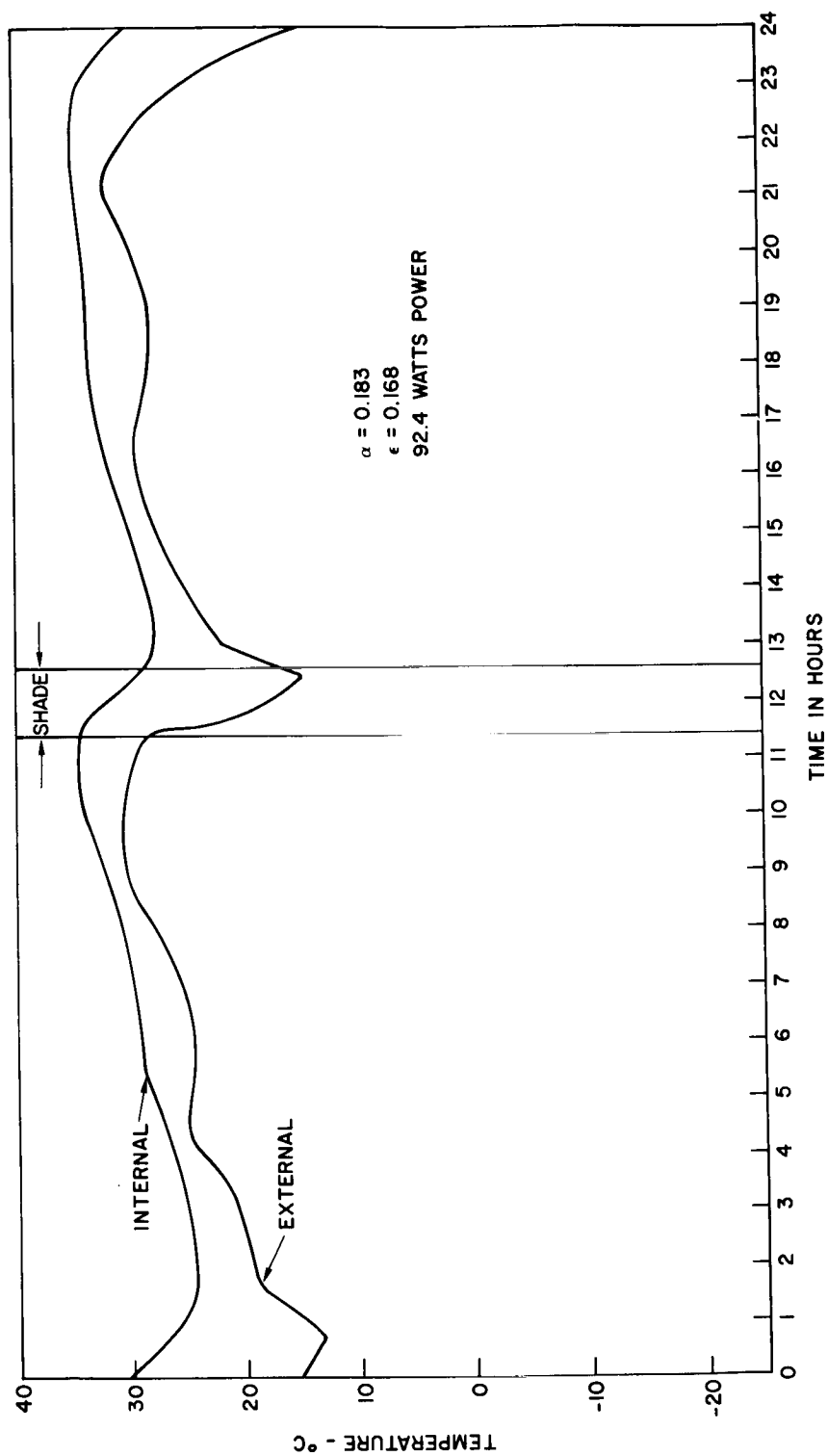


Figure 15-12. ATS-4 feed.

## SECTION 16

### POWER SYSTEM DESIGN CONSIDERATIONS

#### INTRODUCTION

In the design of the power system, the following environmental and performance parameters were assumed:

1. Orbit - synchronous
2. Daytime regulated load - 200 watts
3. Nighttime regulated load - 100 watts
4. Loss due to radiation - 25 percent (2 years)
5. Paddle temperature -  $60^{\circ}$  C
6. Pitch and roll -  $\pm 8.5$  degrees each
7. Yaw -  $\pm 1$  degree

These assumptions were the initial conditions for the design. However, other considerations were either known or assumed. The configuration of the solar array was confined to two paddles, parallel to the spacecraft pitch axis and arranged in a cruciform manner. It was also known that a +28-volt  $\pm 2$  percent regulated bus was required. A simplified block diagram of such a regulated bus system is shown in Figure 16-1. This system provides a 28-volt regulated bus from energy derived from solar cells and batteries during daylight and from batteries during night. The system implies two additional considerations not stated in Figure 16-1. The batteries must be charged in a controlled manner, and there is some maximum voltage to which the system must be limited to protect the electronics.

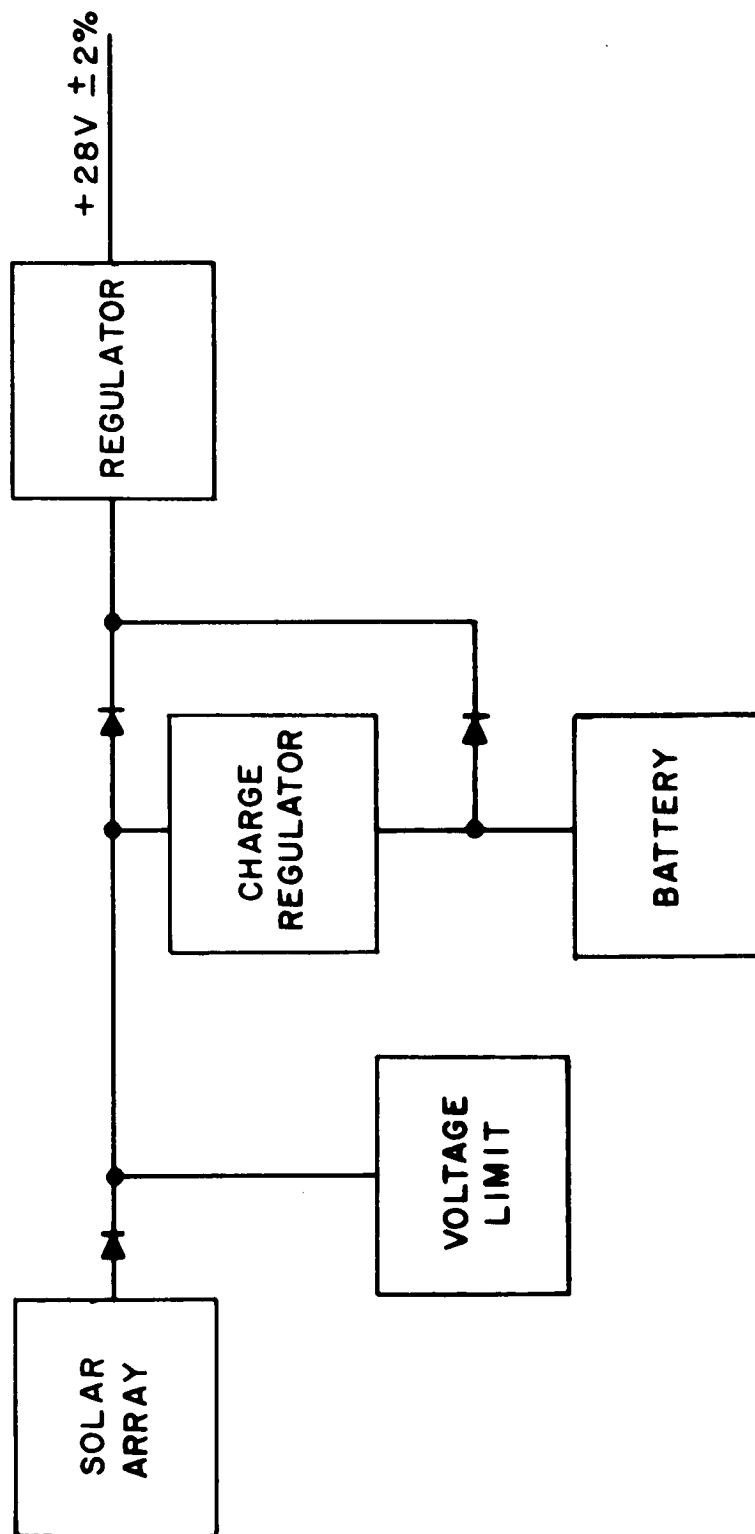


Figure 16-1. Regulated bus power system.

Normally, a power system design analysis starts with the regulated bus and works back to the battery, charge controller, limiter, and the solar array. However, this report describes the solar array before the batteries because the solar array characteristics (maximum and minimum voltage, etc.) must be known to size the batteries. With that exception, this report progresses in the normal sequence.

## REGULATION

A tightly regulated bus can be derived from any one of three series regulator configurations -- buck, boost, or buck-boost. The output voltage of a buck regulator is lower than the input voltage. Conversely, the output voltage of a boost regulator is higher than the input voltage. A buck-boost regulator then will function properly when the input voltage is either higher or lower than the specified output voltage. A buck-boost regulator was chosen for two reasons: Firstly, to avoid the necessity for the chopping transistors to switch the total source current; and secondly, because the regulator can operate over a wider range of input voltages, negating the maximum/minimum voltage limitations normally associated with the array and battery. For example, a buck regulator typically requires an input voltage 0.5 volt above its output to maintain regulation. Assuming a series worst-case discharge voltage of 1.1 volts per cell means that  $28.5/1.1 = 26$  series batteries are necessary to maintain regulation. If a higher end of discharge voltage is assumed, the buck-boost regulator still operates with fewer series batteries, because its input voltage can swing above and below the output. A major difficulty with a simple boost system is the  $I^2R$  loss associated with the increased solar array currents flowing through the long cables to the unregulated bus system. A buck-boost regulator was chosen since it utilizes the best features and negates the disadvantages of both its counterparts.

The regulator must supply not only the average 200 watts daytime power, but the peak demand as well. Table 16-1 lists the peak loads of the spacecraft. A 10 percent margin results in a 400-watt regulator.

Table 16-1  
Peak Power Loading

System	Power (watts)
Controls	70
Station keeping	33
Command and telemetry	49
Antenna (peak stall)	35
X-Band	80
UHF	72
Interferometer	15
Other	10
Total	364

Redundancy considerations indicate the desirability of a standby regulator in case of failure of the first. To save weight and packaging, the second regulator could share the heavy filtering components and be mounted in the same package with the first. (A regulator package of this type weighs approximately 18 pounds.) When loss of regulation is sensed, the faulty regulator is switched out, and the standby takes over. Ground command switchover will also be provided. The efficiency of this regulator at the given voltage and power level is typically 85 percent or better. This efficiency was assumed in the power calculations.

### SOLAR ARRAY

A sketch of the solar paddle alignment, looking into the yaw axis, is shown in Figure 16-2.

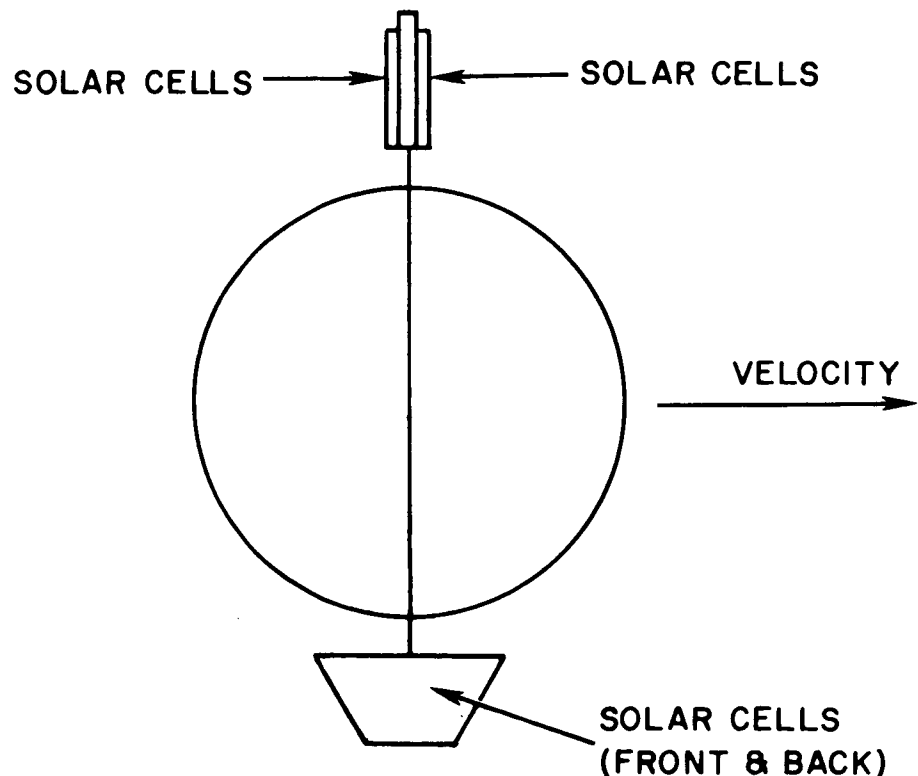


Figure 16-2. Solar paddle alignment.

The solar array uses 10.5 percent, air-mass zero efficiency N-on-P solar cells covered with 6-mil-thick quartz. Each of the two paddle surfaces provides 40 square feet of area for mounting the solar cells. Since the orbit is synchronous and the spacecraft is earth-pointing, it can be seen that as the spacecraft revolves about the earth, first one paddle surface sees the sun and then gradually the other. As the first paddle surface goes out of view of the sun, its back surface comes into view. Figure 16-3 shows the varying angles that the paddles make with the sun vector.

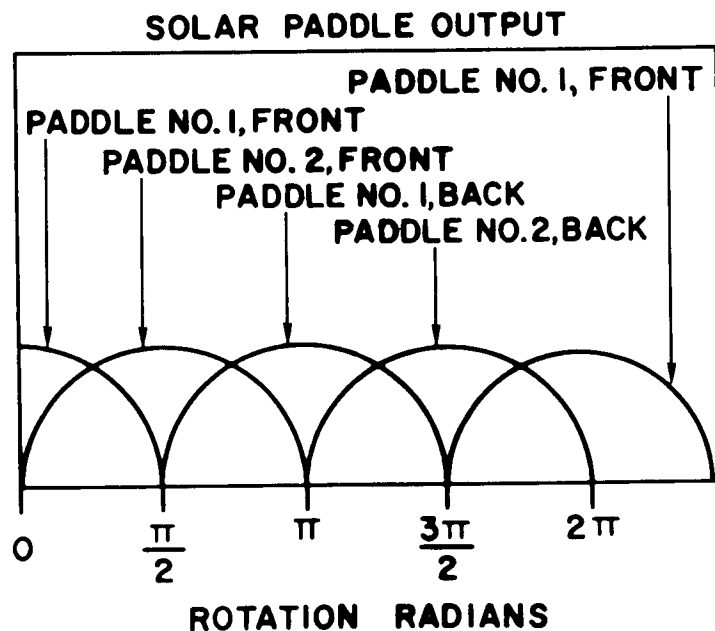


Figure 16-3. Solar paddle output.

Each paddle surface acts as a single half-wave rectifier, and the total output is the sum of these rectifier outputs phased 90 degrees apart. The average output of a single half-wave rectifier is given by

$$P_{\text{avg}} = \frac{P_{\text{max}}}{2\pi} \int_{-\pi/2}^{\pi/2} \cos \theta \, d\theta$$

$$P'_{\text{avg}} = \frac{P_{\text{max}}}{\pi}$$

Where  $P'_{avg}$  and  $P_{max}$  are the output of a single paddle surface. The assumption in this equation that the output power follows the cosine curve is not strictly true. This situation can be remedied by assuming that the power follows the cosine curve except at an angle of 75 degrees from the normal, where it goes to zero. The modified equation for the average power is then

$$P'_{avg} = \frac{P_{max}}{2\pi} \int_{-\frac{5\pi}{12}}^{\frac{5\pi}{12}} \cos \theta \, d\theta$$

$$P'_{avg} = 0.965 \frac{P_{max}}{\pi}$$

Since  $P_{max}$  represents the output of one surface, then

$$P_{avg \, total} = 4 \left( \frac{0.965}{\pi} P_{max} \right) .$$

This equation represents the average power output when the sun is in the equatorial plane and when pitch, roll, and yaw are zero. However, the apparent motion of the sun is 23.5 degrees above and below the equatorial plane. It can be shown that the effect of this motion changes the output by

a constant factor equal to the cosine of 23.5 degrees. The average power equation can be further modified thus:

$$P_{\text{avg total}} = \frac{(4) (0.965) (\cos 23.5^\circ) (P_{\text{max}})}{\pi}$$

$$P_{\text{avg total}} = \frac{(4) (0.965) (0.917) (P_{\text{max}})}{\pi}$$

It can be shown further that roll affects only one paddle and modifies it by a term equal to the cosine of the amount of roll; however, pure pitch merely changes the phase of the array output and not the magnitude. Therefore, the average power must again be modified. The result is

$$P_{\text{avg}} = \frac{(3.53) (0.965) (P_{\text{max}})}{\pi}$$

If the average power required from the array is known, the size of the paddles can be determined.

The general equation for energy balance is

$$P_A t_D = \frac{P_{LD} t_D}{\eta_R} + P_{SLD} t_D + \frac{1}{\eta_B} \left( \frac{P_{LN}}{\eta_R} + P_{SLN} \right) t_N$$

where

- $P_A$  = Average array power,
- $P_{LD}$  = Average regulated day load power,
- $P_{SLD}$  = Average daytime shunt loss power,
- $P_{LN}$  = Average regulated nighttime load power,
- $P_{SLN}$  = Average regulated nighttime shunt loss power,
- $t_D$  = Satellite day = 22 hours, 50 minutes,
- $t_N$  = Satellite night = 70 minutes,
- $\eta_B$  = Battery discharge to charge efficiency, and
- $\eta_R$  = Load regulator efficiency.

A worst-case battery discharge-to-charge efficiency is arrived at by assuming a warm environment, 35° C. At this temperature, and including trickle charge, a charge-to-discharge current ratio (C/D) could be conservatively specified to be 1.35/1. This is somewhat conservative, but of little impact, as will be seen later. An end-of-charge to end-of-discharge voltage ratio can be assumed to be 1.46/1.1.

The battery watt-hour charge efficiency is given by

$$\eta_B = \frac{(1.0 \times 1.1)}{(1.35 \times 1.46)} = 56\%$$

A more typical value is 65 percent; however, 56 percent is used for the margin value, since it does not seriously affect the array size of this mission.

Although not necessarily true, for simplicity the assumption has been made that all shunt losses are unregulated. The nighttime loss is assumed to be 5 watts and the daytime loss 15 watts. Substituting these numbers into the equation for the average array power gives

$$\overline{P}_A = \left( \frac{200}{0.85} + 15 \right) + \frac{1}{0.56} \left( \frac{100}{0.85} + 5 \right) \left( \frac{\frac{7}{6} \text{ hrs}}{\frac{137}{6} \text{ hrs}} \right)$$

$$\overline{P}_A = 250 + \frac{1}{0.56} (122.5) \left( \frac{7}{137} \right)$$

$$\overline{P}_A = 261 \text{ watts}$$

To supply the loads as specified, the array must average 261 watts over the charging period of 22 hours and 50 minutes. To deliver an average of 261 watts, each paddle must have a maximum output, when normal to the sun, that equals

$$P_{\max} = \frac{(261) (\pi)}{(0.965) (4)} = 212 \text{ watts}$$

A worst-case condition occurs when the sun is at 23.5 degrees declination, and the spacecraft is rolled 8.5 degrees. Although the average load requirement has decreased approximately 5 percent to the daylight load of 250 watts average, the array output has decreased by the cosine of 32 degrees (23.5 + 8.5) for one paddle, and by the cosine of 23.5 degrees for the other. Since the array output consists of two components,

$$P_{\max} (\cos 32^\circ) \cos \omega t \text{ and } P_{\max} (\cos 23.5^\circ) \sin \omega t$$

and all components are defined, a plot of the output can be constructed as in Figure 16-4.

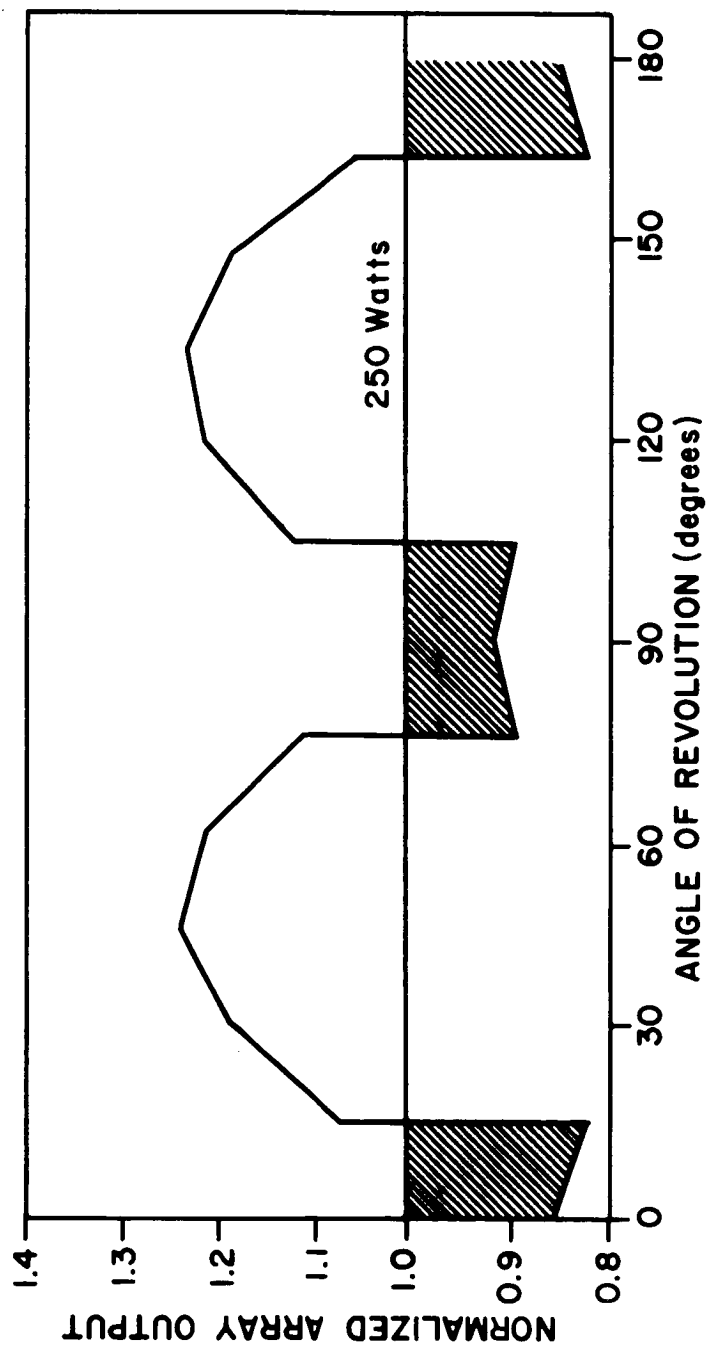


Figure 16-4. Output of the array as a function of angle of revolution.

In Figure 16-4, all power levels have been normalized to the maximum output,  $P_{\max}$ , of a single paddle surface normal to the sun. The abscissa represents the satellite motion about the earth axis. The sun is 23.5 degrees above the equatorial plane, and the spacecraft has rolled 8.5 degrees away from the sun. The pitch is ignored since it affects only the phase of the plot. Yaw motion of  $\pm 1$  degree is also neglected since it has little effect. Each 15 degrees of revolution corresponds to 1 hour of time. Because of the varying output, it is possible that some of the average power required would be supplied by the batteries. If this occurs, then the  $P_{\max}$  point must be designed so that the array supplies not only the average load requirement, but also the necessary power to recharge the batteries. As a first trial, it can be assumed that  $P_{\max}$  equals the average 250-watt load. This is shown on the graph. The shaded area under 250 watts represents battery discharge. As another worst case, it can be assumed that the array is required to recharge the batteries completely after each discharge. Integrating the deepest discharge area over 2 hours and dividing by  $\pi/2$ , results in 13.8 watts as the average discharge. Dividing by the D/C efficiency of 56 percent yields 24.7 watts as the average charge power required. Integrating the charge portion of the curve yields 30.8 watts average, an excess of 6.1 watts. Then

$$P_{\text{avg}} = \frac{(3.53) (0.965) (250)}{\pi}$$

$$P_{\text{avg}} = 271 \text{ watts}$$

$$271\text{w} - 6\text{w} = 265 \text{ watts avg}$$

$$P_{\text{max}} = \frac{(265) (\pi)}{(3.53) (0.965)}$$

$$P_{\text{max}} = 245 \text{ watts}$$

Changing the  $P_{\max}$  to 245 watts shifts the 250-watt daytime load level to 1.02 on the curve. The resulting ratio of discharge-to-charge areas is 0.56, the required ratio for this analysis.

The solar array must be designed so that at end of life each paddle surface must be capable of supplying 245 watts, minimum, when the sun vector and paddle normal vector coincide. At this zero sun elevation, the average power from the array will be

$$P_{\text{avg}} = \frac{(4) (0.965) (0.917) (245)}{\pi}$$

$$S/L = 0$$

$$P_{\text{avg}} = 276 \text{ watts}$$

At 23.5 degrees elevation and 8.5 degrees roll, the output will be

$$P_{\text{avg}} = \frac{(3.53) (0.965) (245)}{\pi}$$

$$S/L = 23.5^\circ$$

$$R = 8.5^\circ$$

$$P_{\text{avg}} = 265 \text{ watts}$$

Finally, how much power will the paddles deliver at launch? Above 30°C, temperature effects degrade the performance by 0.5 percent/°C. Since a temperature of 60°C has been assumed, the output will be degraded by 15 percent. Radiation degradation of 25 percent has been assumed. This implies 18 percent current degradation and 9 percent voltage degradation. (At the time of this writing, no data concerning the actual radiation levels at synchronous altitude were available. When such data are available, the 25 percent figure may have to be modified.) However, the assumed radiation and temperature effects modify the paddle maximum by

$$P_{\text{max launch}} = \frac{P_{\text{max end of life}}}{(0.75) (0.85)} = \frac{245}{(0.75) (0.85)}$$

$$P_{\text{max}} = 385 \text{ watts}$$

A design of 400 watts per paddle yields almost a 5 percent margin. Assuming 10.5 percent, air mass zero efficient cells with 6-mil-thick cover glass, a packing factor of 85 percent and 13 percent interconnection losses, it can be shown that 40 square feet of surface area will yield 400 watts.

Figure 16-5 is a normalized graph of the solar array output for four interesting conditions. The curved portion of the graph represents the solar array output when the sun is contained in the equatorial plane. The segmented straight line portion of the graph represents the output when the sun is 23.5 degrees out of the equatorial plane and when the spacecraft is rolled 8.5 degrees. (The latter graph is similar to Figure 16-4). Note that the discontinuities are fictitious in both cases, but are drawn for ease of representation and analysis. Also, the segmented straight line portion of the graph really should be drawn similar to the curved one, but artistic license is taken again for clarity.

The lower dashed line represents the 250-watt day load before radiation degradation. No daytime battery cycling occurs. The array is normalized to 340 watts, the output of one paddle at 60° C. The upper dashed line represents the 250 watts load after 25 percent array degradation. The array is normalized to 255 watts; note that daytime battery cycling occurs during the unfavorable sun and spacecraft orientation. Cycling also occurs, to a lesser extent, at this sun elevation when the spacecraft has not been reoriented 8.5 degrees. The power levels noted on the graph represent the instantaneous output before and after radiation degradation.

By extrapolating Nimbus and IMP paddle weights, a 40-square-foot paddle would weigh 64 pounds, not including booms. The solar array consists of two paddles of cruciform configuration, with 40 square feet of surface area per surface, and 10.5 percent, air mass zero efficiency N-on-P solar cells with 6 mils of quartz cover glass mounted on all four surfaces. Such an array in the ATS-4 orbit will deliver a minimum of 275 watts average power and will weigh 128 pounds, excluding boom weights.

## BATTERY

Since the loads and the solar array output have been defined, the battery can now be designed. Two important parameters are operating voltage and depth of discharge. A minimum end-of-discharge voltage was chosen to be 1.1 volts per cell, while the maximum allowable charge voltage

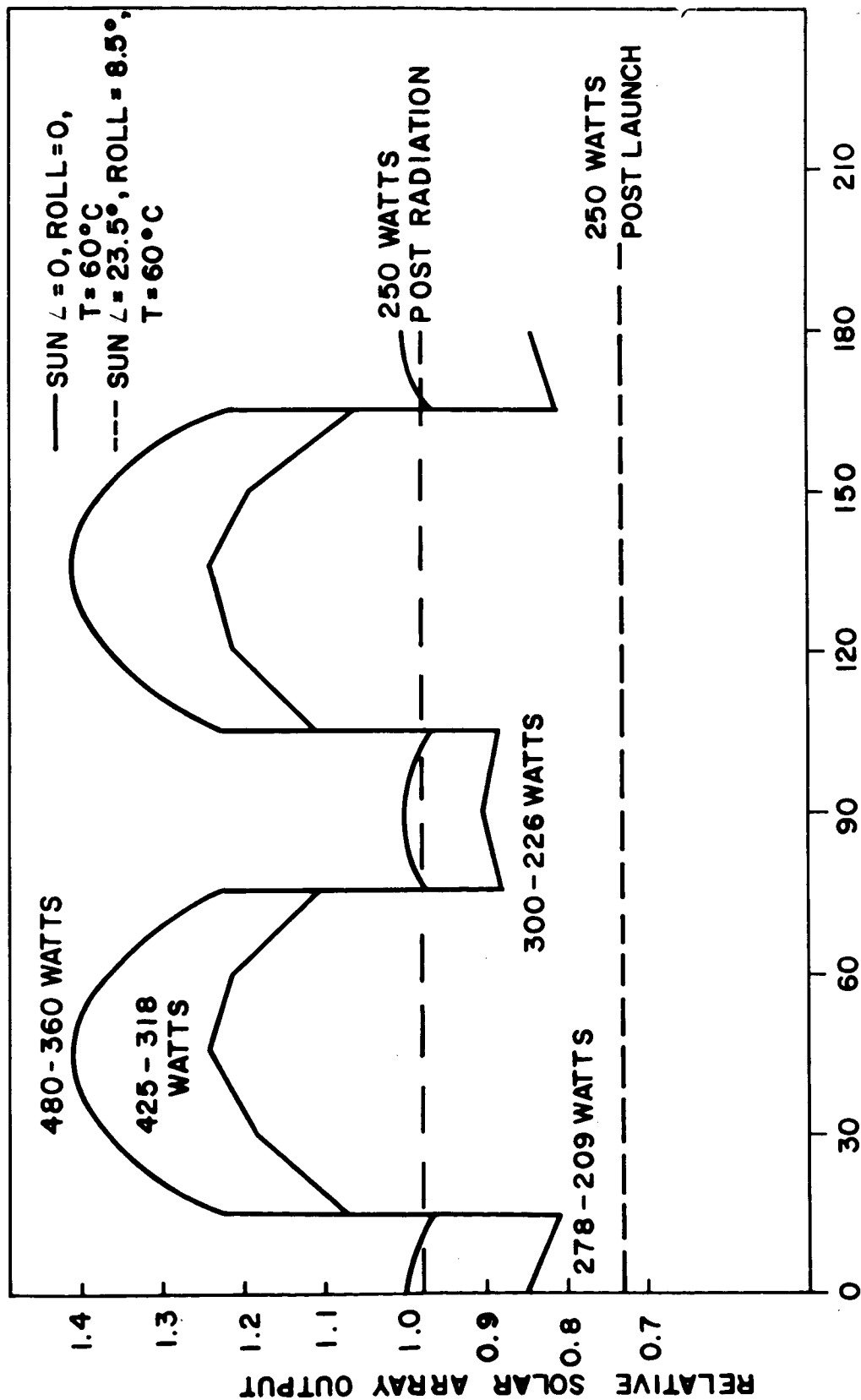


Figure 16-5. Normalized graph of the solar output for four conditions.

was chosen to be 1.50 volts per cell. This represents the maximum allowable charge voltage at 0° C. The average value of this voltage range is 1.30 volts per cell. This value divided into 28 volts yields the number of required series cells: 22.

Calculating the necessary capacity

$$\text{Amp-hours} = \frac{\text{watt-hours}}{\text{volts}} = \frac{\left(\frac{100}{0.85} + 5\right) \frac{7}{6}}{(1.1) (22)}$$

$$\text{Amp-hours} = 5.9$$

Normally, the depth of discharge is maintained at a maximum of 15 percent when thousands of repetitive cycles are expected. However, the eclipse time for a synchronous orbit varies throughout the year, and the peak 70-minute eclipse occurs only twice a year. (See Figure 16-6.) For this reason, a 25 percent depth of discharge was considered allowable. An even greater depth of discharge would be allowable if the array analysis did not indicate that daytime cycling is expected after radiation degradation. Then the necessary capacity is

$$\frac{5.9 \text{ amp-hours}}{25\%} = 23.6 \text{ amp-hours}$$

This is convenient because 24 amp-hours can be derived from two 12-amp-hour batteries discharged in parallel. The parallel configuration results in some redundancy in case of failure. Four 6-amp-hour packs could be used, but the integration and handling problems would increase, as would the cost.

A third electrode nickel-cadmium battery provides the necessary cycle lifetime and overcharge protection. Since long periods of continuous sunlight can occur, protection against overcharge must be supplied. The third electrode develops a voltage that is a function of internal pressure. When the voltage reaches a preset level, it signals the battery charger to reduce the charge current to 200 milliamps.

The weight of the cells, plus 50 percent for electronics and packaging, results in a single battery weight of 36.5 pounds. The size required for a battery pack is 6 inches wide, 8 inches high, and 11 inches deep.

After long periods of use, a nickel-cadmium battery often loses some of its capacity. This phenomenon is not completely understood; however, it is known that temperatures above 25° C greatly accelerate the effect. Therefore, the batteries must be operated in a temperature environment between 0° C and 25° C. In order to extend the life of the battery, provision is made to discharge each battery slowly through a resistor to an average voltage of one volt per cell and then to recharge. This action should regain some of the lost capacity if the discharge time is extended to perhaps three days. Each battery would be conditioned while the satellite is in full sunlight just prior to the beginning of the eclipse period. To discharge a 12-amp-hour cell over a three day period:

$$\text{Rate} = \frac{12 \text{ amp-hours}}{72 \text{ hours}} = 167 \text{ ma average discharge current;}$$

$$\frac{\text{Average voltage} = 1.2 \text{ volts}}{\text{Average current} = 167 \text{ ma}} = 7.2 \text{ ohms.}$$

Assuming 8 ohms per cell multiplied by 22 cells yields a letdown resistance of 159 ohms. Since 160 ohms is a standard size, this value could be used. The maximum power dissipation is

$$\frac{(1.25 \times 22)^2 \text{ volts}}{160 \text{ ohms}} = 4.7 \text{ watts.}$$

#### BATTERY CHARGE REGULATOR (BCR)

The charge current into any battery must be controlled so as not to damage the battery with the high end-of-charge or overcharge rates. A PWM temperature-controlled, constant-voltage regulator was selected for ATS-4. The PWM feature provides high efficiency while the constant voltage protects against high end-of-charge voltage. The unit is simply a voltage regulator whose output voltage is a function of temperature. As the battery temperature varies, the battery end-of-charge voltage varies inversely. The temperature of the battery is sensed with a thermistor,

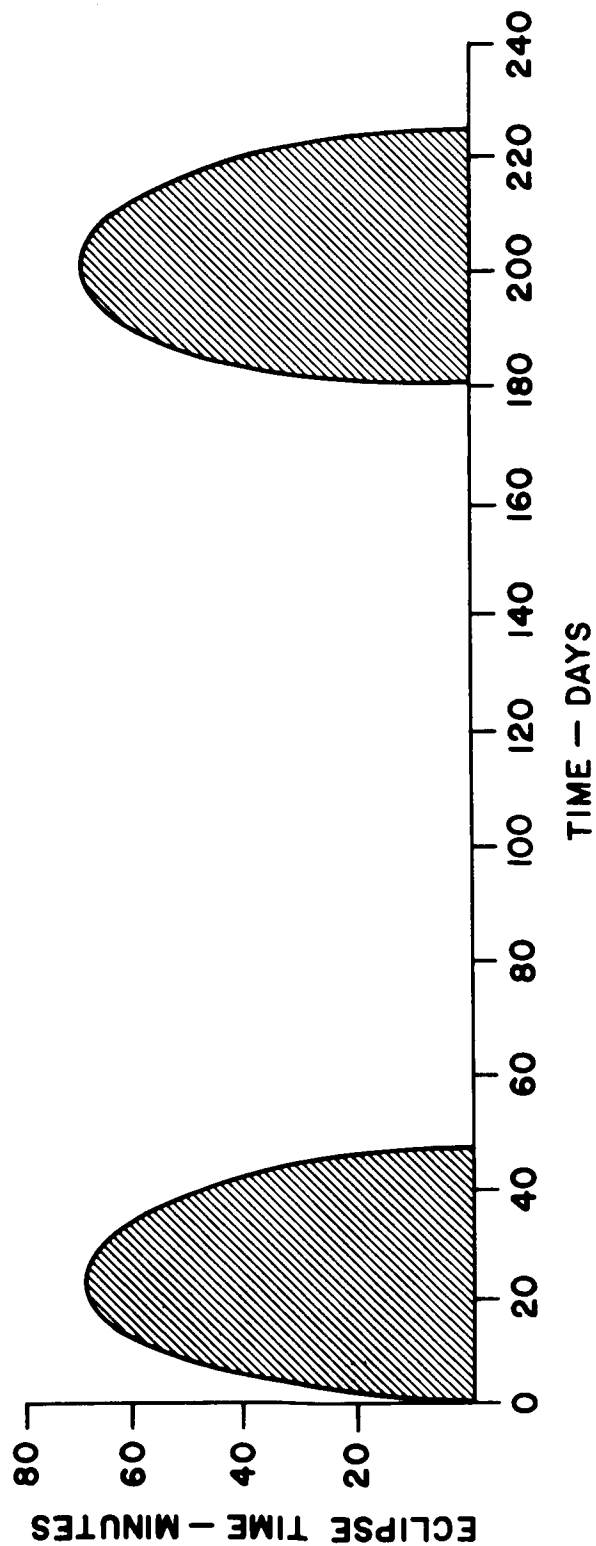


Figure 16-6. Satellite eclipse periods.

and the BCR regulates to the maximum allowable battery voltage for that temperature. When the third electrode cell signals that the proper charge-to-discharge ratio has been provided, the regulator switches to a constant current mode of 200 milliamps. This rate, capacity rating divided by 60 (C/60), is considered safe for long periods of continuous overcharge. Circuitry for ground command trickle charge is provided.

For reliability and isolation, each battery pack has a series charge regulator. The proper ground command can also provide a regulator bypass in case of malfunction. Provision for opening the ground leg of the battery by command has been provided in case multiple failures cause high overcharge rates.

### VOLTAGE LIMITER

The final component of the system is the voltage limiter. This circuit is necessary because some of the electronic components of the system have maximum voltage limitations. This situation is particularly true in the case of high-current transistors since it is difficult to find transistors in the 10-amp range that allow 100 volts to be impressed across them. If the components could withstand the maximum output voltage of the array, then no voltage limiter would be necessary. The array would operate at the particular point on its output characteristic in such a manner that only the required power would be delivered. However, the inclusion of the limiter clamps the array at a maximum voltage in such a manner that excess power can be delivered and therefore must be dissipated in the limiter. This situation is illustrated in Figure 16-7.

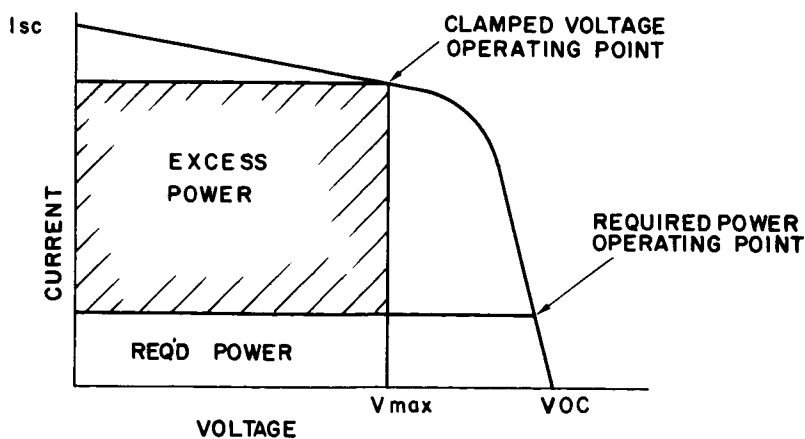


Figure 16-7. Voltage limited array.

The excess power is not quite as great as that shown since the required power to the right of  $V_{\max}$  adds to the required power on the left when operating in the clamped mode. This would decrease the excess shown. However, the illustration demonstrates the concept of clamped arrays and excess power. Under conditions of maximum array output and a minimum load that equals 50 watts, as much as 450 watts can be dissipated in the limiter. This requirement can be reduced by using a partial shunt regulator. This regulator, instead of operating across the full unregulated bus, limits the bus to a maximum by shorting out a portion of the array. This operation is demonstrated in Figures 16-8 and 16-9.

The curves shown have the following characteristics in relation to Figure 16-6.

$$I_{sc} = I_{sc1} + I_{sc2}$$

$$V_{oc} = V_{1oc} + V_{2oc}, \text{ and}$$

$$V_{\max} = V_1 + V_2.$$

The tap point must be chosen so that  $V_2$  plus the saturation voltage of the transistor does not exceed the maximum clamp voltage under conditions of a cold array and minimum load. A 50-watt minimum load reduces the 450-watt dissipation requirement to 140 watts. Each paddle must be supplied with a limiter so that when a paddle has zero output (edgewise to the sun), regulation is maintained.

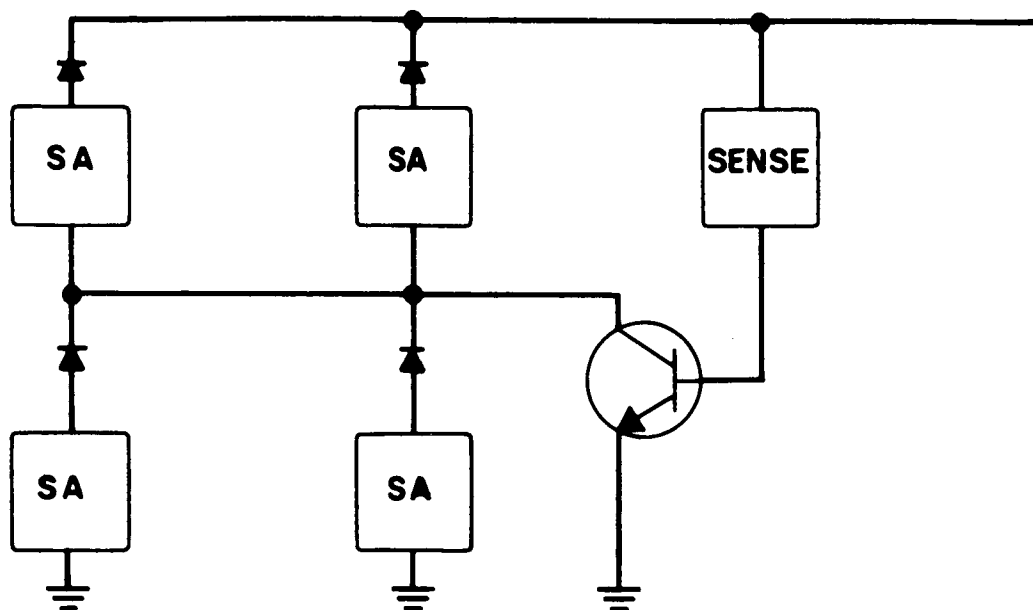


Figure 16-8. Partial shunt regulator.

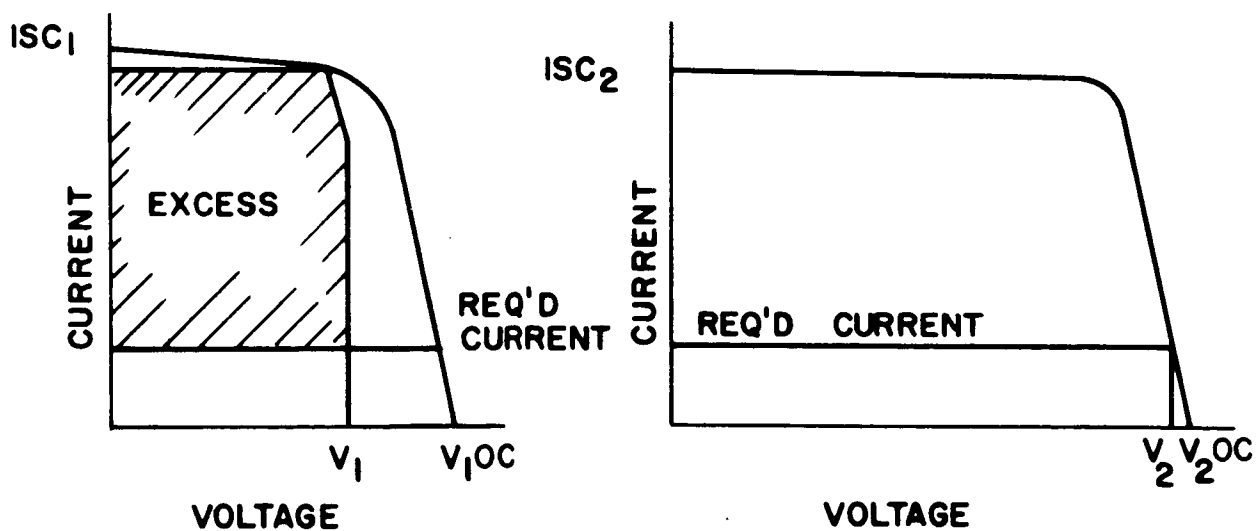


Figure 16-9. Split array characteristics.

## TELEMETRY

The telemetry should be chosen so that information describing system operation can be obtained. Another telemetry function is to provide predicted design information such as the solar array output under space conditions. Table 16-2 shows the desirable telemetry points. These telemetry points should greatly facilitate post launch and anomaly analysis.

Table 16-2  
Telemetry Requirements

Subsystem	Function	Quantity req.
Solar array	Paddle voltage	4
	Paddle current	4
	Paddle temperature	4
Battery	Battery voltage	2
	Charge current	2
	Discharge current	2
	Temperature	2
	3rd elect. voltage	2
	3rd elect. cell voltage	2
Busses	Voltage-regulated	1
	Voltage-unregulated	1
	Current-regulated	1
	Current-unregulated	1
Relays	On-off status	7
Margin		<u>5</u>
	Total	40

## COMMAND REQUIREMENTS

Since the system has been defined, it merely remains to sum the operational modes to arrive at the number of necessary ground commands (Table 16-3).

Table 16-3  
Command Requirements

Subsystem	Commands	Quantity req.
Regulators	Switch to standby	1
Batteries	Switch to trickle charge	2
	Conditioning	2
	Charger bypass	2
Margin	Open circuit	2
		<u>5</u>
	Total	14

## POWER SUMMARY

Table 16-4 summarizes the array and battery performance for several conditions. Since the 25 percent depth of discharge is a result of satellite eclipse, it is not affected by the solar array output. However, the 14 percent discharge occurs during the sunlit portion of the orbit. The 14 percent results when the array average power is 265 watts. Since the array will deliver 275 watts, the depth of discharge will be closer to 11 percent.

Table 16-4  
Power Summary

Mode	Array		Batteries
	Pwr. req. (watts)	Delivered (watts)	Depth of discharge (percent)
Launch Sun = 0 P&R = 8.5°	265	420	25
Two years Sun = 0 P&R = 8.5°	265	315	25
(Worst case) Two years Sun = 23.5° P&R = 8.5°	265	275	14

### WEIGHT SUMMARY

Table 16-5 indicates the estimated system weights. It should be remembered that the solar array weight is exclusive of booms.

Table 16-5  
Weight Summary

Subsystem	Weight (lbs)
Solar array	128
Voltage limiter (2)	6
Battery (2)	73
Regulator (2)	18
Total	225

## LAUNCH PHASE

It has been shown that the system design fulfills the operational requirements of the satellite under worst-case assumptions. It remains to be shown that the system supplies the necessary power from launch throughout acquisition. Figure 16-10 shows the power requirements during this time and the average array power supplied for a January launch. The output from an oriented array is also shown. It has been assumed that 30 minutes of initial shadowing occurs during the ascent phase. It can be seen that more than enough power is available from the solar array to supply the launch-acquisition phase.

## CONCLUSION

Throughout the analysis, attempts have been made to assume worst-case conditions. The designed system has been shown to easily meet these conditions. Since worst-case conditions usually do not occur throughout the mission, the resulting margin is a measure of the reliability and the growth potential of the satellite. Obviously, trade-offs can be made with regard to reducing the system weight, but only with a corresponding reduction of reliability and growth potential. The proposed system easily supplies the stated 200-watt daytime load and 100-watt nighttime load when the sun is at the worst angle and after two years of radiation damage. Figure 16-11 is a simplified block diagram of the proposed system and its command capability.

## BATTERY WEIGHT REDUCTION

Although it has been shown that two packs of 12 amp-hour batteries supplies satisfactorily and reliably the required power demands, the question arises whether a reduction in capacity, and therefore weight, will still supply the necessary requirements. The answer, of course, is yes, although there will be a corresponding reduction in system margin. Although no data are available for a 24-hour orbit, tests have shown that a Gulton, 6-amp-hour, 3rd electrode battery has been cycled several thousand times to 40-percent depth of discharge in a 1.5-hour orbit. Cautious extrapolation of these tests implies that two similar packs can survive two years life in the proposed ATS-4 satellite. The following justifications are offered.

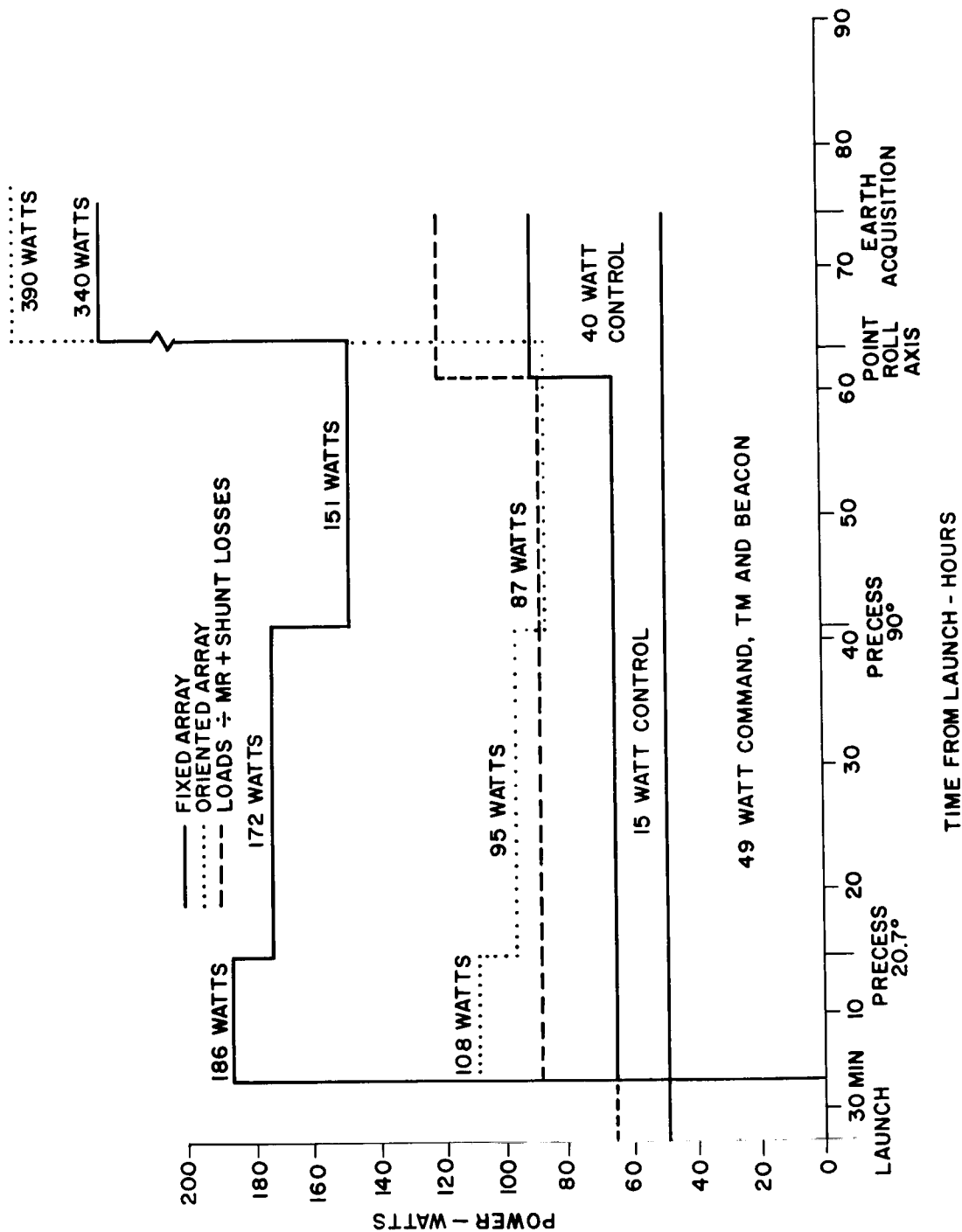


Figure 16-10. Launch sequence.

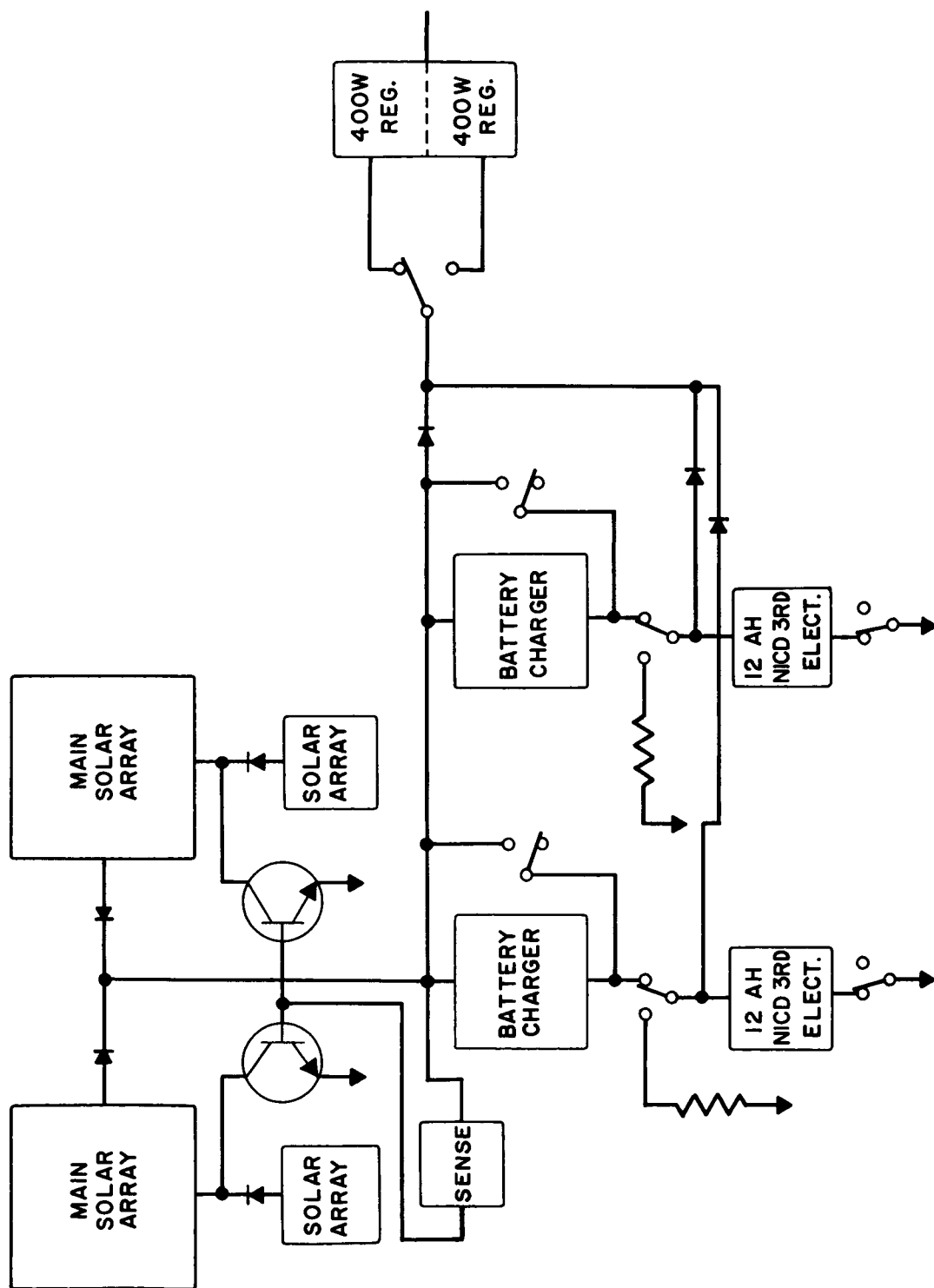


Figure 16-11. Power system block diagram.

1. The 50 percent depth of discharge of two packs of 6-amp-hour batteries is the worst case. The actual depth builds up to this maximum and then subsides twice a year.
2. The cycle is not repetitive (the tests were), in that the discharge depth varies substantially throughout the year.
3. The batteries will not be subjected to a warm environment; maximum allowable temperature is 25° C.
4. The batteries will be periodically reconditioned in orbit.
5. The batteries are protected from overcharge by the third electrode cell.

Life tests should begin immediately to substantiate the justifications. If the results prove negative, the three packs would have to be used to reduce the depth of discharge. However, three packs of 6-amp-hour cells would only be 11 pounds lighter, and would eventually cost more than two packs of 12-amp-hour cells. Table 16-6 shows the trade-offs of the proposed batteries.

Table 16-6  
Battery Characteristics

Capacity	Number of packs	Weight (lbs)	Wgt. savings (lbs)	Depth of discharge (max. percentage)
12	2	73	--	25
6	2	41	32	50
6	3	62	11	33

## ORIENTED ARRAY

Since the proposed paddle configuration results in a huge, expensive array, the following paragraphs discuss the savings of an oriented array. It has been shown that the lowest solar array output occurs when the sun is 23.5 degrees above or below the equatorial plane and when the spacecraft is rolled 8.5 degrees. A simple calculation shows the necessary power, assuming no battery discharge, to supply the 250 watts average power demand.

$$P'_{\text{array}} = \frac{\text{load power}}{\cos (23.5^{\circ} + 8.5^{\circ})} = \frac{250 \text{ watts}}{0.848} = 295 \text{ watts}$$

$S\angle = 23.5^{\circ}$   
 $R = 8.5^{\circ}$

The power at launch and at a temperature of 30° C would be

$$P_{\text{array}} = \frac{P'_{\text{array}}}{(\text{radiation}) (\text{temperature})} = \frac{295}{(0.75) (0.85)} = 463 \text{ watts}$$

Each paddle surface would only have to be approximately 23 square feet, and solar cells would only cover two surfaces. These dimensions are similar to the Nimbus paddles and therefore would weigh approximately 54 pounds total. A final advantage is incurred because the batteries are no longer subjected to daytime cycling as is the case with fixed paddles. Table 16-7 summarizes the foregoing discussion.

Table 16-7  
Solar Array Comparisons

Type	Size/paddle (ft <sup>2</sup> )	Total weight (lbs)	Wgt. savings (lbs)	Cost factor
Fixed array	40	128	--	700k
Oriented array	25	54	74	300k

## SECTION 17

### COMMAND AND TELEMETRY SYSTEM

#### INTRODUCTION

The Command and Telemetry System (CTS) for the ATS-4 has been designed to provide the optimum system flexibility for meeting the ATS-4 mission requirements. During the lifetime of the spacecraft, CTS requirements will vary widely from undeployed to fully deployed, station keeping, normal operation, etc. Certain events will occur for relatively short periods (e.g. deployment, station keeping, etc.). These will, however, require virtually the full capacity of the CTS. The flexibility in accommodating these variations in requirements has been incorporated in the CTS design.

#### COMMAND SYSTEM

The command requirements of the ATS-4 are, by system design, constrained to real-time employment. Frequency and delayed-time command requirements of the spacecraft are minimal, thereby reducing the command system complexity. The system envisioned would be of a straightforward design, conforming to all requirements of the GSFC Aerospace Data Systems Standards.

The present ATS-4 command requirements are given below: (A detailed breakdown is shown in Table 17-1).

- a.  $\approx$  160 latching-type relay commands.
- b.  $\approx$  171 10-bit digital-command-type words.
- c.  $\approx$  8 timed tone-execute commands for "real time" control of spacecraft functions.

To provide this command capability, the following system is proposed. (Expansion capability is provided.)

1. 256 commands in an X-Y matrix to provide current drivers for latching-type relays (16-by-16 X, Y matrix).
2. 10-bit command word (4-bit address, 6-bit command) -- total of 12 address and 64 commands/address. (2 bits of the address will specify relay driver or command word.)

3. "Tone-execute" command capability.
4. Command rate of 2 commands per second.
5. Internal-spacecraft command verification and execute indication in telemetry bit stream.
6. No stored commands.
7. No frequency generation.

A basic block diagram of a system which will provide this capability is shown in Figure 17-1; a more detailed description of the various command system functions follows.

#### X-Y MATRIX

If a command contains a "one" in both high-order bit locations, it will be determined to be a matrix command and the lower-order eight bits will be employed to provide the "X" and "Y" addresses. This matrix will provide a 50-ms. pulse to the relays located in the various spacecraft systems. These commands can typically be used for turning an experiment on or off, switching to a redundant mode, etc.

#### COMMAND WORDS

The command words supplied by the command system will be 10 bits in length. They can be used by the various spacecraft systems which require a digital number. Specific uses of this type of command could be for setting a particular limit value into a system (e. g., incrementing a stepping motor a given number of times, loading a starting value into a system, etc.)

#### TIMED-TONE EXECUTE

The timed-tone execute commands can be employed to provide "real-time" control of the spacecraft by the ground station. A typical application of this type of command would be for the thrusters. Initially, a command would be sent, arming the thrusters. Thereafter, a tone would be sent from the ground station which, when detected, would cause the desired thruster action to occur. Duration of the action would be a function of the width of the control pulse, which would be variable. After the desired actions had occurred, a second command would be sent, disarming the system and thereby protecting it from being activated by any spurious tones. It will be noted that while the

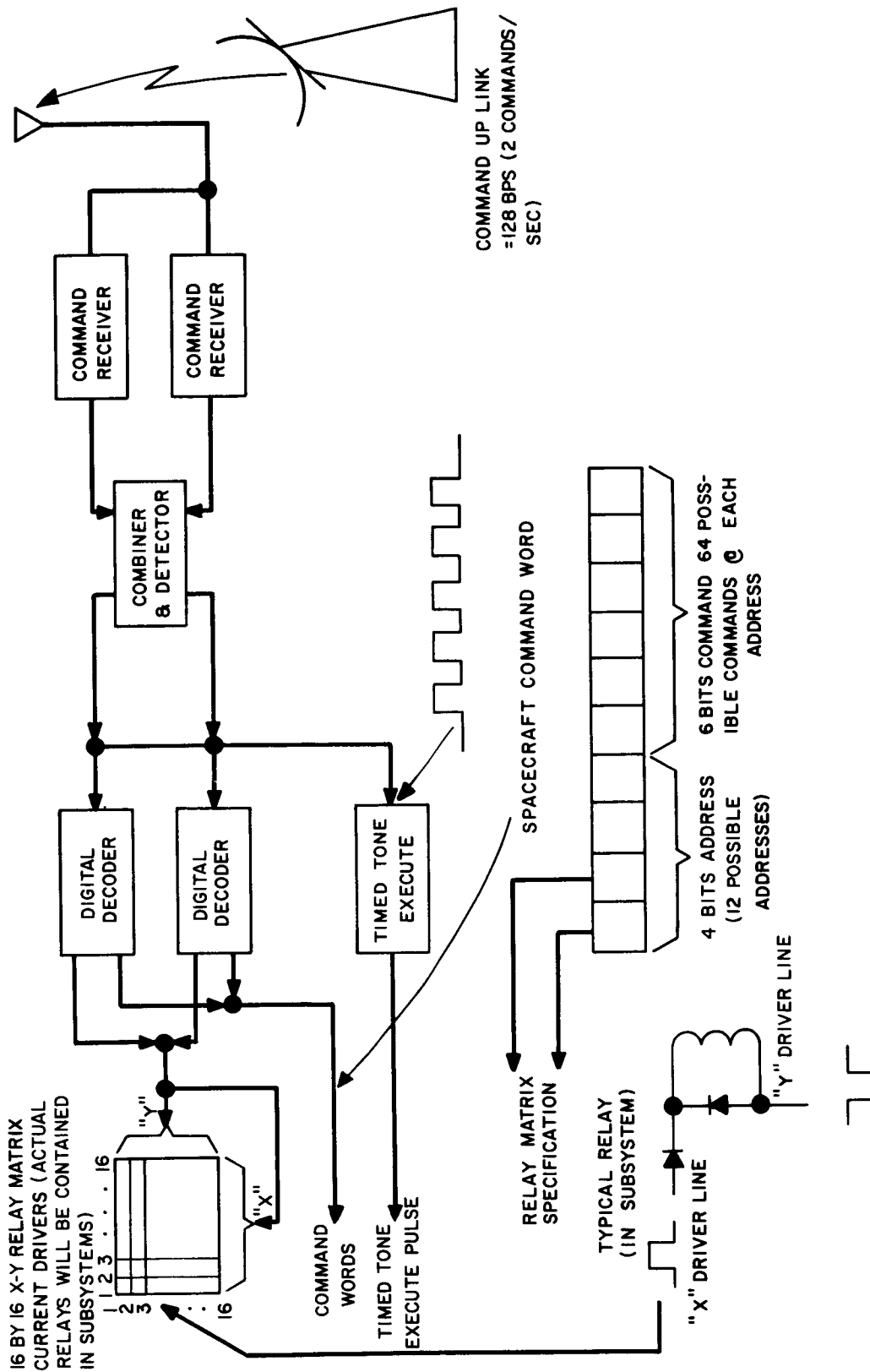


Figure 17-1. Command system.

tone-execute system is being used, it will not be possible to enter other commands into the system.

## COMMAND RATE

Commands will be received by the system at a 128-bps rate. Each word received from the ground will be 64 bits in length. The actual internal-spacecraft command will be 10 bits in length; however, the ground word will contain both the 10-bit command and its complement.

## VERIFICATION

Internal spacecraft verification of the command will be performed prior to spacecraft execution. A provision will be included in the telemetry bit stream to indicate that the command has been received, verified, and executed.

Electrical interface requirements for the command system are listed in Table 17-2.

## TELEMETRY SYSTEM

The requirements of ATS-4 are such that only certain parameters require continuous TM readout, with the intermittent requirements varying from time periods of a few minutes to several hours. To best satisfy these TM requirements, a data-processing system is proposed which can vary the sampling rates and sampling points through the employment of various stored programs.

This system for the ATS-4 is based upon the adaptable or programmable concept which allows wide variations in sampling rates, points, and formats, and thereby obviates many of the restrictions imposed by hardwired systems. The data-processing system capabilities are listed below:

1. Adaptable (programmable) concept to be employed which will allow wide variations in sampling rates, points, and formats.
2. Two basic data-transmission rates:
  - 40 samples/second (prior to deployment);
  - 400 samples/second (after deployment).
3. Sample words will be 10 bits in length.

4. 8-bit A-to-D conversion capability.
5. Can accept analog, 10-bit serial digital, or 10-single bit (i.e., on-off) digital information.
6. Distributed commutation to minimize harness.
7. Optional ground programming mode.
8. Optional auxiliary telemetry points for failure analysis.
9. No low-level signal conditioning.

A more detailed description of these capabilities is as follows:

#### PROGRAMMABLE CONCEPT

The ATS-4 telemetry requirements are such that a wide variation of sampling rates are required. A breakdown of the various requirements indicates that a basic rate of greater than 400 samples per second would be required if a hardwired system were to be employed. However, information from many of the channels is required only periodically (e.g., thrusters, antenna deployment, etc.) and for only relatively short time periods. Consequently, a programmable system could operate at a lower-bit rate, therefore at a higher S/N ratio and, via programming, still be capable of accommodating the periodic requirements. In addition, the system proposed is not tailor made for one mission, but can serve as a basic system for a number of spacecrafts. (This will allow a design similar to that of the Nimbus D Spacecraft Telemetry System to be utilized.) Another advantage of the programmable concept is the large number of inputs which can be accommodated. (It will be noted that a certain number of channels could be set aside and used only for failure analysis without limiting the operational requirements of the system.) Furthermore, because of the adaptable nature of the system, additions or deletions to the telemetry format can be readily made during the actual construction of the spacecraft. It is further emphasized that all alterations to the telemetry format will be electrical changes only, with no hardware alterations necessary.

The internal configuration of the proposed data processing system is illustrated in Figure 17-2. The heart of the system is the memory, which will be capable of storing several different programs. To insure reliable operation, the memory will be made up of several sections. One section, having read-only (RO) properties, is capable of having programs inserted at any time up to launch via a hardwire connection. This section would, as a minimum, contain

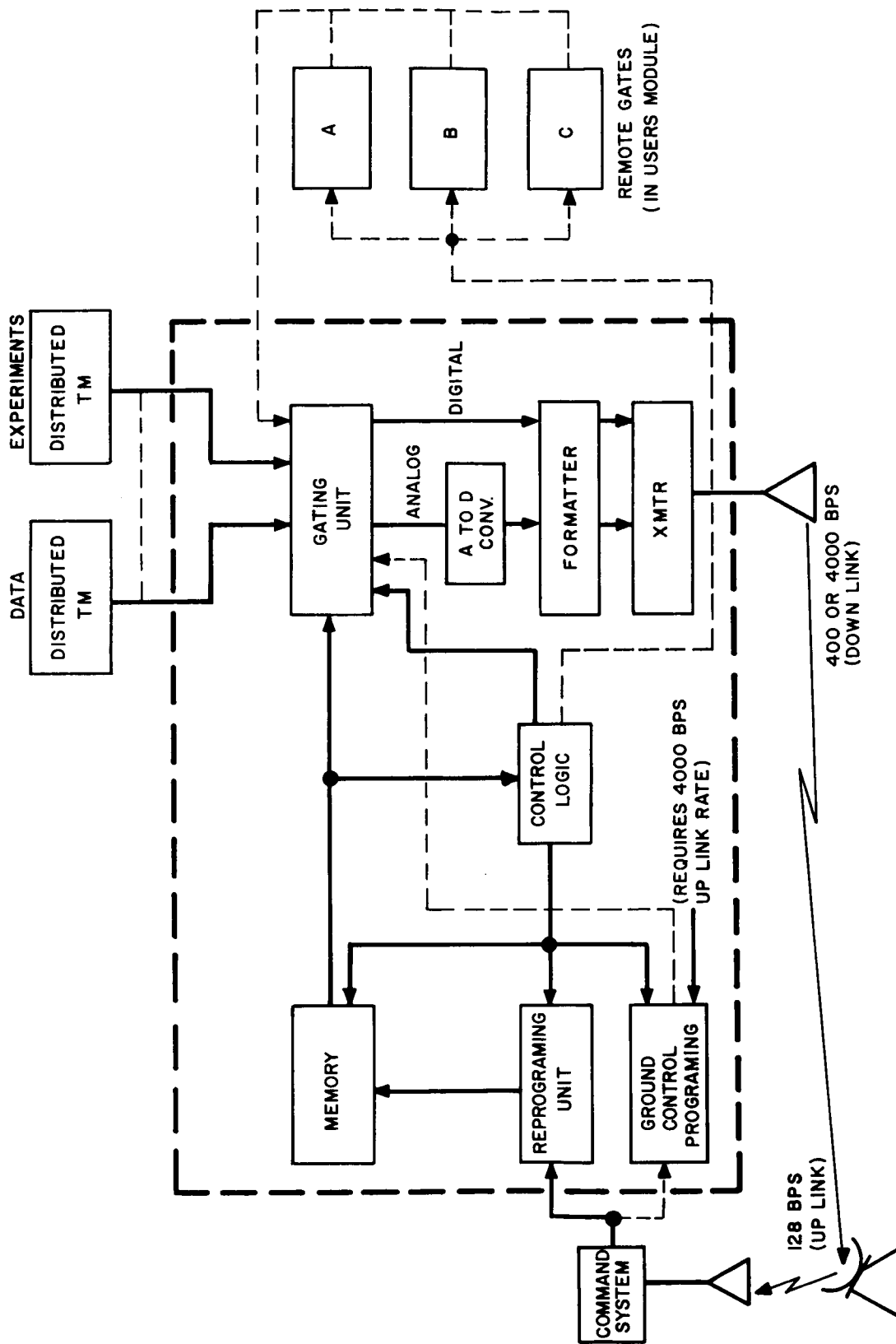


Figure 17-2. Telemetry system.

the normal operational program. A second section of memory, having non-destructive-readout (NDRO) properties, would be employed to provide a reprogramming capability at any time, either prior to or after launch.

In the actual operation of the system, programs would be loaded into the memory either via the command link or a hardwire connection. The specific program being executed would be cycled through under internal logic control. The bit patterns fetched from memory would be examined and utilized to open a gate from one of the approximately 1000 data or telemetry points the system can handle. (Present ATS-4 requirements, as shown in Table 17-1, are 493 analog, 21 ten-bit digital, and 199 single-bit digital.) Special command words in the programs will be used to provide subcommutation, frame identification, sync words, supercommutation, and the other necessary functions.

#### TRANSMISSION RATES

The data processing system will be capable of transmitting 10-bit samples at two basic rates: 40 samples/second (400 bps) and 400 samples/second (4000 bps). The lower rate will be employed prior to deployment to insure that telemetry data can be collected with a reasonably low error rate. The 400 samples/second will be employed after deployment thereby taking advantage of a more stable antenna pattern to again insure low error rates.

#### SAMPLE WORDS

An analog-to-digital converter is provided in the systems for 8-bit conversion of all analog signals. The data processing system is capable of handling 10-bit accuracy but, because of noise pickup, any higher-order accuracy will be, by necessity, done at the source. The system will also accept 10-bit serial digital signals and single bit (i. e., on-off) signals.

#### DISTRIBUTED COMMUTATION

To minimize harness-wiring interfaces, a distributed commutation system may be employed in several of the displaced subsystems which require a large number of TM points. This will allow the harness to consist of approximately 14 wires rather than the 50 or 100 it may have required.

All information, after it has been passed through the gating unit, will be then sent as serial-bit stream to the beacon transmitter where it will be transmitted to the ground.

Table 17-1  
Command and Telemetry Requirements

	Current Command Requirements			Current Telemetry Requirements		
	X-Y matrix (relay) commands	10-bit S/C command words	Timed-tone execute commands	Analog	10-bit digital	Single bit digital
Controls	60	14	1	15	16	40
TV subsystem	4	-	4	4	-	3
Telemetry transmitter & command receiver	4	-	-	6	-	4
Interferometer	2	7	-	50	-	-
Thrusters	14	22	2	50	2	2
Power	24	-	-	26	-	40
Antenna	11	128	1	319	2	66
Communications transponder	34	-	-	18	-	34
Telemetry & command	7	-	-	5	1	10
Total	160	171	8	493	21	199*

\*199 Single-bit digital samples are equivalent to  $\approx 20$  ten-bit data processor sample words.

## GROUND-CONTROL REPROGRAMMING

An optional mode, which may be employed with the ATS-4 because of its synchronous orbit, is ground-control reprogramming. With this option, programs would be provided to the system via the ground link, bypassing the internal spacecraft memory. Employing this option, would allow real-time control of the spacecraft data processor, and provide a redundant feature in case of partial system failure.

## AUXILIARY TM POINTS

A second option may be in the form of special miniature modules which could be employed as "remote gates" for failure analysis. These modules would be small in size ( $\approx 1'' \times 1'' \times 3''$ ), and would be located in the experimenters package. They would be capable of subcommutating 16 different TM points which would be of interest in failure analysis. Since these modules will normally be in the off condition, their power requirements will not be reflected into the spacecraft power budget. Control of the modules will be via one of the optional programs the data processing system is capable of performing.

Electrical interface requirements of the system are listed in Table 17-2.

## GROUND STATIONS

The ground stations for the ATS-4 CTS will take the configuration shown in Figure 17-3. Signals will be received via a standard receiver system, and synchronization will be accomplished on either the 400- or 4000-bps bit stream. The signal will then be fed to a programmable decommutator which will decommutate the incoming data and provide the appropriate displays and output data. The program which the "decom" operates upon will be one which is essentially the inverse of the particular spacecraft program which is being executed.

The decom also provides data to a small command computer. This computer will allow spacecraft commands to be entered either manually or via a command tape. A command verification mode is also available whereby the execution of a spacecraft command can be verified (via the telemetry) prior to issuing the next command.

An additional mode of the decom computer will be the processing of incoming data to remove redundant information.

In actual operation, the decom and computer system (area within dotted lines) may be one unit of a type which is presently commercially available.

Table 17-2

Interface Requirements

Input voltage +24 to +28 vdc $\pm$ 2%		
Command 4 watts	15 lb	8 x 6 x 13 (4/4) Redundant
Telemetry 6 watts	35 lb	Two 8 x 6 x 13 (4/4) Redundant
<u>Telemetry Interface</u>		
A-to-D convertor will digitize to 8-bit accuracy.		
(Resolution: 1 part in 256)		
Analog inputs to the A-D will range from 0 to +5 vdc.		
Digital inputs to the system will be at the following levels:		
$0.0 \pm 0.5 \text{ v for "0"}$ $\left. \begin{array}{l} 0.25 \\ 5.0 \end{array} \right\} \pm 5.0 \text{ v for "1"}$		
<u>Command Interface</u>		
<u>Matrix</u> current pulses to drive 12-v spacecraft relays		
(pulse duration approximately 50 ms.)		
<u>Command Words</u>		
$0.0 \pm 0.5 \text{ v for "0"}$		
$5.0 \text{ v} \pm 0.5 \text{ for "1"}$		
Maximum load impedance of any user > 20 k		

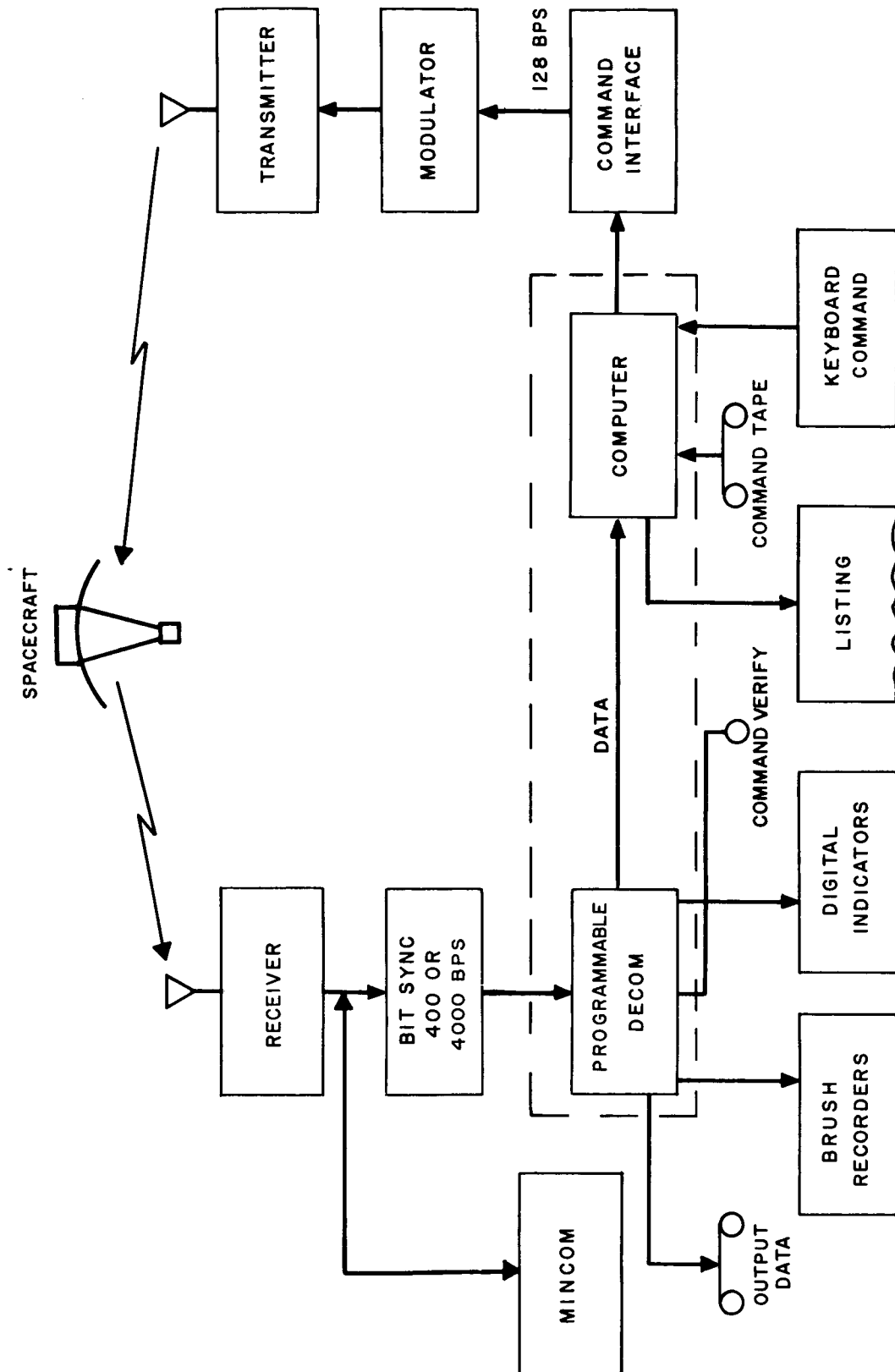


Figure 17-3. Ground station.

## SECTION 18

### TM, COMMAND AND GROUND SUPPORT

#### SUMMARY

In the effort to determine the most effective tracking, telemetry, and command support of ATS-4, and as a result set limits on the associated spacecraft equipment, the following project requirements were applied to the study considerations:

Tracking coverage is necessary in the transfer orbit to determine spacecraft position, velocity, and attitude as a function of time. These data are required to predict and control the spacecraft to the required apogee firing attitude and to predict the firing time and fire the apogee motor. Tracking in this sense includes polarization-angle tracking to enable calculation of spacecraft attitude.

Tracking coverage is necessary in synchronous orbits to determine spacecraft position, velocity, and attitude. These data are required to determine orbit ellipticity and inclination.

Telemetry and command coverage are required during the transfer orbit and thereafter.

#### ORBIT COVERAGE BY GROUND FACILITIES

The tracking and data-acquisition capabilities of Cape Kennedy and of down-range stations are required in conjunction with ground stations managed by Goddard Space Flight Center (GSFC) to provide sufficient coverage for the ATS-4 satellite. Figure 18-1 is included to show the significant events of the proposed ascent trajectory and illustrate coverage by the ground stations.

## DATA ACQUISITION AND COMMAND

Data acquisition and command is discussed in three phases, covering three distinct sections of the launch trajectory and orbit.

1. Launch-to-injection into circular parking orbit
2. Second burn and through reorientation of the Centaur
3. After reorientation

### PHASE 1. LAUNCH-TO-INJECTION INTO CIRCULAR PARKING ORBIT

This phase includes lift-off and point 1 in Figure 18-1. Point 1 marks the location of Atlas burnout, shroud separation and Centaur first ignition.

Tracking data will be available via the C-band Radar Systems located at Cape Kennedy and down range.

Vehicle telemetry will be available via the vehicle telemetry system. This is a pulse-amplitude-modulation/frequency-modulation/frequency-modulation subsystem using IRIG frequency channels 1 through 18 with an effective radiated power of approximately 5 watts in the frequency band of 225 to 260 MHz.

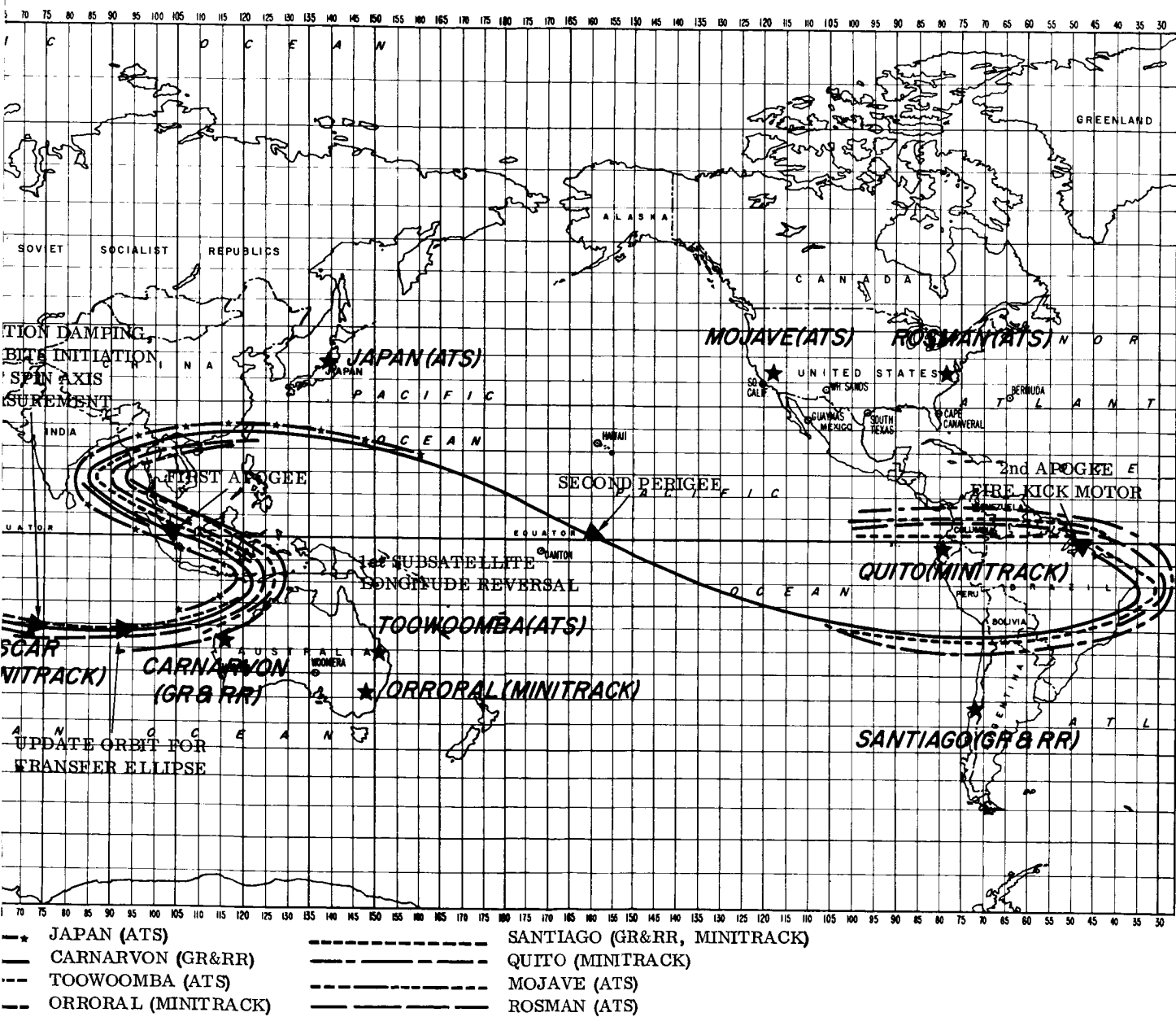
Spacecraft data during this phase could be made available through the Fort Myers GSFC ground station, dependent upon choice of redundancy for spacecraft sources. Commands are generally available only to the Range Safety Officer.

### PHASE 2. SECOND BURN THROUGH REORIENTATION OF THE CENTAUR

This phase covers points 2 (termination of first Centaur burn, injection into circular parking orbit, initiation of coast phase), 3 and 4 (coast phase), 5 (initiation of Centaur second burn and plane change), and 6 (completion of Centaur second burn, transfer orbit established and reorientation of vehicle through 175 degrees of the pitch axis).

If the decision is made to employ a ship for this phase, several methods exist by which spacecraft data could be acquired. One method would be to





SITUATION OF SIGNAL AT ABOVE 6° ELEVATION

Figure 18-1. Station acquisition at above 6° elevation.

couple selected spacecraft data with the vehicle telemetry; another method would use an existing Minitrack VHF transmitter which contains a modulator (see Phase 3 below for transmitter description). Acquisition of spacecraft data via the present vehicle telemetry system is not considered further, since space telemetry in the 225- to 260-MHz band is supposedly to cease operation prior to ATS-4 launch. It is very likely, however, that vehicle telemetry in this band will be moved to the S-band frequency (2200 to 2300 MHz). Generally, tracking and telemetry data are acquired from the vehicle for a very short period during the trajectory; therefore, relatively few interference problems should be encountered.

### PHASE 3. AFTER REORIENTATION

The S-band frequencies between 1750 and 1850 MHz for ground-to-spacecraft and between 2200 and 2300 MHz for spacecraft-to-ground transmission will be used for this program in conjunction with the transponder developed for unified operation with Goddard Range and Range Rate System (GR&RR) for command reception, telemetry transmission, and tracking data (GR&RR technique) retransmission. A new transponder antenna will be required, providing linear polarization and wider beamwidth than is available from the present transponder antenna design. A unified S-band (tracking, telemetry, and command) transponder can be built using present technology (4-watt phase-modulated output power) with a discriminator type of demodulator for command detection. It is anticipated that this transponder will weigh 10 pounds and require 38 watts while transmitting and 6 watts while receiving with dual command receivers for increased reliability.

The present Applications Technological Satellite Program uses VHF command in the 148- to 154-MHz band and telemetry in the 135.9- to 138-MHz band while utilizing a specially developed range and range-rate system (similar to the GR&RR technique) at the communication frequencies of 6 GHz ground-to-spacecraft and 4 GHz spacecraft-to-ground. The logic for deviating from these frequencies is:

There are more than ten spacecraft on the present ATS-B spacecraft command frequency and more than 30 spacecraft using the 136- to 138-MHz spacecraft telemetry band. The STADAN loading study for the future shows an increase over this number. In addition, the VHF telemetry band channelization is based upon a 30-KHz total-data bandwidth. This generally is not the best selection for wideband data such as television, which may be desirable during the 30-foot parabolic-antenna deployment.

Figure 18-1 shows that the GR&RR equipped stations (Madagascar, Carnarvon, Santiago, and Rosman) have more total orbital coverage than the present ATS-equipped stations. Quito would be available for telemetry reception dependent on spacecraft data-acquisition schedules and priorities by 1970. It is also anticipated that the remaining dish sites will have S-band capability during this time frame.

A lightweight Minitrack transmitter can be added as a backup system to provide Minitrack data from Johannesburg, Madagascar, Orroral, Santiago, and Lima during the transfer orbit. A small transmitter can be supplied which weighs less than one pound and has a volume of 10 cubic inches with a phase-modulated output of 2 watts at 136 MHz and consumes 6 watts of DC power. The phase-modulated output of the Minitrack transmitter can provide backup for lower telemetry data rates of 400 bits per second even when the satellite reaches synchronous orbit.

Because of the above considerations and the known performance of several other programs which have successfully communicated with synchronous-type spacecraft, all problems associated with ground support, telemetry, command, range, and range-rate measurements are considered solvable. With the high transmitter power available at each ground station, good signal strength is available at the spacecraft. Thus no major problems are anticipated in the command link. For telemetering data to the ground, for range and range-rate measurements, and for polarization angle measurements, a very careful tradeoff of the factors which effect the link signal-to-noise ratio must be made to arrive at the approach selected for the final system.

## SECTION 19

### ORBIT DETERMINATION

The Cowell Orbit Determination System will be used for the ATS-4 program. This system accounts for the following perturbations affecting the orbit:

Zonal harmonics  
Lower-order tesseral harmonics  
Higher-order tesseral harmonics  
Lunar gravitation  
Solar gravitation  
Solar radiation  
Atmospheric drag

During the transfer orbit the following stations will track the satellite and obtain tracking data as indicated:

Rosman	(Range and range rate)
Santiago	(Range and range rate)
Carnarvon	(Range and range rate)
Madagascar	(Range and range rate)
Minitrack network	(Direction cosines)
Stadan 40-foot and 85-foot paraboloids	(X, Y angle data)

During the near-synchronous and synchronous orbits, primary tracking will be by range and range rate from Rosman and Santiago.

Approximately three hours after lift-off, sufficient tracking data will have accumulated to determine the orbit. The output of the orbit determination program will be position and velocity of the satellite as functions of time.

Approximately two hours after each maneuver, sufficient tracking data will have accumulated to redetermine the orbit. If due to the temperature rise resulting from the firing of the apogee motor, the range and range rate transponder cannot be turned on until the temperature has fallen to a safe level, then this delay must be added to the two hour estimate for orbit redetermination.

#### ATTITUDE DETERMINATION

Attitude determination for the ATS-4 satellite will be performed by a program almost identical with that used in the ATS-B program.\*

During the transfer orbit, the sun-sensor data and Polang data will be used for attitude determination. Approximately 4-1/2 to 5 hours after lift-off, sufficient data will have accumulated to permit determination of the satellite attitude to an accuracy of 1 to 2 degrees.

During the synchronous orbit, if the attitude is redetermined it will require between 12 and 24 hours of data to obtain an accuracy of between 1 and 2 degrees. The output of the attitude determination program will be the right ascension and the declination of the satellite spin axis.

#### MANEUVER CONTROL

The same referenced document describes in detail the programs and methods used to control and perform the following functions:

Fire the apogee motor

Reorient the satellite

---

\* "ATS-B Maneuver and Control Program Documentation," August 1966.

Remove orbit inclination

Remove orbit eccentricity

Change drift rate

Calibrate the peroxide fuel system

The programs are also designed to evaluate each maneuver and to determine the accuracy with which target conditions are met.

## SECTION 20

### ATS-4 EXPERIMENTS

#### A. COMMUNICATIONS EXPERIMENTS AND DEMONSTRATIONS CONSIDERATIONS

##### INTRODUCTION

This section is both an outline of specific demonstration-type communications experiments to be considered for the ATS-4 program and a survey of potential applications of ATS-4 high-gain spacecraft antenna technology. Under the first heading, such systems as television relay to small ground terminals, multiple-access "man-pack" satellite communications, experimental weather forecast/facsimile broadcast services, conventional and spread-spectrum aircraft-satellite communications, and satellite-satellite data acquisition links have been analyzed. Under the second heading, certain advanced systems such as TV and FM direct broadcast, libration point communications to the hidden side of the moon, and deep space applications of ATS-4 large aperture antenna technology have been looked at briefly to determine channel capacities, power requirements, and other link parameters.

In this study, ATS-4 communications frequency assignments of 401 MHz (up-link) and 466 MHz (down-link) at UHF and 8.0 GHz (up-link) and 7.3 GHz (down-link) at X-band have been made. This choice fairly well encompasses the range of frequencies at which it is technically feasible to operate a large aperture, gravity-gradient stabilized parabolic reflector in synchronous orbit. Below UHF, apparent antenna gain (assuming constant radiation efficiency) falls off rapidly to the point where the large dish has no advantage over smaller, cheaper, and simpler structures. Above X-band, the surface tolerances attainable with a large light-weight structure in a thermal environment must be expected to degrade the radiation efficiency of the antenna to the point where smaller and highly rigid structures would be more effective.

Thus, although future large aperture antenna missions may involve operating frequencies other than those considered here (e.g. Apollo S-band relay), the present choice covers frequencies below and above those at which such missions are likely, and hence indicates upper and lower bounds on antenna gains, power requirements, channel capacities, and other link parameters.

##### ANTENNA AND TRANSPONDER CHARACTERISTICS AND FUNDAMENTAL LINK PARAMETERS

Assuming nominal deployment of the antenna and successful three-axis stabilization of the ATS-4 spacecraft, the electrical characteristics of the

large aperture parabolic reflector can be computed from standard formulas (Reference 1)\* and are summarized in Table 20-1. The numbers given, particularly antenna gains and beamwidths at X-band, are indicative of what can be achieved with a 30-foot dish in orbit and do not necessarily reflect eventual ATS-4 antenna design objectives, which will be compromised somewhat by the multiple mission nature of the program.

Table 20-1

Electrical Characteristics of ATS-4 Large Aperture Antenna

Antenna Diameter	Radiation Efficiency	Operating Frequency (MHz)	Apparent Gain (db)	3 db Beamwidth (degrees)
30 feet	50 percent (assumed)	401	28.7	5.6
		466	30.0	4.8
		7.3	53.9	0.31
		8.0	54.7	0.28

At a synchronous orbit altitude of  $36.3 \times 10^3$  km and a minimum earth elevation angle of 5 degrees, the maximum earth-spacecraft slant range is  $41.1 \times 10^3$  km. The resulting maximum free space losses at the several operating frequencies are given in Table 20-2, together with approximate diameters of main-beam earth coverage at the sub-satellite point, computed from the 3-db beamwidths of Table 20-1.

If the antenna is grossly defocused at UHF, global coverage could be achieved at a cost of about 10 db in apparent antenna gain. For world-wide data acquisition systems this type of sub-optimum operation would have certain advantages. However, since beam-steering is available to center the main-lobe of the undefocused beam anywhere on the surface of the earth, defocusing with its concomitant penalty of 10 db in system channel capacity would not appear to have any particular merit in an assessment of ATS-4 UHF capabilities. Therefore, defocused UHF operation will not be considered further in this study, except to note its impact on specific systems.

All ATS-4 communications operations considered here presuppose inclusion in the spacecraft of a frequency translating transponder. Independent UHF

---

\* Unless otherwise noted, all numbers quoted in this section have their source in this reference.

and X-band transponder subsystems have been proposed, and are discussed in Section 12 of this report. The transponders proposed would be extremely versatile units, capable of either linear or hard-limiting operation to accommodate a large variety of communications signals.

Table 20-2\*

Spacecraft-to-earth Path Losses and Approximate Earth Coverages

Operating Frequency	Free Space Loss (db)	Diameter of Earth Coverage, Sub-satellite Point (km)
401 MHz	-176.9	3520
466 MHz	-178.2	3040
7.3 GHz	-202.1	192
8.0 GHz	-202.9	160

Table 20-3 below summarizes assumed transponder characteristics, based on the detailed descriptions given in Section 12.

Table 20-3

Summary of Assumed Transponder Characteristics

Communications Subsystem	Receive Frequency	Transmit Frequency (MHz)	3-db Bandwidth (MHz)	Receiver Noise Figure (db)	Maximum CW Power Output (watts)
UHF	401 MHz	466	10	3	40
X-band	8.0 GHz	7.3	40	7	24

The various antenna, transponder, and link parameters presented in Tables 20-1 through 20-3 define the ATS-4 communications subsystems completely. The next step in this study is to consider specific missions.

---

\* A comparison of Tables 20-1 and 20-2 indicates that at all frequencies, the antenna gain and free space loss sum to -158.2 db, a constant of the system. This fact is important in considering links to an isotropic or fixed gain antenna.

## ATS-4 MISSION OBJECTIVES INVOLVING SMALL (MOBILE) TERMINALS

Preliminary ATS-4 mission objectives call for the demonstration of spacecraft stabilization techniques in a series of experiments. These experiments will be performed in conjunction with the large aperture spacecraft antenna system, providing communications, position determination, data acquisition, and control functions for small (mobile) terminal applications. A number of such demonstration-type experiments have been considered for the program and are discussed in the following pages, grouped according to type of operation under one of six classifications:

1. Satellite TV Relay
2. Narrowband satellite broadcast services
3. Man-pack type multiple-access communications
4. Air-traffic communications and control
5. Satellite data acquisition
6. Satellite position determination.

### SATELLITE TV RELAY

#### General

For purposes of classification, TV transmission systems involving communications satellite relay may be divided into two categories: those serving home viewers indirectly (through a central signal redistribution scheme) and those serving home viewers directly (direct broadcast TV). Up to the present, of course, all systems have been of the former type because of the severely limited effective radiated power (erp) available with both subsynchronous satellites (Telstar and Relay) and synchronous satellites (Syncom and Early Bird). In every case both sensitive (high gain/low noise) ground receiving facilities and the use of wideband frequency modulation (trading bandwidth for signal-to-noise ratio) have been required for satisfactory video performance on the critical satellite-to-ground down-link.

The ATS-4 large aperture antenna in conjunction with the proposed UHF and X-band communications subsystems will develop erps several orders of magnitude greater than those achieved in any previous satellite relay system. It is therefore of interest to investigate the extent to which this capability can be

used to provide TV transmission to small ground terminals including, if possible, direct broadcast to the home.

### System Configuration and Applicable Standards

Four system configurations have been chosen for study and are listed in Table 20-4.

Table 20-4

#### Summary of Systems Studied

System	General Description
1	UHF direct-broadcast to home receivers using conventional vestigial sideband amplitude modulation (VSB-AM)
2	UHF relay to small community type central receivers using VSB-AM
3	UHF relay to central receivers using frequency modulation
4	X-band relay to central receivers using frequency modulation

System 1, which is included mainly for purposes of completeness, has been considered previously in some detail by Gould (Reference 2), who termed it a "Spacious Fantasy". System 2 may be viewed as a space application of the well-developed technology of UHF line-of-sight TV relay (Reference 3). Systems 3 and 4, although similar in concept to previous satellite TV relay operations, clearly reflect the advantages of ATS-4 erps in terms of enormously reduced ground receiving facility complexity and cost.

Unfortunately, a good deal of subjectivity exists in most discussions of video picture quality. Even in situations where performance is limited only by additive white gaussian receiver thermal noise, there is no universally accepted measure of acceptable quality. For purposes of this study, it will be both convenient and sufficient to avoid the whole issue of picture quality and performance indices by using the CCIR Standards for international microwave radio-relay of television signals in discussing Systems 2, 3, and 4, and downgrading these standards in arbitrary 6 db in discussing System 1. Detailed explanations of

CCIR TV noise measurement procedures and terminology are given in Reference 4, which deals mainly with European 405, 625, and 819 line systems, and treats the U.S. 525 line system only lightly. The several performance parameters used in the present analyses have been taken directly from References 4 and 5, and are summarized in Table 20-5.

Table 20-5

Summary of TV Parameters and Design Objectives

TV System	Baseband Limit	Design Objective Weighted Signal/Noise Ratio		Noise Weighting Factor	
525 line	4 MHz	46 db	52 db	6.1 db	10.2 db
Scan, black and white		(system 1)	(systems 2, 3 & 4)	(white noise)	(triangular noise)

The use of the parameters in Table 20-5 is best explained by example. However, for Systems 1 and 2 (VSB-AM) the weighted post-detection peak signal/rms noise ratio is computed by adding the weighting factor for white noise to the predetection peak signal/rms noise ratio, measured in a band of 4 MHz. Second detector losses are ignored. For Systems 3 and 4 (FM), the weighted post-detection peak signal/rms noise ratio is computed by adding the weighting factor for triangular noise to the peak signal/rms noise after the frequency discriminator, again measured in a band of 4 MHz.

Analysis of each system considered is simplified by ignoring the aural subcarrier. Assuming the usual intercarrier sound system, this simplification can affect the analysis of Systems 1 and 2 by at most 3 db (Reference 2) and probably much less; Systems 3 and 4 would be affected by only a fraction of a db in the worst case, although aural-video intermodulation due to phase nonlinearities would be a potential problem in these wideband FM systems (Reference 8).

Analysis of System 1

The rationale for running through the numbers for UHF direct broadcast TV is that despite the fact that design objective performance turns out to be many decibels away from what can be realized using the present ATS-4 system, the concept remains of considerable interest for future high-power satellite missions. The ATS-4 down-link frequency of 466 MHz is adjacent to a large block of sparsely populated FCC UHF 6-MHz VSB-AM TV allocations, running from 470 MHz (channel 14) up to 890 MHz (channel 83). At the present time,

some of these channels are assigned on an area basis to commercial and educational TV, and a few are used for TV radio-relay to outlying areas. It seems probable that any future direct broadcast TV system would be assigned to operate in one of these many UHF channels. Therefore, a look at the numbers for the ATS-4 system working directly into a typical UHF home receiver is of value in assessing spacecraft power and antenna requirements for such advanced missions.

To simplify the analysis it is assumed that the down-link limits the system. Therefore, to complete the analysis it is necessary only to specify the parameters of the postulated typical home receiver. An overall noise figure of 12 db has been chosen with a receiving antenna gain of 15 db, corresponding to a superior UHF array. By applying these values to the information in Tables 20-1 through 20-5, the calculation is summarized in Table 20-6.

Table 20-6

Link Calculation for System 1

Parameter	Link Calculation
Satellite xmit power (40 watts)	+ 16.0 dbw
Xmit losses	- 1.0 db
Xmit antenna gain	+ 30.0 db
Erp	+ 45.0 dbw
Free space loss	-178.2 db
Receive antenna gain (superior UHF array)	+ 15.0 db
C, received signal power	-118.2 dbw
$\eta$ , receiver noise density (12 db NF, including losses)	-192.6 dbw/Hz
$C/\eta$ , down-link channel capacity (see Appendix I)	+ 74.4 db-Hz
$B_i$ intrinsic bandwidth (4 MHz)	+ 66.0 db-Hz
$C/\eta B_i$ , predetection signal/noise ratio	+ 8.4 db
White noise weighting factor	+ 6.1 db
Weighted postdetection signal/noise ratio	+ 14.5 db
System design objective	+ 46.0 db
Difference to be made up	- 31.5 db

The calculation in Table 20-6 shows that System 1 falls more than 30 db short of meeting its design objective. Therefore, increasing the ATS-4 UHF transponder power by a factor of a thousand to 40 kw would make direct-broadcast to the home technically feasible. This figure compares favorably with the results of Gould's analysis (Reference 2).

As a check on the above calculations, the direct-broadcast TV problem can be observed from a somewhat different point of view. Instead of postulating home receiver characteristics and computing output signal/noise ratios, the field strength developed by the ATS-4 system at 466 MHz has been investigated and compared with the field strengths recommended for various classes of TV service by the FCC and the Television Allocations Study Organization (TASO). These recommendations are given in Reference 6 and are summarized in Table 20-7.

Table 20-7

Summary of Recommended UHF TV Field Strengths

Organization	Grade of Service	Recommended Field Strength for Channels 14-83	
		$\mu\text{v/m}$	dbu
FCC	Principal City	10,000	80
	Grade A	5,000	74
	Grade B	1,600	64
TASO	Primary	7,500	75
	Secondary	630	56
	Fringe	180	45

The relationships between field intensities in  $\mu\text{v/m}$ , dbu, and synchronous satellite erp are discussed in Appendix II. The proposed ATS-4 UHF subsystem can develop a maximum field strength of  $25\mu\text{v/m}$  or +28 dbu, numbers far below those specified for minimum service at channel 14. Increasing the erp by 31.5 db (RF levels around 40 kw) would raise the field intensity at the ground to about  $1,000\mu\text{v/m}$  or +60 dbu. This would be equivalent to strong secondary reception in the TASO recommendations.

Analysis of System 2

System 2 is a space application of the well-developed technology of VSB-AM UHF radio-relay of TV signals. The only differences in the analysis of this system and System 1 are the ground receiving system parameters to be assumed and the performance design objective. For a community-type central receiving system, it is reasonable to postulate an overall noise temperature of  $600^\circ\text{K}$  and an antenna gain of 25 db, corresponding to an elaborate UHF array or a 15-foot parabolic dish. The calculation is summarized in Table 20-8.

Table 20-8

## Link Calculation for System 2

Parameter	Link Calculation
Satellite xmit power (40 watts)	+ 16.0 dbw
Xmit losses	- 1.0 db
Xmit antenna gain	+ 30.0 db
Erp	+ 45.0 db
Free space loss	-178.2 db
Receive antenna gain (elaborate array or 15' dish)	+ 25.0 db
C, received signal power	-108.2 dbw
$\eta$ , receiver noise density ( $T = 600^\circ$ )	-200.8 dbw/Hz
$C/\eta$ , down-link channel capacity	+ 92.6 db-Hz
$B_i$ , intrinsic bandwidth (4 MHz)	+ 66.0 db-Hz
$C/\eta B_i$ , predetection signal/noise ratio	+ 26.6 db
White noise weighting factor	+ 6.1 db
Weighted postdetection signal/noise ratio	+ 32.7 db
System design objective	+ 52.0 db
Difference to be made up	19.3 db

As was the case with System 1, System 2, falls far short of meeting design objectives. The difference of approximately 20 db suggests that by accepting a sub-CCIR picture quality and by using somewhat greater satellite power, System 2 would be well within the realm of technical feasibility for future missions. A System 2 demonstration with proposed ATS-4 capabilities, however, would be at best a highly marginal and questionable operation. There does not seem to be any possibility of increasing UHF receiving system sensitivity much beyond the  $600^\circ$  K system temperature and the 25-db gain antenna postulated. For this reason, a more efficient down-link modulation technique is necessary to achieve CCIR quality at UHF. This technique, discussed in the following paragraphs, involves trading bandwidth for signal/noise ratio.

### Analysis of System 3

The frequency-modulation TV relay system discussed here (and later in relationship to System 4) is one which has been optimized (Reference 7) to yield CCIR quality 4 db above FM threshold. The optimization procedure may be described as a constraint that the postdetection signal/noise correspond to CCIR quality at the same time the predetection carrier/noise ratio is +14 db, measured in a noise bandwidth given by Carson's rule (Reference 13). A cubic equation is involved, whose solution is tedious and best accomplished by means of a digital computer. Free use is made of the computer print-out of Reference 7 in the link

calculations of Table 20-9. The ground station parameters are the same as those for System 2.

Table 20-9

### Analysis of System 3

Parameter	Link Calculation
Design objective postdetection weighted signal/noise ratio	+ 52.0 db
Triangular noise weighting factor	+ 10.2 db
Resulting unweighted postdetection signal/noise ratio	+ 41.8 db
Required intrinsic carrier/noise ratio $C/\eta B_i$ (from Reference 7)	+ 22.7 db
$B_i$ , intrinsic system bandwidth (4 MHz)	+ 66.0 db-Hz
Required channel-capacity, $C/\eta$	+ 88.7 db-Hz
Available channel-capacity, $C/\eta$ (from Table 20-8)	+ 92.6 db-Hz
Overall system performance margin (in excess of postulated 4-db threshold margin)	+ 4.1 db
Resulting Carson's rule RF bandwidth	28.8 MHz

The 4.1-db margin in the calculation given in Table 20-9 means that by degrading the down-link channel capacity by 4.1 db (by reducing satellite erp, using a noisier receiver, or using a simpler antenna) the system will yield CCIR quality and still have 4-db fade margin before FM threshold. Comparing System 3 to Systems 1 and 2, the advantages of wideband FM transmission are obvious. A serious disadvantage of the system, however, is the large RF bandwidth required (almost 30 MHz), equivalent to five FCC UHF TV channels stacked side by side. This precludes, apparently, any possibility of using System 3 in an ATS-4 demonstration, although operational systems using wideband FM in the upper end of the allocated band (near channel 83) might be practical at some future time. For purposes of ATS-4 demonstrations, it is necessary to examine System 4.

### Analysis of System 4

System 4 is of particular interest because of the relatively minimal microwave ground receiving facility required. Postulated are a 2-foot parabolic dish and a  $1000^{\circ}\text{K}$  system temperature. Drawing on Tables 20-1 through 20-9, the analysis is summarized in Table 20-10.

Table 20-10

## Analysis of System 4

Parameter	Link Calculations
Satellite xmit power (24 watts)	+ 13.8 dbw
Xmit losses	- 1.0 db
Xmit antenna gain	+ 53.9 db
Erp	+ 66.7 dbw
Free space loss	+202.1 db
Receive antenna gain (2-foot dish)	+ 30.4 db
C, received signal power	-105.0 dbw
$\eta$ , receiver noise density	-198.6 dbw/Hz
C/ $\eta$ , down-link channel capacity	+ 93.6 dbw-Hz
Required channel capacity C/ $\eta$ (from Table 20-9)	+ 88.7 db-Hz
Performance margin (in excess of postulated 4-db threshold margin)	+ 4.9 db
Resulting RF Carson's rule bandwidth	28.8 MHz

As was the case with System 3, an adequate performance margin exists. System 4 shows how the availability of a high gain antenna in synchronous orbit can enormously simplify ground receiving facility requirements. By way of comparison, early microwave satellite TV relay systems using similar FM parameters depended on sites like Andover with about 58 db of gain (at 4.1 GHz) and a system temperature around 50° K (Reference 8) to achieve high-quality video performance. The availability of a spectrum allocation for a System 4 ATS-4 demonstration-experiment seems likely; therefore, such an operation might well be considered for inclusion in the ATS-4 program. One serious disadvantage of System 4 which must be stressed, however, is the relatively small area which would be served; coverage would be limited to a 3-db diameter of about 200 km at the subsatellite point (Table 20-2). This would serve any single city, but would make simultaneous service to, say, New York and Washington, D. C. something of a problem.

## FM BROADCAST SERVICE

It is readily demonstrated by resorting to link calculations that the proposed ATS-4 UHF subsystem does not develop enough erp at 466 MHz to make commercial quality FM broadcast to home receivers (using inexpensive converters) technically feasible. As noted in the discussion of direct broadcast TV, ATS-4 can be expected to develop maximum field strengths of some 25  $\mu$ v/m

or +28 dbu. FCC (Reference 3) recommends a minimum field strength of +34 dbu for FM broadcast in the commercial band (88 to 108 MHz). Extrapolating this figure to 466 MHz by the square of the frequency ratio (reflecting the smaller effective area of a simple dipole receiving antenna at the high frequency and ignoring the increased line losses and converter noise figures) suggests a minimum required field strength of some +50 dbu at ATS-4 frequencies, some 22 db greater than that available. This deficit is not so great as to make commercial quality FM broadcast to high-gain/low-noise home receiving systems technically unfeasible, but it is certainly large enough to obviate service to the average home user. For quality service of the latter type, satellite RF levels in the kilowatt range would be required, working into an ATS-4 type antenna.

Nevertheless, noncommercial-type FM broadcast services at UHF remain of considerable interest for potential industrial, government, and military users who could afford a somewhat more sensitive receiving facility than the home user.

Possible applications of an ATS-4 type UHF FM broadcast system include 24-hour central weather reporting and subscription facsimile services. The latent demand for the latter type of service has been pointed out by A. G. Cooley (Reference 9).

Design objectives for the FM broadcast system considered here are taken from applicable military standards for FM voice and facsimile broadcasting in the UHF band (Reference 10) rather than FCC standards because of the somewhat specialized nature of the proposed operation.

The information signal is assumed to be either 4-KHz speech or a 4-KHz voice frequency facsimile system. The facsimile system proposed would have typically a scan rate of 120 lines/minute, a scan width of 18 inches, with a resolution of 100 elements per inch. The keying frequency would then be given by

$$(2 \text{ lines/second}) (18 \text{ inches/line}) (100 \text{ elements/inch}) = 3.6 \text{ KHz}$$

and hence would effectively constitute a 4-KHz voice frequency signal.

Military design objectives for transmission of 4-KHz signals by FM in the UHF band are a signal-to-noise ratio of 47.8 db and a maximum RF bandwidth per emission of 40 KHz. The signal-to-noise ratio quoted is for transmission of a sinusoidal signal of the maximum amplitude consistent with system capacity and unweighted noise measured in a 4-KHz band. This is equivalent to +38 dba<sub>0</sub> (U.S. telephone terminology - FIA weighting at the zero-transmission point) and/or 25,000 picowatts (European telephone terminology - psophometric

weighting at the zero transmission point); for details, see References 10, 11, and 12.

The assumed ground facility has a gain of 15 db and a noise temperature of 1000°K. The calculation is summarized in Table 20-11.

Two formulas from FM theory are required to complete the analysis

Equation 1: Carson's rule  $B_{rf} = 2 (\Delta f + B_i)$  (Reference 13)

Equation 2: FM output signal/noise ratio  $= \frac{3}{2} \left( \frac{\Delta f}{B_i} \right)^2 \frac{C}{\eta B_i}$  (Reference 14).

Table 20-11

#### Analysis of UHF FM Broadcast Service

Parameter	Link Calculation
$B_i$ intrinsic bandwidth	4 KHz
$B_{rf}$ , Carson's rule bandwidth (Ref. 10)	40 KHz
$\Delta f$ , allowable peak deviation	16 KHz
$\Delta f/B_i$ , allowable index of modulation	4
Design objective output signal/noise ratio	47.8 db
$C/\eta$ , required channel capacity (solving Eq. 2)	+70.0 db
$C$ , received carrier power (Table 20-6)	-118.2 dbw
$\eta$ , receiver noise density	-198.6 dbw/Hz
$C/\eta$ available channel capacity	+80.4 db
Margin above performance objective	+10.4 db
Margin above 10-db FM threshold	+24.4 db

The analysis shows the proposed system to have a substantial margin over design objectives. The simplicity of the required ground receiving equipment would recommend this type of demonstration-experiment for inclusion in the ATS-4 program. The relatively broad earth coverage afforded by the 30-foot dish at 466 MHz (Table 20-2) is still another argument in favor of this system.

#### MULTIPLE-ACCESS "MAN-PACK" COMMUNICATIONS

Two "man-pack" multiple-access voice communications systems meeting military design objectives have been studied for possible experimental use with the ATS-4. Important characteristics of the two systems are summarized in Table 20-12.

Table 20-12

## Characteristics of "Man-pack" Systems

System	Multiplexing Technique	Number of Duplex Channels	Band of Operation	Modulation Technique
1	Frequency Division Multiplex (FDM)	10 (with companding)	UHF	SSB
2		10 (no companding)	X-band	FM

Both systems would require essentially linear transponders to avoid severe intermodulation effects (References 12 and 15); design objectives for both systems have been taken directly or extrapolated from Reference 10.

Analysis of System 1

Table 20-13 summarizes the analysis of System 1. A thorough discussion of the loading factors and peak factors used in computations for SSB-FDM systems is to be found in Reference 14. Syllabic speech companders are required in System 1 to bring performance up to the design objective. The conservative 16-db compression/expansion improvement assumed, as well as the multi-channel peak and loading factors for compandored channels, has its source in a paper by Rizzoni (Reference 16).

Without companders, the system would be many decibels short of the military design objective, but would still be a useful voice channel.

Frequency stability of the inserted carrier is an important consideration in the detection of SSB signals, and assuming a maximum allowable inaccuracy (in precision or stability) of several tens of hertz, the requirement would be an easily achieved part in  $10^{-7}$ .

The analysis for the up-link parallels that for the down-link and will not be given in detail. The essential result is that a single channel SSB transmitter, operating into the UHF array used in the down-link, would operate at a mean power of 2.5 watts and would require a peak rating of some 60 watts. This analysis assumed that all 10 duplex channels were on the air or in use at the same time, and the loading and peak factors used took into consideration the statistics of ordinary talkers. In a modest multiple-access operation of this type, the use of these statistics is probably pessimistic and leads to an over-

Table 20-13

## Analysis of System 1, Down-link

Parameter	Link Calculation
Design objective for overall system noise performance	+38 dba <sub>0</sub>
Equivalent TT/noise ratio, 4 KHz unweighted (Refs. 4 and 11)	+42.5 db
Down-link TT/noise objective, allowing 3 db for up-link noise and intermodulation effects	+45.5 db
Down-link TT/ $\eta$ design objective, assuming 16-db subjective companding improvement	+65.5 db-Hz
Peak satellite erp (3 db greater than CW erp of Table 20-1)	+48.0 dbw
Multichannel peak factor, 10 compandored channels	+12.3 db
Mean satellite erp, 10 compandored channels	+35.7 dbw
Loading factor, 10 compandored channels	+2.5 db
Satellite TT erp	+33.2 dbw
Free space loss	-178.2 db
Receiving antenna gain (UHF array)	+12.0 db
Received TT power	-133.0 dbw
$\eta$ , receiver noise density (1000°K)	-198.6 dbw/Hz
Available TT/ $\eta$ , down-link	+65.6 db-Hz
Margin over design objective	+0.1 db

designed system. At any rate, the present results indicate the general technical feasibility of a compandored UHF SSB-FDM "man-pack" multiple-access ATS-4 communications experiment.

### Analysis of System 2

For System 2, the assumed "man-pack" receiver parameters are a 2-foot dish and a noise temperature of  $1000^{\circ}\text{K}$ . As with System 1, the down-link is analyzed in detail and discussion of the up-link is limited to a statement of ground transmitter power requirements. A conservative 2-db backoff from the rated 24 watts of TWT output power is assumed, ensuring essentially linear amplification of the 20 (equal power) FM carriers, corresponding to 10 duplex FM channels (Reference 17).

Table 20-14

#### Analysis of System 2 (Down-Link)

Parameter	Link Calculation
Required $C/\eta$ per channel, assuming no up-link noise and intermodulation effects (from Table 20-11)	+70.0 db-Hz
Required $C/\eta$ per channel, allowing 3 db for up-link noise and intermodulation effects	+73.0 db-Hz
Available satellite erp (2 db back-off from figure of Table 20-10)	+64.7 dbw
Available satellite erp per channel (20 carriers)	+51.7 dbw
Free space loss	-202.1 db
Receive antenna gain (2-foot dish)	+30.4 db
C, received carrier power per channel	-120.0 dbw
$\eta$ , receiver noise density ( $1000^{\circ}\text{K}$ )	-198.6 dbw/Hz
Available $C/\eta$ , per down-link channel	+78.6 db-Hz
Margin over required $C/\eta$	5.6 db-Hz

Per channel, up-link CW power requirements, assuming no interference from other sources, would be roughly 1 watt, working into an on-beam 2-foot dish. Power control could be a consideration in system operation, for if one user were to operate so that his up-link transmission arrived at the satellite many decibels stronger than the FM carriers of the other users, potential "power-grabbing" would occur. For the relatively large number of simultaneous carriers considered, however, the problem should not be too serious.

The minimum RF bandwidth of an X-band multiple-carrier FM "man-pack" system would be 800 KHz, assuming 40 KHz per carrier (Reference 10). To reduce intermodulation effects, it would probably be worthwhile to use somewhat more spectrum spacing the carriers instead of separating them by 40 KHz. Babcock (Reference 18) has studied the spacing problem, and his "optimum" spacings to avoid intermodulation spectra lead to somewhat inefficient use of the spectrum. Doyle (Reference 15) concludes that elaborate spacing schemes are not worth the trouble they cause; thus, it may be argued that the most convenient and practical solution would be to assume 50-KHz carrier separations in keeping with FCC recommendations for fixed and mobile FM voice links (Reference 19).

The excellent technical quality attainable with relatively simple although admittedly specialized "man-pack" systems of the two types discussed here suggest that such an operation, at X-band or UHF, be considered as a demonstration-experiment in the ATS-4 program. It should be noted that the comments relative to weather broadcast and facsimile services earlier in this document apply to the "man-pack" systems discussed, as do the statements regarding earth coverage of the 30-foot dish (Table 20-2).

Figure 20-1 illustrates receive and transmit spectra for the two FDM "man-pack" systems presented in this portion of the study.

## AIR TRAFFIC COMMUNICATIONS AND CONTROL

The following discussion is not intended to be a comprehensive treatment of ATS-4 potentialities and capabilities for systems of air traffic communications and control. The field is so new, and the requirements and characteristics of future operational systems (including frequency assignments) so vaguely defined that a detailed analysis would be beyond the scope of this in-house study. Rather, the discussion is limited to a general statement of the background of aircraft-satellite communications, a comparison of ATS-B VHF Repeater and ATS-4 UHF channel capacities in the satellite-to-aircraft link, and to a brief analysis of a hypothetical S-band (1.7 GHz) link between an ATS-4 spacecraft and an in-flight airplane.

### Background

Early attempts at aircraft-satellite communications conducted jointly by Air Transport Association (ATA), Bendix, NASA-Hughes, and Pan American (subsequently termed the ATA tests) and reported in Reference 20 were successful in establishing the general feasibility of using a satellite relay for aircraft communications and control over remote areas. Teletype transmissions at rates up to 100 wpm were achieved on both the ground-satellite-aircraft up-link

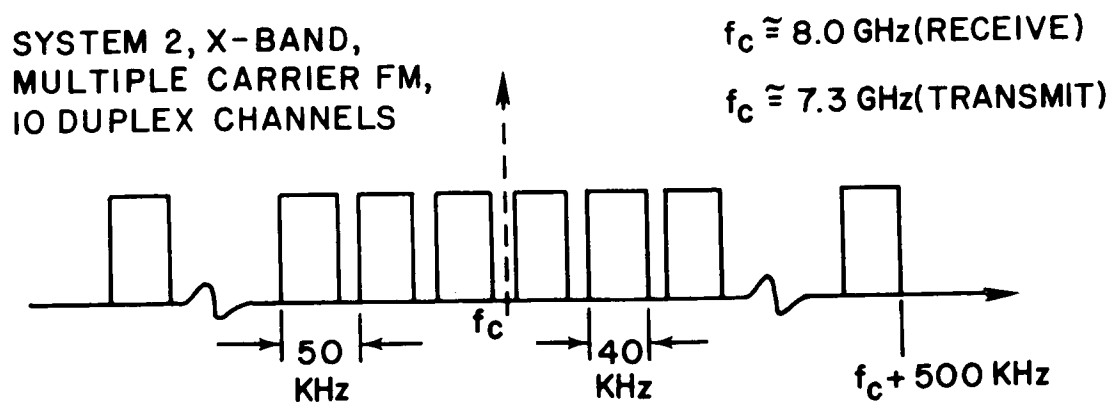
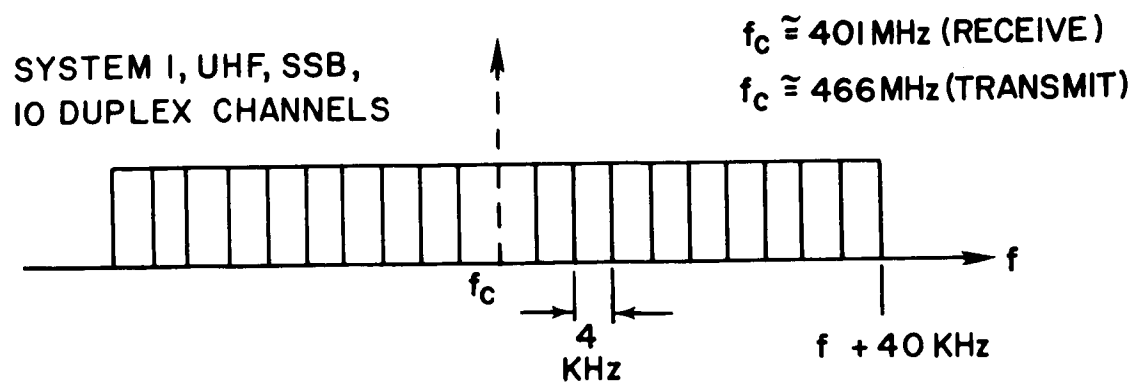


Figure 20-1. Receive and transmit spectra for FDM multiple-access communications, Systems 1 and 2

and the aircraft-satellite-ground down-link via a VHF telemetry channel of the Syncom II satellite. Performance was highly variable, but enough good copy was received in both modes of operation to encourage further interest in and development of aircraft-satellite communications technology. One such development, of course, is the VHF repeater which has been demonstrated in successful tests of the recently launched ATS-B spacecraft (Reference 21).

The communications package of the ATS-B VHF transponder has an overall bandwidth of some 100 KHz and develops an erp of +23.5 dbw as compared to an erp of only -3.5 dbw in the original Syncom II VHF system, affording a 27-db increase in the channel capacity of the critical satellite-aircraft link, and opening the way for FM voice communications and other wideband signaling techniques.

#### ATS-B at VHF Versus ATS-4 at UHF

ATS-B, with its phased-array antenna giving global coverage and developing +23.5 dbw of erp at 136 MHz, has a channel capacity of some +58 db-Hz in a typical link to an airborne receiver having a 3-db gain antenna, 3-db polarization loss, and a system temperature of 1000°K. Analyses in Reference 21 and preliminary experiments conducted by FAA, private industry, and the military indicate that this link (satellite-aircraft links are in general many decibels weaker than aircraft-satellite links) can support an "acceptable" 4-KHz voice channel using FM parameters close to those used in the systems detailed in Tables 20-11 and 20-13 of this study.

By way of comparison, ATS-4 with its +45 dbw of erp at 466 MHz in a similar link would have a channel capacity of about +66 db-Hz, somewhat fatter but still below that required to meet military design objectives for the FM voice link.

ATS-4 coverage at 466 MHz is somewhat short of global (without defocusing the beam), but studies (Reference 22) have shown that by positioning the spacecraft in equatorial orbit near 87 degrees W longitude and pointing the large aperture antenna at 54 degrees W longitude by 20 degrees N latitude, the main-beam would virtually blanket the North Atlantic, presumably a requirement for any future operational system in that part of the world.

Since ATS-4 UHF frequencies are not used for present air-traffic control and since future systems are unlikely to use these frequencies (Reference 23), the fact that ATS-4 is only at best some 8 db better than ATS-B in the critical satellite-aircraft link does not suggest a bright future for ATS-4 in the area of UHF air-traffic communications and control. Beam-defocusing, of course,

would produce world-wide coverage and reduce ATS-4 channel capacity to an aircraft below that of ATS-B.

#### S-band Aircraft-Satellite Communications with ATS-4

Much of the variability in performance in the ATA tests (Reference 20) was attributed to multipath propagation due to specular sea-water reflections. Even in the presence of large received signal-to-thermal-noise ratios, intersymbol interference and resulting teletype error rates were at times completely unacceptable. The severity of multipath interference in any satellite-aircraft link over water, and the validity of the geometrical model of Figure 20-2 (taken from Reference 24) have recently been confirmed in Air Force tests conducted by Lincoln Labs at M. I. T. (Reference 25). Further evidence of the impact of multipath on the VHF aircraft-satellite communications is anticipated in the results of present and future experiments with ATS-B.

To a large extent, the difficulty in overcoming multipath problems at VHF lies in the problem of designing an aircraft antenna that has a broad enough beam to ensure satellite coverage while at the same time providing discrimination against multipath signals. Steerable antennas at VHF, of course, are not practical for commercial aircraft applications. If one considers, however, S-band frequencies for the aircraft-satellite link, it is clear that steerable antennas become practical from the point of view of size. A 2- or 3-foot dish mounted in an aerodome built into the structure of the aircraft would provide considerable gain as compared to dipoles at S-band and would eliminate multipath problems due to its relatively narrow beam and low side-lobes.

Table 20-15 is a gross analysis of a hypothetical ATS-4 aircraft link at 1.7 GHz. One watt of satellite RF power, a 3-foot steerable parabolic dish mounted in the airplane, and an aircraft system receiving noise temperature of  $1000^{\circ}\text{K}$  are the basic assumptions. It is seen that ample channel capacity exists for supporting high quality FM voice communications. One serious disadvantage to the system as described is the relatively narrow beamwidth of the ATS-4 30-foot antenna at 1.7 GHz, corresponding to a coverage of some 1000 km at the subsatellite point. Any operational S-band satellite-aircraft system would probably work with a less directional spacecraft antenna, making up the difference by using increased RF power. The calculation does show, however, the technical feasibility of such a communications link.



Table 20-15

## Hypothetical ATS-4 Link to In-flight Aircraft at S-band

Parameter	Link Calculation
Satellite transmit power (1 watt)	+ 0.0 dbw
Satellite antenna gain (30-foot dish at 1.7 GHz)	+41.3 db
Satellite erp	+41.3 dbw
Nominal path loss	-189.1 db
Aerodome losses (assumed)	-3.0 db
Aircraft receive antenna gain (3-foot dish at 1.7 GHz)	+21.5 db
C, received signal power	-129.3 dbw
$\eta$ , receiver noise density (1000°K)	-198.6 dbw/Hz
C/ $\eta$ , S-band satellite-aircraft channel capacity	+69.3 db-Hz

## DATA ACQUISITION

The sensitive receiving capability of the proposed ATS-4 communications subsystems combined with the flexibility of a high-gain steerable antenna in geosynchronous orbit suggests several novel applications in the area of data acquisition. Three potential applications are discussed below: satellite-to-satellite relay of Interrogation, Recording, and Location System (IRLS) data from a Nimbus-type spacecraft to ATS-4, satellite-to-satellite relay of S-band video from a Nimbus-type spacecraft to ATS-4, and launch phase Apollo support S-band data links.

ATS-4 IRLS Applications

The IRLS experiment (Reference 26) is a proposed data collection operation in which many sensors monitoring oceanographic, geophysical, and meteorological conditions in remote areas around the world (unmanned sea buoys, platforms, or balloons) relay their data to a central point through a sub-synchronous satellite of the Nimbus series. The spacecraft would have a UHF transponder to collect signals at 401 MHz and relay them at 466 MHz to a central point via NASA Command and Data Acquisition stations located at Fairbanks, Alaska, and Rosman, North Carolina.

The pseudo-noise ranging technique to be used in the IRLS is not compatible with the concept of direct interrogation of platforms by a geosynchronous satellite, although enough channel capacity would exist to make some operations feasible. The propagation delays involved in such a link would produce time ambiguities which could not be resolved without major redesign of the IRLS. However, addition of a 401-MHz transmit capability to the Nimbus spacecraft would

enable ATS-4, as presently conceived, to monitor IRLS platforms indirectly, replacing the direct Nimbus-Rosman link with a Nimbus-ATS-4-Rosman link. This link would have the advantage of greatly increasing the percentage of time Nimbus would be available to interrogate platforms. The concept of using 401 MHz as both a receive and transmit frequency for Nimbus, while somewhat unusual, is technically feasible since all IRLS transmissions to and from Nimbus are in bursts, permitting time-division-multiplexing of spacecraft receive and transmit functions.

The nominal channel capacity of the platform-Nimbus up-link is given as 64.1 db-Hz (Reference 26). Using this as a design objective for the proposed Nimbus-ATS-4 link, the required Nimbus erp is computed in Table 20-16.

Table 20-16

Nimbus-ATS-4 IRLS Relay, Power Requirements

Parameter	Link Calculation
Design objective $C/\eta$ ratio	+64.1 db
$\eta$ , ATS-4 receiver noise density (600°K)	-200.8 dbw/Hz
Nominal Nimbus-ATS-4 path loss	-176.0 db
ATS-4 receive antenna gain	+28.7 db
Required Nimbus erp	+10.6 dbw

ATS-4 Nimbus S-band Video Link

The next system to be considered is hypothetical in that it assumes the existence of an ATS-4 wideband receiving capability at 1.7 GHz. This frequency was not included in those selected for the present study (Table 20-1); nevertheless it is of interest to assess the potential channel capacity of such a system. Present Nimbus operations involve transmission of reduced data rate recorded video signals to the Fairbanks and Rosman 85-foot receiving facilities at S-band (1.7 GHz). Satellite transmitter power is nominally 5 watts, and the nominal antenna gain is 3 db.

Following the line of reasoning used in the IRLS-ATS-4 application discussed above, Table 20-17 compares the channel capacity of the existing Nimbus-Rosman link with that attainable in a hypothetical Nimbus-ATS-4 S-band link. Beam steering of the large aperture antenna is assumed, keeping the subsynchronous satellite always in the main-beam of the ATS-4 receiving system.

Table 20-17

## Nimbus-ATS-4 versus Nimbus-Rosman S-band Channel Capacities

Parameter	Nimbus-Rosman	Nimbus-ATS-4
Link frequency	1.7 GHz	1.7 GHz
Nimbus erp	+10.0 dbw	+10.0 dbw
Free space loss	----- *	-189.1 db
Receive antenna gain	----- *	+41.3 db
C, received signal power (Reference 27)	-99.0 dbw (typical measured value)	-137.8 dbw
System noise temperature	250°K (typical)	+600°K
$\eta$ , receiver noise density	-204.6 dbw/Hz	-200.8 dbw/Hz
C/ $\eta$ , link channel capacity	+105.6 db-Hz	+63.0 db-Hz

\*Path loss and antenna gain are not indicated for the Nimbus-Rosman link because actual measured received signal strengths were available.

The enormous difference, some 43 db, reflects the higher gain, lower system temperatures, and shorter path length involved in the Nimbus-Rosman link. Nevertheless, the channel capacity to ATS-4 could support digital data rates of  $4 \times 10^5$  bps with error rates under  $10^{-3}$ , enough for non-real time transmissions. Real time video in such a link would require a high gain antenna on the Nimbus spacecraft or orders of magnitude greater RF power levels.

#### Apollo S-band Launch Phase Support

During the critical launch phase of the Apollo mission, the spacecraft will be stationed in a subsynchronous parking orbit for a sufficiently long time to make continuous communications a severe problem. An ATS-4 spacecraft could be of considerable value in supplementing the presently planned Apollo

communications network of ships, aircraft, and ground stations during launch phase. The following gross analysis indicates the technical feasibility of such an operation with an ATS-4 spacecraft equipped with a 2.3 GHz receive capability.

Table 20-18

Approximate Data Rate for Hypothetical Launch-phase  
Apollo-ATS-4 Data Relay Link

Parameter	Link Calculation
Frequency (Apollo unified S-band system)	2.3 GHz
Apollo spacecraft erp (assumed)	+12.0 dbw
Free space loss to ATS-4 (max.)	-193.0 db
ATS-4 receive antenna gain	+43.0 db
C, received signal power	-138.0 dbw
$\eta$ , receiver noise density (600°K)	-200.8 dbw/Hz
C/ $\eta$ , link channel capacity	+62.8 db-Hz
Energy per bit/ $\eta$ ratio for bit $P_e = 10^{-3}$	+6.5 db
Attainable Apollo ATS-4 data rate (56.3 db)	$4 \times 10^5$ bits/sec

## POSITION DETERMINATION

Consideration of potential ATS-4 applications in the area of position determination will be limited to a brief discussion of ATS-4 usage in the Omega Position Location Equipment (OPLE) experiment (Reference 28). The proposed OPLE system is a world-wide data collection operation which has a precision position location capability ( $\pm 3$ km) based on use of the Omega Navigation System recently developed by the U. S. Navy.

Involved are a large number of free-floating meteorological platforms and weather balloons, dispersed over the earth and synoptically monitored by a geo-synchronous satellite which relays collected data to NASA's Rosman receiving facility. The existing VLF Omega system would provide each platform (or balloon) with information as to its position. This information, together with real-time meteorological sensor data, would be transmitted upon interrogation to the monitoring satellite for relay to Rosman.

Two frequency configurations have been discussed, a preliminary system at VHF (149 MHz up / 136 MHz down) and an operational system at UHF (401 MHz up / 466 MHz down). This latter scheme is, of course, one

which has been selected for ATS-4 UHF operations, and hence it is clear that ATS-4 might serve as the spacecraft relay in an OPLE experiment.

Using platform and satellite parameters from Reference 28, Table 20-19 compares the up-link channel capacities of the OPLE UHF system as proposed and the OPLE system working with ATS-4.

Table 20-19

OPLE Up-link Comparison

Parameter	OPLE as Proposed	OPLE with ATS-4
Platform transmit power	+2.6 dbw	+2.6 dbw
Platform antenna gain	0.0 db	0.0 db
Path loss	-176.9 db	-176.9 db
Satellite antenna gain	+14.0 db	+28.7 db
Misc. losses	-2.0 db	-2.0 db
C, received signal power	-162.3 dbw	-147.6 dbw
Receiver noise temperature	500°K	600°K
$\eta$ , receiver noise density	-201.6 dbw/Hz	-200.8 dbw/Hz
$C/\eta$ , up-link channel capacity	+39.3 db-Hz	+53.2 db-Hz

The table shows that the OPLE system, working with ATS-4 at UHF, would have an up-link almost 14 db better than that discussed in Reference 28. This would mean that platform RF power, for example, could be reduced to the milliwatt region or, alternately much higher data rates could be used.

A requirement to have truly world-wide coverage, however, would entail defocussing of the ATS-4 beam, reducing the advantage to only 4 db. Nevertheless, it is clear that ATS-4 as proposed would be a more than suitable spacecraft for OPLE UHF experiments.

## SUMMARY

A relatively broad spectrum of ATS-4 applications, experiments, and demonstrations has been discussed in widely varying depth, all involving communications between the large aperture antenna in synchronous orbit and small, including mobile, terminals. A great many assumptions entered into the analysis of any single system, and it is felt that a detailed side-by-side tabulation of all systems considered, including identification of all assumptions, would be unwieldy and somewhat misleading. Nevertheless, it is

desirable to summarize the work in some concise way. Therefore Table 20-20 has been prepared, identifying the systems studied, noting the design objective source or reference system used, and indicating the results of the analysis in terms of performance margins, plus or minus, with respect to the design objective or the reference system.

Table 20-20

Summary of Systems Considered - ATS-4 Working with Small Terminals

ATS-4 Application	Design Objective Source or Reference System	Margin with Respect to Design Objective or Reference System
UHF direct broadcast home TV	CCIR (downgraded) and/or FCC-TASO flux density recommendations	-31.5 db
UHF TV radio relay	CCIR	-19.3 db*
UHF TV radio relay using wideband FM	CCIR	+4.1 db*
X-band TV radio relay (wideband FM)	CCIR	+4.9 db
UHF FM direct home broadcast	FCC flux density recommendations	-22.0 db*
UHF FM broadcast services (weather and/or facsimile)	Applicable military standards	+10.4 db*
UHF SSB "man-pack" using compandors	Applicable military standards	+0.1 db*
X-band FM "man-pack"	Applicable military standards	+5.6 db
UHF air traffic communications and control	ATS-B VHF repeater link	+8.0 db*

\* For defocussed operation at UHF, change by 10 db.

Table 20-20 (Concluded)

## Summary of Systems Considered - ATS-4 Working with Small Terminals

ATS-4 Application	Design Objective Source or Reference System	Margin with Respect to Design Objective or Reference System
Hypothetical S-band air traffic communications and control	ATS-B VHF repeater link	+11.3 db
Satellite-to-satellite IRLS data relay	Platform-Nimbus UHF link	Nimbus erp of 10.6* dbw required
Satellite-to-satellite video data relay	Nimbus-Rosman S-band link	-42.6 db ( $4 \times 10^5$ bps still feasible)
Satellite-to-satellite Apollo launch phase data relay	-----	$4 \times 10^5$ bps feasible
Position location systems	Proposed OPLE system	+13.9 db*

\* For defocussed operation at UHF, change by 10 db.

## ADVANCED MISSIONS

The several applications discussed in the previous section concerned the category of communications between an ATS-4 spacecraft in synchronous orbit and small (not necessarily earthbound) terminals. This section of the study considers very briefly non-geocentric space applications of ATS-4 antenna technology. The two systems discussed are libration point communications to the hidden side of the moon and interplanetary probes.

## LIBRATION-POINT LUNAR COMMUNICATIONS

Figure 20-3 shows the geometry of the five earth-moon libration points (References 29 and 30). Given the proper initial conditions, a light mass positioned at any of these points will rotate with the moon about the earth, remaining fixed in earth-moon space.

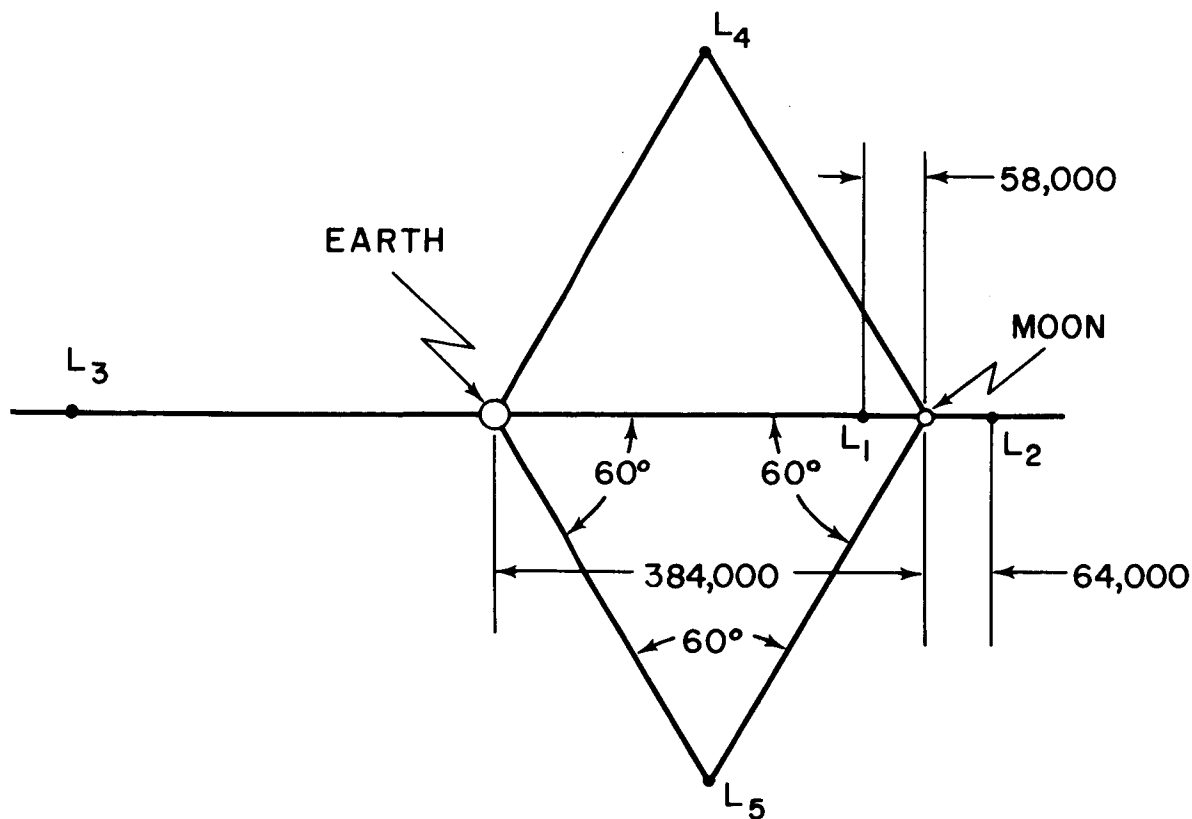


Figure 20-3. Geometry of the five earth-moon libration points, labelled  $L_1$ ,  $L_2$ ,  $L_3$ ,  $L_4$ , and  $L_5$ . Distances in kilometers

Since the moon's period of revolution about the earth is equal to its rotational period, any body that remains fixed in earth-moon space will be a synchronous satellite of the moon. This suggests several applications of ATS-4 large aperture antenna technology. Two hypothetical systems have been selected for study.

#### Lunar-earth Communications via $L_4$ or $L_5$

The first system is that of a lunar base on the hidden side of the moon having a 10-foot dish and 10 watts of power communicating with earth via a satellite located at  $L_4$  or  $L_5$ . The satellite has an ATS-4 type 30 foot dish for receiving signals from the lunar base at 8.0 GHz, and relays them at a level of 10 watts to earth at a frequency of 7.3 GHz, via a second, smaller (5-foot) dish. The earth receiving station is assumed to have an 85 foot dish and a noise temperature of 50°K. The channel capacity of the overall link is computed in Table 20-21.

Table 20-21

Lunar-Earth Channel Capacity Using Relay at  $L_4$  or  $L_5$ 

Parameter	Lunar-Earth Channel Capacity
Lunar base xmit power (10 watts)	+10.0 dbw
Xmit antenna gain (10-ft dish @ 8.0 GHz)	+45.5 db
Lunar base erp	+55.5 dbw
Path loss to libration point (384,000 km)	-222.5 db
Receive antenna gain (30-ft dish @ 8.0 GHz)	+54.7 db
C, received signal power at satellite	-112.3 dbw
$\eta$ , satellite noise density (600°K)	-200.8 dbw/Hz
C/ $\eta$ , lunar-satellite channel capacity	+88.5 db-Hz
Satellite xmit power (10 watts)	+10.0 dbw
Xmit antenna gain (5 ft dish @ 7.3 GHz)	+33.7 db
Satellite erp	+43.7 dbw
Receive antenna gain (85 ft dish @ 7.3 GHz)	+63.5 db
C, received carrier power	-114.6 dbw
$\eta$ , receiver noise density (50°K)	-211.6 dbw/Hz
C/ $\eta$ , satellite-earth channel capacity	+97.0 db-Hz
Overall link channel capacity	88.0 db-Hz

This channel capacity is within 1 db of that required to support a CCIR quality video link using wideband FM (Table 20-10), or from another point of view, is sufficient to permit digital data rates up to 100 megabits with bit error rates under  $10^{-3}$  (Table 20-17).

Point-to-point Lunar Communications via  $L_2$ 

In this hypothetical system, an ATS-4 type spacecraft is assumed to be located at  $L_2$ . The maximum frequency at which the 3-db mainbeam of a 30-foot dish at  $L_2$  will give global coverage of the moon is about 800 MHz. Choosing this frequency and assuming 1 watt per channel, spacecraft transmit power, a gross estimate of channel capacity in a link to the lunar surface is computed in Table 20-22. The up-link, assumed reciprocal, is not analyzed.

Table 20-22

Channel Capacity of Point-to-point Lunar  
Communications System Using  $L_2$

Parameter	Channel Capacity
Satellite xmit power	+0.0 dbw
Xmit antenna gain (30 ft dish @ 800 MHz)	+35.0 db
Satellite erp	+35.0 dbw
Path loss to lunar surface (64, 000 km)	-187.1 db
Receive antenna gain (assuming 10 ft dish)	+25.6 db
C , received signal power	-126.5 dbw
$\eta$ , noise density (assuming 1000°K)	-198.6 dbw/Hz
C/ $\eta$ , channel capacity	+72.1 db-Hz
Overall link channel capacity (reciprocal up-link)	+69.1 db-Hz

This channel capacity is essentially that required to meet military design objectives for FM voice communications (Tables 20-11 and 20-14). In terms of digital transmission, such a link could accommodate data rates in excess of a megabit with error rates under  $10^{-3}$ .

#### INTERPLANETARY MISSIONS

The material presented in this section is intended to indicate the RF power levels required for typical interplanetary missions using an ATS-4 type transmitting antenna on the probe spacecraft. The enormous distances involved in such missions preclude real-time transmission of wideband data unless both high gain antennas and substantial spacecraft power are available.

Three typical real-time digital signals are considered at widely varying data rates. They are vocoded speech at 2.4 kbps, 6-bit PCM speech at 48 kbps, and 4-bit PCM slow-scan TV at 480 kbps. A link frequency of 7.3 GHz is assumed, and the earth receiving system is taken to be an 85-foot dish (63 db gain at 7.3 GHz) and 50°K system noise temperature.

Spacecraft RF power levels required to achieve the three data rates while maintaining a bit error rate under  $10^{-3}$  are shown in Table 20-23 for four interplanetary missions.

Table 20-23

Power Requirements for Several Interplanetary Missions Using  
ATS-4 Type Transmitting Antennas

Mission	Distance (km)	Free Space Loss (db)	Power Required (dbw)		
			2.4 kbps	48 kbps	480 kbps
Venus-earth (min)	$3.5 \times 10^7$	262	-26.3	-13.3	-3.3
Mars-earth (min)	$5.3 \times 10^7$	264	-24.3	-11.3	-1.3
Venus-earth (max)	$2.5 \times 10^8$	277	-11.3	+1.7	+11.7
Mars-earth (max)	$5.4 \times 10^8$	284	-4.3	+8.7	+18.7

## APPENDIX I

Throughout this study, the parameter  $C/\eta$ , received signal power divided by (white, gauss) noise power per unit bandwidth, has been termed "channel capacity" and used extensively as a common denominator in analyzing and comparing a broad spectrum of communications systems. This appendix is included for the benefit of the reader who may not be familiar with this approach to characterizing communication system capability.

$C/\eta$ , which is measured in units of time<sup>-1</sup>, bandwidth, or some dimensionless quantity per unit time, is also sometimes called "noise bandwidth" (it is that bandwidth  $W$  in which the signal-to-noise power ratio  $C/(\eta W)$  is unity) and has also been discussed as a "system capacity quotient" (Reference 31). The importance, both theoretical and practical, of the  $C/\eta$  ratio in communication system analysis and design may be appreciated by appeal to a simple argument involving Shannon's famous theorem from information theory (Reference 32).

For present purposes, this theorem may be stated non-rigorously as follows. Given a transmission channel characterized by a rectangular band-pass  $W$ , an average communication signal power  $C$ , and an average additive white gauss noise power  $N$ , the function

$$S(W, C, \eta) = W \log(1 + C/N)$$

defines the maximum information transmission rate which can be supported without error. The function or quantity  $S$  has the units of information per unit time, where the actual information measure is arbitrary and depends on the logarithm base, as yet unspecified.

Shannon's theorem does not tell one how to build equipment to approach this maximum transmission rate, nor does it spell out what other factors (transmission and encoding-coding delays) may be involved in realizing  $S$ . However, considering  $S$  as a function of  $W$  only ( $C$  and  $\eta$ , the noise power per unit bandwidth or spectral density considered fixed), the fact that  $S(W)$  is strictly monotonic increasing with  $W$  suggests that for fixed signal power  $C$  and constant spectral density  $\eta$ ,  $S(W)$  can be maximized by using signaling or modulation techniques which use greater and greater bandwidth.

Working with Shannon's "natural units" of information, in the limit for large  $W$ , using the relationship

$$\ln(1 + x) \cong x, \quad x \ll 1$$

one has that

$$\lim_{W \rightarrow \infty} S(W) = S_{\infty} = C/\eta \quad \text{natural units per second.}$$

Information theory, then, asserts that in a communications system with fixed power and fixed noise spectral density but variable bandwidth, the information transmission rate is ultimately limited by the ratio  $C/\eta$  and will be approached as one goes to larger and larger transmission bandwidths. Examples of signaling techniques which trade signaling bandwidth for performance are, of course, wideband FM and the various digital systems (PCM, delta modulation, etc.).

The Parameter  $C/\eta$  used in this study is thus seen to be a special value of Shannon's function, i. e.  $S_{\infty}$ , the "infinite bandwidth channel capacity."

## APPENDIX II

This appendix is included to present in concise form the relationships between power density in watts/m<sup>2</sup> (or dbw/m<sup>2</sup>), electric field strength in volts/m (or dbu), and the power density and field strength developed by a given satellite erp at geosynchronous altitude. This material has important application in the analysis of direct broadcast (TV or FM) satellite systems.

If E is the electric field intensity in volts/m, it can be expressed in dbu (decibels relative to one microvolt/m) by the formula

$$E_{\text{dbu}} = 20 \log_{10} E + 120. \quad (1)$$

If E is the electric field intensity in volts/m, the power density P in watts per meter squared is given by the formula

$$P = \frac{E^2}{120\pi}. \quad (2)$$

If E is the electric field intensity in volts/m, the power density in dbw per meter squared is given by the formula

$$P_{\text{dbw/m}^2} = 10 \log_{10} \left[ \frac{E^2}{120\pi} \right] = 10 \log_{10} P. \quad (3)$$

If W is the synchronous satellite erp in dbw, the power density produced at the ground is given by the formula

$$P_{\text{dbw/m}^2} = W + 10 \log_{10} \left[ \frac{1}{4\pi R^2} \right] = W - 163.3, \quad (4)$$

where the value of R used is the maximum slant range  $41.1 \times 10^3$  km.

Figure 20-4 plots the relations between formulas (1), (2) and (3).

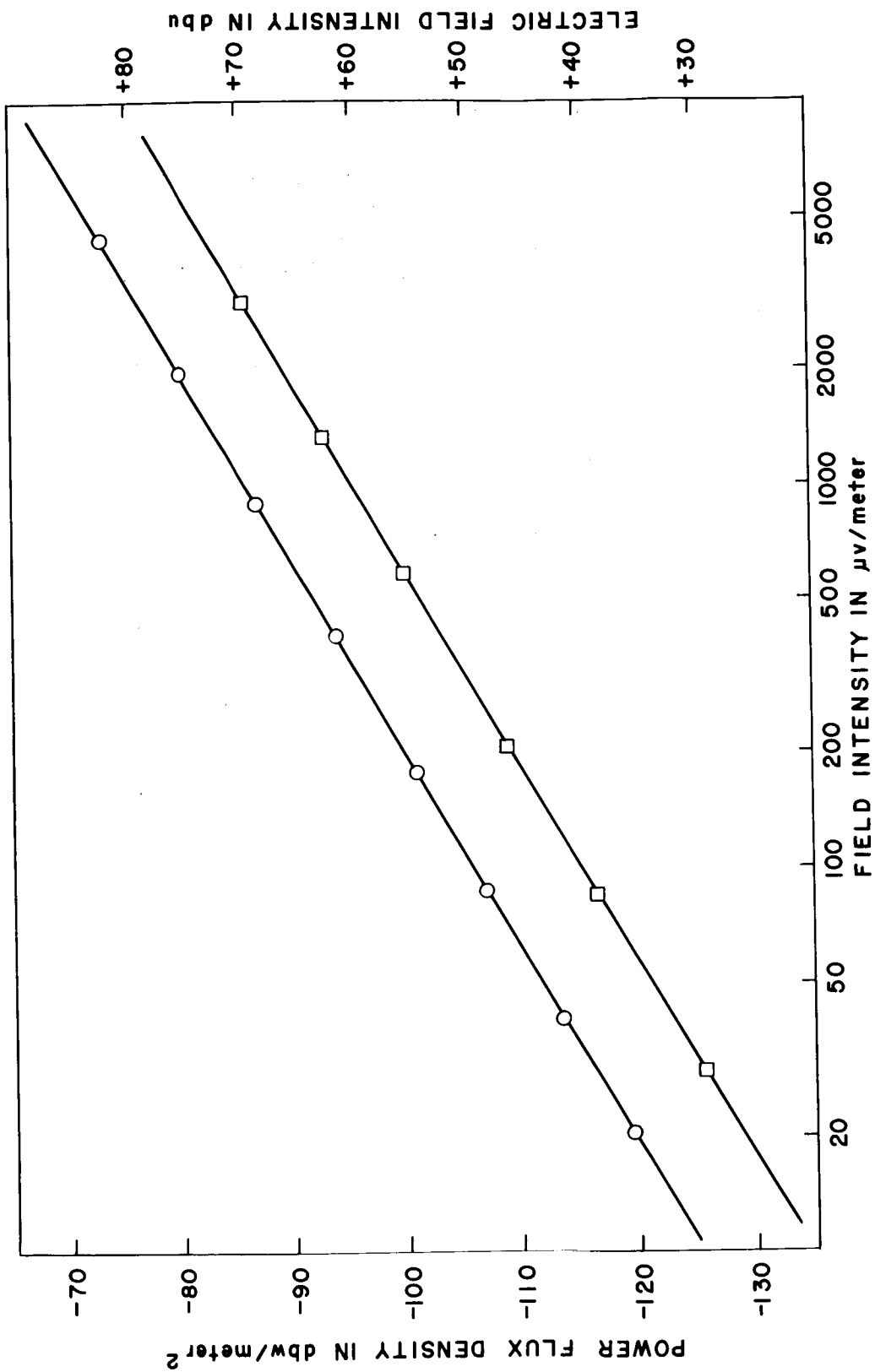


Figure 20-4. Showing Interrelationships between  $\mu\text{v}/\text{m}$ , dbu, and dbw/m<sup>2</sup>.

## REFERENCES

1. G. M. Northrup, "Aids for the Gross Design of Satellite Communication Systems," IEEE Trans. Comm. Tech., Vol. Com-14, No. 1., February 1966.
2. R. G. Gould, "TV Broadcast from an Earth Satellite," IRE Trans. Comm. Sys., Vol. CS-10, No. 2, June 1962.
3. B. W. St. Clair, "UHF Television Translators," in NAB Engineering Handbook, A. P. Walker, McGraw-Hill, New York, 1960.
4. W. J. Bray, "The Standardization of International Microwave Radio-Relay Systems," Proc. IEE., Paper No. 3412E, March 1961.
5. CCIR Document 2238-E.
6. H. T. Head, "The Measurement of FM and TV Field Strength," in NAB Handbook (see Ref. 3).
7. Unpublished work of J. E. Miller, Communications Research Branch, GSFC.
8. "Telstar," NASA SP-32, GSFC, June, 1963.
9. A. G. Cooley, "The Possible Use of Facsimile in Broadcasting," in NAB Handbook (see Ref. 3).
10. "Military Communication System Technical Standard," MIL-STD-188B, Washington D. C., February 24, 1964.
11. H. C. Franke, "Noise Measurements on Telephone Circuits," Tele-Tech and Electronic Industries, March 1955.
12. P. J. Heffernan, "Analysis of Non-linear Noise in FDM Telephony Transmission over an SSB-PM Satellite Communication System," NASA TN-2365, Washington, D. C., July 1964.
13. "Transmission Systems for Communications," 3rd Edition, Bell Telephone Laboratories, Winston-Salem, 1964 (page 468).
14. J. Fagot and P. Magne, "Frequency Modulation Theory," Pergamon Press, New York, 1961 (Eq. 2, 112, P. 118).

15. W. Doyle, "Crosstalk of Frequency-Multiplexed Signals in Saturating Amplifiers," RAND Memorandum RM-3576-NASA, April, 1963.
16. E. M. Rizzoni, "Compandor Loading and Noise Improvement in Frequency Division Multiplex Radio-Relay Systems," Proc. IRE, Vol. 48, No. 2, February, 1960.
17. E. D. Sunde, "Intermodulation Distortion in Multicarrier FM Systems," IEEE Int. Con. Rec., Part 2, March, 1965.
18. W. C. Babcock, "Intermodulation Interference in Radio Systems," BSTJ, January, 1953.
19. "Frequency Allocations," RCA Frequency Bureau, Washington, D. C., December, 1965.
20. "VHF Aircraft Satellite Relay - Final Report of Flight Tests," Bendix Radio Division, Baltimore, Md., April, 1965.
21. "Quarterly Progress Report No. 1," Contract NAS 5-9593, Hughes Aircraft Company, October 31, 1965.
22. W. Sollfrey, "Earth Coverage patterns with High-Gain Antennas on Stationary Satellites," RAND Memorandum RM-4894-NASA, February, 1966.
23. O. J. DeZoute, "Future Satellite Communication Subsystem Investigation," FAA Report No. RD-65-77, July, 1965.
24. "First Quarterly Report," Contract NAS 5-10255, Technical Communications Corporation, October, 1966.
25. Unpublished results of measurements made by M.I. T. Lincoln Labs with their LES 3 and 4 satellites.
26. J. R. Cressey and G. D. Hogan, "The Interrogation, Recording and Location System Experiment." Proc. National Telemetry Conference, 1965, Paper WA 61.
27. NDHS Pass Summary, Interrogation Orbit # 105R (unpublished data sheets, Tracking Systems Directorate, GSFC).

28. C. Laughlin, G. Hilton, R. Hollenbaugh and R. Lavigne, "Meteorological Experiment Using the Omega System for Position Location," NASA Document X-731-65-416, GSFC, October, 1965.
29. L. Steg and E. Shoemaker, "Libration Point Satellites," in A Review of Space Research, NAS-NRC Publ. 1079, 1962.
30. D. Jamison, "Synchronous Communication Satellites of the Moon," Proc. IEEE, Vol. 54, No. 7, July, 1966.
31. J. W. Schwartz, J. M. Aein, and J. Kaiser, "Modulation Techniques for Multiple Access to a Hard-Limiting Satellite Repeater," Proc. IEEE, Vol. 54, No. 5, May, 1966.
32. C. E. Shannon, Mathematical Theory of Communication, University of Illinois Press, Urbana, 1949.

## B. WHEEL-GRAVITY-GRADIENT BOOM HYBRID

The technology for passive gravity-gradient attitude control systems is being fully developed by ATS A, D, and E. Passive techniques produce an attitude control system with a response time related to orbital frequency, high static errors when subjected to disturbance torques, and no off-vertical pointing capability. The wheel-gravity-gradient boom hybrid is an active control system in that the attitude reference is not derived from the gravity field thus it does not suffer the performance limitation of a passive system. The gravity-gradient boom is gimballed with 2 degrees of freedom and serves two functions: to provide a source of reaction torque for attitude maneuvers (thus reducing the required wheel torque) and to provide a source of external torque to prevent wheel saturation and to minimize the momentum storage requirement. The wheel and control electronics provide control system damping; therefore, a low torque passive damper is not required.

A system study is being conducted by the Westinghouse Air Arm Division. This study will produce a recommended system design, a recommended gimbal design, and a digital computer simulation of the control system. The contractor was given the ATS-4 performance specification, and it is anticipated that the wheel-gravity-gradient boom system will satisfy the ATS-4 operational control requirements.

Since the wheel-gravity-gradient boom hybrid attitude control system is a new technology (not proven in flight), it will be carried on ATS-4 as an experimental system and will be deployed only after the major antenna experiments have been carried out. The concept is shown in Figure 20-5.

## C. SCANNING CELESTIAL ATTITUDE DETERMINATION SYSTEM (SCADS)

### INTRODUCTION

A star mapping system is proposed to provide a simple means for determining three-axis satellite attitude information for ATS-4 during the transfer ellipse mode, circular orbit, and the three-axis stabilized mode.

The SCADS concept consists of a single on-board sensor head and a ground-based computer data reduction system. The sensor head, by observing the known star field, provides signals from which the star field can be positively identified and three axis vehicle attitude information derived.

The primary objective of the experiment is to utilize SCADS to provide three-axis attitude to within 0.1 degree or better and spin period to 0.03 percent during the transfer and synchronous spin stabilized orbital phases. The attitude

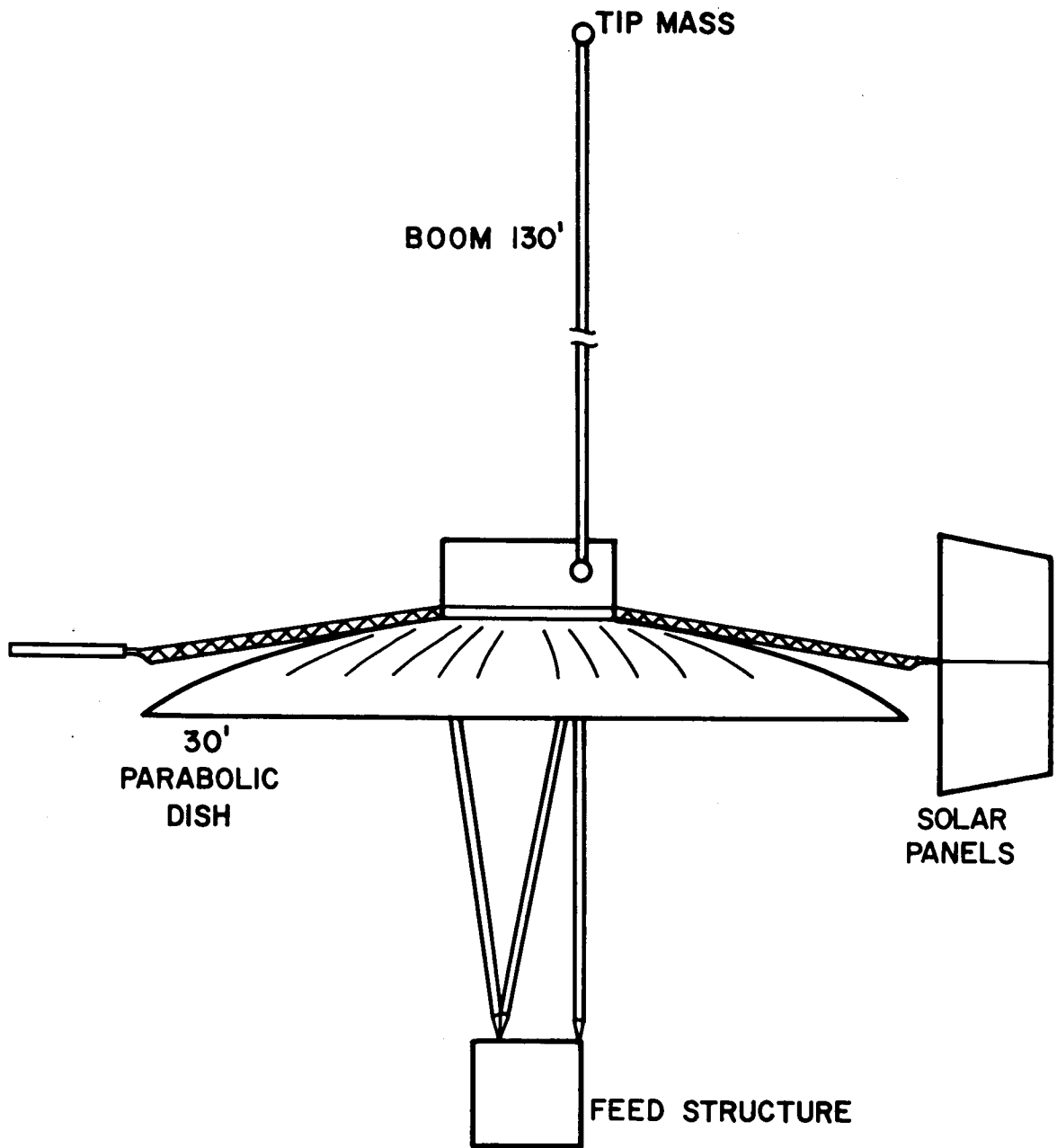


Figure 20-5. Commandable gravity gradient configuration.

data provided by SCADS will be used to supply the direction of the incremental velocity necessary to produce the synchronous orbit. A second objective of this experiment is to utilize SCADS to provide three-axis attitude data during the three-axis controlled synchronous mode to within 0.01 degree. The attitude data will be used to evaluate the control system performance.

The basic scanning instrument is comprised of a lens, an opaque reticle with a hairline radial slit, and a photodetector. The reticle will be rotated by the ATS-4 spacecraft during the spin stabilized modes and by a motor during the three-axis synchronous mode. As the reticle rotates, the instantaneous star image within the optical field of view will pass through the slit and impinge through onto the photodetector. In this manner, the photodetector produces an output for each star viewed by the scanning instrument.

The first step in the computer solution is that of star identification. The star identification problem consists of establishing a pairing of a transit time with the name (number) of the star which furnishes that transit. The right ascension and declination of stars brighter than a threshold setting controlled by ground command are examined to ascertain which of these stars could yield a measured transit time. The relative star magnitudes assist in the star identification when the assumed pointing direction is unknown. When the approximate pointing direction is given (within 5 to 10 degrees), the relative star magnitudes are not required. After the star identification phase is completed, the parameters which define attitude may be computed.

The SCADS system will consist of two basic parts. These are scanning sensor head and associated signal processing electronics and power supply. The components contained within the sensor head include a lens system, photomultiplier tube, motor with gearhead, reticle, and angle encoder. The volume required for the sensor head will be approximately 40 cubic inches, based on a housing 4-1/2 inches in diameter and 8-3/4 inches in length. The electronics package dimension will be 2 inches by 6-1/2 inches by 6 inches. The complete SCADS system will weigh approximately 7 pounds. Characteristics of the system are given below.

#### Power Requirements

Spin stabilized mode - 2.5 watts

Three axis stabilized mode - 5 watts during use

#### Telemetry

Data 2 - 10 bit words/second or 20 bits/second

### Diagnostic Telemetry

Lens cap status  
Unit temperature  
High voltage power supply  
Low voltage power supply  
Sun protection status, etc.

Total = 10 low rate channel (1/min)

### Commands

1 - word - to set threshold  
9 - relay - On-Off

A breadboard SCADS system and motion simulator were fabricated to demonstrate the practicality of spacecraft attitude determination from celestial coordinate measurements. The system was designed to simulate and measure the nutation about the spin axis for a spin stabilized satellite.

The accuracy that was achieved with a 10-second scanning period was 40 seconds of arc in pointing direction. In the precession mode, with a spin period of 10 seconds and a precession period of 20 seconds in the opposite direction, the cone angle of 0.7 degree was determined to within 15 seconds of arc rms.

#### D. ELECTRIC PROPULSION EXPERIMENT

The electric propulsion experiment will serve to demonstrate the in-space operational feasibility of an advanced colloid microthruster. Colloid thrusters fall within the category of electrostatic thrusters because the exhaust beam kinetic energy is obtained by the acceleration of charged particles within the electrostatic fields maintained by an accelerating electrode structure. Colloid thrusters differ from ion engines in that the charged particles are multimolecular rather than atomic.

Of the several colloid thruster concepts which have been experimentally investigated over the past 7 years, only one has yielded significant performance. The characteristic feature of that concept is the use of a charged particle source, which employs the phenomenon of electrostatic spraying of liquids. The propellant, a low vapor pressure, moderately conductive liquid, is sprayed from the tips of metallic capillary tubes which are maintained at a high electrical potential. The capillary potential imposes large electrical stresses in the liquid meniscus at the capillary tip, causing the meniscus to rupture and eject extremely small, charged droplets. The very low power required for this charged particle generation technique is the feature which makes colloid thrusters highly competitive to ion engines, especially at thrust levels below 1 millipound.

Conventionally, electrostatic thruster operation consists of three separate processes: charged particle generation, acceleration, and exhaust beam neutralization. Within the past 2 years, the state-of-the-art in charged particle generation by electrostatic spraying has advanced to the point where the particle formation and acceleration process can be accomplished simultaneously. The advancement has eliminated the requirement for an accelerating electrode structure and, with it, the problem of accelerating electrode erosion, which has been one of the more serious developmental problems of ion engines. There is presently under development a colloid microthruster, which uses a thermionic neutralizer. This microthruster is scheduled for experimental test aboard a DOD satellite and promises a power requirement of approximately one-fifth that of ion engines of comparable thrust level. Nearly half its power is required for the neutralizer.

An advanced version of the colloid microthruster produces positively and negatively charged particles simultaneously, but from adjacent capillary tubes, thereby eliminating the requirement for a thermionic neutralizer and reducing the power requirement by almost one-half. There are presently two Air Force sponsored research efforts devoted to this thruster concept.

The primary object of the experiment aboard ATS-4 is to determine the adequacy of the autoneutralizer characteristic of the advanced micro-thruster. This determination can be made implicitly from a measurement of the thrust output. The sizing and location of the experiment aboard the spacecraft must be consistent with the thrust measurement requirement. If desired, the thruster may be sized (thrust) to serve an operational function such as north-south station keeping. A thrust level of 200 micro-pounds would require less than 20 watts (perhaps as few as 10 watts) at 800 to 1000 seconds specific impulse. The propellant requirement would be 6-1/2 to 8 pounds per year of continuous operation. The total package weight could be expected to be 15 to 20 pounds.

#### E. DEVELOPMENT OF INTERFEROMETER ATTITUDE SENSOR FOR ATS-4 EXPERIMENT

##### PURPOSE

The ATS-4 spacecraft is required to demonstrate attitude control for pointing the main beam of the large aperture antenna to  $\pm .1$  degree for all three axes. In order to fulfill this requirement, it is necessary that on-board attitude sensors have an accuracy approaching an order of magnitude better than  $\pm .1$  degree.

If the interferometer experiment is successful, it could be used to fully exploit the conduct of the other ATS-4 experiments. This experimental sensor would serve as a redundant system to the conventional ATS-4 sensors. It could be considered for use as the primary attitude sensor for future missions.

##### OBJECTIVE

The interferometric principle has long been adaptable to high accuracy measurement. The MINITRAC system is basically an RF type of interferometer. The RF interferometer principle has also been successfully applied to terrestrial navigation systems, improved aircraft landing systems, and manned (Gemini) spacecraft docking systems. Similarly, this principle exhibits the potential of being developed into a spacecraft attitude sensor that would have the accuracy (better than  $\pm .1$  degree) required for implementing the ATS-4 mission. It is the objective, therefore, to develop an interferometer attitude sensor for possible implementation of a flight experimental on board the ATS-4 spacecraft. The basic interferometer attitude sensor will consist of two antennae whose phase centers are separated by a

distance and an electrical phase-comparing element. In operation, a transmitted radio wave intersecting the two antennae will result in a measurable phase shift between the signals received by each antenna. The amount of phase shift will be dependent upon the angle of arrival of the wave to the baseline axis (interferometer axis) between the antennae. By mounting pairs of antennae so that they are orthogonal to the main axis of a spacecraft, and configured to represent the X-Y axes, the resulting measured phase gradients will be indicative of spacecraft attitude. For this application, the radio wave is considered to be planar at the time of arrival at the antennae, since the interferometer will be at a great distance (orbital altitude) from the transmitter.

#### TECHNICAL APPROACH

The technique to be studied by the contractor will be that of a spacecraft phase comparison receiver system. Operation will be at X-band frequency to afford optimum antennae separation, in wave lengths, for obtaining the required accuracy. The maximum linear antennae baseline dimension will be 4 feet to provide a reasonable and realistic antennae mounting configuration for a possible spacecraft experiment. The antennae design configuration shall be such that its aperture plane(s) can be mounted orthogonally to the main axis of a spacecraft for a flight experiment, so that the measured, phase gradients will be indicative of the spacecraft's attitude. Either a coarse-vernier (dual baseline) antennae system or a dual frequency technique will be employed to resolve ambiguities. The technique will be based on the use of two ground stations, each transmitting the required signal(s) in a prescribed manner to the interferometer receiver for making the required attitude determination measurement. The transmitted signals will be circularly polarized. The field of view of the interferometer will be at least twice the angle for full earth coverage for possible operation as an experiment on board a spacecraft at synchronous attitude. This will permit the spacecraft's main axis to be pointing at one horizon and receiving interferometric measurement signals from the opposite horizon. Interferometer receiver characteristics (sensitivity, stability, bandwidth, etc.) will be optimized so as to receive a minimal transmitted signal (transmitter power of a maximum few hundred watts operating into a small dish several feet in diameter) during a synchronous altitude flight experiment. On-board signal processing circuitry to be developed under the initial contract will be limited to that necessary to make the required comparison between individual phase measurements and express the result(s) in an electrical format suitable either for telemetering back to an earth terminal for final attitude computation or for further on-board processing so as to interface into the ATS-4 attitude control system. Means will be provided, as part of the spacecraft receiver

system, for in-flight calibration and for sensing and determination of system errors, both electrical and mechanical. The interferometer receiver system will be designed to operate from an unregulated 28 volt nominal dc supply. Power and weight will be optimized. Packaging geometry, excluding the antennae subsystems, will be flexible. Development of the interferometer to operate at X-band will represent a more significant technological advancement than at a lower frequency, since it is more difficult to measure electrical phase to the accuracy required in the 7 to 10 GHz region.

## SPACE LINK CHARACTERISTICS

Of importance in performing an interferometer attitude spacecraft measurement experiment will be the radio frequency (RF) space link characteristics. This is especially important at the present time, since the project envisions a synchronous altitude receiving system for phase gradient measurement relative to a RF signal transmitted from a minimal type ground terminal of a transportable nature. The system will operate at X-band frequency - 8 GC, for example. A good carrier-to-noise ratio (C/N) must be achievable for successful conduct of the experiment.

System and link characteristics for this experiment are presented in Table 20-24. It shows that an adequate C/N ratio is achievable.

Table 20-24.

### System and Link Characteristics

Operating frequency = 8 GHz  
 Ground transmitter power = 100 watts (20 dbw)  
 Ground antenna - 2 ft diameter dish,  $G_t = 32$  db, Beamwidth =  $4-1/2^\circ$   
 S/C antenna - Horn 10 db BW =  $34^\circ$   
 S/C receiver noise figure = 10 db  
 Receiver bandwidth = 1 KHz

#### Receive Carrier Power

Transmitter power ( $P_t$ )	=	20 dbw
Transmitter antenna gain ( $G_t$ )	=	32 db
Space loss	=	-200 db
Polarization loss	=	-3 db
Misc. loss	=	-5 db
Receiver antenna gain	=	10 db
		<hr/> -146 dbw

Table 20-24. (Concluded)

System and Link Characteristics

Receive Noise Power

Boltzmann's Constant ( $1.38 \times 10^{-23}$ W/Hz/°K)	=	-228.6	dbw
Effective system temperature (1500° K) *	=	31.8	db
Bandwidth (1KHz)	=	50	db
		<hr/>	
		-156.8	dbw
Predetection C/N = $\frac{-146 \text{ dbw}}{-156.8 \text{ dbw}}$	=	20.8	db

\*(1500° K = 300°K galactic temp + 120°K x NF)

## SECTION 21

### SUMMARY

It can be concluded that the ATS-4 program meets the criterion specifics for NASA Phase A planning. It is feasible, practical, and desirable.

An assessment has been made which shows that the SLV-3C Atlas-Centaur with the TE-364-3 apogee motor will inject 1797 pounds into orbit. It is considered practical to design the ATS-4 spacecraft to this design constraint. The stated objectives—demonstration of a 30-foot diameter deployable antenna, provision of spacecraft fine pointing and an oriented platform at synchronous altitude for advanced technology experiments—are considered both feasible and practical. The 30-foot diameter spacecraft antenna and the fine pointing control system will provide a significant advance to the technology of radio communications. The oriented platform at synchronous altitude permits the conducting of a number of experiments in spacecraft attitude determination, spacecraft attitude control, and communications systems.

As in all programs which must advance the state-of-the-art to achieve significant technology advancements, there are some outstanding difficult problem areas. The pacing problem in this program is the antenna reflector. A reflector study contract is now under way. It is anticipated that this planned engineering effort will be adequate to solve the problem on a timely base. Another problem, not pacing at this time, is the antenna feed and feed support system. Launch packaging constraints introduce certain constraints on the antenna feed support structure. These in turn affect the antenna gain and patterns. The gain loss varies from 1-1/2 db to 2-1/2 db through the operating frequency range. A study of this problem is under way, and it is anticipated that these gain losses can be reduced considerably. There are many other engineering problems in the program. It is anticipated that these problems will follow the normal pattern where some become critical and are solved during the course of the program. Others are solved with normal engineering effort.